

X

11 6 AUG 2005

PHASE INVERSION CASTING OF  
POLY(ACRYLONITRILE) BASED MEMBRANES

THESIS  
SUBMITTED TO THE  
UNIVERSITY OF PUNE  
FOR THE DEGREE OF  
DOCTOR OF PHILOSOPHY  
IN CHEMISTRY




BY  
MADHURI SHINDE  
CHEMICAL ENGINEERING DIVISION  
NATIONAL CHEMICAL LABORATORY  
PUNE 411008  
INDIA

DECEMBER, 2002

## DECLARATION

Certified that the work incorporated in the Thesis "**Phase inversion casting of Poly(acrylonitrile) based membranes**", submitted by Ms. Madhuri. H. Shinde was carried out by the candidate under my supervision. Such material as has been obtained from other sources has been duly acknowledged in the thesis.



(Dr. B.D.Kulkarni )

Research Guide

# University of Pune



## Declaration of result of the Doctor of Philosophy ( Ph.D )

Smt. Shinde Madhuri Himmatrao

(श्रीमती शिंदे माधुरी हिम्मतराव)

University has accepted thesis submitted by the above mentioned candidate for award of Ph.D., as per reports of referees and examiners of open defence of the thesis. Accordingly, it is hereby notified that, the above mentioned candidate is declared to have passed the examination of Ph.D. and has become eligible for the award of Ph.D. Degree.

### RELEVANT DETAILS ARE AS UNDER:

1. Faculty : Science
2. Subject : Chemistry
3. Title of the Thesis : "Phase Inversion Casting of Poly(acrylonitrile) Based Membranes"
4. Place of Research : National Chemical Laboratory, Pashan, Pune 411008.
5. Name and Address of the Guide : Dr. B. D. Kulkarni, National Chemical Laboratory, Pashan, Pune 411008.
6. Date of Registration : 28th December, 2000.
7. Date of Declaration of Result : 15th September, 2003.

Ganeshkhind, Pune 411007.  
Ref. No. PGS/Ph.D./4021  
Date: 19/9/2003

For Controller Of Examinations

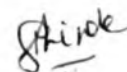
## ***ACKNOWLEDGEMENTS***

I wish to express my deep sense of gratitude to my research guide, Dr. B.D. Kulkarni, for his guidance, patience and support throughout the course of these investigations. I wish to thank the Director, N.C.L for allowing me to present the work in the form of the thesis. I am also thankful to CSIR for granting me the fellowship.

I would like to mention a special word of thanks to Dr. S. S. Kulkarni for his constant encouragement and help throughout the course work even after leaving NCL for the past four years. I would like to also thank my Senior colleagues Dr. D. A. Musale and Dr. S. K. Karode for their useful suggestions and ever helping hand throughout my study tenure even after being busy with their own tight job schedules etc. I am absolutely wordless for these people.

I must thank my colleagues, Shubhangi, Mahendra, Singh, Anuja and all others for their help and cooperation during my thesis completion.

Finally, I would like to mention a special word of thanks to my husband Ajit for his patience, support and help given to me during my course work. Lastly, I would like to thank my parents and in-laws for their constant support and help rendered to me.



Madhuri. H. Shinde

## CONTENTS

	Page No
List of Figures	vi
List of Tables	xv
List of symbols	xviii
Abbreviations	xix
ABSTRACT	1
CHAPTER 1	6
1.1 Commercially available PAN membranes	9
1.2 Characterization of interactions of salts with DMF	10
1.2.1 IR studies	10
1.2.2 NMR studies	12
1.2.3 Raman spectroscopy	15
1.2.4 Miscellaneous characterization techniques	17
1.2.5 Metal:DMF solvation stoichiometry	18
1.3 Characterization of interactions of PAN with DMF	20
1.4 Characterization of interactions of inorganic halides with model PAN compounds - organonitriles	21
1.5 Characterization of interactions of inorganic halides with PAN	25
1.6 PAN solution properties	27
1.6.1 PAN solution viscosity study	27
1.6.2 Dilute solution study	28
1.6.2.1 Theoretical models	28
1.6.2.2 Experimental studies of dilute PAN solution rheology	31
1.6.3 Concentrated solution studies	31
1.6.3.1 Theoretical models	31
1.6.3.2 Experimental studies of dilute PAN solution rheology	33
1.7 Effect of solution composition on membrane morphology	34

1.7.1 Phase boundary map	34
1.7.2 Membrane morphology determined by mechanism of phase inversion	36
1.7.3 PAN membrane morphology	39
1.7.3.1 Organic additives	40
1.7.3.2 PAN blends and co-polymers	40
1.8 Other polymeric membrane morphology studies	41
1.8.1 Organic additives	41
1.8.2 Salt additives	43
1.8.2.1 Polysulfone (PSF)	43
1.8.2.2 Polyamide / imides	44
1.8.2.3 Vinyl polymers	46
1.9 Aim and Objectives for this work	48
1.10 Description of thesis organization	49
CHAPTER 2	56
2.1 Polymer synthesis and characterization	56
2.1.1 Materials	56
2.1.2 Polymer synthesis	57
2.1.3 Copolymer synthesis	58
2.1.4 Polymer Characterization Results	58
2.1.4.1 Elemental analysis	58
2.1.4.2 Fourier Transform Infrared Spectroscopy (FTIR)	59
2.1.4.3 NMR spectroscopy	65
2.1.4.4 Intrinsic viscosity	66
2.2 Solution studies	67
2.2.1 Dilute Solution studies	67
2.2.2 Concentrated solution viscosity	68
2.2.2 Cloud point study	68

2.3 Membrane preparation and characterization	69
2.3.1 Membrane Preparation	69
2.3.1.1 Membrane preparation for PAN-A	69
2.3.1.2 Membrane preparation for PAN-B and PAN-C	70
2.3.2 Permeability measurements	71
2.3.3 Bubble point/pore size distribution measurements	72
2.3.4 Membrane structure	73
 CHAPTER 3	 74
3.1 Experimental	74
3.1.1 Fourier Transform Infrared (FTIR) spectroscopic measurements	74
3.1.2 Dilute solution viscosity studies	75
3.2 Specific interactions between Salts, DMF and PAN: FTIR studies	75
3.2.1 FTIR studies of DMF+ salts	75
3.2.2 FTIR studies of PAN+DMF	80
3.2.3 FT-IR studies of Salt + DMF + PAN	90
3.3 PAN-DMF-salt interactions: Dilute solution rheology studies	104
3.3.1 Solvent viscosity	104
3.3.2 Dilute Solution viscosity	105
3.3.3 Intrinsic Viscosity calculations and interpretation	110
3.3.3.1 Mark-Houwink (M-H) constant estimation	113
3.3.4. Activation energy correlations	120
3.4 Discussion summarizing Chapter III	126
 CHAPTER 4	 128
4.1 Rheological properties	128
4.1.1 Concentrated solution viscosity	129
4.2 Phase boundary studies	132
4.3 Membrane morphology	135

4.3.1	Surface SEM	135
4.3.2	Cross-section SEM	138
4.3.2.1	Effect of polymer concentration: Comparison of 7-17% polymer concentration variation for PAN-A and PAN-A-Z membranes	138
4.3.2.1	Effect of Salt additive: Comparison of Additive type for PAN-A membranes cast from 11 and 13% polymer concentration	146
4.4	Permeation results	150
4.4.1	Bubble pt / Pore size distribution	
4.4.1.1	Effect of additive on bubble point / pore size	151
4.4.1.2	Effect of polymer concentration on bubble point / pore size of PAN-A and PAN-A-Z	154
4.4.2	Water permeability measurements	155
4.4.3	Ultrafiltration studies	157
4.5	Correlation of membrane structure / performance with solution properties	161
CHAPTER 5		164
5.1	Rheological properties	164
5.1.1	Concentrated solution viscosity	165
5.1.2	Low shear rate viscosity	165
5.1.3	Solvent effect on viscosity in concentrated PAN solutions	170
5.1.4	Shear dependent rheology	176
5.2	Phase boundary studies	178
5.3	Membrane properties	183
5.3.1	Pore size and pore size distribution:	183
5.3.2	Pure water permeation	187
5.3.3	Protein rejection	188
5.4	Membrane morphology studies	189
5.4.1	Effect of PAN grade	195



5.4.2 Effect of salts	195
5.5 Membrane morphology, Comparison of PAN-A with copolymer PAN-1	196
5.6 Correlation of PAN membrane structure / performance with solution properties	198
CONCLUSIONS AND SCOPE FOR FUTURE WORK	202
REFERENCES	210
APPENDICES	220
Appendix Chapter I	220
Appendix Chapter III	222
Appendix Chapter IV	226
Appendix Chapter V	229

## List of figures

	Chapter 1	Page No.
Figure 1.1	Proposed structure of the complex of DMF with metal salts	19
Figure 1.2	Illustration of polymer chain configuration in dilute, semi-dilute and concentrated solutions.	28
Figure 1.3	Schematic phase diagram of the polymer-solvent--non-solvent system showing the precipitation pathway of the casting solution during membrane formation.	35
Figure 1.4	Phase separation in ternary systems for membrane preparation Path (a) solvent evaporation and non-solvent addition leading to gelation without phase separation.....	37
Figure 1.5	Proposed solvation structure for the aromatic polyamide in an amide solvent.	46
<b>Chapter 2</b>		
Figure 2.1	FTIR spectra of a 7 % w/w PAN-A solution in pure DMF.	60
Figure 2.2	FTIR spectra of a 7 % w/w PAN-B solution in pure DMF.	61
Figure 2.3	FTIR spectra of a 7 % w/w PAN-C solution in pure DMF.	62
Figure 2.4	FTIR spectra of a 7 % w/w copolymer PAN-1 solution in pure DMF.	63
<b>Chapter 3</b>		
Figure 3.1a	Effect of salt addition on $>C=O$ stretching frequency of DMF.	76
Figure 3.1b	Effect of salt addition on OC-N stretching frequency of DMF.	76
Figure 3.1c	Effect of salt addition on O-C-N bending frequency of DMF.	77
Figure 3.2	Depiction of various populations of DMF molecules in DMF-salt solutions. Also shown are the assignments for	78

	the O-C-N bending frequency.	
Figure 3.3a	FTIR spectra of a PAN-A film made from 3% w/w PAN solution in pure DMF.	83
Figure 3.3b	FTIR spectra of a PAN-B film made from 3% w/w PAN in pure DMF.	84
Figure 3.3c	FTIR spectra of a PAN-C film made from 3% w/w PAN in pure DMF.	85
Figure 3.4a	FTIR spectra of a 7 % w/w PAN-A solution in pure DMF.	86
Figure 3.4b	FTIR spectra of a 7 % w/w PAN-B solution in pure DMF.	87
Figure 3.4c	FTIR spectra of a 7 % w/w PAN-C solution in pure DMF.	88
Figure 3.5	Illustration of various DMF populations in PAN-DMF solution.	89
Figure 3.6a	Effect of PAN addition on $>C=O$ stretching in neat DMF.	90
Figure 3.6b	Effect of PAN addition on OC-N stretching in neat DMF.	91
Figure 3.6c	Effect of PAN addition on O-C-N bending in neat DMF.	91
Figure 3.7a	Effect of LiCl and PAN addition on $>C=O$ stretching in DMF.	92
Figure 3.7b	Effect of LiCl and PAN addition on OC-N stretching in DMF.	92
Figure 3.7c	Effect of LiCl and PAN addition on O-C-N bending in DMF.	93
Figure 3.7d	Effect of LiCl on nitrile stretching in PAN + DMF.	93
Figure 3.8a	Effect of $ZnCl_2$ and PAN addition on $>C=O$ stretching in DMF.	94
Figure 3.8b	Effect of $ZnCl_2$ and PAN addition on OC-N stretching in DMF.	94
Figure 3.8c	Effect of $ZnCl_2$ and PAN addition on O-C-N bending in DMF.	95
Figure 3.8d	Effect of $ZnCl_2$ on nitrile stretching in PAN + DMF.	95
Figure 3.9a	Effect of $AlCl_3$ and PAN addition on $>C=O$ stretching in DMF.	96

Figure 3.9b	Effect of AlCl <sub>3</sub> and PAN addition on OC-N stretching in DMF.	96
Figure 3.9c	Effect of AlCl <sub>3</sub> and PAN addition on O-C-N bending in DMF.	97
Figure 3.9d	Effect of AlCl <sub>3</sub> on nitrile stretching in PAN + DMF.	97
Figure 3.10a	Frequency shifts in PAN-DMF-LiCl binary and ternary system for >C=O and OC-N stretching.	101
Figure 3.10b	Frequency shifts in PAN-DMF-ZnCl <sub>2</sub> binary and ternary system for >C=O and OC-N stretching.	102
Figure 3.10c	Frequency shifts in PAN-DMF-AlCl <sub>3</sub> binary and ternary system for >C=O and OC-N stretching.	102
Figure 3.11	Effect of salt addition on viscosity ratio of DMF+salt vs neat DMF at 25°C.	105
Figure 3.12a	Arrhenius plots of $\eta$ vs 1/T for PAN-A (0.1%) polymer solution with and without additives as function of temperature (298-318 K).	106
Figure 3.12b	Arrhenius plots of $\eta$ vs 1/T for PAN-A (0.2%) polymer solution with and without additives as function of temperature (298-318 K).	106
Figure 3.12c	Arrhenius plots of $\eta$ vs 1/T for PAN-A (0.3%) polymer solution with and without additives as function of temperature (298-318 K).	107
Figure 3.12d	Arrhenius plots of $\eta$ vs 1/T for PAN-B (0.1%) polymer solution with and without additives as function of temperature (298-318 K).	107
Figure 3.12e	Arrhenius plots of $\eta$ vs 1/T for PAN-B (0.2%) polymer solution with and without additives as function of temperature (298-318 K).	108
Figure 3.12f	Arrhenius plots of $\eta$ vs 1/T for PAN-B (0.3%) polymer solution with and without additives as function of temperature (298-318 K).	108
Figure 3.12g	Arrhenius plots of $\eta$ vs 1/T for PAN-C (0.1%) polymer solution with and without additives as function of Temperature (298-318 K).	109
Figure 3.12h	Arrhenius plots of $\eta$ vs 1/T for PAN-C (0.2%) polymer solution with and without additives as function of Temperature (298-318 K).	109
Figure 3.12i	Arrhenius plots of $\eta$ vs 1/T for PAN-C (0.3%) polymer	110

	solution with and without additives as function of Temperature (298-318 K).	
Figure 3.13a	Plot of $\ln[\eta]$ vs $\ln M$ for solvent type DMF at various temperatures.	115
Figure 3.13b	Plot of $\ln[\eta]$ vs $\ln M$ for solvent type DMF-L at various temperatures;	116
Figure 3.13c	Plot of $\ln[\eta]$ vs $\ln M$ for solvent type DMF-Z at various temperatures;	117
Figure 3.13d	Plot of $\ln[\eta]$ vs $\ln M$ for solvent type DMF-A at various temperatures	118
Figure 3.14	Mark-Houwink plot from the viscosity data at 25°C for all the four solvents i.e. neat DMF, DMF+LiCl, DMF+ZnCl <sub>2</sub> , DMF+AlCl <sub>3</sub>	119
Figure 3.15a	Activation energy (E <sub>a</sub> ) values for PAN-A as a function of polymer concentration for solvent types DMF, DMF-L, DMF-Z and DMF-A.	120
Figure 3.15b	Activation energy (E <sub>a</sub> ) values for PAN-B as a function of polymer concentration for solvent types DMF, DMF-L, DMF-Z and DMF-A.	121
Figure 3.15c	Activation energy (E <sub>a</sub> ) values for PAN-C as a function of polymer concentration for solvent types DMF, DMF-L, DMF-Z and DMF-A.	121
Figure 3.16	Correlation between the activation energy (E <sub>a</sub> ) and the coil overlap parameter, $[\eta]_c$ .	123
Figure 3.17	Correlation between the activation energy (E <sub>a</sub> ) and the coil overlap parameter $\beta$ categorized by solvent type i.e. neat DMF, DMF-L, DMF-Z and DMF-A	124
Figure 3.18	Correlation between the activation energy (E <sub>a</sub> ) and the coil overlap parameter $[\eta]_c$ for the solvent type i.e. neat DMF, DMF-L, DMF-Z and DMF-A for the three polymer PAN-A, PAN-B and PAN-C	125

#### Chapter 4

Figure 4.1a	Log viscosity (at $3.75 \text{ sec}^{-1}$ shear rate) as a function of PAN-A concentration in solutions with various solvents: DMF, DMF-L, DMF-Z and DMF-A	130
Figure 4.1b	Concentrated solution viscosity as a function of polymer concentration at a fixed shear rate of $3.75 \text{ sec}^{-1}$ .	131
Figure 4.2	Ternary phase diagram plotted (theoretical points) for PAN-A, PAN-A-L, PAN-A-Z and PAN-A-A solutions using the lcp equation (4.1)	133
Figure 4.3	Water sensitivity plot for PAN-A, PAN-A-L, PAN-A-Z and PAN-A-A showing water volume fraction at the cloud point as a function of PAN concentration.	134
Figure 4.4a	Frequency distribution of the surface pore size for PAN-A, -A-L, -A-Z and A-A membranes cast (supported) from 13% polymer solutions. The legend shows the pore size in nm.	135
Figure 4.4b	Surface view of 13% polyester supported PAN-A membrane at a magnification of 50k	136
Figure 4.4c	Surface view of 13% polyester supported PAN-A-L membrane at a magnification of 50k	136
Figure 4.4d	Surface view of 13% polyester supported PAN-A-Z membrane at a magnification of 50k	137
Figure 4.4e	Surface view of 13% polyester supported PAN-A-A membrane at a magnification of 50k	137
Figure 4.5a-h	Cross-sectional views of PAN-A membranes as a function of polymer concentration at (a,b) 7%, (c,d) 11%, (e,f) 13% and (g,h) 17%.	139
Figure 4.6a-g	Cross-sectional views of PAN-A-Z membranes as a function of polymer concentration at (a,) 7%, (b,c) 11%, (d,e) 13% and (f,g) 17%	143
Figure 4.7a-h	Cross-sectional views of PAN-A membranes cast from	146

	11% polymer concentration as a function of combined DMF+ salt additive type: (a,b) neat DMF, (c,d) DMF-Z (e,f) DMF-L and (g,h) DMF-A.	
Figure 4.8a-d	Scanning electron micrographs for the cross-sectional view of membranes of 13% polymer concentration (a) PAN-A (b) PAN-A-L (c) PAN-A-A at 300x magnification and (d) skin layer of PAN-A-Z at 50k magnification	149
Figure 4.9a	Average membrane bubble points of isopropanol-wetted PAN-A, PAN-A-L, PAN-A-Z and PAN-A-A (polyester-supported) membranes cast from 13% polymer concentration solutions.	151
Figure 4.9b	Average membrane bubble points of water-wetted PAN-A, PAN-A-L, PAN-A-Z and PAN-A-A (polyester-supported) membranes cast from 13% polymer concentration solutions.	152
Figure 4.10	Pore size distribution curve for the 13% polymer concentration membrane (supported) of PAN-A, PAN-A-L, PAN-A-Z and PAN-A-A. Calculations based on air-isopropanol displacement data.	153
Figure 4.11a	Pore size distribution curve for PAN-A membranes (cast on glass plate) cast from 7, 11, 13 and 17% polymer concentration solutions.	154
Figure 4.11b	Pore size distribution curve for the water wetted supportless PAN-A-Z membranes cast from different polymer concentrations.	154
Figure 4.12	Average water permeation rates of PAN-A, PAN-A-L, PAN-A-Z and PAN-A-A (polyester-supported) membranes cast from 13% polymer concentration solutions. Based on data for operating pressure 200kPa, temperature 25°C in stirred cell.	155
Figure 4.13	Water permeation rates as a function of polymer	156

	concentration (7-15%).for PAN-A and PAN-A-Z membranes cast on polyester support. The water permeability was measured at 70kPa, temperature 29°C	
Figure 4.14	Water permeability for PAN-A ,PAN-A-L,PAN-A-Z, PAN-A-A supportless membranes as a function of polymer concentration range of 7-17%. The water permeability was measured at 70kPa, temperature 29°C.	157
Figure 4.15	Average PEG, lysozyme and BSA rejections for PAN-A, PAN-A-L, PAN-A-Z and PAN-A-A supported membranes cast at 13% polymer concentration. Operating pressure 100kPa, temperature 25°C, stirred cell.	159
Figure 4.16	BSA rejection data for machine cast PAN-A and PAN-A-Z membranes cast on polyester support as a function of polymer concentration (11-15%). Operating conditions : pressure 70kPa, buffer 7.5 pH, 0.1g/dl BSA in stirred cell.	160
<b>Chapter 5</b>		
Figure 5.1a	Viscosity of PAN-A (DMF), PAN-A-L, PAN-A-Z and PAN-A-A solutions as a function of polymer concentration at a shear rate of 3.75 sec <sup>-1</sup> and 30°C.	166
Figure 5.1b	Viscosity of PAN-B (DMF), PAN-B-L and PAN-B-A solutions as a function of polymer concentration at a shear rate of 1 sec <sup>-1</sup> and 30°C.	167
Figure 5.1c	Viscosity of PAN-C, PAN-C-L and PAN-C-A solutions as a function of polymer concentration at a shear rate of 1 sec <sup>-1</sup> and 30°C.	169
Figure 5.2	Correlation of $\eta_0$ at 30°C with the coil overlap parameter $\beta$ for all three PAN grades.	170
Figure 5.3a	Correlation of $\eta_0$ with $\beta$ ( $\equiv c[\eta]$ ) for the various DMF, DMF-L, DMF-Z and DMF-A based solutions for all three PAN grades.	172



Figure 5.3b	Correlation of $Y$ (eqn 5.2 ) with $\beta$ ( $\equiv c[\eta]$ ) for the various DMF, DMF-L, DMF-Z and DMF-A based solutions for all three PAN grades.	173
Figure 5.4a	Correlation of $\eta_0$ at 30°C with the Bueche parameter ( $\lambda \equiv MW c$ ) for all three PAN grades.	174
Figure 5.4b	Correlation of $\eta_0$ at 30°C with the Bueche parameter ( $\lambda \equiv c MW$ ) for the various DMF, DMF-L, DMF-Z and DMF-A based solutions for all three PAN grades.	175
Figure 5.5a	Reduced shear viscosity vs reduced shear rate for PAN-A in DMF, DMF+L, DMF+Z and DMF+A.	176
Figure 5.5b	Reduced shear viscosity vs reduced shear rate for PAN-B in DMF, DMF+L and DMF+A.	177
Figure 5.5c	Reduced shear viscosity vs reduced shear rate for PAN-C in DMF, DMF+L and DMF+A	177
Figure 5.6	Ternary phase diagram for PAN-B (P) in solvents (S) DMF, DMF+L, DMF+Z and DMF+A in contact with non-solvent (NS) water.	178
Figure 5.7	Ternary phase diagram for PAN-C (P) in solvents (S) DMF, DMF+L, DMF+Z and DMF+A in contact with non-solvent (NS) water.	179
Figure 5.8a	Predicted curves for the water sensitivity of PAN-A solutions as a function of polymer volume fraction with and without salt additives.	181
Figure 5.8b	Predicted curves for the water sensitivity of PAN-B solutions as a function of polymer volume fraction with and without salt additives.	181
Figure 5.8c	Predicted curves for the water sensitivity of PAN-C solutions as a function of polymer volume fraction with and without salt additives.	182
Figure 5.9a	Pore size distribution in isopropanol of PAN-A, PAN-A-L, PAN-A-Z and PAN-A-A 13% solutions cast on polyester	185

	support	
Figure 5.9b	Pore size distribution measured by isopropanol –air displacement tests of PAN-B, PAN-B-L and PAN-B-A membranes (supportless) cast from 7% polymer solutions	185
Figure 5.9c	Pore size distribution measured by isopropanol –air displacement tests of PAN-C, PAN-C-L and PAN-C-A membranes (supportless) cast from 7% polymer solutions	186
Figure 5.10	Water flux (lmh) data at 70kPa and 30°C for membranes cast from 7 % PAN- A, 15% PAN-A 7% PAN- B and 7% PAN-C solutions with DMF, DMF-Z, DMF-L and DMF-A solvents	187
Figure 5.11a-g	Cross-sectional views of PAN-B and PAN-C membranes with and without additives (a,b) 7% PAN-B and PAN-C from neat DMF (c,d,e) 7% PAN-B and PAN-C from DMF-L (f,g) 5% PAN-B from DMF-Z.	190
Figure 5.12a-h	Cross-sectional views of PAN-1 membranes cast from neat DMF at (a,b) 13% and (c,d) 17% solutions. Views (e,f) 13% and (g,h) 17% show the analogous views for PAN-1 cast from DMF-Z.	197

## List of Tables

<b>Chapter 1</b>		<b>Page No</b>
Table 1.1	Summary of previous IR studies demonstrating complexation of DMF with various salts.	13
Table 1.2	Reported proton-NMR shifts of DMF-Lewis acid complexes in methylene chloride	14
Table 1.3	Summary of previous NMR studies demonstrating complexation of DMF with various salts.	15
Table 1.4	Summary of previous Raman spectrometry studies demonstrating complexation of DMF with various salts.	17
Table 1.5	Solubilities of inorganic halides and their solvates formed with DMF	19
Table 1.6	Summary of previous IR studies demonstrating complexation of organonitriles with various salts.	24
Table 1.7	Summary of previous IR studies demonstrating complexation of PAN+DMF+salts.	27
Table 1.8	Summary of the experiments performed on dilute solutions of PAN.	32
<b>Chapter 2</b>		
Table 2.1	Typical proportions of the redox-initiator system used for preparation of the polymer of the higher molecular weight.	57
Table 2.2	Wt % elemental composition of the three acrylonitrile homopolymers and the copolymer of acrylonitrile with acrylamide.	59
Table 2.3	Spectral band (FTIR) assignment for PAN homopolymers: PAN-A, B and C.	64
Table 2.4	Spectral band (FTIR) assignment for the Polyacrylonitrile and acrylamide (88:12) copolymer PAN-1.	65
Table 2.5	Proton NMR peak assignment for the homopolymers PAN-A,	65

	B and C.	
Table 2.6	Proton NMR peak assignment for the Polyacrylonitrile and acrylamide (88:12) copolymer.	66
Table 2.7	The intrinsic viscosity and molecular weight calculated using the Mark-Houwink equation.	66
<b>Chapter 3</b>		
Table 3.1	The effect of salt addition on the >C=O stretching, OC-N stretching and O-C-N bending frequencies of DMF	77
Table 3.2	The ionic radii of various cations	79
Table 3.3	The effect of DMF on the three polymers focussing mainly on >C=O stretching, OC-N stretching and O-C-N bending frequencies of DMF and -C≡N stretching of PAN.	81
Table 3.4	IR frequencies (cm <sup>-1</sup> ) for >C=O stretching, OC-N stretching and O-C-N bending of DMF and -C≡N stretching of the polymer in the PAN-A+salt+DMF system.	98
Table 3.5	IR frequencies (cm <sup>-1</sup> ) for >C=O stretching, OC-N stretching and O-C-N bending of DMF and -C≡N stretching of the polymer in the PAN-B + salt + DMF system.	99
Table 3.6	IR frequencies (cm <sup>-1</sup> ) for >C=O stretching, OC-N stretching and O-C-N bending of DMF and -C≡N stretching of the polymer in the PAN-C + salt + DMF system.	99
Table 3.7	One point intrinsic viscosity estimates by three different methods at a polymer concentration of 0.2 g/dl	112
Table 3.8	The intrinsic viscosities measured at 25°C and the molecular weight values calculated using reported Mark Houwink constants ( $K' = 3.17 \times 10^{-4}$ dl/g; $a = 0.75$ ).	114
Table 3.9	The Mark-Houwink constants at 25°C for the four solvents i.e. neat DMF, DMF+LiCl, DMF+ZnCl <sub>2</sub> , DMF+AlCl <sub>3</sub> .	119

#### Chapter 4

Table 4.1	Parameter $a$ and $b$ calculated by fitting eqn (4.1) to experimental lcp data.	133
Table 4.2	Summary of observations for cross-sectional SEM views (Figures 4.5a-h) of PAN-A cast from 7-17% polymer solutions in neat DMF.	141
Table 4.3	Summary of observations for cross-sectional SEM views (Figures 4.6a-g) of PAN-A-Z cast from 7-17% polymer solutions in DMF+ZnCl <sub>2</sub> .	145
Table 4.4	Summary of observations for cross-sectional SEM views (Figures 4.6a-g) of PAN-A cast from 11% polymer solutions in various DMF+salt combined solvents.	148
Table 4.5	Spiral wound module performance for bacteria removal. Operating conditions: ambient temperature, 10 <sup>9</sup> Ecoli counts/ml in feed, 70kPa.	161
<b>Chapter 5</b>		
Table 5.1	Summary of lcp equation (4.1) parameters obtained by regression analysis of experimental cloud point data.	180
Table 5.1	Average bubble point (kg/cm <sup>2</sup> ) in water –air displacement tests for membranes cast from various PAN materials and salt additive	184
Table 5.2	Average bubble point (kg/cm-1 <sup>2</sup> ) in isopropanol –air displacement tests for membranes cast from various PAN materials and salt additives	184
Table 5.3	Water permeability, air-water bubble point and BSA rejection at 70kPa - 30°C / 0.1 % BSA concentration in stirred cell for PAN-B membranes.	188
Table 5.4	Water permeability, air-water bubble point and BSA rejection at 70kPa – 30°C / 0.1 % BSA concentration in stirred cell for PAN-A membranes.	189
Table 5.5	Summary of observations for the cross-sectional views of PAN-B and PAN-C membrane cross-sectional views in Figure 5.11.	193

## List of Symbols

$C$	Solute concentration (mg/ml)
$R$	Observed Solute rejection
$J$	Permeate flux ( $l\ m^{-2}\ h^{-1}$ )
$LR$	Log Reduction
$r$	End-to-end chain distance ( $\text{\AA}$ )
$A$	Membrane area ( $cm^2$ )
$c^*$	Critical concentration
$\sigma'$	Interfacial tension ( $dynes\ cm^{-1}$ )
$\eta$	Intrinsic viscosity [eta] (dl/g)
$k'$	Huggins paramter
$\phi$	Universal constant (eqn 3.1)
$\alpha$	Chain expansion factor (eqn 3.1)
$a$	Exponent in the Mark Houwink equation
$K'$	Exponent in the Mark Houwink equation
$\zeta$	Frictional Coefficient
$\beta$	Beuche parameter [ $c(\eta)$ ],
$\eta_0$	Zero shear rate viscosity
$\rho$	Density ( $g\ cm^{-3}$ )
$k$	Boltzmann's constant
$\gamma$	Shear rate

### *Subscripts*

$f$	Feed
$p$	Permeate
$r$	Retentate
$sp$	specific viscosity
$M$	Martins constant
$a$	activation energy ( $E_a$ )

## Abbreviations

PAN	Poly(acrylonitrile)
DMF	N, N Dimethyl Formamide
BSA	Bovine serum albumin
PEG	Poly(ethylene)glycol
DMSO-d <sub>6</sub>	Deuterated Dimethylsulfoxide
SEM	Scanning Electron Microscopy
FTIR	Fourier Transform Infrared Spectroscopy
PEI	Polyetherimide
PSF	Polysulfone
CA	Cellulose acetate
PES	Polyether sulfone
LiCl	Lithium Chloride
ZnCl <sub>2</sub>	Zinc Chloride
AlCl <sub>3</sub>	Aluminium Chloride

## Abstract

This thesis entitled "**Phase Inversion Casting of Poly(acrylonitrile) Based Membranes**".

The performance of ultrafiltration membranes is mainly defined by flux and rejection properties, which are affected by membrane morphology. Control of membrane morphology is critical for success in some applications (electronics, water purification) that require high flux coupled with extremely high rejections (99.999+%) for contaminants such as virus or bacteria. Based on previous empirical studies, we found that addition of  $ZnCl_2$  to a casting solution of poly(acrylonitrile) (PAN) in N,N dimethyl formamide (DMF) results in membranes with significantly less large pores/defects and consequently higher rejection for *E. coli*. However, the role of the  $ZnCl_2$  additive was not clearly identified. This thesis aims at a better understanding of the formation of PAN microporous membranes cast from solutions in DMF plus various metal chlorides. The work focuses on the effect of **PAN molecular weight** and that of various **metal chloride additives** ( $LiCl$ ,  $ZnCl_2$  and  $AlCl_3$ ) on the solution and separation properties of the membranes formed. The approach taken to improve our understanding of the basic issues involved can be summarized as:

1. Spectroscopic studies to describe the interaction between salt, solvent and polymer
2. Measurement of solution properties and correlation with spectroscopic studies
3. Detailed description of membrane morphology and correlation with the relevant solution properties

### *Experimental techniques:*

Three grades of PAN were used. PAN-A is a commercially available polymer which was purified and spectroscopically analyzed to confirm its structure as principally ( $-CH_2-CH(CN)-$ ). The molecular weight (MW) estimated from the intrinsic viscosity  $[\eta]$  and reported Mark-Houwink constants is  $\sim 50k$ . Two higher molecular weight grades of PAN were synthesized and purified in the laboratory; these are designated as



PAN-B and PAN-C. The MW of PAN-B was estimated to be ~168k while that of PAN-C was ~250k. Since, the commercial PAN-A may also contain a small degree of hydrolyzed groups, for comparison, a PAN (acrylamide: acrylonitrile) (12:88) copolymer was also synthesized. This copolymer was used in limited work- the focus of the thesis remains on the three PAN grades described above.

Both dilute and concentrated solutions in DMF were made with the three PAN polymers in the presence of mono-, bi -and trivalent inorganic additives: LiCl, ZnCl<sub>2</sub> and AlCl<sub>3</sub>. The concentration of each additive in DMF was standardized at a constant ionic strength (0.834 M). The notations used for both the solutions as well as the membranes cast from these are in the format: PAN-x-y where: x represents the PAN grade ie. PAN-A, -B or -C , and y represents the additive ie. either blank (DMF only), L = LiCl, Z = ZnCl<sub>2</sub> , A = AlCl<sub>3</sub> . Depending on the context, this same nomenclature denotes either the solution type or the corresponding membrane formed from this solution.

Solution viscosities were measured in the dilute polymer concentration range (0.1-0.3%) at 25-45°C. Solution viscosities were also measured at 30°C in a cone and plate viscometer at the higher concentrations, c, more typical of casting solutions. These data were used to estimate the shear thinning indices and also the dependence of the solution viscosity on the coil overlap parameter ( $\beta = [\eta] c$ ). Cloud point measurements for the various PAN-water-DMF+salt systems were made at low PAN concentrations and extrapolated to higher concentrations using a linearized ternary phase boundary equation.

Membrane characteristics were principally measured by water flux, solute rejection, pore size distribution by bubble point measurements in water and iso-propanol, and by scanning electron microscopy (SEM).

## *Results and Discussion*

**I. Fourier-transform infra-red (FT-IR) and dilute solution rheology** were used to study interactions between the various salts, DMF and PAN. FT-IR studies were done for each salt additive, first in the combined solvent i.e. DMF + salt. These salt + solvent combinations are denoted DMF-L, -Z or -A for the 3 chloride additives. FT-IR spectra measured with 3-7 % PAN solutions in the various solvents show that the salts interact strongly with DMF and also have weaker effects on PAN.

The  $>C=O$  stretching frequency observed in pure DMF remained essentially unchanged in both DMF-L and DMF-A, whereas a red shift was observed in case of DMF-Z. This observation can be correlated with the electronic cloud density around these cations. The energy involved in complexation of the electronegative carbonyl O of DMF with a cation is the highest for  $Al^{3+} > Li^+ > Zn^{2+}$ . Both anion ( $Cl^-$ ) and cation affect salt interaction with the O-CN group. Red shifts (following the trend of  $Al^{3+} > Zn^{2+} > Li^+$ ) observed in the OC-N stretching frequency can be attributed to the increasing electron cloud density of  $Cl^-$  near slightly electropositive nitrogen (compared to oxygen).

In the competition between the -OCN group of DMF and the -CN group of PAN for forming a complex with the salt, DMF is clearly the preferred interaction partner. The simultaneous presence of both salt and PAN gives rise to various new frequencies for both the  $>C=O$  and OC-N stretching frequencies of DMF. Significant differences are seen between the various DMF-PAN-salt ternary solutions in terms of the O-CN and particularly the  $>C=O$  stretch in DMF. Comparing the frequency shifts in these ternary systems with the binary PAN-DMF systems indicates that the nitrile group of PAN is weakly affected by the presence of the salt.

The intrinsic viscosities for PAN-A are higher in DMF+salt solutions compared to those in neat DMF. The  $[\eta]$  values for PAN-B are essentially unchanged with the salt while those for the highest MW grade, PAN-C decrease with salt addition. The calculated Mark-Houwink exponents indicate that the general effect of the salt is to decrease the

PAN chain expansion. The increase in  $[\eta]$  for the lower MW PAN-A may be attributed to interchain bridging promoted by the salts. Plotting the viscosity activation energies,  $E_a$ , against the coil overlap parameter,  $\beta$ , further supports these conclusions.

**II. Rheological, phase-boundary and membrane properties** of various DMF+salt solutions based on the lower MW commercial product PAN-A were specifically studied. Above the critical concentration entanglement point, the viscosity of the salt containing solutions increases more rapidly than that of neat PAN/DMF solution. The presence of additives in the dope solution clearly alters the ternary phase boundary. Cloudpoint measurements show that PAN-A-Z tolerates only a small amount of water before precipitation while PAN-A-L tolerates more water than solutions of PAN in DMF alone.

SEM studies of the membrane structure show PAN-A, PAN-A-A and PAN-A-Z with large macrovoids in the underlying asymmetric structure; while these macrovoids are considerably reduced for PAN-A-L. This is consistent with the ternary cloud point data, which imply that the skin layer in PAN-A-Z and PAN-A would form rapidly with the exchange of only a small amount of water. The skin layer in PAN-A-Z membranes shows a fused nodular surface with a well-defined transition layer between it and the macroporous substructure. In the case of PAN-A-L, precipitation would occur only after a considerable amount of DMF : water exchange had already taken place.

Ultrafiltration studies were done with various solutes: polyethylene glycol, lysozyme, (BSA) albumin, and casein, in a stirred cell configuration. While small differences are seen in the rejection for various solutes (BSA, lysozyme, PEG-9000), PAN-A-Z and PAN-A-A have fewer large pores / defects and consequently higher rejection for bacteria. This suppression of surface defects correlates with the higher solution viscosity attributed to polymer chain bridging. The relatively high flux is due to retaining the macrovoid-containing substructure; this can be attributed to the low water tolerance of the casting solutions. Pan-A-Z has 1000x higher bacterial reduction capability and ~80% of the water permeability of the corresponding membrane from DMF alone.

**III. Rheological, phase-boundary and membrane properties** of various salt containing solutions based on the **higher MW grades PAN-B and PAN-C**, were compared with those seen for PAN-A. As the PAN MW increases, interchain entanglements become significant. Concentrated solution viscosities increase sharply with the increase in PAN MW; this effect is the most pronounced with  $\text{ZnCl}_2$ . By contrast, solution viscosities decrease with  $\text{LiCl}$  and  $\text{AlCl}_3$  additives. PAN-A-DMF solutions show more shear thinning than solutions containing salts. For PAN-C we see the opposite trend and PAN-B shows similar power-law indices for DMF, DMF-L and DMF-A solvent systems. Low-shear viscosities measured as a function of polymer concentration in the various solvents show a good correlation with the coil overlap parameter and that  $\text{ZnCl}_2$  is the most effective additive for increasing solution viscosity in the concentrated solution range.

Cloud point studies with PAN-B show that all the salt containing solutions tolerate less water than the solution in DMF only; this trend can be expressed as  $Z < L < A < \text{neat DMF}$ . As the PAN MW increases, the measured bubble point (at a given PAN concentration) also increases (i.e. the pore radii decreases) and the water flux decreases. SEM of PAN-B cast without any additive shows a microporous sublayer full of macrovoids while membranes with PAN-B+ salt additives show a collapsed structure. The collapsed substructure can be attributed to the low polymer concentrations attainable in the casting dope and also from the lower solution viscosity with  $\text{LiCl}$  and  $\text{AlCl}_3$ . The cloud point curves for the highest MW grade, PAN-C, are relatively unaffected by the salt additives. SEM of the PAN-C membranes shows an absence of asymmetric skin formation and a collapsed sub-structure.

# Chapter I

## INTRODUCTION

Fluid separation membranes have been developed considerably since 1970 when the first asymmetric or “skinned” high-permeability Reverse Osmosis (RO) membrane was made by Sourirajan [1970]. RO and ultrafiltration (UF) processes have now become well established separation processes. The performance of ultra- and micro- filtration membranes is mainly defined by flux and rejection properties. For a given polymer, these properties are determined by the membrane morphology.

In many UF processes, (cheese whey, biological recovery), the desired product stream contains larger solutes (e.g. proteins) that do not permeate the membrane. Such processes require the membrane to exhibit high flux and fractionation capability with a moderately high rejection (95-99%) for the larger solutes. By contrast, other applications (water purification, electronics etc.) require high flux coupled with extremely high rejections (99.999+%) for contaminants such as virus or bacteria. Control of membrane morphology is critical for success in such applications. This thesis examines the effect of various membrane fabrication parameters on the resulting morphology and performance of polyacrylonitrile (PAN) flat-sheet membranes intended for water purification.

The morphology of UF membranes prepared by phase-inversion of a polymer solution can be affected markedly by the choice of organic or inorganic additives in the solution. This chapter summarizes relevant background and literature on such additives in polymer solutions and their effect on the separation properties of the membrane that is formed.

### **Ultrafiltration (UF) : Introduction And Terminology :**

In UF, macrosolutes are separated from microsolute. Solute in the range of 10 to 1000Å (or 500 to 500,000 daltons) are separated by this process. The driving force for transport across an UF membrane is a pressure difference across the membrane. Ultrafiltration is considered to be a size-exclusion based, pressure driven process. UF is mainly used for clarification, concentration and fractionation of macromolecules

[Kulkarni et al, 1992a]. Large scale applications of UF are in industries such as wastewater/effluent treatment, food and dairy [Cheryan, 1985], downstream processing, biotechnology, paper and pulp, electronics, medical and therapeutics etc. [Cheryan, et al 1986, Kulkarni et al, 1992b].

The relevant terms common to UF processes are defined below:

The volumetric flux through the membrane,  $J_v$ , is defined as the permeate volume,  $V$ , per unit area,  $A$ , per unit time,  $t$ :

$$J_v = \frac{V}{A \cdot t} \quad (1.1)$$

Ultrafiltration membranes separate macromolecular solutes from a mixture of solutes of different sizes. The observed solute rejection,  $R$ , is defined as:

$$R = 1 - \frac{C_p}{C_r} \quad (1.2)$$

where,  $C_p$  and  $C_r$  is the solute concentration in the permeate and retentate respectively.

UF membranes are generally characterized in terms of their Molecular Weight Cut-Off (MWCO) value which is defined as the smallest molecular weight (MW) of the species for which the membrane has more than 90% rejection. The typical MWCO values of UF membranes range between 0.5-500 kDa (kDa =  $10^3$  daltons).

The use of ultrafiltration (UF) membranes for purification of water is an established process [ref]. UF processing is sometimes preferred to other standard techniques because it can reduce both small contaminants such virus as or humic acid in addition to larger species such as bacteria or spores. Typically, log reduction (L.R.) is used to quantify the bacterial rejection ability of a UF membrane. Log reduction is defined as:

$$L.R. = \log_{10} \left( \frac{C_r}{C_p} \right) = \log_{10} \left( \frac{1}{1-R} \right) \quad (1.3)$$

There is a need for high bacterial rejection rates, especially when a UF membrane is to be used in stand-alone membrane water treatment.

The performance of the membrane is defined mainly by its flux and rejection properties, which, in turn, are governed by the membrane morphology. Simply decreasing the membrane total thickness will increase the membrane flux; however, this is limited by mechanical stability constraints. In order to overcome this limitation, asymmetric membranes were developed in which a thin separating layer is supported by a mechanically robust porous layer [Sourirajan, 1970]. Phase inversion methods are a well-established technique for preparation of asymmetric membranes. During the phase inversion process, a homogeneous solution is converted into two continuous phases, one which is rich in the membrane material and forms the structure (e.g. polymer) and a second which is rich in the pore forming material (e.g. liquid solvent). Phase inversion refers to the polymer going from a discontinuous phase in solution to a continuous membrane structure.

#### **Motivation for thesis work: PAN UF membranes for water purification**

Based on some empirical studies, we found that the addition of a divalent salt,  $ZnCl_2$ , to a casting solution of poly(acrylonitrile) in *N,N* dimethyl formamide (DMF) results in PAN membranes with improved water purification capability in comparison to the membrane prepared without the additive. The mode pore size of the improved membrane was similar to that cast from neat DMF; however, the modified membranes had significantly less number of large pores/defects of size greater than 0.3  $\mu m$ . Consequently, these membranes exhibited higher rejection for *E. coli*. This work resulted in the form of a patent [Kulkarni et al, 1996] and a water treatment device incorporating these membranes has been developed.

Further work is necessary to understand the role of the salt additive in the casting solution. It has still not been possible to clearly delineate basic thermodynamic effects relating to the polymer solution from the kinetics of phase separation. The phase

inversion of poly(acrylonitrile) (PAN) solutions in the presence of various inorganic additives in a non-solvent such as water is not well understood. Also, the literature on the subsequent effect of these additives on the pore size distribution of the membranes cast therefrom is limited. This thesis addresses some of these issues.

### **Review of relevant literature**

The thesis focuses on PAN UF membranes cast from solutions in DMF plus various metal chlorides. The literature related to complexation of various inorganic additives with DMF and PAN as well as the implications for membrane morphology is subdivided as follows.

- 1.1 Review of current commercially available PAN membranes.
- 1.2 Characterization of interactions of salts + DMF
- 1.3 Characterization of interactions of PAN + DMF
- 1.4 Characterization of interactions of salts with nitrile containing model compounds for PAN
- 1.5 Characterization of interactions of salts + dissolved PAN
- 1.6 Characterization of interactions of salts + other dissolved polymers
- 1.7 Solution property characterization
- 1.8 Morphology control of PAN membranes
- 1.9 Morphology control of other polymeric membranes

### **1.1 Commercially available PAN membranes**

Polyacrylonitrile (PAN) is a commercially used membrane material due to its good chemical and physical stability combined with low cost. Today PAN-based UF membranes are commercially available and used in several applications such as water treatment, concentration of whey or protein, concentration of oil/water mixtures, etc. In these applications the membrane appears to demonstrate high stability against chemical cleaning agents and resistant to sodium hypochlorite, citric acid and weak alkaline solutions [Scharnagla et al 2001]. PAN based membranes do not degrade under biological attack as is sometimes found for cellulosic membranes. Polysulfone (PSF)



based membranes are preferred to PAN in many applications because of the higher temperature and mechanical strength of PSF. However, the low cost and biological resistance of PAN makes it a potentially interesting material for a rural water purification membrane system. A summary of the information from various PAN membrane vendors is presented in Appendix I-1.

## **1.2 Characterization of interactions of salts with DMF**

Several researchers have used infra-red spectroscopy (IR) to characterize the interaction of DMF with salt additives. Other characterization methods used have been NMR, Raman spectroscopy and other miscellaneous techniques.

### ***1.2.1 IR studies***

Several IR studies have found that metal halides interact with DMF primarily through a complex formation between the carbonyl O of DMF and the cation. The details of these studies are summarized below.

The most relevant study is that of Waghorne and Rubalcava [1982] who studied the interactions of different metal ions with DMAc and fully deuterated DMF by IR spectroscopy. The metal ions examined were classified in two categories: (i) those containing d-electrons ( $Zn^{2+}$ ,  $Cd^{2+}$ ) and (ii) those with closed shell electrons ( $Li^+$ ,  $Ba^{2+}$ ,  $Mg^{2+}$ ,  $Al^{3+}$ ). They observed that the carbonyl stretching frequency at  $1635\text{cm}^{-1}$  for deuterated DMF changed to 1642, 1632 and  $1644\text{ cm}^{-1}$  after the addition of  $Li^+$ ,  $Zn^{2+}$  and  $Al^{3+}$  salts respectively. The O-CN stretching frequency was also changed from  $620\text{cm}^{-1}$  to 630, 645 and  $685\text{ cm}^{-1}$  for  $Li^+$ ,  $Zn^{2+}$  and  $Al^{3+}$  salts, respectively. They also observed that anions do not influence the positions of the absorption bands of the complexed amide, concluding that the changes in the carbonyl stretching frequency arise directly from cation to amide interactions. The change in carbonyl and O-CN stretching frequencies was correlated with the cation electrostatic potential (calculated from their ionic radii and charge). A linear relationship was found between this electrostatic potential and the carbonyl frequency for cations containing d-electrons. For cations containing closed shell electrons, the carbonyl frequency increases at lower potentials and then levels off.

Kim et al [1985] studied several metal complexes of DMF ( $\text{MX}_2 \cdot n\text{DMF} \cdot m\text{H}_2\text{O}$ ;  $n = 1-2$ ;  $m = 0 - 2$ ) where M was a transition metal (Mn, Co, Zn, Ni, Cu) and X was a halide (Cl, Br) by IR spectroscopy. He showed that the coordination of DMF takes place through the carbonyl 'O' atom. The anions in the inner coordination sphere serve as monodentate ligands except for  $\text{CuBr}_2 \cdot \text{DMF}$  in which Br serves as a bridge.

Yilmaz et al [1997] further studied the preparation, characterization and thermal reactivity of N,N-dimethylformamide complexes of the chloride salts of these same transition metal chlorides. The coordination adducts of  $\text{MnCl}_2$ ,  $\text{FeCl}_3$ ,  $\text{CoCl}_2$ ,  $\text{NiCl}_2$  and  $\text{CuCl}_2$  with DMF were isolated and characterized by elemental analysis, magnetic moments, UV-visible spectroscopy, IR spectroscopy and thermal analytical techniques. The bonding of DMF through its oxygen to these transition metals was indicated by a shift of the CO stretching vibration to lower frequency [similar to the results for Zn reported by Waghorne and Rubalcava, 1982]

Jungbauer et al [1964] studied the -N-C=O bending vibration in complexes of DMF with metal halides. The peak at  $657 \text{ cm}^{-1}$  is attributed to the -N-C=O bending vibration. This absorption shifts to higher frequencies in complexes with metal halides: Specifically, the peak at  $657 \text{ cm}^{-1}$  shifts to  $688 \text{ cm}^{-1}$  in case of complexation with Zinc halide.

Lassigne and Baine [1971] studied solvation of  $\text{LiClO}_4$  by DMF using IR spectroscopy. They observed two new bands at  $365$  and  $420 \text{ cm}^{-1}$  for  $\text{DMF-LiClO}_4$  solution (which were absent in pure DMF). These were attributed to specific cation - solvent interactions through the electronegative atoms, N and O of DMF. The carbonyl band of DMF in dioxane (dioxane does not interact with DMF nor  $\text{LiClO}_4$ ) appears at  $1686 \text{ cm}^{-1}$ . After addition of  $\text{LiClO}_4$  in DMF, another band is seen at  $1670 \text{ cm}^{-1}$ , the intensity of which increased with increase in concentration of  $\text{LiClO}_4$ . These results conclude that bonding between  $\text{Li}^+$  ion and DMF takes place through carbonyl oxygen, as resonance in the DMF molecule causes oxygen to be the primary negative charge site.

Yang et al [1996] performed further FT-IR studies on the complexation of lithium ions with DMF / PAN. The absorption peak at  $1668 \text{ cm}^{-1}$  which is the carbonyl peak of DMF becomes much wider from  $1580-1690 \text{ cm}^{-1}$  after addition of  $\text{LiClO}_4$ . The widening is attributed to two overlapping peaks: one at  $1668 \text{ cm}^{-1}$  attributed to the

unbonded carbonyl of DMF and another peak at  $1640\text{cm}^{-1}$  attributed to the complexed carbonyl.

Chai and Samalenko [1971] studied complexation of  $\text{AlCl}_3$  with DMF by IR spectroscopy. The results are in accordance with formation of 1:1 complexes as  $\text{AlCl}_3 : 6\text{DMF}$  and  $\text{Al}(\text{NO}_3)_3 : 5\text{DMF}$  which were isolated as crystalline solids. IR spectra revealed both free and coordinated (through oxygen atom to above compounds) DMF molecules.

The relevant information for this thesis gleaned from the IR studies described above is summarized in Table 1.1.

### *1.2.2 NMR studies*

The NMR spectrum of DMF distinguishes two different kinds of methyl protons (cis and trans to the carbonyl oxygen). This distinction is attributed to the restricted rotation of the carbon-nitrogen bond which has a partial double bond character. The proton resonance spectrum of DMF and boron trichloride) showing two different methyl sets was first measured by Gerrard et al [1960].

Kuhn et al [1965] studied the complexation of DMF and various Lewis acids ( $\text{ZnCl}_2$ ,  $\text{AlCl}_3$ ,  $\text{BF}_5$ ,  $\text{BCl}_3$ , etc ) in methylene chloride using H-NMR. The NMR spectra of the complexes show the two sets of methyl protons of DMF in all the DMF-Lewis acid complexes. If the Lewis acids were to coordinate with DMF through the nitrogen atom, the partial double bond character of the carbon nitrogen bond would be destroyed and the difference between the two methyl groups would disappear. Since the NMR spectra continues to show two separate peaks for the two different sets of methyl groups, as shown in Table 1.2, it would appear that the double bond character of the carbon nitrogen bond is retained and the coordination of the Lewis acid is through the carbonyl oxygen.

Table 1.1: Summary of previous IR studies demonstrating complexation of DMF with various salts.

Additive to DMF	Interaction identified	Change in spectra		Comments	Reference
		C=O stretching $\text{cm}^{-1}$	OCN bending $\text{cm}^{-1}$		
Li salts	Cation complexes with amide C=O	1635 → 1642	620 → 630	Anions do not complex deuterated DMF	Waghorne & Rubalcava [1982]
Zn salts		1635 → 1632	620 → 645		
Al salts		1635 → 1644	620 → 685		
Zn salts	NC = O bending		657 → 688	Associated with -CH	Jungbauer [1964]
LiClO <sub>4</sub>	Li complex with electronegative carbonyl O	1686 → 1670			Lassigne & Baine [1971]
		New pks (365 and 420)			
LiClO <sub>4</sub>		1668 → 1640 (b) *		Li <sup>+</sup> bonds with C=O as well as C≡N in PAN	Yang [1996]
		1668 → (ub)*			

\*(b) - bonded \*(ub)- unbonded

**Table 1.2:** Reported proton-NMR shifts of DMF-Lewis acid complexes in methylene chloride [Kuhn et al, 1965].

Complex	Cis Methyl*	Trans Methyl*	Aldehyde@
DMF	75	80	475
ZnCl <sub>2</sub> .2 DMF	89	97	488
AlCl <sub>3</sub> .1 DMF	100	107	489

\*The shifts are in cps downfield from external acetonitrile reference.

The cis and trans values are reported in reference to the aldehyde proton

@ The aldehyde shifts are in cps downfield from internal TMS standard.

Alexander [1982]) performed NMR ( $Zn^{67}$ ) study of zinc ions in water and in some non-aqueous solvents (MeOH, DMF and some binary mixtures). Anhydrous  $Zn(NO_3)_2$  solution in DMF and MeOH shows an upfield, concentration-independent chemical shift at -27 and -19 ppm respectively in comparison with the aqueous standard solution. Addition of DMF or methanol to an aqueous solution of Zn salt results in a diamagnetic shift but for the addition of acetonitrile, a paramagnetic shift is observed. In all these cases the signal was broadened, e.g.: for  $ZnCl_2$  solutions; the line width increased from approx. 40 to approx. 600 Hz in going from water to 35% aqueous methanol.

Dunn and Samson [1969] found chemical shifts for DMF :  $ZnCl_2$  (2:1) to be +13 Hz for CO-H and +14, +17 Hz for N-CH<sub>3</sub>, indicating complexation of the salt with DMA through the carbonyl oxygen. Yasuhiro et al [1998] studied the formation of  $Al^{3+}$  chloro-complexes with DMF by spectrophotometry, calorimetry and  $Al^{27}$  NMR spectroscopy. It was claimed that the data can be explained in terms of formation of mono- and dichloro-complexes of Al in DMF entropies.

The relevant information for this thesis gleaned from the NMR studies described above is summarized in Table 1.3.

**Table 1.3:** Summary of previous NMR studies demonstrating complexation of DMF with various salts.

Additive to DMF	Interaction identified	Comments	Reference
Boron salts	C=O	Two different sets of methyl protons observed	Gerrard & Wallis [1960]
Zn salts	C = O	H-NMR Shifts observed DMF →75,80 ppm	Kuhn [1965]
Al salts		ZnCl <sub>2</sub> →89,97 ppm AlCl <sub>3</sub> →100,107 ppm	
Zn salts	C=O	-27 ppm shift seen in Zn-NMR diamagnetic shifts also observed	Alexander [1982]

### 1.2.3 Raman spectroscopy

Kabisch et al [1984] studied the complex formation and solvation of LiBr and ZnBr<sub>2</sub> in DMF by Raman spectroscopy. They found a shift to higher frequency of the OC-N bending vibration in DMF from 660cm<sup>-1</sup> to 686 cm<sup>-1</sup> on addition of Zn<sup>+</sup> and to 671cm<sup>-1</sup> on addition of Li<sup>+</sup> ions. A continuing unshifted 660 cm<sup>-1</sup> band reflects the presence of a significant fraction of C=O group not coordinated to any of the cations. They also observed that the fraction of DMF solvating Li<sup>+</sup> ions is larger than for Zn<sup>2+</sup> ions.

Alia et al [2000] used FT-Raman spectroscopy to investigate lithium trifluoromethanesulfonate (triflate) solutions in three dipolar aprotic, electron donor solvents, namely acetone, DMF, and DMSO. New bands in the Raman spectra which are characteristics of the solvating molecules, allowed calculation of the solvation numbers of Li<sup>+</sup> at different molar concentrations (1-3.5 mol dm<sup>-3</sup>). Deconvolution of the triflate anion S-O symmetric stretching band permitted assessment of the ionic pairing.

Alia et. al [2001] further studied solutions of lithium or silver (triflate) in a mixed solvent formed by acrylonitrile (ACN) and N,N-dimethylformamide (DMF) by FT-Raman spectroscopy. The composition of the solvation sphere in both ions was calculated by measuring the effect of the salts on the nitrile CYN stretching at  $2228\text{ cm}^{-1}$  and in the NC anti-symmetric stretching of DMF at  $658\text{ cm}^{-1}$ . Relative to ACN, DMF preferentially solvates both cations. The preference is less pronounced in the case of  $\text{Ag}^+$ , Remarkably,  $\text{Li}^+$  is solvated exclusively by DMF molecules in the equimolar (ACN:DMF) mixed solvent.

Powell et al [1985] studied compounds of the form  $\text{MX}_2 : (\text{amide})_n$  where (M = Mn, Fe, Co, Ni, Cu, Cd, Hg, Pd and Pt; X = Cl, Br; amide = formamide, N-methyl formamide and N, N-dimethyl formamide; n = 1, 2 and 4) using IR and Raman spectroscopy. Complete assignments of the spectra were proposed. The majority of the complexes were found to be oxygen co-ordinated. The exceptions were  $\text{NiCl}_2(\text{NMF})_4$ ,  $\text{NiCl}_2(\text{DMF})_2$  and  $\text{CuCl}_2(\text{DMF})_2$  which showed signs of both oxygen and nitrogen co-ordination.

Gurunadham et al [1982] performed an intensity study of Raman bands of dimethyl formamide (DMF) and dimethyl sulfoxide (DMSO) in solutions of different concentrations. The intensities of the Raman bands due to the C : O stretching in DMSO were obtained in the solvents  $\text{CCl}_4$ ,  $\text{H}_2\text{O}$ ,  $\text{D}_2\text{O}$  and  $\text{MeCOOH}$ . The intensities of these bands are extremely sensitive to variations in concentration. The results are interpreted in terms of strong interactions such as the formation of H bonding in these systems.

The relevant information for this thesis gleaned from the Raman spectroscopy studies described above is summarized in Table 1.4.

**Table 1.4:** Summary of previous Raman spectrometry studies demonstrating complexation of DMF with various salts.

Additive to DMF	Interaction identified	Comments	Reference
Li salts	O-C-N	660→686 cm <sup>-1</sup>	Kabisch [1984]
Zn salts		660→671 cm <sup>-1</sup>	
Li salts	Solvation by DMF	Li <sup>+</sup> ions are more solvated compared to Ag <sup>+</sup> ions	Alia [2001]
Ag salts			
MX <sub>2</sub> (amide) <sub>n</sub>	M= Mn, Fe, Co, Ni, Cu, Cd, Hg, Pd X = Cl, Br; Amide = formamide, NMF and DMF n = 1, 2 and 4	Oxygen coordination except NiCl <sub>2</sub> and CuCl <sub>2</sub> where both oxygen and nitrogen coordination is observed	Powell [1985]

#### 1.2.4 Miscellaneous characterization techniques

Striegel et al [1999] studied the polarizability and inductive effect contributions to solvent-cation binding observed in electrospray ionization mass spectrometry (ESI). ESI was used in conjunction with computer modeling to investigate binding tendencies of alkali metal cations to low molecular weight solvents. Intensities of peaks in ESI mass spectra corresponding to solvent-bound alkali metal cations were found to decrease with increasing ionic radii (Li<sup>+</sup> > Na<sup>+</sup> > K<sup>+</sup> > Cs<sup>+</sup>) in either dimethylacetamide (DMAc) or DMF. When a lithium or sodium salt was added to an equimolar mixture of DMF, DMAc, and dimethylpropionamide (DMP), the intensities of ESI mass spectra peaks decreased in the order DMP > DMAc >> DMF. These trends were attributed to a combination of at least three factors. An inductive effect from the alkyl group adjacent to the carbonyl function on each solvent contributes through-bond electron donation to stabilize the alkali metal cation attached to the carbonyl oxygen. However, the shift in the partial negative charge at the oxygen binding site with increasing n-alkyl chain length (evaluated via computer modeling), cannot fully account for the mass spectrometric data. The increasing polarizability and augmented ability to dissipate thermal energy with increasing size of the solvent molecules are postulated to



act in conjunction with the inductive effect. Further evidence of these contributions to solvent-cation binding in ESI-MS is given by the relative intensities of [solvent + Li]<sup>+</sup> peaks in mixtures containing equimolar quantities of alcohols, indicating preferential solvation of Li<sup>+</sup> in the order n-propanol > ethanol > methanol. These experiments suggest a combined role of polarizability, the inductive effect, and solvent molecular size in determining relative intensities of solvated cation peaks in ESI mass spectra of equimolar mixtures of homologous solvents.

Gallardo et al [1989] studied the enthalpies of interaction of alkali metal halides with N-Methylacetamide and DMF in water at 25°C. They found that the tertiary amide- interacts with the salt more strongly than the secondary amide.

Rode and Fussengger [1959] say that binding of single Li<sup>+</sup> ion to C=O oxygen atom increases the double bond character of C-N leading to a higher barrier of rotation. And at higher concentrations because of ion pair formation, two or more Li<sup>+</sup> ions may be situated in neighborhood of solvent molecules, leading to binding of second Li<sup>+</sup> ion to nitrogen. Therefore this tetrahedral arrangement of atoms at nitrogen atom decreases the  $\pi$  character of C-N bond and so it facilitates internal rotation. Gopal and Rastogi [1970] studied the ion-solvent interaction of some tetraalkyl ammonium and alkali metal halides in polar, hydrogen bonded, non-hydrogen bonded solvents (N-Methylacetamide, N-Methylpyrrolidone, N,N-Dimethylformamide) from viscosity data. While R<sub>4</sub>N<sup>+</sup> ions act as net structure breakers, common salts like LiCl, KI etc act as net structure promoters in N-Methylacetamide and N-Methylpyrrolidone. In DMF no structure building or breaking appears to occur in presence of electrolytes.

### ***1.2.5 Metal:DMF solvation stoichiometry***

Kazuhiko et al [1993] studied the solvation structure of divalent transition-metal ions (Mn, Fe, Co, Ni, Cu, and Zn) in N,N-dimethylformamide and N,N-dimethylacetamide by the EXAFS method. All these metal ions showed a coordination number of 6, suggesting a six-coordinate octahedral structure in DMF.

Khotsyanovskii and Telyakova [1971] studied bromide complexes in DMF. (Zn<sup>2+</sup>-Br<sup>-</sup>-DMF) potentiometrically and polarographically. Four complexes with the general compound ZnBr<sub>n</sub><sup>2-n</sup> form in the system. The anhydrous system gave ZnBr<sub>2</sub>-

2DMF, having the DMF coordinated to Zn through the carbonyl O. X-Ray diffraction proved ZnBr<sub>2</sub>.DMF to be tetrahedral.

Schneider [1963] studied DMF solvates of metal perchlorates. DMF can replace water in solvent sheets of metal ions by coordination through the carbonyl 'O' of DMF. The complex salts {M(DMF)<sub>6</sub>(ClO<sub>4</sub>)<sub>n</sub>} where (M=Cr<sup>3+</sup>, Fe<sup>3+</sup>, Al<sup>3+</sup>, Ga<sup>3+</sup>, M<sup>n3+</sup>, Zn<sup>2+</sup>) and {M(DMF)<sub>4</sub>(ClO<sub>4</sub>)<sub>2</sub>} (M = Be<sup>2+</sup>, Ca<sup>2+</sup>) were prepared by adding cooled DMF dropwise to strong aqueous solutions of metal perchlorates. Paul and Shreenathan [1965] studied the solubility and solvate formation of inorganic additives in DMF. The solubilities (g/100g solvent) of the salts in DMF at 25 °C and the solvates formed are shown in Table 1.5.

**Table 1.5:** Solubilities of inorganic halides and their solvates formed with DMF [from Paul and Shreenathan 1965].

Inorganic Halide	Solubility (g/100g solvent)	Solvate Formed
LiCl	27.53	LiCl.DMF
ZnCl <sub>2</sub>	6.32	ZnCl <sub>2</sub> .2DMF
AlCl <sub>3</sub>	3.742	AlCl <sub>3</sub> .6DMF

As the anion/cation size ratio increases, the solubility of the compound increases; the polarization of the solvent is greater as the size of the anion increases. On the basis of the donor properties of the oxygen atom in DMF, the salt-DMF complex can be represented as Figure 1.1 where, M is the metal atom and X may be Cl, Br, or NO<sub>3</sub>.

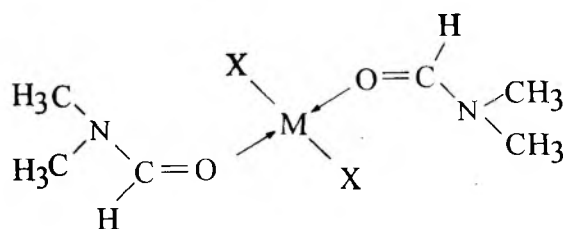


**Figure 1.1:** Proposed structure of the complex of DMF with metal salts

Tarasov et al [1982] studied the formation of solvate-separated ion pairs in dimethyl formamide solutions of aluminum trihalides. A  $Al^{27}$  NMR study of  $AlCl_3$  ( $AlBr_3$ )-DMF-MeCN solutions with and without added  $CCl_4$  showed the formation of  $[Al(DMF)_6]Cl_2^+$ ,  $[Al(DMF)_6]Cl_2^+$ , and  $[Al(DMF)_6]Br_2^+$  ion pairs with formation constants 0.46, 0.19, 0.21, respectively, in neat DMF and 2.37, 5.52, 0.91 in MeCN solutions.

### 1.3 Characterization of interactions of PAN with DMF

PAN is generally poorly soluble in many solvents except for polar solvents such as N-Methyl-2-Pyrrolidone (NMP), DMF and DMAc, DMSO, ethylene carbonate,  $\gamma$ -butyrolactone, conc.sulfuric and nitric acid, and conc. salt solutions of LiBr,  $ZnCl_2$ , NaCNs in water. Polyacrylonitrile is a polar polymer and is partly self-associated through dipole-dipole interactions at the CN groups. Solvent DMF breaks this self-association but is itself bound to the nitrile groups by dipole-dipole interactions. The difficult removal of solvent DMF from PAN spun fiber is attributed to these dipole interactions [Padhye and Karandikar, 1985]

The steric effect of solvent molecules in the dissolution of polyacrylonitrile from five different N,N-dimethylformamide derivatives was studied by Minagawa et al [1996] using Raman spectroscopy. The carbonyl band in each solvent shifted to a higher frequency when nitriles (PAN) were added. The extent of the shift was directly related to the structure and geometry of the substituent in each solvent molecule. The Raman carbonyl shift correlates directly with the intensity of the interaction between the solvent and the nitrile group.

Summarizing, Polyacrylonitrile is a polar polymer and is partly self-associated through dipole-dipole interactions at the CN groups. Solvent DMF breaks this self-association but is itself bound to the nitrile groups by dipole-dipole interactions. PAN goes into solution by forming donor-acceptor complexes with the solvent.

#### 1.4 Characterization of interactions of inorganic halides with model PAN compounds - organonitriles

Information regarding complex formation between the nitrile N and cations can be obtained from spectroscopic studies with organonitriles. These model compound studies support the more limited studies discussed in section 2.5 which measure interactions between salts and PAN.

An early infrared absorption study [Coerver and Curran, 1958] showed that addition of inorganic halides to organonitriles increased the  $-C\equiv N$  frequency and also the absorption of the nitrile group indicating the formation of a nitrogen-metal bond. In case of acetonitrile addition compounds the spectra are complicated by the presence of a second absorption peak at a slightly higher frequency than that assigned to the  $-C\equiv N$  vibration. The free nitrile peak at  $2290\text{ cm}^{-1}$  shifts to 2335, 2338, 2271 and  $2271\text{ cm}^{-1}$  in addition compounds with  $\text{BF}_3$ ,  $\text{BCl}_3$ ,  $\text{TiCl}_4$  and  $\text{SnCl}_4$  respectively.

Hoskins et al [1991] performed an IR study of acetonitrile in aqueous inorganic salt solutions and compared it with related polyacrylonitrile solutions. The IR spectra of acetonitrile (AcN) were obtained in the (CN) stretching region for the pure liquid, in water and in aqueous salt solutions of  $\text{NaSCN}$ ,  $\text{NaI}$ ,  $\text{LiI}$ ,  $\text{CaI}_2$  and  $\text{ZnCl}_2$ . The CN absorption bands of AcN in aqueous inorganic salt solutions were very similar to those found in aqueous solutions of poly(acrylonitrile-co-vinyl acetate) containing inorganic salts. The effect of the aqueous salt solutions on the (CN) stretching absorptions at  $2270\text{ cm}^{-1}$  was divided into three types:

1. solutions containing  $\text{NaSCN}$  and  $\text{NaI}$  which cause a shift in the (CN) absorption band relative to that in pure AcN with  $= + 6\text{ cm}^{-1}$ ,
2. solutions containing  $\text{ZnCl}_2$  which give rise to two absorption bands with shifts of  $= + 6$  and  $+ 60\text{cm}^{-1}$ , and
3. those containing  $\text{LiSCN}$  and  $\text{CaI}_2$ , which also produce two absorption bands but with shifts of  $= + 6$  and  $+ 22\text{ cm}^{-1}$ .

Padhye and Karandikar [1985] measured IR spectra of the  $-C\equiv N$  stretching region for AcN in DMF / LiBr solution. In addition to the strong absorption at  $2230\text{ cm}^{-1}$  assigned to the monomer, an additional band at  $2249\text{ cm}^{-1}$  was observed in the presence

of LiBr. The latter band is absent in the spectrum of the pure DMF solution without LiBr.

Alia et al [1997] performed a detailed Fourier-transform Raman spectroscopic study of the association between acrylonitrile (propenenitrile) and cobalt and Ni ions in aqueous solution. A new  $\nu(\text{CN})$  band at  $2268 \text{ cm}^{-1}$  was attributed to cation-associated acrylonitrile, displaced by  $+32 \text{ cm}^{-1}$  from the wavenumber corresponding to the solvent (water/acrylonitrile mixt). The proposed equilibrium involves the interchange of one molecule of water and one molecule of acrylonitrile in the first solvation sphere of the cation, namely:



The association constant calculated at infinite dilution was  $0.32 \text{ mol}^{-1}$  was greater than that corresponding to the same equilibrium with nickel ions ( $0.22 \text{ mol}^{-1}$ ). This difference is explained by the higher hydration energy of the nickel ion.

Jamroz et al [1997] studied solvation of trivalent cations  $\text{Al}^{3+}$ ,  $\text{Fe}^{3+}$ , and  $\text{Cr}^{3+}$  with mixtures of water and deuterated acetonitrile over a wide concentration range. CN stretching vibrations of the  $\text{CD}_3\text{CN}$  molecules were used as probes of the structural environments. The CN band in each case is a superposition of four sub-bands, which may be attributed to the  $\text{CD}_3\text{CN}$  bonded in the first, second, and third coordination shells of the cation and to the free acetonitrile. The changes of the integral intensities of the sub-bands with the  $\text{H}_2\text{O}:\text{Me}^{3+}$  molar ratio show that water tends to dislodge acetonitrile from the coordination spheres of the cation. The composition of the first coordination sphere is determined only by the  $\text{H}_2\text{O}:\text{Me}^{3+}$  molar ratio, whereas the composition of the second and third spheres depends on the concentration of both solvents.

Farona and Bremer [1966] studied complexation of halogenopentacarbonyl-manganese with succinonitrile by IR spectroscopy. The infrared spectra of  $\text{Mn}(\text{CO})_3(\text{NCCH}_2\text{CH}_2\text{CN})\text{X}$  complexes exhibit three strong carbonyl bands. In addition to the CO bands, a CN stretching frequency is observed for the derivatives at  $2070 \text{ cm}^{-1}$  representing a decrease in the CN stretching frequency by about  $185 \text{ cm}^{-1}$  from that observed for free succinonitrile. There is no trace of any peak at or above  $2257 \text{ cm}^{-1}$  suggesting that complexation occurred via the triple bond.

Barthel et al [2000] studied the ion solvation of LiClO<sub>4</sub> and LiSCN in acetonitrile, benzonitrile, and propylene carbonate using FTIR spectroscopy in the temperature range from 5 to 45°C. New bands due to a fraction of solvent molecules in the primary solvation shell of the lithium ions were detected in the region of the CN stretching mode of the nitriles and of the CO stretching mode of propylene carbonate.

Saum (1960) found that the CN group in organonitriles affects the physical properties of nitriles in a manner indicative of polar interactions between molecules. Possible interpretations for these interactions are:

- 1 intermolecular hydrogen bonding between CN nitrogen and hydrogen on carbon alpha to the CN group.
- 2 dipole interactions between a given CN group and several nearest neighboring CN groups (i.e. random dipole-dipole interactions).
- 3 dipole pair bonding between closely associated groups.

Kiyoshi et al [1979] studied the mechanism of dissolution of PAN in concentrated aqueous solution of magnesium or calcium thiocyanate. The interaction between alkaline earth metal salts and the model aliphatic dinitriles succinonitrile (I), glutaronitrile (II), and adiponitrile (III) was studied by IR, Raman spectroscopy and potentiometry. In the presence of Mg(NO<sub>3</sub>)<sub>2</sub> or Ca(NO<sub>3</sub>)<sub>2</sub>, the IR spectra of II and of III showed a new strong band assignable to coordinated CN groups in the range 2270~2290 cm<sup>-1</sup> in addition to a normal peak for free CN groups near 2250 cm<sup>-1</sup>. When I was added to an aqueous solution of MgCl<sub>2</sub> or CaCl<sub>2</sub>, the concentration of free Mg<sup>2+</sup> or Ca<sup>2+</sup> decreased. Upon addition of I to an aqueous solution of Mg(SCN)<sub>2</sub> or Ca(SCN)<sub>2</sub>, the concentration of free thiocyanate ion decreased. Thus, Mg<sup>2+</sup> or Ca<sup>2+</sup> can form complexes with aliphatic dinitriles via their CN groups. Thiocyanate ion also can bind nitriles; however, Cl does not.

The relevant information for this thesis gleaned from the above studies on the interaction of organonitriles with salts is summarized in Table 1.6.

Table 1.6: Summary of previous IR studies demonstrating complexation of organonitriles with various salts.

Additive	Interaction identified	Comments	Reference
Inorganic halides	-C≡N	↑ in the frequency Nitrogen to metal bond formation Free nitrile → 2290 cm <sup>-1</sup> BCl <sub>3</sub> → 2335cm <sup>-1</sup> ; BF <sub>3</sub> → 2338cm <sup>-1</sup> PbCl <sub>4</sub> → 2271cm <sup>-1</sup> ; TiCl <sub>4</sub> → 2271cm <sup>-1</sup>	Coerver & Curran [1958]
NaCNS + NaI	-C≡N	+ 6 cm <sup>-1</sup> (All shifts w.r.t. pure CH <sub>3</sub> CN)	Hoskins [1991]
Zn salts		+6 and +60 cm <sup>-1</sup>	
LiCNS +CaI <sub>2</sub>		+6 and +22 cm <sup>-1</sup>	
i)CH <sub>3</sub> CH <sub>2</sub> CN+DMF ii)CH <sub>3</sub> CH <sub>2</sub> CN+DMF + LiBr	-C≡N	i) 2230 cm <sup>-1</sup> ii) additional band at 2249 cm <sup>-1</sup>	Padhye & Karandikar [1985]
Co salts + acrylonitrile + H <sub>2</sub> O	-C≡N	Cation + acrylonitrile→32 cm <sup>-1</sup> comp. Solv.water/acrylonitrile	Alia [1997]
Succinonitrile Halogen pentacarbonyl- Manganese	-C≡N	No band at 2257 cm <sup>-1</sup> (nitrile) ↓ CN stretching frequency compared to free succinonitrile: 2255→2070cm <sup>-1</sup>	Farona & Bremer [1966]

## 1.5 Characterization of interactions of inorganic halides with PAN

FT-IR studies by Wu and Liedberg [1988] on the complexation of  $\text{Cu}^+$  ions with PAN solutions found that two new bands at  $2334\text{ cm}^{-1}$  and  $2191\text{ cm}^{-1}$  appear and the original band ( $2243\text{ cm}^{-1}$ ) for  $-\text{C}\equiv\text{N}$  mode of vibration disappears after heat treatment for 5 hrs at  $200^\circ\text{C}$ . This indicated two types of complexes:

1. End-on coordination to copper ions through the nitrogen lone pair orbitals of the  $\text{C}\equiv\text{N}$  (band at  $2334\text{ cm}^{-1}$ ); and
2. Coordination of copper to nitrile group through  $\pi$  electrons ( $2191\text{ cm}^{-1}$ ).

This study suggested that Cu ion complexes with PAN reduce the inter/intrachain dipole-dipole interactions, allowing the polymer chain to become more ordered as it breaks the dipole-dipole interactions so the cluttered chains become free and get a specific order type.

Yang et al [1996] performed FT-IR studies to show that  $\text{Li}^+$  ions form a complex with the carbon and nitrogen groups of PAN in DMF solvent. Since not all of the  $\text{C}\equiv\text{N}$  bonds interact with the  $\text{Li}^+$  ion, the spectra shows both the original peak at  $2243\text{ cm}^{-1}$  plus a new signal at  $2269\text{ cm}^{-1}$  due to the interactions of  $\text{Li}^+$  ions with  $\text{C}\equiv\text{N}$ .

Similarly, Huang et al [1996] studied the mechanism of lithium ion transport in PAN based polymer electrolytes by IR, NMR and X-Ray diffraction techniques. They observed a shoulder at about  $2270\text{ cm}^{-1}$  on the high frequency side of the  $\text{C}\equiv\text{N}$  stretch mode of PAN at  $2244\text{ cm}^{-1}$ . The intensity of the shoulder increased with rising concentration of  $\text{LiClO}_4$ . PAN plasticized with ethylene carbonate and  $\text{LiClO}_4$  showed relatively high ionic conductivity at room temperature. This high ionic conductance is attributed to  $\text{Li}^+$  ions, which are coupled to the  $\text{C}=\text{N}$  groups in gelled-state PAN.

PAN can be dissolved in concentrated aqueous solutions of  $\text{ZnCl}_2$  (40-60%) and fibers can be spun from these solutions [1967, US. 3,346,685]. Bock, et al. [1966] found an interaction of the nitrile lone pair electrons with  $\text{Zn}^{2+}$ , associated with a shift to higher frequency of the nitrile stretch of  $40\text{-}60\text{ cm}^{-1}$ . This type of interaction is sufficient to suppress dipole-dipole interactions of the  $-\text{CN}$  group permitting polymer





dissolution. By contrast, stronger Lewis acids such as  $VCl_4$ ,  $AlCl_3$  are not stable in aqueous solutions.

Padhye and Karandikar [1985] studied the effect of LiBr on solvent (DMF / DMSO) removal from solution-cast PAN. They showed that by adding Li salts to the dope solution before casting films, removal of the solvent becomes easy. Based on IR results with AN/DMF/LiBr, they suggested that LiBr forms coordinate linkages with the nitrile group, thereby blocking solvent bonding. Rae et al [2000] studied the PAN/ $FeCl_3$  complexes using FTIR, XPS, x-ray diffractometry and TEM. They observed that  $FeCl_3$  is preferentially coordinated with the solvent, DMF; then the DMF-coordinated  $FeCl_3$  interacts electrostatically with the PAN to reduce the dipole-dipole moment of the nitrile groups. The resulting crystal system is consequently transformed from hexagonal to triclinic.

The Raman and IR spectra of DMF/PAN/ $LiClO_4$  were analyzed by Biying et al [1997]. The interaction between DMF and PAN, probably resulting from the dipole interaction between the O=C-N group of DMF and the nitrile group of PAN, is weak. Compared with the Raman spectra of DMF/ $LiClO_4$  system, the addition of PAN promotes ion association between  $Li^+$  ions and DMF. However, in spite of the wide range of molar ratios of DMF/PAN/ $LiClO_4$  studied, no ion association is observed between the nitrile group of PAN and the  $Li^+$  ions in the DMF/PAN/ $LiClO_4$  system.

The relevant information for this thesis gleaned from the above studies on the interaction of PAN+DMF+salts is summarized in Table 1.7.

**Table 1.7:** Summary of previous IR studies demonstrating complexation of PAN+DMF+salts.

Additive to DMF	Interaction identified	Interactions and comments	Reference
Cu salts	-C≡N	Original nitrile band at 2243 cm <sup>-1</sup> Two new bands at 2234 and 2191cm <sup>-1</sup> showing binding via  lone electron pair of C≡N and through.π electrons	Wu & Leidberg [1988]
Li salts	C=O	1668→1640 cm <sup>-1</sup> (bonded) + original 1668 (unbonded)	Yang [1996]
	-C≡N	2243→2269cm <sup>-1</sup> (bonded) + original 2243 cm <sup>-1</sup> (unbonded)	
Li salts	-C≡N	No interaction with PAN in presence of DMF	Biyang [1997]
Li salts	-C≡N	Red shift of 40-60cm <sup>-1</sup>	Bock [1966]
Fe salts	C=O	Salt complex with DMF interacts with PAN	Rae [2000]

## 1.6 PAN solution properties

### 1.6.1 PAN solution viscosity study

The viscosity of a polymer solution is a measure of the polymer-solvent interactions. The casting solution viscosity is generally considered a useful parameter in controlling the final membrane morphology. Polymer solution viscosity is generally discussed in three concentration regimes: dilute, semi-dilute and concentrated, illustrated in Figure 1.2. As the polymer concentration increases, intermolecular interactions progressively become predominant. At a critical concentration  $c^*$  the polymer molecule domains begin to overlap and entanglements develop. Concentration  $c^*$  separates the dilute and semi-dilute regimes: in dilute solutions the polymer coils are separate while in more concentrated solutions the coils overlap. In the concentrated solution region, the number of polymer coils increases further and become strongly entangled.

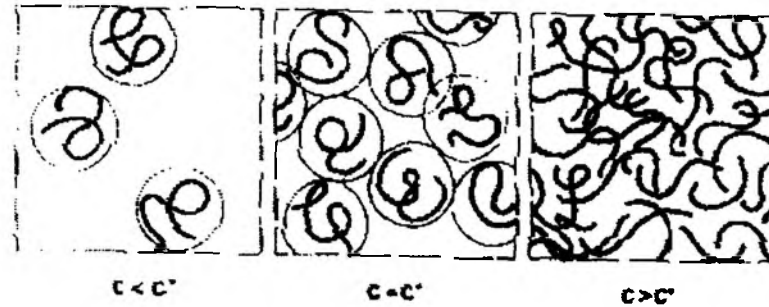


**Figure 1.2:** Illustration of polymer chain configuration in dilute, semi-dilute and concentrated solutions.

### ***1.6.2 Dilute solution study***

#### **1.6.2.1 Theoretical models**

Rheology studies at low polymer concentration can be used to define the polymer – solvent system without the complications introduced by polymer chain interactions at higher polymer concentration. The relative viscosity,  $\eta_r$  is the dimensionless ratio of solution viscosity,  $\eta$  to solvent viscosity,  $\eta_0$ :

$$\eta_r = \frac{\eta}{\eta_0} \quad (1.4)$$

The specific viscosity  $\eta_{sp}$  is defined as the fluid viscosity increase due to all polymer solute molecules:

$$\eta_{sp} = \frac{\eta - \eta_0}{\eta_0} \quad (1.5)$$

The reduced viscosity,  $\eta_{red}$  defined as  $\eta_{sp} / c$ , is the fluid viscosity increase per unit of polymer solute concentration,  $c$ . The intrinsic viscosity,  $[\eta]$  is the limit of the reduced viscosity as the polymer solute concentration approaches zero. Parameter  $[\eta]$  is

related to important characteristics of the polymer solution as shown by the following equation [Beever, 1968]:

$$[\eta] = \phi \alpha^3 (\overline{r^2})^{3/2} / MW \quad (1.6)$$

where,  $\phi$  is a universal constant, and MW is the polymer molecular weight. Length  $(\overline{r^2})^{3/2}$  is the mean square end-to-end distance of the unperturbed coil i.e. in a theta solvent. The coil expansion coefficient,  $\alpha$ , is the ratio of the end-to-end distance of a random coil in a particular solvent over the unperturbed end-to-end distance of the same polymer molecule.

The intrinsic viscosity is commonly determined by either the Huggins [ $\eta_{red}$  vs.  $c$ ] or Kraemer [ $\ln(\eta / \eta_0)$  vs.  $c$ ] plots. The Huggins equation is defined as:

$$\eta_{red} = \frac{\eta_{sp}}{c} = [\eta] + k' [\eta]^2 c \quad (1.7)$$

The Kraemer equation is defined as:

$$\ln\left(\frac{\eta_r}{c}\right) = [\eta] - k'' [\eta]^2 c \quad (1.8)$$

Combining the Huggins and Kraemer equation,  $[\eta]$  can also be calculated by “one-point” methods as exemplified by equation below:

$$[\eta] = \frac{\sqrt{2}}{c \sqrt{\eta_{sp}}} - \ln(\eta_r) \quad (1.8)$$

noting that as  $c \rightarrow 0$ , and  $k' + k'' = 1/2$

The Huggins coefficient  $k'$  is independent of the molecular weight; it increases from values around 0.35 in strong solvents to values as high as 1.4 for solutions in poor

solvents [Turner et al (a) 1950, Turner et al (b) 1947]. Thus intrinsic viscosity  $[\eta]$  is higher in good solvents, while  $k'$  is higher in poor solvents. In poor solvents, coiling of the polymer chain to a compact shape is favored because the forces between the polymer segments overcome the strong polymer-solvent forces which are characteristic of good solvents [Turner et al.]. Increase in specific viscosity at high concentration in poor solvents is caused by intermolecular association resulting in a gel.

Staudinger et al [1930] showed that solution viscosity depends on both the polymer molecular weight and the extension in space of the polymer chains. The molecular weight of polymers is related to the intrinsic viscosity by the Mark-Houwink equation:

$$[\eta] = K' M^a \quad (1.9)$$

where,  $M$  is viscosity average molecular weight and  $K'$  and  $a$  are the Mark-Houwink constants. There is a specific set of Mark-Houwink constants for every polymer-solvent combination. The constant  $a$  is a scalar which relates to the "stiffness" of the polymer chains. If the polymer molecules in solution were rigid rods,  $a=2$ ; while if the polymers were hard spheres,  $a=0$ . More realistically, in a theta solvent,  $a=0.5$ , and in a thermodynamically good solvent,  $a=0.8$ .

For low polymer solution concentration and low polymer molecular weight, solution viscosity is independent of the shear rate. The solution viscosity measured under these conditions is Newtonian or "zero" shear viscosity. However, as the polymer concentration and/or the polymer molecular weight increases, the solution viscosity becomes shear dependent or non-Newtonian. Most non-Newtonian polymer solutions are shear thinning i.e. viscosity decreases with increasing shear rate. The solution viscosity used to determine the intrinsic viscosity in the Huggins or Kraemer's plots must be the "zero" shear viscosity determined in the low shear or Newtonian region.

### 1.6.2.2 Experimental studies of dilute PAN solution rheology

Bercea et al [1999] studied extremely dilute PAN solutions in DMF. They determined the critical overlapping concentration  $c^*$  separating the dilute and extremely dilute regimes for PAN in DMF using viscometry. They observed a deviation in the Huggins dependence for dilute solutions and a scaling law between the reduced viscosity and the concentration for the extremely dilute solutions was determined. They concluded that the critical overlapping concentration depends on the molecular weight and on the viscosity of the polymer solutions.

Morariu et al [1999] studied the conformational characteristics of oligo- and poly- acrylonitrile solutions in the dilute region using GPC and viscometry. They observed a change in the Mark-Houwink dependencies of  $[\eta]$  vs  $M_n$  as the molecular weight changes. They observe an increase in the exponent  $a$  with the increasing molecular weight range. They conclude that the chain stiffness and chain ends influence the chain dimensions in the dilute solutions.

The experiments performed on the dilute solutions of PAN are not very informative from experimental point of view; available information is tabulated in Table 1.8.

### ***1.6.3 Concentrated solution studies***

#### 1.6.3.1 Theoretical models

The terminology used in this section is defined as follows:

For non-dilute polymer solution the polymer chain interaction in solution is a function of the coil overlap parameter or Berry number,  $\beta$  ( $\beta=[\eta]c$ ). The zero shear viscosity at moderate concentrations follows equations of the general form:

$$\eta_0 = \eta_s F(c[\eta]) \quad (1.10)$$

Such equations can be useful in unifying data for different concentrations and molecular weights in the same polymer -solvent system.

**Table 1.8:** Summary of the experiments performed on dilute solutions of PAN.

Interaction identified	Comments	Reference
intrinsic viscosity $[\eta]$ measurements of UHMW Pan in very dilute solutions	observe high $[\eta]$ values than normal for very dilute solutions attributed to entanglement effects	Zhu et al [1996]
PAN+DMF+Inorganic salt $\text{Ni}^{2+}$ , $\text{Co}^{2+}$ , $\text{Cu}^{2+}$ , $\text{Ag}^{3+}$ and $\text{Cr}^{3+}$	changes in IV attributed to changes in chain conformation	Abdurakhmanova et al [1974]
interaction of VIB metals (Cr, Mo, W) with PAN in DMSO	changes in molecular weight, attributed to association of macromolecules and salts of VI group	Dubrovina et al [1998]
dilute solution viscosity of PAN in DMF and water absorbed sensitivity studied	higher values of eta sp/c M-H-constants used	Toshio et al [2000]

A specific form of the general equation is the commonly used Martin's equation (equation 1.11)

$$\eta_0 - \eta_s = \eta_s c [\eta] \exp(k_M c [\eta]) \quad (1.11)$$

A better fit to the data is obtained by replacing  $[\eta]$  with  $M^a$  and choosing  $a$  to fit data. It is found that  $a$  is close to the Mark Houwink constant [Graessley, 1974]. ✓

Viscosity of concentrated polymer solutions is usually shear rate dependent. Several equations correlate the dependence of polymer solution viscosity on shear rate. For example, the Cross equation (1.12) is given as follows:

$$\frac{\eta_0 - \eta}{\eta - \eta_\infty} = \left( K \dot{\gamma} \right)^m \quad (1.12)$$

where,  $\eta_0$  and  $\eta_\infty$  refer to asymptotic values of viscosity at very low and very high shear rates ( $\dot{\gamma}$ ) respectively. K is a constant parameter with the dimensions of time and m is a dimensionless constant. For the case that  $\eta \ll \eta_0$  and  $\eta \gg \eta_\infty$ , and with a simple redefinition of parameters, the Cross model can be written as:

$$\eta = \left( K_2 \dot{\gamma} \right)^{n-1} \quad (1.13)$$

Equation 1.13 is the power law model; n is called the power law index and  $K_2$  is called the consistency. Logarithmic plots of  $\eta$  versus  $\dot{\gamma}$  typically exhibit a pronounced linear region at high shear rates with negative slopes between 0.4-0.9. A way to present solution viscosity v/s shear rate data is as a function of reduced variables where the subscript “ref” usually refers to a low shear rate condition:

$$\frac{\eta}{\eta_{ref}} = \left( K_2 \right)^{n-1} \left( \frac{\dot{\gamma}}{\dot{\gamma}_{ref}} \right)^{n-1} \quad (1.14)$$

### 1.6.3.2 Experimental studies of dilute PAN solution rheology

Stoiko et al [1996] studied different conditions for making UF membranes from solutions of PAN in DMF. They studied the effect of various additives ( $\text{LiNO}_3$ , water and formamide) to solutions of polyacrylonitrile terpolymer (92% acrylonitrile, 7% methyl methacrylate, 1% vinyl sulfonate, Mw: 63,000) in DMF. These additives are considered to be structure forming agents for membranes cast from their solutions. Changes in viscosity and rheological characteristics of the polymer solutions were correlated with pore radii, efficiency and selectivity of the membranes. Formamide is a weak coagulant for this polymer solution. Increasing the formamide concentration up



to 2wt % results in increased solution viscosity; however, at higher formamide concentrations, the viscosity decreases.

Lobanov et al [1969] (abstract only) studied the effect of LiCl added to solutions of PAN in DMF. Small additions of LiCl to concentrated solutions of PAN/DMF decreased the viscosity of the solution to 70-80% of the starting viscosity. Polatovskaya et al [1969] also observed that Lifer salts (LiCl, MgCl<sub>2</sub>, NaCNS or ZnCl<sub>2</sub>) added to PAN spinning solutions in DMF decrease the solution viscosity and also delay the fiber precipitation process.

## **1.7 Effect of solution composition on membrane morphology**

### **1.7.1 Phase boundary map**

Knowledge of the phase separation process is the key to understanding membrane properties and structures. The effect of composition in a ternary system (polymer-solvent-nonsolvent) can be understood by following the precipitation pathway on a phase boundary map [Strathmann et al, 1988].

Figure 1.3 [Porter, 1988] depicts a phase diagram of a three component mixture which exhibits a miscibility gap over a wide range of compositions. If a non-solvent is added to a homogeneous solution consisting of a polymer and solvent, the composition of which is indicated by the point A on the solvent-polymer line, and, if the solvent is removed from the mixture at about the same rate as the non-solvent enters in, the composition of the mixture will change following the line A-B. At point C the composition of the system will reach the miscibility gap and two separate phases will begin to form: a polymer rich phase represented by the upper boundary of the miscibility gap and a polymer poor phase represented by the lower boundary of the miscibility gap.

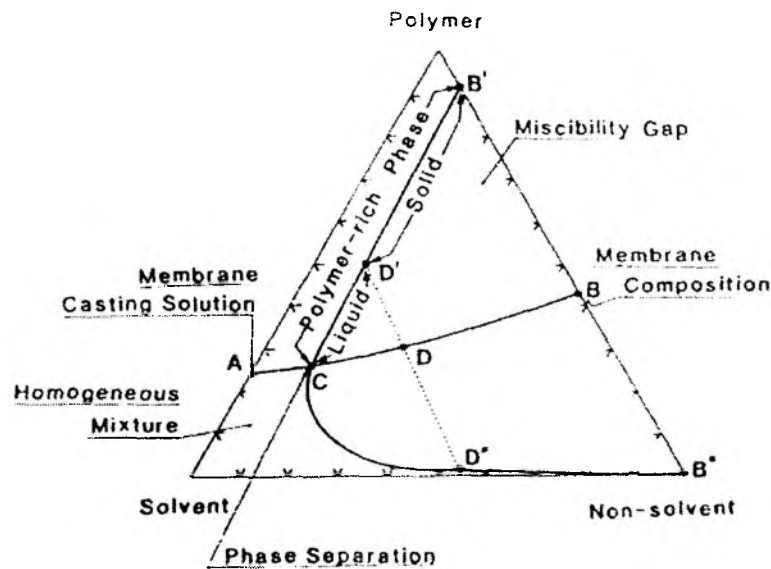


**Figure 1.3:** Schematic phase diagram of the polymer-solvent--non-solvent system showing the precipitation pathway of the casting solution during membrane formation.

At a certain composition represented by point D in Figure 1.3, the polymer concentration in the polymer rich phase will be so high that it is considered to be a solid. At this point, the membrane structure is more or less determined. Further exchange of the solvent and non-solvent will lead to the final composition of the membrane, the porosity of which is determined by the point B. The point B represents a mixture of both the polymer rich phase and the liquid solvent rich phase as represented by the points B and B' respectively. The liquid-liquid demixing curve shown in Figure 1.3 is known as binodal curve. A second curve lying just within the binodal is the spinodal curve which separates the metastable region of the composition map from a stable region.

The experimentally measured cloud point curve obtained by following the point of insipient phase separation does not lie on the binodal curve except for a monodisperse polymer system; but is commonly taken to represent it. Theoretical calculation of the binodal involves resolution of extremely non-linear equations in terms of the solvent and non-solvent volume fractions in the polymer rich and polymer lean phases. Analysis can be simplified on the basis of linearized cloud point curves [Boom et al (1993)] for ternary

systems consisting of one non-solvent (NS), one solvent (S) and one polymer (P). The conditions for validity of this linear correlation function are:

(a) that the polymer is strongly incompatible with the non-solvent and both the polymer and the non-solvent are miscible with the solvent, and

(b) that only liquid-liquid demixing occurs.

The linearized cloud point (LCP) curve (equation 1.15) is interpreted in terms of the various parameters occurring in the Flory-Huggins theory (eqn 2.5):

$$\ln\left(\frac{\phi_{NS}}{\phi_P}\right) = b \ln\left(\frac{\phi_S}{\phi_P}\right) + a \quad (1.15)$$

where,  $\phi$  represent volume fractions. The intercept  $a$  depends on enthalpy factors and is a function of the Flory-Huggin's interaction parameters. For details, please see Boom et al,1993.

Parameter  $b$  depends on the respective molar volumes:

$$b = \frac{v_{NS} - v_P}{v_S - v_P} \quad (1.16)$$

### ***1.7.2 Membrane morphology determined by mechanism of phase inversion***

The membrane pore structure is generated by phase separation. After immersion of a thin polymer solution layer in a non-solvent bath, a solvent - non-solvent exchange brings the initially thermodynamically stable system into a condition for which the minimum Gibbs free energy is attained by the mixture separating into two coexisting phases.

The membrane morphology is determined by kinetic and thermodynamic parameters associated with the phase inversion process [Strathmann 1985, Cabasso ]. Figure 1.4 is taken from a recent publication by Nunes et al [1997] who describe various membrane morphologies resulting from different paths of phase separation, If the solvent-non-solvent exchange brings the system first to a meta-stable condition (Path A), a nucleation and growth mechanism (NG) is favored. A dispersed phase consisting

of droplets of a polymer poor solution is formed in a concentrated matrix. If no additional non-solvent influx or temperature change were to occur, the composition inside the nuclei would be that expected at the equilibrium and would not change with time. Only the size of the droplets would increase with time.

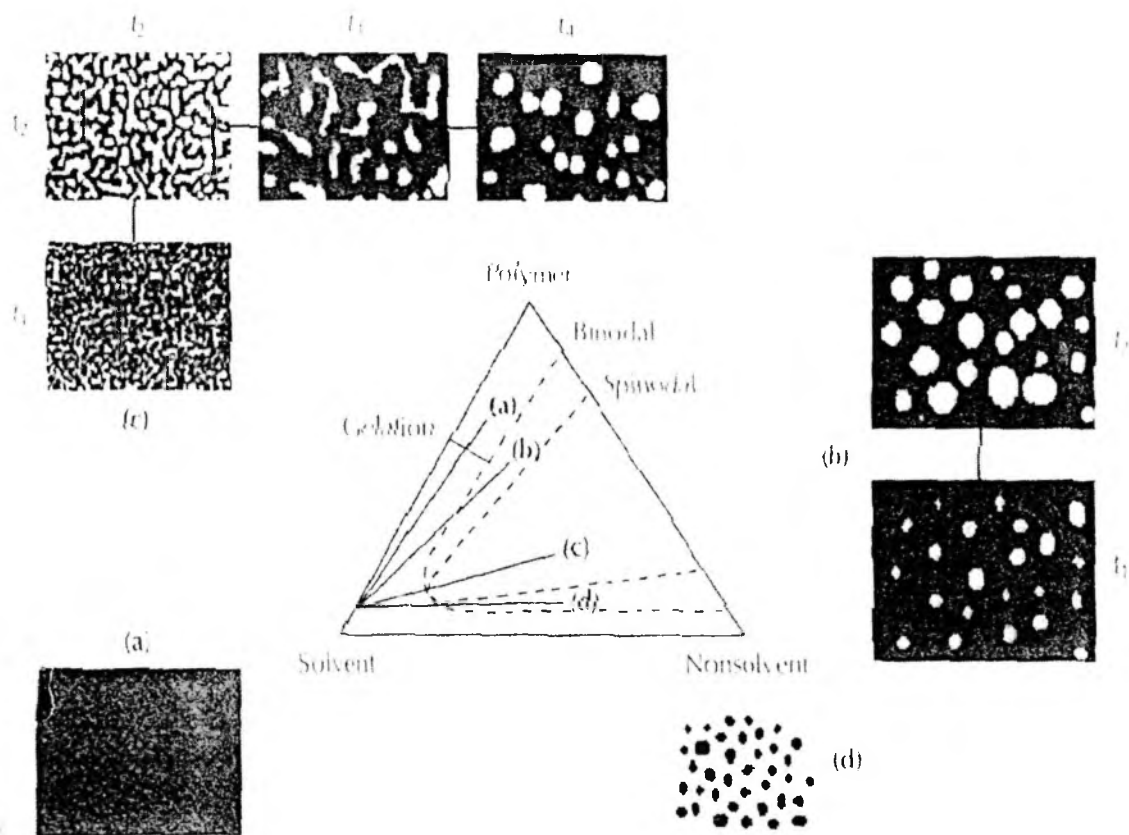


**Figure 1.4:** Phase separation in ternary systems for membrane preparation Path (a) solvent evaporation and non-solvent addition leading to gelation without phase separation. Non-porous membrane is formed. Path (b) Solvent-non-solvent exchange leading to phase separation (NG) in the metastable region with a polymer rich matrix Path (c) Solvent-non-solvent exchange leading to phase separation(SD) in the unstable region. Membrane with interconnected pores is formed if gelation starts before the beginning of coalescence. Path (d) NG phase separation with a polymer poor matrix, no membrane is formed. [NG=nucleation and growth and SD= spinodal decomposition].

If the demixing path crosses the critical point, going directly into the unstable region (Path B), spinodal decomposition (SD) pre-dominates. A concentration fluctuation appears in the initially homogeneous system and progresses with increasing

amplitude, leading to separation in two co-continuous phases. Here again the polymer poor phase will form the pores. The initial steps of phase separation, either by NG and SD can be relatively well described according to theories of phase separation. However, at later stages, both NG and SD usually progress to a coalescence phase and the final structure can only be predicted with difficulty.

At least as important as the starting mechanism of phase separation is the point where the developing structure is fixed. In parallel to demixing, as the concentration of the polymer solution changes by solvent-non-solvent exchange, the mobility of the system decreases. Reasons for that may vary from physically unfavorable polymer-solvent (or non-solvent) interaction leading to stronger polymer-polymer contacts, to vitrification of the polymer concentrated phase as the solvent concentration decreases, or, in some cases, partial crystallization. If the system gels and solidifies directly after the first steps of phase separation (for instance at  $t_2$ ), the membrane will have a fine pore structure, which keeps the original characteristics given by the initial demixing mechanism. If NG demixing stops during the initial stages, a morphology of closed cells would be favored. At later NG stages, the nuclei would grow and touch each other forming interconnected pores. By contrast, SD demixing would favor the formation of an interconnected pore structure from the beginning. An asymmetric structure is usually formed across the membrane since the solvent non-solvent exchange leads to different starting conditions for phase separation at solution layers far from the surface.

Stropnik et al [2000] studied turbidity and shrinkage phenomena to elucidate the elementary processes in polymeric membrane formation by phase inversion. They postulated four elementary processes: (i) direct accumulation of polymer, the nucleation and growth of the (ii) polymer lean as well as the (iii) polymer rich phase and (iv) spinodal phase separation.

Besides the NG and SD demixing mechanisms, other factors influence the morphology. The whole membrane structure usually can be classified as sponge-like or finger-like. Finger-like cavities are formed in many cases. This macrovoid structure may contribute to a lack of mechanical stability in membranes to be used at high pressures.

The viscosity of the casting solution is an important variable determining

membrane morphology. Viscosity can hinder the rate of solvent and non-solvent during the phase inversion process. It is also indicative of polymer chain mobility required for growth in the nucleation mechanism and also affects the point at which the membrane morphology is effectively set.

The membrane pore size distribution is affected by parameters such as polymer concentration, dope solution composition, nature of additives, gelation bath temperature and its composition. [Scharnagla et al 2001, Stoiko et al 1996, Petrov et al 1991, Kim et al 2002 ] The effect of inorganic additives on the precipitation behaviour of various polymer solutions is discussed below.

Strathman [1971] and Frommer et al [1971] suggest that the action of casting solution additives is to modify the difference in the chemical potential of the non-solvent (water) between the casting solution and the wash bath.

The effect of additives on the membrane morphology is compiled in the next section

### ***1.7.3 PAN membrane morphology***

Scharnagla et al [2001] fabricated PAN membranes for ultra- and microfiltration on a non-woven support by phase inversion on the most important parameters determining membrane morphology were polymer concentration of the casting solution and the temperature of the precipitation bath. The membrane morphologies varied from large finger-like pores to homogeneous microporous structures. The flux of the membranes was 100 - 2000 l-m<sup>2</sup>-h. The water permeability was found to decrease with increasing polymer concentration and with a lowering in the precipitation bath temperature. Protein rejection studies were performed using Dextran T<sub>250</sub>; the Dextran rejection increased with a decrease in the temperature of the bath.

The only information available on the effect of salts in the casting solution is the work of Cho et al [1994] who observed that PAN fibers spun from a spinning dope containing ZnCl<sub>2</sub> have a denser and finer structure than those in the absence of the salt. This was attributed to ZnCl<sub>2</sub> in the dope retarding the coagulation rate. Fibers spun

from solutions containing  $ZnCl_2$  in the dope also had improved tensile strength and modulus.

Though the effect of inorganic salts on the polymer membrane fabrication of PSF, PVDF, PES, PEI and some cellulosic polymers is reported in the literature, there is no similar study for polyacrylonitrile. However, studies have been made of PAN membrane morphology from solutions containing various organic solvents and additives. These are summarized below.

#### 1.7.3.1 Organic additives

Kim et al [2002] studied the morphological changes of Polyacrylonitrile membranes after addition of 1-4-dioxane. The additive did not change the membrane morphology; in the cross sectional view; all the membranes had large macrovoids. The surface views of the membranes appear to indicate that the additive decreased the membrane pore slightly.

Th 8572

The effect of glycerol added to the dope solution (glycerol concentration range 0.5- 4wt %) on the membrane pore size and structure was examined by Petrov et al [1991]. With increasing glycerol concentration, membranes with higher pore density and smaller pore size were formed, increasing the selectivity to lower molecular weight compounds.

Stoiko et al [1996] studied the effect of formamide as an additive in DMF and polyacrylonitrile terpolymer solutions / membranes. With increasing formamide concentrations, finger like pores in the cast film become longer and occupy a greater part of the layer. The resulting greater degree of asymmetry improves membrane efficiency and selectivity.

#### 1.7.3.2 PAN blends and co-polymers

Xiuli et al [1998] studied the morphological structure and properties such as miscibility, tensile strength, flux and rejection of hollow-fiber membranes prepared from PAN blended with small amounts of PVDF. The hollow fiber was made from spinning solutions composed of polymer (PAN : PVDF=10 : 0, 9 : 1, 7 : 3), additive (PVP, PEG-600) and solvent (DMAC) precipitated in water. The membrane morphologies were

examined by SEM. The blend membranes possess higher flux than PAN membrane with same rejection.

Kobayashi et al [1998] studied the rejection of *Escherichia coli* by charged and un-charged polyacrylonitrile ultrafiltration membranes. Three types of PAN UF membranes were made from various materials: neat PAN and PAN with charge groups of sulfonate sodium salt (SSS) and trimethylammonium chloride (TMA). These UF membranes were prepared from solutions with various polymer concentrations in dimethylsulfoxide (DMSO) by phase inversion in a water coagulation bath. With increasing polymer concentration in the cast solution, the pore size, as measured by molecular size rejection, of the resultant UF membrane decreased. SEM studies compared the membrane morphology by varying the DMSO concentration (10, 30, 50, 70 wt %) in the water bath. The membrane morphology shows a typical asymmetric structure, consisting of a top thin layer supported with a finger like structure. The observation of fingerlike macrovoids implies that the PAN segments coagulate instantaneously in water medium while at high DMSO concentrations a spongy structure is formed. High concentration of DMSO in the bath results in a very loose coagulation of the PAN segments leading to decreased *E.coli* rejection. .

## **1.8 Other polymeric membrane morphology studies**

Polyethersulfone, Polysulfone and PVDF membrane morphologies have been extensively studied with both organic and inorganic salt additives to solutions in aprotic solvents such as NMP or DMF.

### ***1.8.1 Organic additives***

Pereira et al [2001] studied the effect of Lewis Acid - Base (LAB) complexes in polymer solutions on precipitation kinetics and membrane formation. Their work investigated membranes using polyethersulfone (PES) and LAB's comprising N-Methylpyrrolidone (NMP) and dicarboxylic / monocarboxylic acids from a homologous series. The results indicated that the solvent-additive interaction, which is a function of their capacity to form complexes and the acid chain length directly, affects the viscosity



and the miscibility region. These parameters affect the precipitation velocity, which then affects the membrane transport properties. They observed that the solutions containing the acids as additives present a larger miscibility gap compared to water as an additive.

Fritzsche et al. [1990] studied the structures of hollow fiber membranes spun from polysulfone solutions made in NMP with propionic acid and from formylpiperidine (FP) with formamide (FA). They compared the structures of both the hollow fibers so formed, and found these to depend on the complex formation and its dissociation on contact of the non-solvent. Hollow fibers spun from propionic acid : N-methyl pyrrolidone complex had a thinner active separating layer than those made from formylpiperidine / formamide mixture.

Tao et al [1998] studied the effect of nonsolvent additives to the casting solution on performance of PES MF membranes. Three nonsolvent additives (NSA) (ethylene glycol, diethylene glycol and n-butanol) with different polarity and solvating power were examined in terms of water flux and maximum membrane pore size. The compatibility of the three NSA with PES/DMAc (N,N-dimethylacetamide) were investigated in terms of cloud point for systems of PES/DMAc/NSA and PES/DMAc/NSA/H<sub>2</sub>O. For the same NSA, polymer concentration and coagulation conditions, the increase of a (the ratio of near-to-cloud-point) value could lead to the changing of membrane structure.

Kim et al [1998] studied the effect of PEG as a pore-former additive on the membrane formation from PSF/NMP. They observed that on increasing the ratio of PEG to NMP or by increasing the PEG molecular weight, the coagulation value decreases or the solution becomes thermodynamically less stable. They also observed that PEG causes the surface pore size to become bigger and the top-layer to become more porous. The distance from the top surface to the starting point of macrovoid formation becomes larger. They observed an increase in the water flux and solute rejection on increase in the molecular weight of PEG additive or the ratio of the PEG additive to NMP. The permeation properties agree well with the SEM photographs.

## ***1.8.2 Salt additives***

### **1.8.2.1 Polysulfone (PSF)**

Kim et al [1996] found that addition of  $\text{ZnCl}_2$  to polysulfone (PSF) solution in NMP may cause association between the PSF chain molecules leading the solution to a gel like state. The precipitation of PSF solutions containing  $\text{ZnCl}_2$  required less water than the salt-less solutions. The addition of  $\text{ZnCl}_2$  lowered the water permeation rate and increased the rejection of the resulting membrane. This was attributed to the formation of smaller pores and a narrower pore size distribution without significant change in the overall membrane porosity. SEM was not able to see any significant differences in membrane structure. This implies that  $\text{ZnCl}_2$  affects mainly the skin layer rather than the entire membrane. The membranes with the additive had clearly finger typed structure as revealed from the cross-sectional views of the S.E.M studies similar to the membranes without additive. Infrared spectroscopic study shows the addition of  $\text{ZnCl}_2$  (3% w/w) in the PSF solution in N-Methylpyrrolidone (NMP) caused a red shift of  $3\text{ cm}^{-1}$  in the symmetric vibrational stretching of sulfone group ( $1152.2\text{ cm}^{-1}$ ); this is attributed to the interaction of  $\text{ZnCl}_2$  with sulfone group.

Seong et al [1990] studied the system PSF/DMF/water + additive; the additives employed were NaCl, NaOH, KCl, LiCl,  $\text{CaCl}_2$  etc. They observed shifts in the binodal curve for the additive containing system towards the polymer-solvent axes by the presence of electrolyte in water; the extent of the change in the binodal curve was dependent on the nature of the salt additive with no clear trend.

Bottino et al [1988] prepared UF membranes from binary solutions of polyvinylidene fluoride (PVDF) in dimethyl formamide (DMF), dimethyl acetamide (DMAc) or NMP containing LiCl. The porosity of the membrane increased, and the bursting pressure decreased due to the LiCl. The permeate flux and rejection for Dextran increased, compared to membranes without LiCl in the dope solution.

Ying et al [1990] studied the morphology of phase inversion membranes prepared from PVDF-LiCl-DMF and PVDF-LiCl-DMAc solutions. The membranes obtained were studied by Scanning electron Microscopy (S.E.M.) and showed both finger type and spongy type structures. The active layer of the membranes was the

bottom surface and the sponge type structure was observed near the bottom surface of the membrane instead of the top surface of the membrane.

#### 1.8.2.2 Polyamide / imides

Lee et al [2002] studied the physical properties of poly(amic acid) (PAA) casting solutions in *N*-methyl-2-pyrrolidone (NMP) containing lithium chloride (LiCl) and characterized them using viscometry and dynamic light scattering and finally related these properties to the morphologies of asymmetric membranes prepared from these solutions. They observed that at a fixed polymer concentration, the increase in viscosity of PAA solutions with increasing LiCl content is mainly determined by the viscosity of the salt-solvent medium. This implies that LiCl-NMP interactions are stronger than those between LiCl-PAA. The LiCl-NMP complexes reduce the solvent power of NMP for PAA inducing polymer aggregation (clustering) and/or transient cross-links in the solutions. Dynamic light scattering for salt containing solutions at low PAA concentrations showed the existence of such aggregations. Solutions without salt showed a single relaxation, but solutions with LiCl exhibited multiple relaxation modes; two diffusional modes of cooperative and aggregates, and one angle independent transient network mode. The polymer aggregates and transient cross-links form a gel-like structure in the casting solution and hinder macrovoid formation during phase inversion, resulting in asymmetric membranes with a primarily sponge-like structure.

Kurdi et al [2001] studied the influence of casting solution structure on the microporosity and performance of polyetherimide (PEI) gas separation membranes prepared by a coagulation+post-leaching of solution additives method. This method uses a delayed wet-phase-inversion step where there is poor mutual affinity between the solvent and non-solvent in the coagulation bath. The membrane structure formed by this method is usually of the closed type; however appropriate post - leaching the additive component opens the membrane structure. Their computational chemistry and chemical structure study indicated that a lithium cation solvated in NMP (*N*-methyl-2-pyrrolidinone) forms a complex with two NMP molecules. This complex was determined by computational chemistry to be stable in isopropanol but not in methanol or water. They observed that increasing the additive (LiNO<sub>3</sub>) concentration in the

casting solution lead to a greater number of micropores in the 0.7–1.2 nm range, while the peak in the micropore distribution remained unchanged at 1.0 nm. Molecular mechanics calculations indicated that the PEI polymer chain can form coils having an inner section of 0.7 nm -1.0 nm. The inherent size of the PEI polymer coils remains unchanged with the addition of  $\text{LiNO}_3$  but the number of polymer coils increases. Larger micropores were present at higher  $\text{LiNO}_3$  concentrations and caused a decline in the actual separation factor for these membranes.

Kraus et al [1979] observed that low molecular weight salts contained in aromatic polyamide reverse osmosis membranes greatly increase membrane fluxes without a detrimental effect on rejection. Highly dissociated salts, e.g.  $\text{LiClO}_4$  or  $\text{Mg}(\text{ClO}_4)_2$  exert a stronger influence than the commonly used  $\text{LiCl}$ . They also observed that mixtures of different salts might give stronger effects than those obtained with a single additive. It was suggested that the salt effect is related to solvent activity and thus on the kinetics and equilibrium associated with evaporation and coagulation processes.

Highly specific requirement of amide solvents was stressed by Panar et al [1977] for polyamides. The polymer dissolves in fully substituted amides containing very large quantities of  $\text{LiCl}$ . The negatively charged polyamide chain associates with chloride ion, this negative chain being solvated by a weak lithium ion- solvent complex. This overall complex is then soluble in the amide solvent. Their proposed solvation structure for aromatic polyamide in an amide solvent is shown in Figure 1.5.

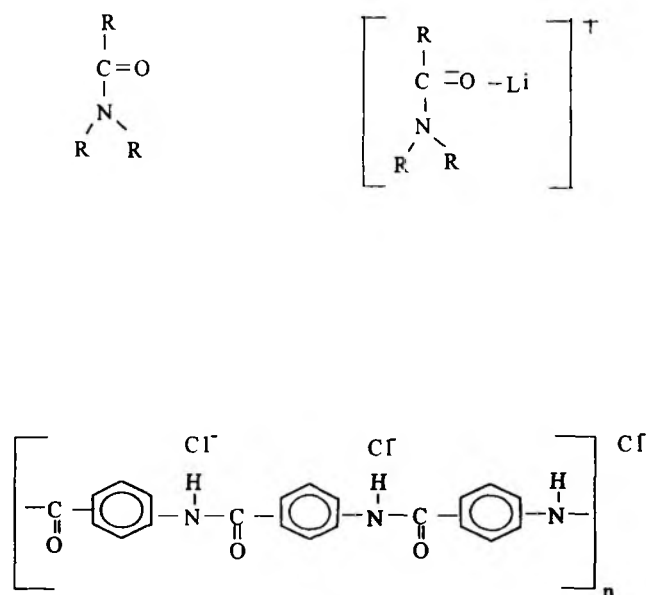


**Figure 1.5:** Proposed solvation structure for the aromatic polyamide in an amide solvent.

Goldammer et al [1979] performed  $^{13}\text{C}$  NMR investigations on the influence of inorganic salts on the solvation of N,N'-dibenzoyl-m-phenylenediamine in N,N-dimethylacetamide. Changes of the solvation sphere of N,N'-dibenzoyl-m-phenylenediamine (as a model substance for aromatic polyamides) in  $\text{AcNMe}_2$  caused by electrolytes such as LiCl, LiBr, or  $\text{BeCl}_2$  were studied by  $^{13}\text{C}$  NMR chem. shift measurements. The observed variations of the chemical shift data were interpreted by a stronger interaction of the solvent molecules with the carbonamide group. The relation of the carbonyl and the amide group interaction with the solvent or the solvated cations depends on the kind of electrolyte. Some possible explanations are discussed to correlate the obtained results with the influence of these electrolytes upon the molecular wt. of the aromatic polyamides prepared in  $\text{AcNMe}_2$ .

### 1.8.2.3 Vinyl polymers

Yih et al [1992] studied the complex formation and nonvolatile-solvent swelling effects for (PMMA/ $\text{CH}_2\text{Cl}_2$ )/(DMF/ $\text{CuCl}_2 \cdot 2\text{H}_2\text{O}$ ) for complex membranes intended for air separation. The effect of membrane casting conditions on gas permeability,

morphology and crystallinity of the complex membranes, as well as the existence and amount of PMMA/(DMF/metal salt) complex formation and the crystallosolvate and adduct phenomena of the casting solutions were studied. The improved gas permeability for the modified PMMA membrane was attributed to the swelling effect and complex formation of the PMMA/DMF/metal salt. Crystallinity increases as the metal salt content increases in the complex membrane. Complex formation was verified by UV, FTIR spectroscopy, wide-angle x-ray diffraction, and DSC studies for this PMMA/(DMF/CuCl<sub>2</sub>·2H<sub>2</sub>O) system.

Zagar et al [2000] studied the solution properties of carboxylated polyurethane's (CPUs) and related ionomers (PUIs) in DMF + LiBr by size exclusion chromatography (SEC), viscometry and in the case of CPUs also by SEC coupled with a multi-angle light scattering detector (SEC-MALS). They observed that in DMF, both kinds of PUs have multimodal molar mass distributions, while the reduced viscosity-concentration profiles indicate an upturn in very dilute regions usually related to the polyelectrolyte effect. However, SEC-MALS measurements of non-carboxylated PU (NPU) and CPUs indicate that these PUs aggregate in DMF. After the addition of LiBr to DMF unimodal molar mass distributions with much larger elution volumes ( $V_e$ ) and linear concentration dependences of reduced viscosity are obtained for both kinds of PUs. LiBr in DMF not only screens the ionic groups of carboxylated PUIs but also specifically interacts with the polar groups of PUs. Thus, LiBr suppresses any electrostatic and/or molecular interactions and consequently eliminating aggregation encountered in SEC characterization of both kinds of PUs in DMF.

Salamova et al [1996] studied the effect of inorganic salts on the main parameters of the dilute aqueous poly(vinylpyrrolidone) solutions. The effect of inorganic salts (co-solute) on the main parameters of dilute aqueous poly(vinylpyrrolidone) (PVP) solutions, such as cloud points, phase diagram, quench temperature and viscosity was studied experimental using various concentrations of salts and said polymer at varying temperatures. Thermodynamic incompatibility of aqueous PVP-salts solutions strongly depends on the character of effect of salts (water-structure breakers or water-structure makers). Inclusion of salts into aqueous PVP solution leads

to decreasing of the  $q$  temperature and intrinsic viscosity, which is, caused by effect of the co-solute ions in enhancing the segment-segment interactions.

### **1.9 Aim and Objectives for this work**

This thesis aims at a better understanding of the formation of PAN microporous membranes cast from solutions in DMF plus various metal chlorides. The work focuses on dope composition parameters affecting membrane structure / morphology. Specifically, it studies the effect of PAN molecular weight and that of various metal chloride additives (LiCl, ZnCl<sub>2</sub> and AlCl<sub>3</sub>) on the solution and separation properties of the membranes formed.

The three salts chosen have a common anion and cations with varying valency and electronic structure. While both Zn and Al are multivalent, Zn also has “soft-shell” d-electrons.

Three PAN materials of increasing MW were used in this thesis. A commercial grade (PAN-A) was procured and two higher MW grades (PAN-B and PAN-C) were synthesized.

The approach taken to improve our understanding of the basic issues involved can be summarized as:

- Spectroscopic studies to describe the interaction between salt, solvent and polymer
- Measurement of solution properties (dilute and concentrated solution rheology, phase boundary map) and correlation with spectroscopic studies
- Detailed description of membrane morphology (SEM, pore size distribution, permeance) and correlation with the relevant solution properties

The detailed objectives of the thesis are as follows:

1. To synthesize PAN of different molecular weights using the acrylonitrile monomer.
2. Detailed FTIR spectroscopic studies to examine the complexation behaviour of the three salt additives with PAN and DMF

3. To study the effect of various inorganic additives such as LiCl, ZnCl<sub>2</sub>, AlCl<sub>3</sub> on the following solution properties of PAN in DMF with the different molecular weight materials.
  - a) Dilute solution viscosity measurements
  - b) Concentrated solution rheology measurements
  - c) Cloud point measurements to investigate the precipitation behaviour of above solutions in water.
4. To cast membranes of different concentrations from the dope solutions of PAN in DMF containing the LiCl, ZnCl<sub>2</sub>, AlCl<sub>3</sub>, as additives with all the three polymers and to characterize them in terms of
  - a) Pure water permeation
  - b) Pore size and pore size distribution by solvent displacement
  - c) morphology assessment by SEM

#### **1.10 Description of thesis organization**

The thesis contains six chapters:

**Chapter I** gives a brief introduction to ultrafiltration (UF) membrane processes and describes the commercially important method of preparing membranes by the phase inversion method. It also includes a survey of previous work relevant to: (i) the complexation of DMF and PAN with various inorganic additives and (ii) the effect of inorganic additives in the casting solution on membrane morphology. The specific objectives and approach of this thesis work are then defined.

**Chapter II** describes the materials and experimental techniques used in the thesis. Three grades of PAN were used. The first, designated as PAN-A, is a commercially available polymer obtained from IPCL, Vadodara. The polymer was purified and techniques like FT-IR, H-NMR, and elemental analysis were used to characterize the structure as principally (- CH<sub>2</sub> -CH(CN) -). Dilute solution viscosity measurements were made at 25°C to estimate the molecular weight (MW) from the intrinsic viscosity [ $\eta$ ] and reported Mark-Houwink constants [Beevers, 1968]. The molecular weight of PAN-A is estimated to be ~50 kDa.



Two other higher molecular weight grades of PAN were synthesized from acrylonitrile monomer; these are designated as PAN-B and PAN-C. Acrylonitrile was extensively purified by several washing steps, followed by vacuum distillation. The monomer was polymerized using a redox-initiator system. The reaction was stirred at 50°C in an inert atmosphere; the reaction time was 1.5 hrs for PAN-B and 2 hrs for PAN-C. The polymer obtained was purified by precipitation- re-dissolution and re-precipitation steps, followed by vacuum drying at 70°C for several days. FT-IR, H-NMR, <sup>13</sup>C- solid state NMR, and elemental analysis were used to confirm that the structure of PAN-B and PAN-C also matched polyacrylonitrile. The MW of PAN-B was estimated to be ~168 kDa while that of PAN-C was ~250 kDa.

Since, the commercial PAN-A may also contain a small degree of hydrolyzed groups, for comparison, we also synthesized a PAN (acrylamide: acrylonitrile) (12:88) copolymer. This copolymer was used in limited work- the focus of the thesis remains on the three PAN grades described above.

Both dilute and concentrated solutions in DMF were made with the three PAN polymers in the presence of mono-, bi -and trivalent inorganic additives: LiCl, ZnCl<sub>2</sub> and AlCl<sub>3</sub>. The concentration of each additive in DMF was standardized at a constant ionic strength (0.83 M). The notations used for both the solutions as well as the membranes cast from these are in the format: PAN-X\_Y where:

X represents the PAN grade i.e., PAN-A, -B or -C, and

Y represents the additive i.e., either blank (DMF only), L = LiCl, Z = ZnCl<sub>2</sub> , A = AlCl<sub>3</sub>.

Depending on the context, this same nomenclature denotes either the solution type or the corresponding membrane formed from this solution.

Solution viscosities were measured in the dilute polymer concentration range (< 0.3%) at 25-45°C. The dilute solution viscosity data was used to calculate the viscosity activation energy for each type of solution. Solution viscosities were also measured at 30°C in a cone and plate viscometer at the higher concentrations, c, more typical of casting solutions. These data were used to estimate the shear thinning indices and also the dependence of the solution viscosity on the coil overlap parameter ( $\beta = [\eta] c$ )

Cloud point measurements for the various PAN-water-DMF+salt systems were made visually at low PAN concentrations and extrapolated to higher concentration values using a linearized cloud point equation [Boom et al, 1993] for the ternary phase boundary.

Membrane characteristics were principally measured by water flux, solute rejection, pore size distribution by bubble point measurements in water and isopropanol, and by scanning electron microscopy (SEM).

**Chapter III** summarizes spectroscopic studies of the interactions between the various salts, DMF and PAN. Salts may modify solution properties by interactions with either solvent molecules or with PAN. FT-IR studies were done for each salt additive, first in the combined solvent i.e. DMF + salt. These salt + solvent combinations are denoted DMF-L, DMF-Z and DMF-A for the 3 chloride additives based on Li, Zn, and Al, respectively. FT-IR spectra were then measured with 3-7 % PAN solutions in both DMF alone as well as with DMF + salt.

Salts can complex with DMF at either its electronegative carbonyl O or the more electropositive N. The  $>C=O$  stretching frequency observed in pure DMF remained essentially unchanged in both DMF-L and DMF-A, whereas a red shift by  $\sim 6\text{ cm}^{-1}$  was observed in case of DMF-Z. This observation can be correlated with the electronic cloud density around these cations. The energy involved in complexation of the electronegative carbonyl oxygen of DMF with a cation is the highest for  $Al^{3+}$ , followed by  $Li^+$  and least for  $Zn^{2+}$ . Both anion (Cl) and cation affect salt interaction with the O-CN group. While the C-N bond order and the corresponding O-C-N stretching frequency was expected to increase due to the carbonyl O - cation complexation, we actually saw a decrease in this frequency. This red shift may be due to the increasing electron cloud density of chloride ions near slightly electropositive nitrogen (compared to oxygen), which prevents the increase in C-N bond order. The red shift in O-C-N stretching frequency follows the trend of  $Al^{3+} > Zn^{2+} > Li^+$  i.e. it is highest for the salt containing the most chloride ions.

Polyacrylonitrile is partly self-associated through dipole-dipole interactions at the nitrile groups. FT-IR shows that DMF can break this polymer self-association but is

itself also bound to the PAN nitrile groups by dipole-dipole interactions. In the competition between the -OCN group of DMF and the -CN group of PAN for forming a complex with the salt, DMF is clearly the preferred interaction partner. This may be due to the higher basicity of DMF compared to the PAN nitrile group. The simultaneous presence of both salt and PAN gives rise to various new frequencies for both the  $>C=O$  and OC-N stretching frequencies of DMF. The nitrile stretching frequency of PAN is the same for all three PAN grades and remains constant even after salt addition salts to DMF. However there are significant differences between the various DMF-PAN-salt ternary solutions in terms of the OCN and particularly the  $>C=O$  stretch in DMF. Comparing the frequency shifts in these ternary systems with the binary PAN-DMF systems indicates that the nitrile group of PAN is weakly affected by the presence of the salt.

The interaction of PAN with DMF and the salt additives can also be probed by dilute solution rheology, which is highly sensitive to polymer chain configuration in solution. The intrinsic viscosities for PAN-A are higher in DMF+salt solutions compared to those in neat DMF. The  $[\eta]$  values for PAN-B are essentially unchanged with the salt while those for the highest MW grade, PAN-C decrease with salt addition. Calculations of the Mark-Houwink constant in solutions made with the salt additives indicate that the general effect of the salt is to decrease the PAN chain expansion; the exponent  $a$  decreases from 0.75 in DMF to  $\sim 0.6$  for DMF+salt solutions. This is consistent with the high affinity of the salts for DMF, measured by FT-IR. The increase in  $[\eta]$  for the lower MW PAN-A may be attributed to interchain bridging promoted by the salts.

Viscosity activation energies,  $E_a$ , calculated in the dilute concentration regime (0.1-0.3 g/dl), correlate well with the coil overlap parameter,  $\beta$ . Plotting  $E_a$  vs  $\beta$  for various solution types show larger +ve slopes for solutions made from neat DMF solutions compared to those with salt additives. Again this appears consistent with the solvent effects described above.

**Chapter IV** describes rheological, phase-boundary and membrane properties of various DMF+salt solutions based on the lower MW commercial product PAN-A. Solution viscosity and the polymer-solvent-nonsolvent (water) phase boundary are

considered critical variables affecting membrane pore formation. PAN-DMF solutions were made at a constant 4wt % level for each salt; the resulting solution and membrane properties were then characterized.

As mentioned above, the addition of both mono and multivalent salts to PAN-A / DMF solution causes an increase in the intrinsic viscosity  $[\eta]$ . Concentrated solution viscosities show that the viscosity of the multivalent salt containing solutions increases more rapidly than that of neat PAN/DMF solution.

The presence of additives in the dope solution clearly alters the ternary phase boundary. Measurements of the cloud point with PAN-A showed that solutions containing  $ZnCl_2$  can tolerate only a small amount of water before precipitation while those with  $LiCl$  or  $AlCl_3$  can tolerate more water than solutions of PAN in neat DMF.

The membrane structure was characterized by SEM studies of the surface and cross-sectional views. PAN-A, PAN-A-A and PAN-A-Z have large macrovoids in the underlying asymmetric structure; while the incidence and size of these macrovoids is considerably reduced in the case of the monovalent salt (PAN-A-L). This is consistent with the ternary cloud point data, which imply that the skin layer in PAN-A-Z and PAN-A would form rapidly with the exchange of only a small amount of water. The skin layer in PAN-A-Z membranes shows a fused nodular surface with a well defined transition layer between it and the macroporous substructure. In the case of PAN-A-L, precipitation would occur only after a considerable amount of DMF : water exchange had already taken place.

Ultrafiltration studies were done with different sized solutes: polyethylene glycol, lysozyme, (BSA) albumin, and casein, in a stirred cell configuration. The addition of di- and trivalent salts to the PAN / DMF casting solution results in membranes with similar rejection for various solutes (BSA, lysozyme, PEG-9000). At the same time, PAN-A-Z and PAN-A-A solutions have fewer large pores / defects and consequently higher rejection for bacteria. This suppression of surface defects correlates with the higher solution viscosity attributed to polymer chain bridging. The relatively high flux is due to retaining the macrovoid-containing substructure; this can be attributed to the low water tolerance of the casting solutions. These findings explain why the addition of  $ZnCl_2$  to the casting solution increases the bacterial reduction capability

of the membrane by 1000x (3-log) while retaining 80% of the water permeability of the corresponding membrane cast from DMF alone.

**Chapter V** describes the rheological, phase-boundary and membrane properties of various salt (LiCl, ZnCl<sub>2</sub> and AlCl<sub>3</sub>) containing solutions based on the higher MW grades PAN-B and PAN-C, and compares these effects with those seen for PAN-A. As mentioned before, MW increases in the order PAN –A < B < C. The main aim here was to see the effect of the increased molecular weight and the interactions with the three salt additives. As the PAN MW increases, dipole-dipole (interchain) interactions also increase and interchain entanglements become significant. The dilute solution properties for all 3 PAN grades were discussed in Ch III, while the rheology of more concentrated solutions are discussed in this chapter.

Concentrated solution viscosities increase sharply with the increase in PAN MW. This effect is the most pronounced with ZnCl<sub>2</sub> as an additive; ZnCl<sub>2</sub> containing solutions with > 5% of PAN-B or >3% of PAN-C are gelled. By contrast, solution viscosities decrease with LiCl and AlCl<sub>3</sub> additives; this may be attributed to these salts breaking existing interchain interactions between the polymer chains. PAN-A-DMF solutions show more shear thinning than solutions containing salts. For PAN-C we see the opposite trend and PAN-B shows similar power-law indices for DMF, DMF-L and DMF-A solvent systems. Low-shear viscosities measured as a function of polymer concentration in the various solvents show a good correlation with the coil overlap parameter. Analysis by the Martin equation shows that ZnCl<sub>2</sub> and AlCl<sub>3</sub> are the most effective additives for increasing solution viscosity in the concentrated solution range.

Cloud point studies with PAN-B show that all the salt containing solutions tolerate less water than the solution in DMF only; this trend can be expressed as Z < L < A < neat DMF. As the PAN MW increases, the measured bubble point (at a given PAN concentration) also increases (i.e. the pore radii decreases) and the water flux decreases. SEM of PAN-B cast without any additive shows a microporous sublayer full of macrovoids while membranes with PAN-B+ salt additives show a collapsed structure. The collapsed substructure can be attributed to the low polymer concentrations attainable in the casting dope and also from the lower solution viscosity with LiCl and AlCl<sub>3</sub>. The cloud point curves for the highest MW grade, PAN-C, are

relatively unaffected by the salt additives. SEM of the PAN-C membranes shows an absence of asymmetric skin formation and a collapsed sub-structure.

Finally, **Chapter VI** summarizes the conclusions followed by suggestions for future work.

## Chapter II

This chapter describes the materials and experimental techniques used in the thesis. The materials used and polymer synthesis procedures are first defined along with the various analytical methods used to characterize the three PAN samples used. Following this, the procedures used for preparing solutions of these PAN materials in various solvent-additive combinations are defined and characterization methods for various solution properties viz. dilute and concentrated solution rheology and cloud-point curves are described. Finally, the procedures used for membrane preparation and performance / morphology characterization are summarized.

### 2.1 Polymer synthesis and characterization

#### 2.1.1 Materials

Acrylonitrile was procured from Thomas and Baker Company, India and further purified according to the process of Chiang and Hu [1985]. Acrylonitrile was washed sequentially with NaOH (3 % solution w/w), then orthophosphoric acid (3 % solution w/w) and finally several times with water. It was then kept overnight under  $\text{CaCl}_2$  followed by distillation under vacuum at  $90^\circ\text{C}$ .

Reagent grade potassium persulfate and sodium bisulfite, sodium hydroxide, methanol, DMF, Lithium Chloride, Zinc Chloride and Aluminum Chloride were procured from S.D. Fine chemicals, India and used as received unless otherwise mentioned. The acrylamide used for the synthesis of the copolymer used was of electrophoresis grade.

Three grades of PAN's are used for the work done in the thesis. The first, designated as PAN-A, is a commercially available polymer, obtained from IPCL, Vadodara. The material was purified prior to use by dissolving the polymer in N'N' Dimethyl formamide (DMF) and precipitating the resulting ~10% w/w solution in excess methanol followed by vacuum oven drying at  $70^\circ\text{C}$  for three to four days.

Two other higher molecular weight grades of PAN were synthesized from acrylonitrile monomer; designated as PAN-B and PAN-C.

### 2.1.2 Polymer synthesis

Higher molecular weight (MW~ 168 kDa and 250 kDa) PAN's were obtained by polymerizing acrylonitrile using a redox initiator system:  $K_2S_2O_8$  and  $NaHSO_3$  under nitrogen atmosphere [Prince and Hornyak, 1967]. The polymers with different MW were obtained by varying the reaction temperature and / or initiator concentration. As described above, acrylonitrile was extensively purified by several washing steps, followed by vacuum distillation before polymerization with the redox-initiator system. The typical proportions of the redox initiator system are tabulated in the following Table 2.1.

**Table 2.1:** Typical proportions of the redox-initiator system used for preparation of the polymer of the higher molecular weight.

Code	Monomer	$K_2S_2O_8$	$NaHSO_3$	Solvent	Molecular weight
PAN-B	80.02g	0.8723g	0.2038g	240.00g	168kDa
PAN-C	60.01g	0.6501g	0.1545g	179.30g	250kDa

The reaction was stirred at 50°C in an inert atmosphere till a solid mass was formed; for PAN-B this stirring time was 1.5 hrs while for PAN-C, the stirring time was 2 hrs. The white solid mass obtained was precipitated in methanol, dried at 70°C and further purified by re-dissolving in DMF and precipitating in methanol, followed by vacuum drying at 70°C for several days.

The polymer was purified and various techniques (FT-IR, H-NMR, and elemental analysis described in section 2.1.4) were used to confirm the polymer structure as essentially (-  $CH_2$  - $CH(CN)$  -). Dilute solution viscosity measurements were made at 25°C to estimate the molecular weight (MW) from the intrinsic viscosity  $[\eta]$  and reported Mark-Houwink constants [Beever, 1968]

The molecular weight of PAN-A is estimated to be ~50kDa. The two higher molecular weight grades of PAN synthesized from acrylonitrile monomer are designated as PAN-B and PAN-C. The MW of PAN-B was estimated to be ~168kDa while that of PAN-C was ~250kDa. The chemical structure of various PANs are also confirmed from  $^1H$ -NMR spectrum measured in deuterated dimethyl sulfoxide (DMSO-d6) using Bruker



NMR spectrometer (Model No.80) working at 200 MHz frequency and elemental analysis, done using a Carlo Erba elemental analyzer (Model No.1108). This characterization is essential as a basis for the further work relating to the solution and membrane formation properties of these polymers and copolymer.

### ***2.1.3 Copolymer synthesis***

Since the commercial PAN-A may also contain a small degree of hydrolyzed groups, we also synthesized a PAN (acrylamide: acrylonitrile) (12:88) copolymer. This copolymer was used in limited work- the focus of the thesis remains on the three PAN grades described above. The copolymer was prepared by the procedure of Bhadani and Kundu [1980]. In order to prepare the copolymer, acrylamide and acrylonitrile in the mole ratio of 12:88, was dissolved first in DMF at 50 % by weight of the total monomer concentration. The 50 % monomer solution in DMF was then degassed and flushed with nitrogen. Specifically 40.89g of acrylonitrile and 9.67g of acrylamide monomers were mixed together in a conical flask to which 100 ml DMF was added. This was immediately followed by the addition of 0.852gm i.e. 0.6ml concentrated HNO<sub>3</sub>. Concentrated HNO<sub>3</sub> (0.0657 moles/l) was added as an initiator and the copolymerization was carried out with constant stirring at 80°C for 10 hrs. The copolymer thus obtained in the form of a viscous mass was precipitated in methanol. It was redissolved in DMF and precipitated in MeOH. The copolymer so obtained was then vacuum dried at 70°C for 4 days. FT-IR, H-NMR, and elemental analysis were used to characterize the structure of the copolymer formed.

### ***2.1.4 Polymer Characterization Results***

#### ***2.1.4.1 Elemental analysis***

Table 2.2 shows the observed wt % elemental composition of the three acrylonitrile homopolymers and copolymer.

**Table 2.2:** Wt % elemental composition of the three acrylonitrile homopolymers and the copolymer of acrylonitrile with acrylamide.

Polymer	C	H	N	O
PAN-A	66.0	6.4	24.7	2.9
PAN-B	65.7	6.7	25.4	2.4
PAN-C	65.7	6.2	25.7	2.4
PAN expected	67.9	5.7	26.4	-
PAN-1	63.0	6.6	21.6	11.3
Expected for 12:88 copolymer	64.6	5.9	25.1	4.3

The elemental analysis of the homopolymers is generally consistent with the expected poly(acrylonitrile) ( $-\text{CH}_2-\text{CH}(\text{CN})-$ ) structure. The higher content of H and O observed in the polymers may be due to absorption of moisture during handling. The elemental analysis of the copolymer is not very consistent in case of the N and O content with a 88:12 ratio of acrylonitrile : acrylamide. The discrepancies may be related to residual DMF solvent, FT-IR shows broad peaks in the hydroxyl group ( $-\text{OH}$ ) region from  $3000-3500\text{cm}^{-1}$ , consistent with some residual solvent remains. It is well known in literature [Padhye and Karandikar, 1985] that the removal of solvent from PAN and its copolymers is difficult as the DMF is bound to the nitrile groups by dipole-dipole interactions.

#### 2.1.4.2 Fourier Transform Infrared Spectroscopy (FTIR)

The FTIR Spectra for PAN-A, PAN-B, PAN-C are shown in Figures 2.1 - 2.3 respectively.

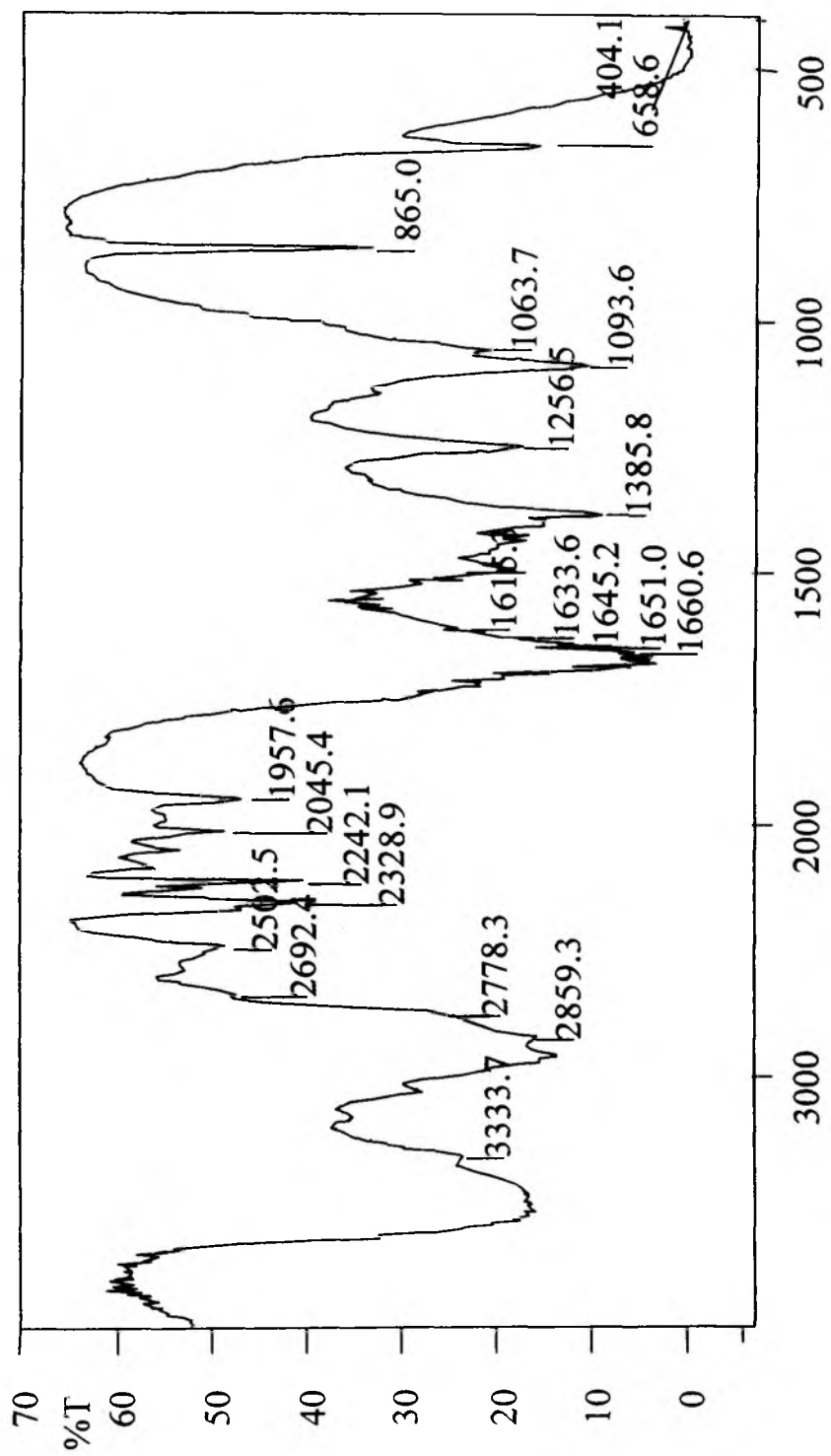


Figure 2.1: FTIR spectra of a 7 % w/w PAN-A solution in pure DMF.

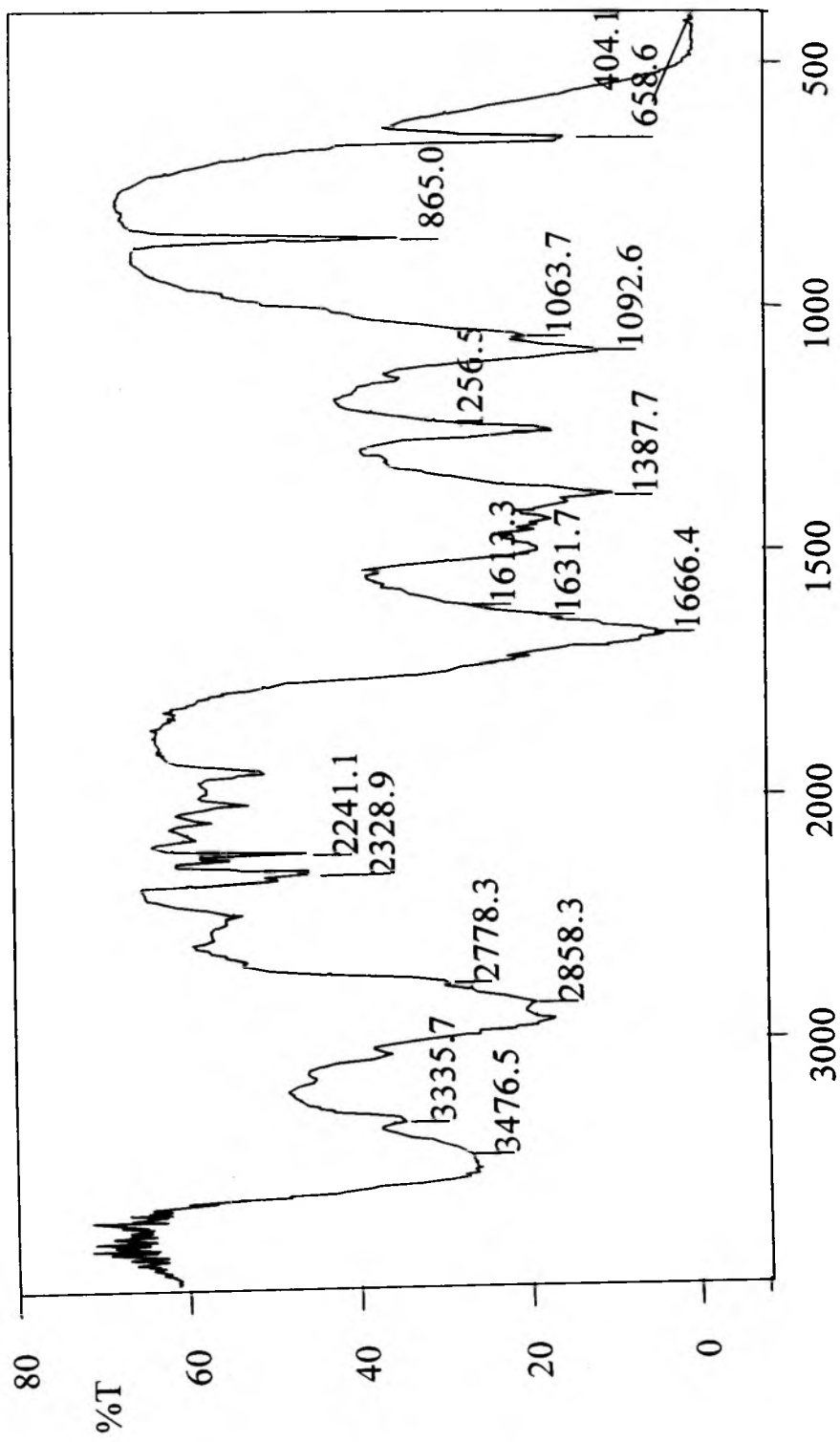


Figure 2.2: FTIR spectra of a 7 % w/w PAN-B solution in pure DMF.

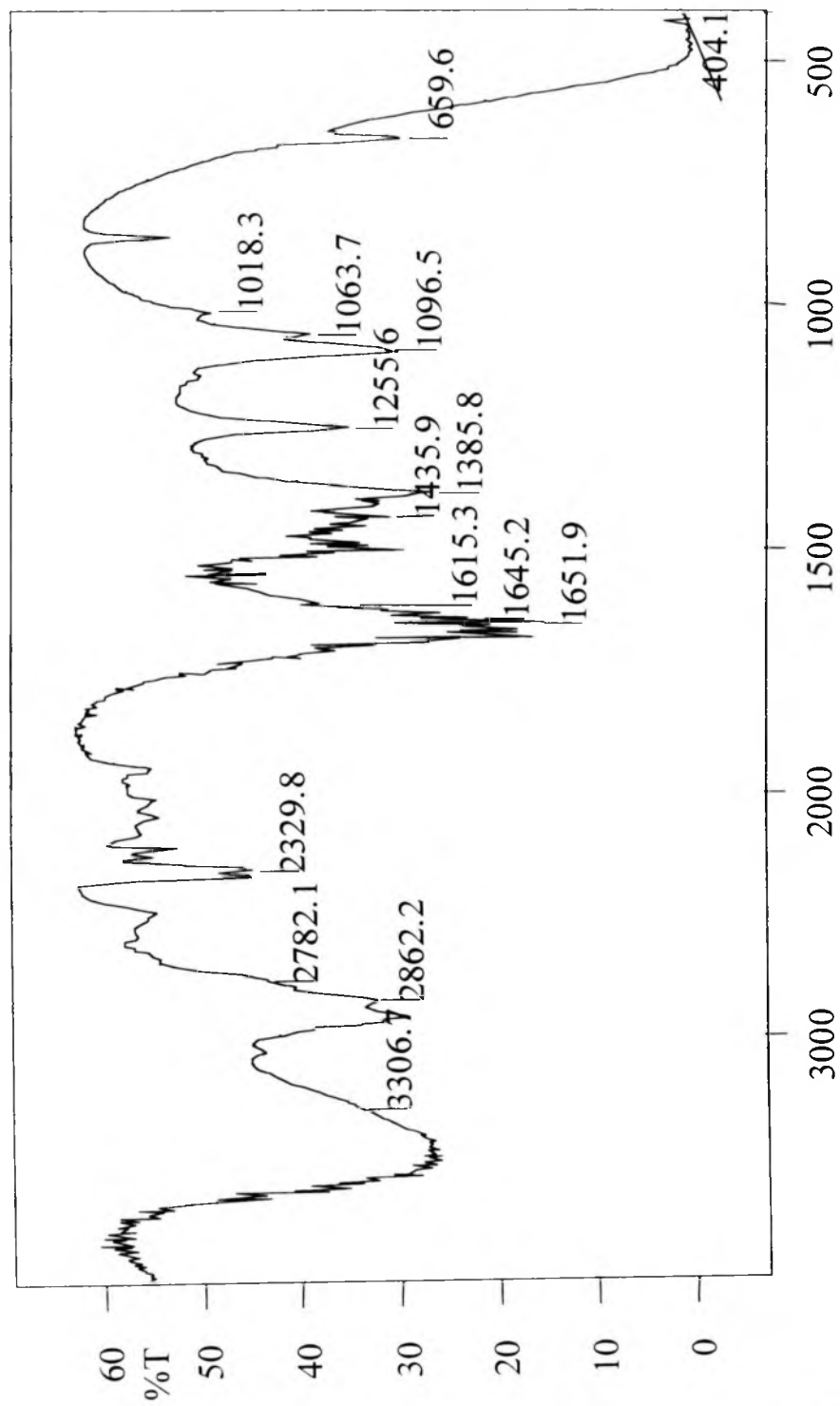


Figure 2.3: FTIR spectra of a 7 % w/w PAN-C solution in pure DMF.

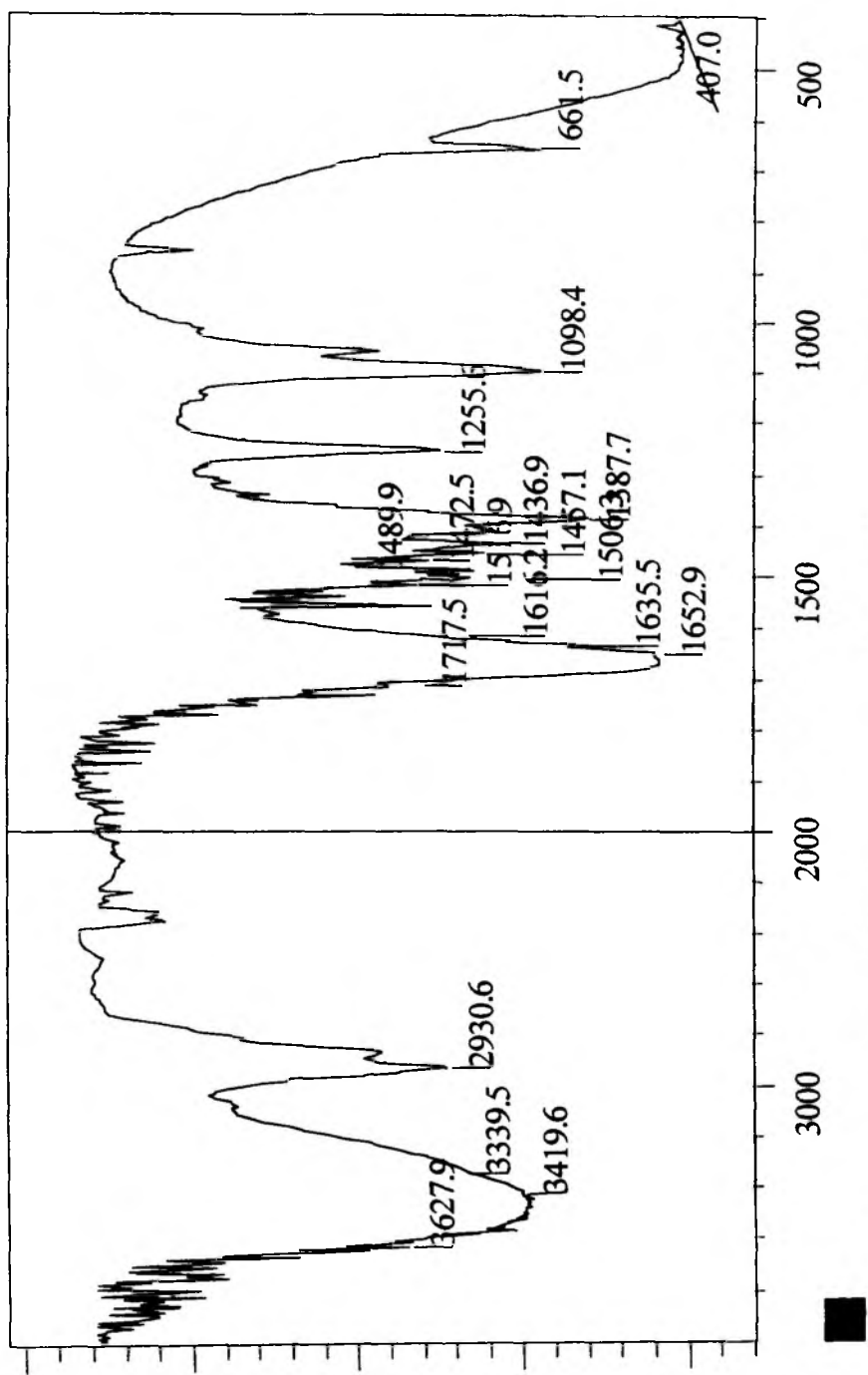


Figure 2.4: FTIR spectra of a 7 % w/w copolymer PAN-1 solution in pure DMF.

The assignment of the various spectral bands in these figures to various chemical functionalities are shown in Table 2.3 [Liang and Krimm, 1958; Jacob and Arof, 2000].

**Table 2.3:** Spectral band (FTIR) assignment for PAN homopolymers: PAN-A, B and C.

660 $\text{cm}^{-1}$	-C-N bending in residual DMF H-CO-N-(CH <sub>3</sub> ) <sub>2</sub>
1660 $\text{cm}^{-1}$	-C=O stretching in residual DMF H-CO-N-(CH <sub>3</sub> ) <sub>2</sub>
1730 $\text{cm}^{-1}$	-C=O stretching PAN
2250 $\text{cm}^{-1}$	-C≡N stretching
2938 $\text{cm}^{-1}$	antisymmetric stretching mode of skeletal-CH <sub>2</sub> group
2950 $\text{cm}^{-1}$	antisymmetric stretching mode of skeletal-CH <sub>2</sub> group
1435 $\text{cm}^{-1}$	-CH <sub>2</sub> bend + -CH bend + -CH <sub>2</sub> wagging vibrations
1385 $\text{cm}^{-1}$	-CH bending vibration
1256.5 $\text{cm}^{-1}$	-CH wagging + -CH <sub>2</sub> wagging + C-C stretching vibration
1063.7 $\text{cm}^{-1}$	C-C stretching + CH <sub>2</sub> rock + C-C-CN bending vibration
3333.7 $\text{cm}^{-1}$	residual moisture absorbed by the polymer

The spectra in Figures 2.1-2.3 in combination with the assignments in Table 2.3 show that the synthesized polymers PAN-B and PAN-C have the expected (-CH<sub>2</sub>-CH(CN)-) structure. The structure of these synthesized materials is very similar to that of PAN-A, which is the commercially available polymer. The signal at 3333  $\text{cm}^{-1}$  may correspond to a small fraction of hydrolyzed groups but is more likely due to moisture absorbed by the polymer samples.

The spectra (Figure 2.4) for the copolymer of acrylonitrile and acrylamide (88:12 mole ratio) is similarly assigned to the various structural features shown in Table 2.4.

**Table 2.4:** Spectral band (FTIR) assignment for the Polyacrylonitrile and acrylamide (88:12) copolymer PAN-1.

1600-1700cm <sup>-1</sup>	-C=O stretching in -CO-NH <sub>2</sub>
2240-2250cm <sup>-1</sup>	-C≡N stretching
3180-3200cm <sup>-1</sup>	-NH <sub>2</sub> stretching
3340-3360cm <sup>-1</sup>	-NH <sub>2</sub> stretching
3420-3460cm <sup>-1</sup>	-NH <sub>2</sub> stretching

#### 2.1.4.3 NMR spectroscopy

The <sup>1</sup>H<sub>1</sub> spectra for PAN-A, PAN-B, PAN-C and PAN-1 showed distinctive peaks which were in agreement with the assignments made by Matsuzaki et al, 1960 as shown in Table 2.5-2.6.

**Table 2.5:** Proton NMR peak assignment for the homopolymers PAN-A, B and C.

2.15 ppm	s, 2H, -CH <sub>2</sub> -
2.50 ppm	m, Residual protons in DMSO-d <sub>6</sub>
2.75 ppm	s, 3H, -CH <sub>3</sub> from residual DMF
2.90 ppm	s, 3H, -CH <sub>3</sub> from residual DMF
3.10 ppm	s, 1H, -CH-
3.70 ppm	s, Water absorbed by DMSO

The FTIR, <sup>1</sup>H<sub>1</sub> Proton as well as the elemental analysis confirm the structure of the synthesized polymers B and C and the commercial grade PAN-A to be that of Polyacrylonitrile (- CH<sub>2</sub> -CH(CN) -).



**Table 2.6:** Proton NMR peak assignment for the Polyacrylonitrile and acrylamide (88:12) copolymer.

2.05 ppm	s, 2H, -CH <sub>2</sub> -
2.50 ppm	M, Residual protons in DMSO-d <sub>6</sub>
2.75 ppm	s, 3H, -CH <sub>3</sub> from residual DMF
2.90 ppm	s, 3H, -CH <sub>3</sub> from residual DMF
3.10 ppm	s, 1H, -CH-
3.3-3.5 ppm	s, Water absorbed by DMSO-d <sub>6</sub>
7.15 ppm	s, 1H, -NH <sub>2</sub> (cis to -C=O group)
7.75 ppm	s, 1H, -NH <sub>2</sub> (trans to -C=O group)
8.0 ppm	s, 1H, H-CO-N(CH <sub>3</sub> ) <sub>2</sub> from residual DMF

#### 2.1.4.4 Intrinsic viscosity

Dilute solution viscosity measurements were made at 25°C to estimate the molecular weight (MW) from the intrinsic viscosity  $[\eta]$  and reported Mark-Houwink constants ( $K' = 3.17 \times 10^{-4}$ ,  $a = 0.75$ ) [Beever, 1968]. The viscosity-average molecular weight increases in the order PAN –A < B < C (see Table 2.7). The copolymer has a comparatively smaller degree of polymerization.

**Table 2.7:** The intrinsic viscosity and molecular weight calculated using the Mark-Houwink equation.

Code	Intrinsic Viscosity $[\eta]$	Molecular weight kDa
PAN-A	1.06	50,003
PAN-B	2.63	1,67,956
PAN-C	3.55	2,50,549
PAN-1	0.81	34,933

## 2.2 Solution studies

Dilute and concentrated solutions in DMF were made with the three PAN polymers in the presence of mono-, bi -and trivalent inorganic additives: LiCl, ZnCl<sub>2</sub> and AlCl<sub>3</sub>. The solvent (DMF) and additives (LiCl, ZnCl<sub>2</sub>, AlCl<sub>3</sub>) used were of reagent grade (SD Fine Chemicals, India). The concentration of each additive in DMF was standardized at a constant ionic strength (0.8338 M). The notations used for both the solutions as well as the membranes cast from these are in the format: PAN-x-y where, x represents the PAN grade i.e. PAN-A, -B -C and the PAN-1 for the copolymer, and y represents the additive i.e. blank (DMF only), L = LiCl, Z = ZnCl<sub>2</sub>, A = AlCl<sub>3</sub>.

Depending on the context, this same nomenclature denotes either the solution type or the corresponding membrane formed from this solution. The notations used for both the solutions as well as the membranes cast from these as mentioned above become as follows:

PAN-A : PAN-A dissolved in DMF alone

PAN-A-L : PAN-A dissolved in DMF plus LiCl

PAN-A-Z : PAN-A dissolved in DMF plus ZnCl<sub>2</sub>

PAN-A-A : PAN-A dissolved in DMF plus AlCl<sub>3</sub>

The same notations are used for the Polymers B and C as well as the copolymer PAN-1 viz. PAN-B, PAN-B-L etc. Depending on the context, this same nomenclature denotes either the solution type or the corresponding membrane formed from this solution.

### 2.2.1 Dilute Solution studies

Solution viscosities were measured in the dilute polymer concentration range (< 0.3%) at 25-45°C. The dilute solution viscosity data was used to calculate the viscosity activation energy for each type of solution. The effect of additive type on intrinsic viscosity of polymer solution was measured for all three polymers and the copolymer using 0.1, 0.2 and 0.3 % w/w solutions made in pure DMF and DMF containing salts (LiCl, ZnCl<sub>2</sub> and AlCl<sub>3</sub>, separately).

The polymers were dried in vacuum oven overnight at 70°C and the salts were dried at 50°C for 6 hr. before dissolving it in the solvent dimethyl formamide. The solutions after addition were dissolved overnight on a magnetic stirrer (speed set at 600 rpm) to obtain a clear solution which was filtered before addition of the polymer.

The solvent and solution flow times were measured with an auto-viscometer (Schott Gerate, Model AVS 440) in a constant temperature bath at 25, 35 and 45°C. Each measurement was carried out in triplicate and the measurement reproducibility was  $\pm 0.01\%$ . Viscosity activation energies were calculated from the dilute solution viscosity measurements.

### 2.2.2 *Concentrated solution viscosity*

Solution viscosities were also measured at 30°C in a cone and plate viscometer at the higher concentrations,  $c$ , more typical of casting solutions. These data were used to estimate the shear thinning indices and also the dependence of the solution viscosity on the coil overlap parameter ( $\beta = [\eta] c$ )

Concentrated polymer solutions in the range of 1-17 % w/v were made with and without the additive for all the three polymers PAN-A, B and C. The solutions with polymers B and C were dissolved in a constant temperature bath at 75°C with intermittent shaking for 12-15 hr. due to the long time required for solubilization at ambient temperature.

The viscosities were measured at 30°C using a Brookfield Cone and Plate viscometer (DV-I) as a function of shear rate. There were two different spindles used cp-40 for the solutions with low viscosities while cp-52 for the very concentrated/viscous solutions. The shear rate range for spindle cp-40 is between 3.75-750  $\text{sec}^{-1}$  while that for spindle cp-52 is 1-200  $\text{sec}^{-1}$ .

### 2.2.3 *Cloud point study*

The precipitation behavior of PAN solutions with and without additives for all the three polymers and the copolymer was studied by determining the cloud point (point of incipient precipitation) in ternary systems consisting of polymer-water-solvent. Solvent in this case represents either DMF alone or DMF+ the individual salt additive.

The cloud point was determined by a sudden increase in the turbidity on addition of small aliquots of non-solvent (distilled water) to the polymer solution. A solution of known concentration (0.1-0.3 % w/v) was taken in a stoppered conical and the non-solvent was added in aliquots with high speed stirring. The opaqueness / turbidity was observed visually.

Cloud point measurements for the various PAN-water-DMF+salt systems were made visually at low PAN concentrations (0.1-0.3 %w/v). The data with these dilute polymer solutions were extrapolated to higher concentration values using a linearized ternary phase boundary equation. The linearized cloud point (LCP) curve (Equation 2.1) is interpreted by Boom et al [1993] in terms of the various parameters occurring in the Flory-Huggins theory.

$$\ln \frac{\phi_{NS}}{\phi_P} = b \ln \frac{\phi_S}{\phi_P} + a \quad (2.1)$$

Where  $\phi$  is the volume fraction and subscripts NS, P and S indicate non-solvent, polymer and solvent respectively.

The intercept  $a$  depends on enthalpy factors and is a function of the Flory-Huggin's interaction parameters. Parameter  $b$  depends on the respective molar volumes as detailed in section 1.7.1.

## 2.3 Membrane preparation and characterization

Membrane characteristics were principally measured by water flux, solute rejection, pore size distribution by bubble point measurements in water and iso-propanol and by scanning electron microscopy (SEM).

### 2.3.1 Membrane Preparation

#### 2.3.1.1 Membrane preparation for PAN-A

Solutions were prepared by dissolving PAN-A (0.01 -17 % w/v) in either DMF alone or in DMF containing 4% (w/w) of each individual additives (LiCl, ZnCl<sub>2</sub> or

Membranes were cast mainly from solutions containing 13% PAN-A dissolved in the above solvent combinations. Solutions were allowed to stand overnight before casting and then knife coated on a continuously moving non-woven polyester backing of 50  $\mu\text{m}$  thickness. The cast film was gelled in water at 20°C after a short air dwell time of 7 seconds. The formed membranes were washed overnight in flowing water, rinsed several times in distilled water and preserved at 10°C until use.

### 2.3.1.2 Membrane preparation for PAN-B and PAN-C

Solutions were prepared by dissolving PAN-B and PAN-C (3 -11 % w/v) in either DMF alone or in DMF containing of individual additives like LiCl, ZnCl<sub>2</sub> and AlCl<sub>3</sub>. The concentration of each additive in DMF was standardized at a constant ionic strength (0.8338 M). These salt concentrations correspond to w/w concentrations of 3.5345 for LiCl, and 3.7845 for ZnCl<sub>2</sub> and 3.3553 for AlCl<sub>3</sub>.

PAN-B and PAN-C membranes were typically hand-cast from solutions containing 7-11% of PAN dissolved in DMF solutions with and without the salt additives. PAN-B and PAN-C were not cast on the continuous web coating machine as was done for PAN-A because of the limited supply of these lab synthesized materials. Solutions were allowed to stand overnight before hand casting on a glass plate with a uniform glass rod. The thickness of the membrane was adjusted to ~150-170  $\mu\text{m}$  with the help of cellophane tape windings on the glass rod and dragging it to obtain a membrane of uniform thickness. The cast film was gelled in water at 20°C after a short air dwell time of 7 seconds. The formed membranes were washed overnight in flowing water, rinsed several times in distilled water and preserved at 10°C until use.

The hand casting method resembled the continuous method; however, potentially important differences are (i) the absence of the polyester web backing in handcast samples and (ii) the differences in salt concentrations (constant w/w concentration in section vs constant ionic strength in this section). To eliminate these issues, several PAN-A membranes were also cast by the identical method as used for the PAN-B and PAN-C described here. PAN-A membranes made by the continuous method described in section 2.3.1.1 are discussed in Chapter IV. The hand-cast membrane performances for all three PAN grades are compared in Chapter V.

### **2.3.2 Permeability measurements**

The distilled water fluxes were measured at 200 kPa in a 13.4 cm<sup>2</sup> stirred cell assembly (Amicon) at 25°C for membranes made from all the three polymers. The membrane piece was cut exactly of the size of the stirred cell assembly and was filled with distilled water followed by the application of a pressure of 200 kPa and the water permeation rate through the membrane was measured using a digital stopwatch for a specific volume measured from which the flow rate was calculated. [Kesting, 1971] The permeation rate for water was measured in triplicate to check the reproducibility, which was within experimental error. The standard deviations of the water fluxes are 20% of the average value.

Protein rejection studies were done in a detailed manner for PAN-A, Due to limited availability of the synthesized polymer material; detailed investigations for membranes made from the two polymers PAN-B and PAN-C could not be done. Only one set of BSA protein rejection data of PAN-B at different polymer concentrations was measured.

The ultrafiltration experiments with PAN-A membrane at 100 kPa and 25°C were carried out in the same assembly as used for the water permeability measurements. The UF test solutions used were (i) BSA (0.1 g/dl) and (ii) lysozyme (0.05 g/dl) solutions prepared in phosphate buffer (pH 7.5) and with (iii) PEG (M.W. 9,000 daltons) solution (0.5 g/dl) in distilled water. All feed solutions were filtered through Whatman paper (No. 1) prior to the UF run. The protein concentrations in the feed and permeate samples were determined using a spectrophotometer (Shimadzu, UV-240) at 280 and 260 nm [Jayaraman, 1981]. PEG concentrations were determined by the method of Sims and Snape [1980]. The PEG estimation depends on a complex formation method which is time based and the complex formed at the 20<sup>th</sup> minute absorbs at 535 nm, which estimates the amount of protein in the samples. The permeate flux and solute rejection data at a volume concentration factor of 1.9 were obtained in duplicate for each solute and averaged. The experimental error within the solute rejection was  $\pm 4\%$ .

PAN-B coupon samples were analyzed in a similar manner to that of PAN-A.

PAN-B coupon samples were analyzed in a similar manner to that of PAN-A.

### 2.3.3 Bubble point/pore size distribution measurements

The determination of the largest pores present on the membrane surface (13.4 cm<sup>2</sup> samples) was made by the standard bubble point technique with both water and isopropanol wetted membranes. The pore and pore size distribution was determined by the well-known bubble point method [Kesting, 1971]. In this method, water imbibed within the membrane pores is displaced by air with a constant increment (*i*) of pressure. Since the water /air interfacial tension is high (73 dynes/cm<sup>-1</sup>), the detection of small pores with this method requires correspondingly higher pressures, which can cause pore structure damage. Therefore instead of water, iso-propanol (IPA) was used as the imbibed phase (interfacial tension 27 dynes/cm<sup>-1</sup>) which enables lower applied pressure measurement of smaller pores.

The pore number density was calculated using Cantor's relation:

$$r_{pi} = \frac{2\sigma \cos \theta}{P_i} \quad (2.2)$$

where,  $\theta$  is the polymer /water (or iso-propanol) contact angle and  $P_i$  is the applied pressure.

The number of pores per unit area ( $n_i$ ) were calculated as follows:

$$n_i = \left[ J_i - \frac{J_{i-1} P_i}{P_{i-1}} \right] \frac{8\mu l}{\pi P_i r_{pi}^4} \quad (2.3)$$

where,  $\mu$  is the viscosity of the flowing fluid and  $l$  is the pore length which is assumed to be equal to the membrane thickness. The fluxes  $J_i$  correspond to the flux measured at the  $i^{\text{th}}$  increment of the pressure ( $P_i$ )

In the case of isopropanol wetted samples, the air flux measurements were also continued till higher pressures (400 kPa) in order to get the leading edge of the pore size

#### ***2.3.4 Membrane structure***

The membrane morphology was studied using a scanning electron microscope. The SEM membrane samples of the polymers PAN-A, B and C with and without additives were prepared by soaking water-wet membrane samples sequentially in two solvents: iso-propanol (30 min.), and hexane (30 min.) followed subsequently by vacuum drying at 50°C for 24 hours. The dried membranes were cryogenically fractured in liquid nitrogen to examine the cross-sectional views. The fractured samples were mounted on small stubs and a silver paste was applied to it as a conductor after which they were sputtered with a fine gold coating prior to viewing the samples.



## Chapter III

This chapter summarizes spectroscopic and dilute solution viscosity measurement studies performed to investigate the nature of interactions between the various salts, DMF and PAN. This information will be used to interpret the casting solution and resulting membrane properties discussed in Chapters IV and V.

### 3.1 Experimental

#### 3.1.1 *Fourier Transform Infrared (FTIR) spectroscopic measurements*

Analytical samples of the commercially available polymer PAN-A and the two synthesized polymers PAN-B and PAN-C (synthesis procedure described in section 2.1.2) were prepared by dissolution in DMF with and without the salt additive as specified. All three salts were added to DMF keeping the ionic strength constant at 0.83M for all the studies reported here. The polymer concentration of the solutions prepared for the FT-IR study used was 7% w/v. The only exceptions were the two higher MW PAN samples with DMF+ ZnCl<sub>2</sub>; PAN-B-Z had only 5% w/v polymer and PAN-C-Z was at 3% w/v due to solubility problems at higher polymer concentrations in these systems. The DMF and LiCl used were of Laboratory Reagent grade (L.R.) from S. D. Fine Chemicals; ZnCl<sub>2</sub> was of Guaranteed Reagent grade (G.R.) from Loba, and AlCl<sub>3</sub> was procured from Sarabhai Chemicals, India.

FT-IR spectra were obtained using a Shimadzu spectrometer (Model 8300 with a resolution of 1-4 cm<sup>-1</sup>.) in the range of 4000-500 cm<sup>-1</sup>. FT-IR studies were done for each salt additive, first with the combined solvent i.e. DMF + salt. These salt + solvent combinations are denoted as DMF-L, DMF-Z and DMF-A for the 3 additives, Li, Zn, and Al chlorides, respectively. After measuring the FT-IR spectra of the DMF-salt solution, FT-IR was used to characterize PAN solutions in DMF alone and then in DMF + salt.

The spectra of the neat polymer solutions were compared to DMF while spectra of polymer solutions with salt present were compared to DMF with the corresponding additive. The polymer (PAN-A) solutions in DMF containing the corresponding salts

are designated as PAN-A-L, PAN-A-Z and PAN-A-A. The solutions of the other two polymers (PAN-B and PAN-C) are similarly designated. Depending on the context, PAN-A may refer either to the polymer itself or to its solution in neat DMF.

### **3.1.2 Dilute solution viscosity studies**

The effect of additive type on the rheology of dilute PAN solutions (0.1-0.3% w/w) was measured for all three polymers using neat DMF and DMF containing salts (LiCl, ZnCl<sub>2</sub> and AlCl<sub>3</sub>, separately) as solvents. An Ubbelohde viscometer with a capillary diameter of 0.64mm was used. The solvent and solution flow times were measured with an auto-viscometer (Schott Gerate, Model AVS 440) in a constant temperature bath at 25, 35 and 45°C. Each measurement was carried out in triplicate and the measurement reproducibility was ±0.01%. The same materials were used for these studies as described above in section 3.1.1.

## **3.2 Specific interactions between Salts, DMF and PAN: FTIR studies**

As described above, FT-IR studies were used as a method of identifying the type and strength of interactions between PAN, DMF solvent and the three salt additives (Li, Zn, and Al chlorides). Literature studies (sections 1.2-1.3) indicate that these salts may modify solution properties by interactions with either solvent DMF molecules or with PAN.

### **3.2.1 FTIR studies of DMF+ salts**

As reported by Jacob and Arof [2000], the major characteristic bands for pure DMF arise from >C=O stretching, OC-N stretching and O-C-N bending vibrations. The FT-IR spectra for pure DMF and salt-DMF solutions in the regions of 1800-1500 cm<sup>-1</sup> (>C=O stretching), 1450-1300cm<sup>-1</sup> (OC-N stretching) and 750-500 cm<sup>-1</sup> (O-C-N bending) are shown in Figures 3.1a, 3.1b and 3.1c respectively. Table 3.1 summarizes the change in the IR spectra for each of these molecular motions.

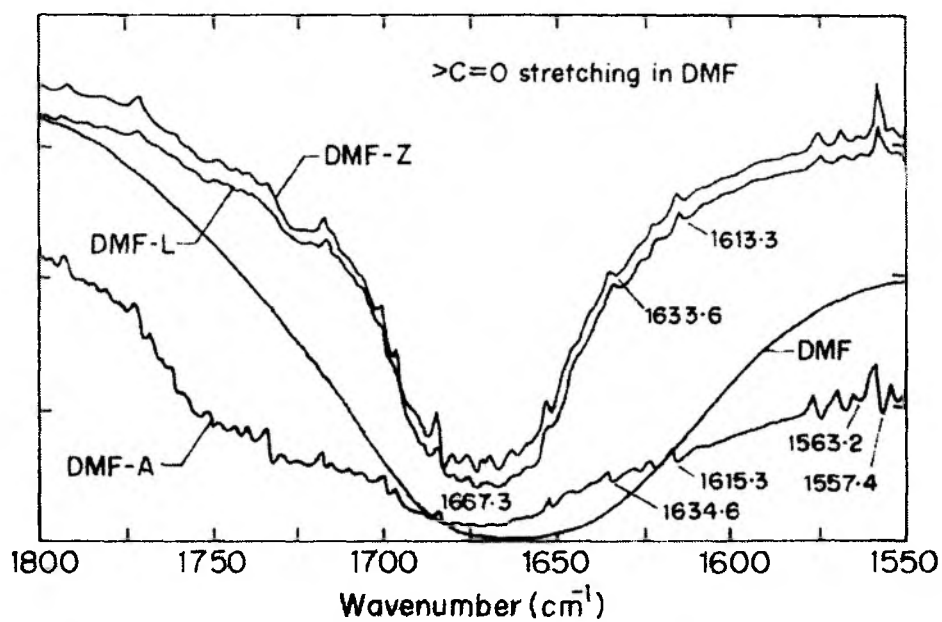


**Figure 3.1a:** Effect of salt addition on >C=O stretching frequency of DMF.

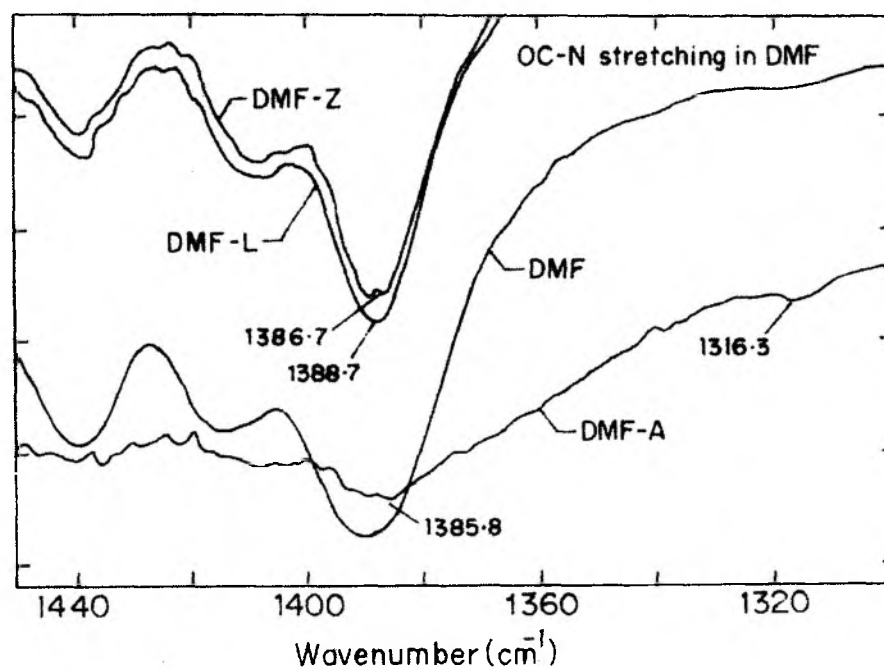


**Figure 3.1b:** Effect of salt addition on OC-N stretching frequency of DMF.

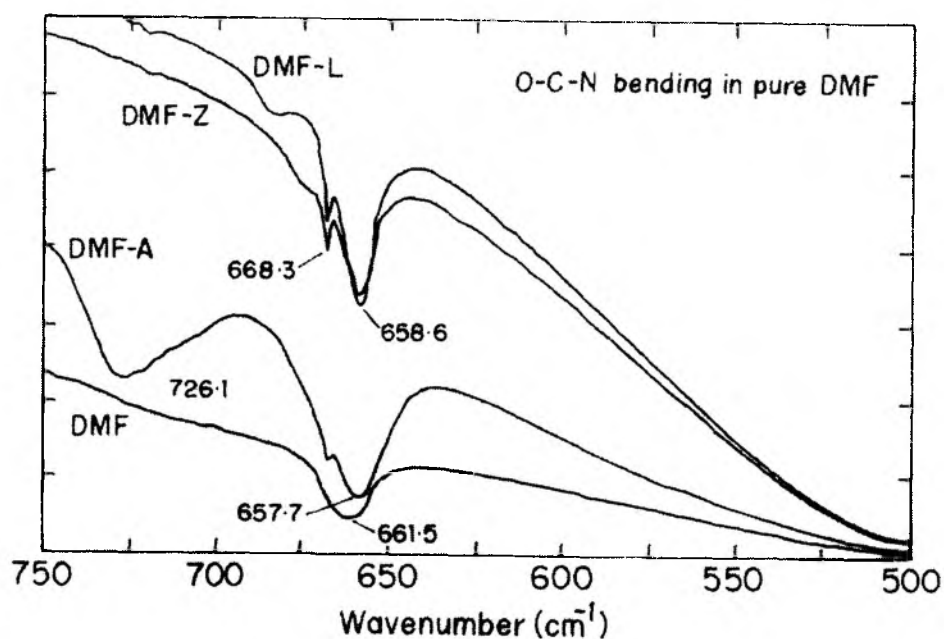


**Figure 3.1c:** Effect of salt addition on O-C-N bending frequency of DMF.

**Table 3.1:** The effect of salt addition on the  $>C=O$  stretching, OC-N stretching and O-C-N bending frequencies of DMF (summary of Figures 3.1 a-c).

Additive to DMF	Interaction identified	Change in IR frequency ( $\text{cm}^{-1}$ )		
		$>C=O$ stretching	OC-N stretching	O-C-N bending*
LiCl	Salt complexes with the electronegative carbonyl O	1667.3 $\rightarrow$ 1667.3	1390 $\rightarrow$ 1388.7	661 $\rightarrow$ 658.6
ZnCl <sub>2</sub>		1667.3 $\rightarrow$ 1661.6	1390 $\rightarrow$ 1386.7	661 $\rightarrow$ 658.6
AlCl <sub>3</sub>		1667.3 $\rightarrow$ 1667.3	1390 $\rightarrow$ 1385.8	661 $\rightarrow$ 657.7

\* In addition a new peak is observed at  $667 \text{ cm}^{-1}$  for all three salt solutions

Literature studies, summarized in Table 1.1 suggest that the salt cations will complex strongly with the electronegative carbonyl O of DMF. The higher electronegativity of oxygen compared to nitrogen implies a higher electron density near oxygen. Hence, it is reasonable that the Lewis acid cation complexes with the carbonyl oxygen of DMF rather than the amide N, as conceptually illustrated in Figure 3.2.

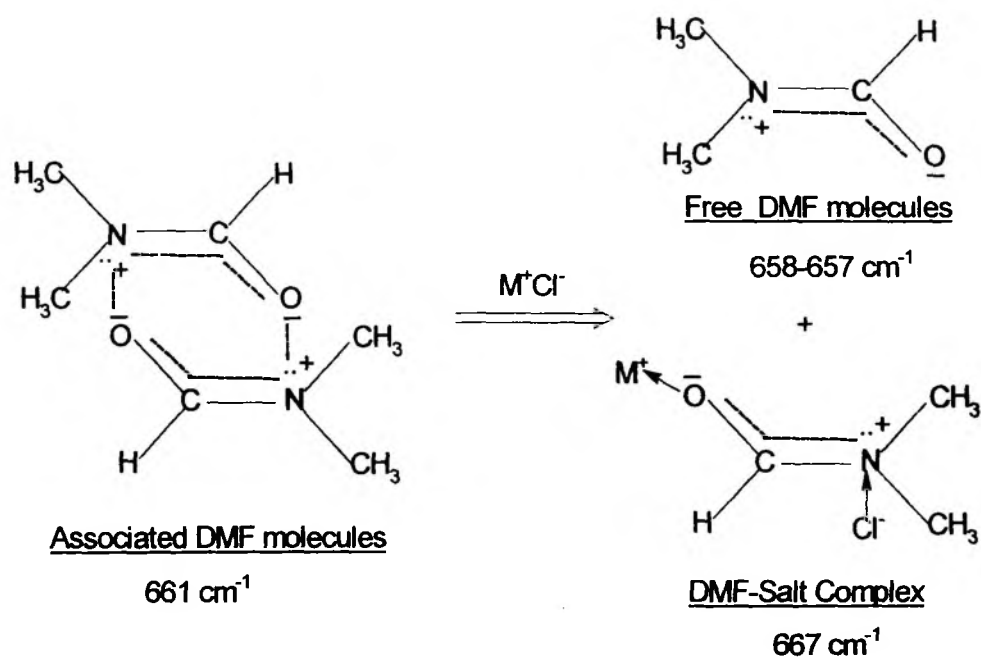


**Figure 3.2:** Depiction of various populations of DMF molecules in DMF-salt solutions. Also shown are the assignments for the O-C-N bending frequency.

The  $>\text{C}=\text{O}$  stretching frequency (Figure 3.1a) observed at  $1667.3$  in pure DMF remained essentially unchanged in both DMF-L and DMF-A, whereas a red shift by  $\sim 6$   $\text{cm}^{-1}$  was observed for DMF-Z. This finding is consistent with Waghorne and Rubalcava [1982] who observed that the carbonyl stretching frequency for deuterated DMF decreased slightly from  $1645$   $\text{cm}^{-1}$  to  $1642$ , and  $1644$   $\text{cm}^{-1}$  after addition of perchlorate salts of  $\text{Li}^+$ , and  $\text{Al}^{3+}$ , respectively, but decreased substantially to  $1632$  after addition of  $\text{Zn}^{2+}$  perchlorate. An explanation for these observations is given below.

A decrease in carbonyl stretching frequency implies a decrease in  $>\text{C}=\text{O}$  bond order. The ionic radii of the various cations are shown in Table 3.2.

**Table 3.2:** The ionic radii of various cations [Waghorne and Rubalcava, 1982]

Ion	Ionic radii, Å	Ionic radius ratio Cl <sup>-</sup> / M <sup>+</sup>
Li <sup>+</sup>	0.68	2.85
Zn <sup>2+</sup>	0.74	2.62
Al <sup>3+</sup>	0.50	3.88
Cl <sup>-</sup>	1.94*	

\* calculated from above Li<sup>+</sup> ion radius and ratio (0.35) of radii of Li<sup>+</sup> and Cl<sup>-</sup> reported by Glasstone [1946]

The ionic radius ratio implies that the electronic cloud is highest around Al<sup>3+</sup> and least around Zn<sup>2+</sup>. Thus, energy required for complexation of the electronegative carbonyl O of DMF with various cations would be highest for Al<sup>3+</sup>, followed by Li<sup>+</sup> and least for Zn<sup>2+</sup>. This reasoning explains why a red shift in >C=O stretching frequency was observed in DMF-Z, whereas insignificant changes were observed in case of DMF-L and DMF-A.

We have observed the OC-N stretching frequency to decrease from 1390 cm<sup>-1</sup> in pure DMF to 1388.7, 1386.7 and 1385.8 cm<sup>-1</sup> after addition of Li<sup>+</sup>, Zn<sup>2+</sup> and Al<sup>3+</sup> chloride salts, respectively i.e. the red shift correlated with the cation valency. By contrast, Waghorne and Rubalcava [1982] observed an increase in the OC-N stretching frequency of deuterated DMF from 1400 cm<sup>-1</sup> to 1412, 1414 and 1420 cm<sup>-1</sup> after addition of Li<sup>+</sup>, Zn<sup>2+</sup> and Al<sup>3+</sup> perchlorate salts, respectively.

We also found the O-C-N bending frequency in pure DMF at 661 cm<sup>-1</sup> to decrease to 658.6, 658.6 and 657.7 cm<sup>-1</sup> after addition of Li<sup>+</sup>, Zn<sup>2+</sup> and Al<sup>3+</sup> chloride salts, respectively. This may be due to formation of free DMF molecules after disassociating DMF dimers through the complex of carbonyl O with the cation. The energy required for the bending vibration in free DMF molecules will be less than that in associated molecules. Additionally a new band is clearly observed at 667 cm<sup>-1</sup> for all the three salts, which may be attributed to the O-C-N bending frequency of DMF-cation complex. Waghorne and Rubalcava [1982] also found the O-C-N bending frequency to

increase from  $620\text{ cm}^{-1}$  to  $630$ ,  $645$  and  $685\text{ cm}^{-1}$  for  $\text{Li}^+$ ,  $\text{Zn}^{2+}$  and  $\text{Al}^{3+}$  perchlorate salt additives, respectively.

These results, in conjunction with those reported by Waghorne and Rubalcava [1982], show that both anion and cation affect the salt interaction with the OCN group. Both sets of data show the greatest change with  $\text{Al}^{3+}$  and least with  $\text{Li}^+$ . The C-N bond order is expected to increase due to complexation of carbonyl oxygen with the cations resulting in an increase in the OC-N stretching frequency and this in fact what is seen with the perchlorate salts. The decrease observed in O-C-N stretching frequency after addition of the chloride salts in the present study, may be due to the increasing electron cloud density of chloride ions near slightly electropositive (compared to oxygen) nitrogen, which prevents the increase in C-N bond order. The larger perchlorate anion may be sterically hindered from a similar interaction. For chloride salts, the red shift in OC-N stretching frequency follows the trend of  $\text{Al}^{3+} > \text{Zn}^{2+} > \text{Li}^+$  i.e. it is highest for the salt containing the most chloride ions.

The existence of both free as well as associated DMF molecules has also been suggested by Kabisch et al [1984] in DMF- $\text{ZnBr}_2$  solution, using Raman spectroscopy. We can thus identify 3 populations in DMF-salt solutions (Figure 3.2): (i) self-associated DMF molecules, (ii) free DMF molecules, and (iii) DMF molecules complexed with the salt through 2 mechanisms: (a) primarily with the salt cation through the carbonyl O and (b) to a lesser extent with the Cl anion through the amide N.

### 3.2.2 FTIR studies of PAN+DMF

Beevers [1968] reports that DMF is a good solvent for PAN and the dissolution of PAN proceeds with solvation of PAN molecules by DMF molecules. The main changes in the 3 molecular motions of DMF ( $>\text{C}=\text{O}$  stretching, OC-N stretching and O-C-N bending vibrations) as a result of PAN solvation are summarized in Table 3.3. This table shows the IR frequency measured for solvent-free PAN films, solvent DMF and the PAN solutions in DMF. Though all 3 homopolymers are nominally the same in terms of chemistry, and the same molar weights are used to prepare the solutions, we see that PAN-A and PAN-B affect the DMF spectra more than PAN-C.

**Table 3.3:** The effect of DMF on the three polymers focussing mainly on  $>C=O$  stretching, OC-N stretching and O-C-N bending frequencies of DMF and  $-C\equiv N$  stretching of PAN.

	DMF frequencies ( $cm^{-1}$ )			PAN frequency
	$>C=O$ stretching	OC-N Stretching	O-C-N bending	$-C\equiv N$ stretching
PAN-A,B,C				2241-2243
DMF	1667.3	1390	661.5	-
DMF+PAN-A	1673.1	1387.5	658.6, 667	2241.1
DMF+PAN-B	1665-1680	1385.8	658.6, 667	2242.1
DMF+PAN-C	1660-1670	1392.5	659.6(h), 667	2242.1

(h)- hump

Padhye and Karandikar [1985] performed an IR investigation of PAN films and of PAN solutions in neat DMF and DMF+LiBr. They suggested that PAN is partly self-associated through dipole-dipole interactions at the  $-CN$  groups. DMF breaks this self-association but is itself bound to the nitrile groups by dipole-dipole interactions. They reported the  $-C\equiv N$  stretching frequency to occur at  $2250cm^{-1}$  in the spectra of DMF-free PAN films, while in PAN-DMF solutions the  $-C\equiv N$  stretching was seen at  $2230 cm^{-1}$ . This shift was attributed to the above mentioned dipole-dipole interactions in solution phase. IR spectra of DMF solution of acrylonitrile with and without LiBr, showed that in addition to the strong absorption band of the monomer at  $2230 cm^{-1}$ , an additional band at  $2249 cm^{-1}$  was observed in DMF+LiBr solutions, indicating a strong interaction of LiBr with  $-C\equiv N$  of acrylonitrile [Padhye and Karandikar, 1985].

Our data does not show the frequency shift between PAN films and solutions, as reported by Padhye and Karandikar [1985]. Figures 3.3a-c show the FT-IR spectra measured on films of PAN-A, B and C, cast from DMF solution and dried at  $70^{\circ}C$  for four days. The  $-C\equiv N$  stretching vibration is observed at  $2241-2243 cm^{-1}$  for all three polymers. Figures 3.4a-c show the corresponding spectra for the same 3 PAN grades in pure DMF solution. We do not see any significant change in the frequency of the  $-C\equiv N$  stretching vibration which continues to show a peak maxima at  $2241-2242 cm^{-1}$ .



However, there are some qualitative differences in the spectra of the films and the solutions. Both nitrile and carbonyl peaks becomes broader and the peaks at  $1070\text{ cm}^{-1}$  and  $1095\text{ cm}^{-1}$  also show some changes. The broadening of the peak corresponding to the O-C-N bending indicates interactions between PAN and DMF.

Even though we do not see the frequency shift for the  $-\text{CN}$  group observed by Padhye and Karandikar [1985], we do see several changes in the DMF spectra between the neat and solution cases. These changes are easier to see in PAN-A and -B solutions; the spectrum for PAN-C shows broader peaks where the maxima is more difficult to identify precisely.

Table 3.3 shows that the  $>\text{C}=\text{O}$  stretching in solution shifts to a higher frequency while the OC-N stretching is red-shifted. The O-C-N bending frequency also shows a red shift accompanied by the emergence of a new peak at  $667\text{ cm}^{-1}$ . Similar changes in the OCN frequencies were also seen in the DMF-salt case where we interpreted these as thermodynamically favored interactions with the solute. However, in the DMF+ salt case, the primary effect is the red shift in the  $>\text{C}=\text{O}$  frequency indicating that this moiety is the preferred interaction site. In the DMF+PAN case, the OCN group is the DMF site with primary affinity for the solute PAN. This is illustrated in Figure 3.5.

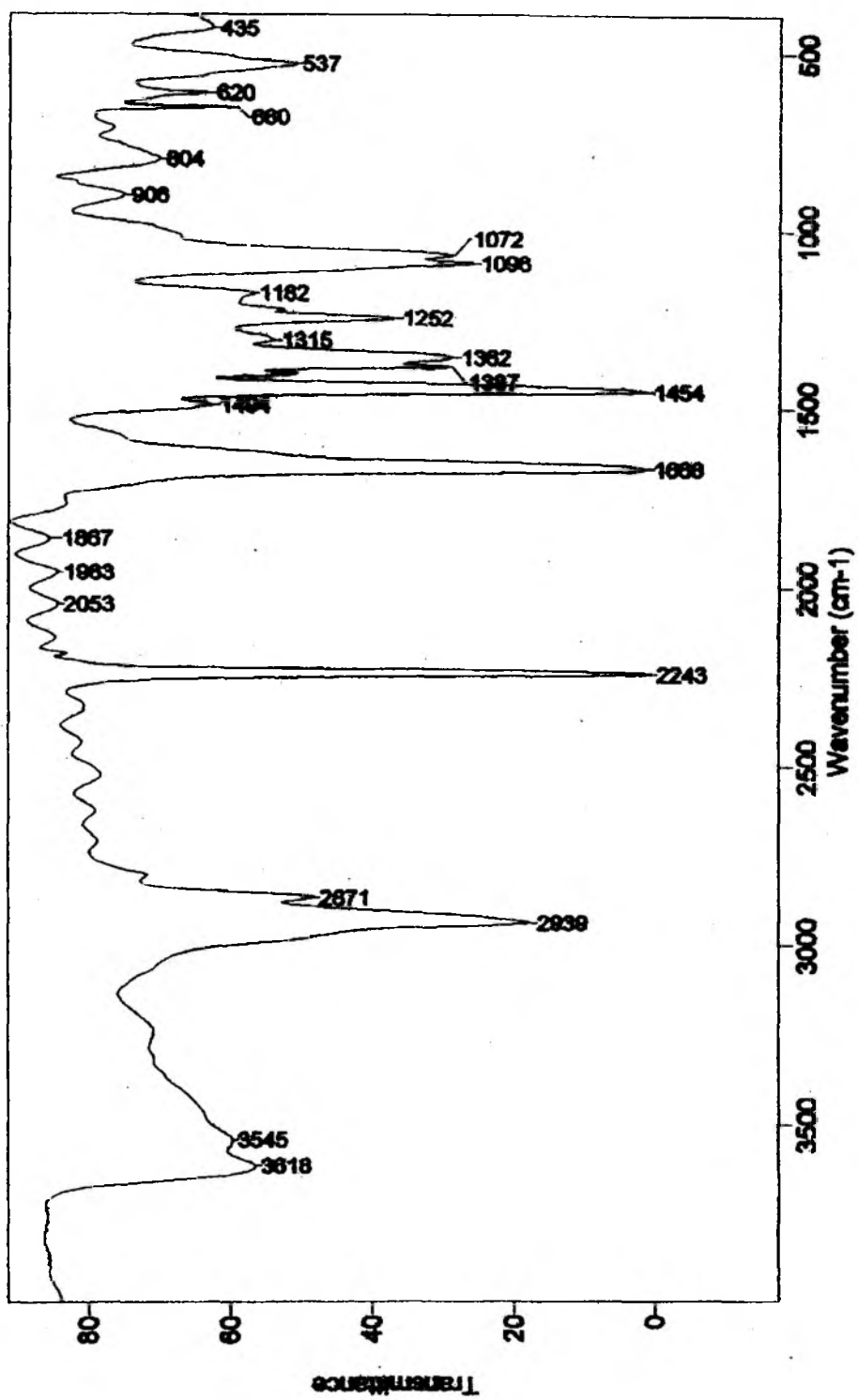


Figure 3.3a: FTIR spectra of a PAN-A film made from 3% w/w PAN solution in pure DMF.

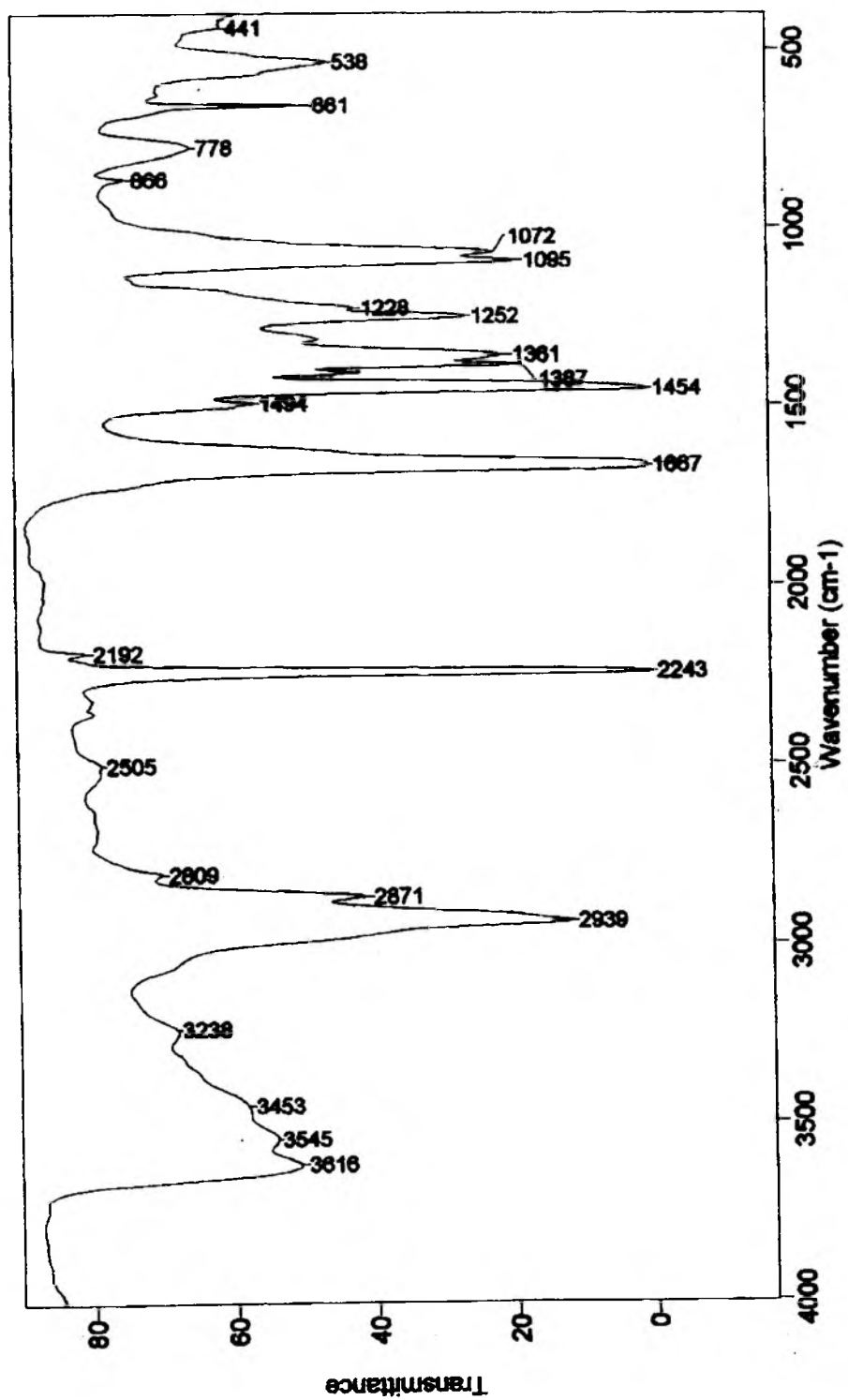


Figure 3.3b: FTIR spectra of a PAN-B film made from 3% w/w PAN in pure DMF.

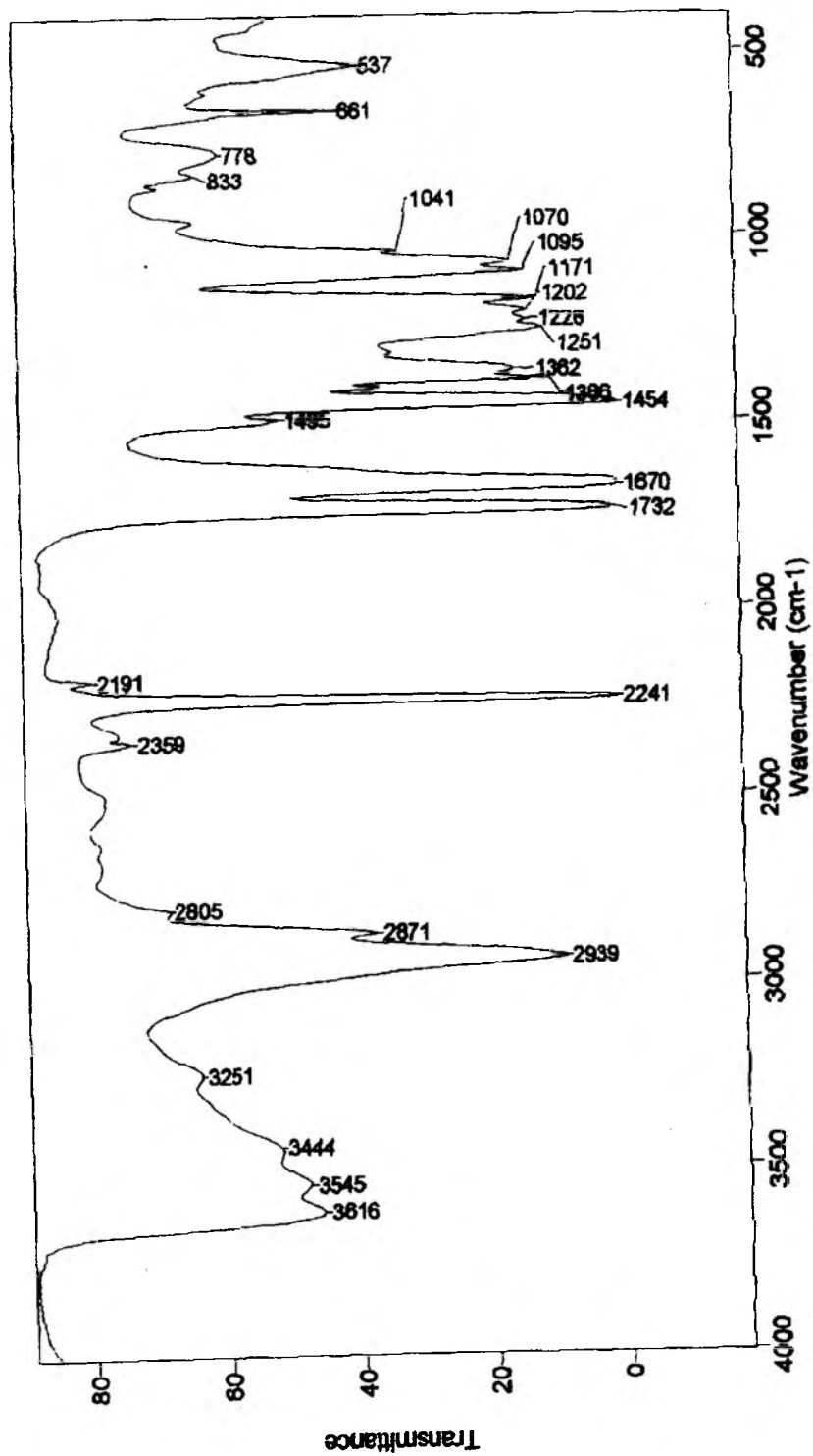


Figure 3.3c: FTIR spectra of a PAN-C film made from 3% w/w PAN in pure DMF.

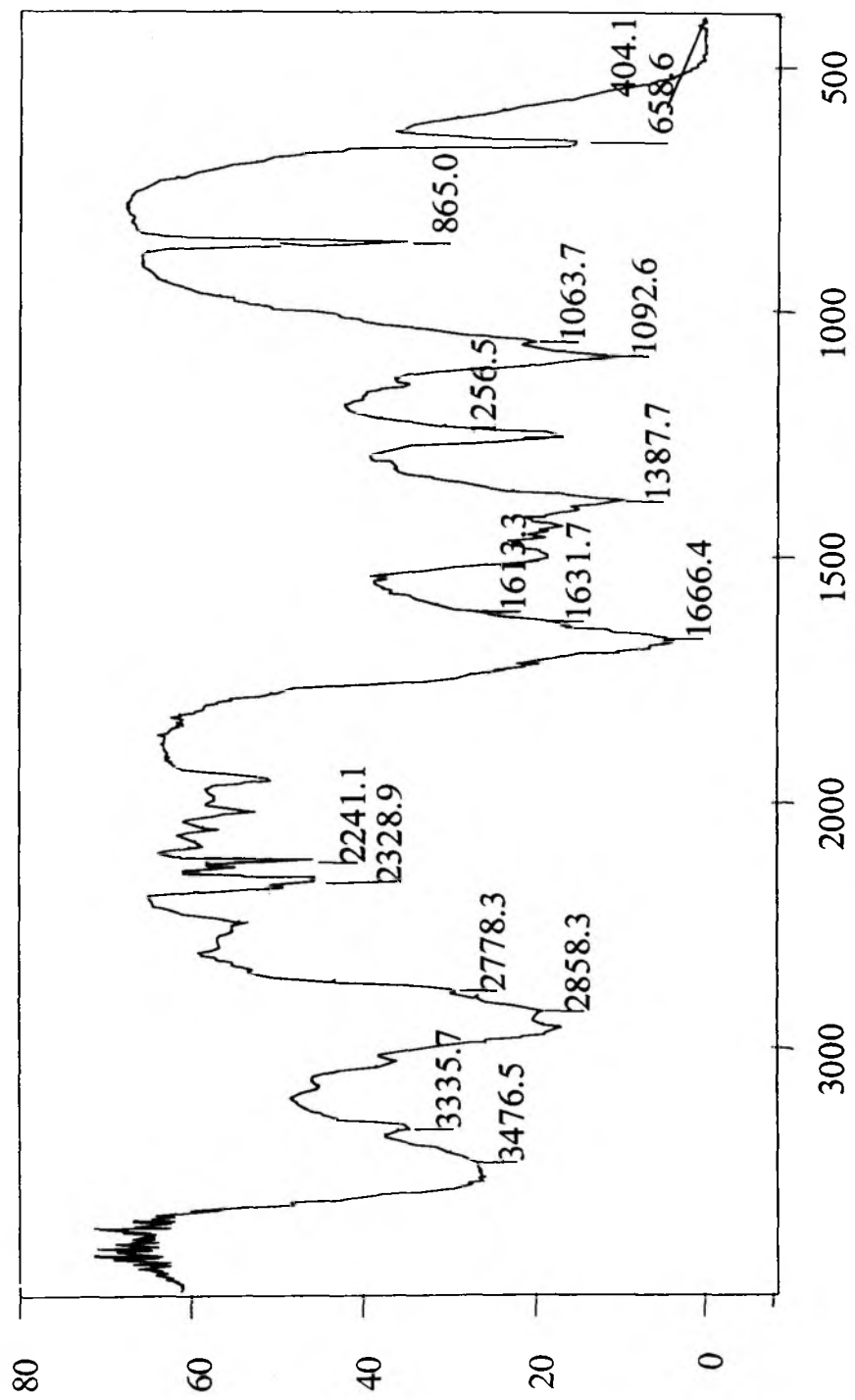


Figure 3.4a: FTIR spectra of a 7 % w/w PAN-A solution in pure DMF.

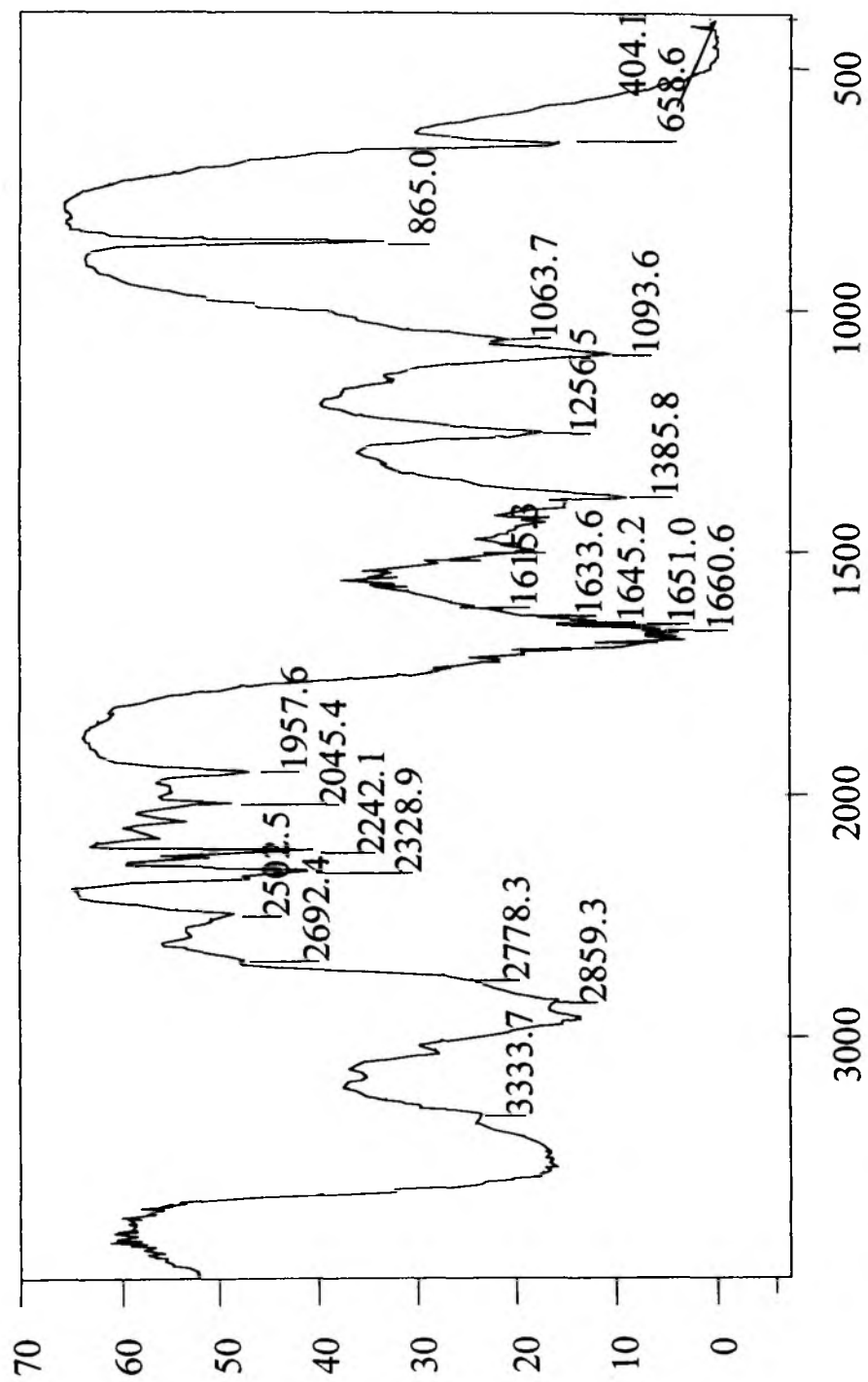


Figure 3.4b: FTIR spectra of a 7 % w/w PAN-B solution in pure DMF.

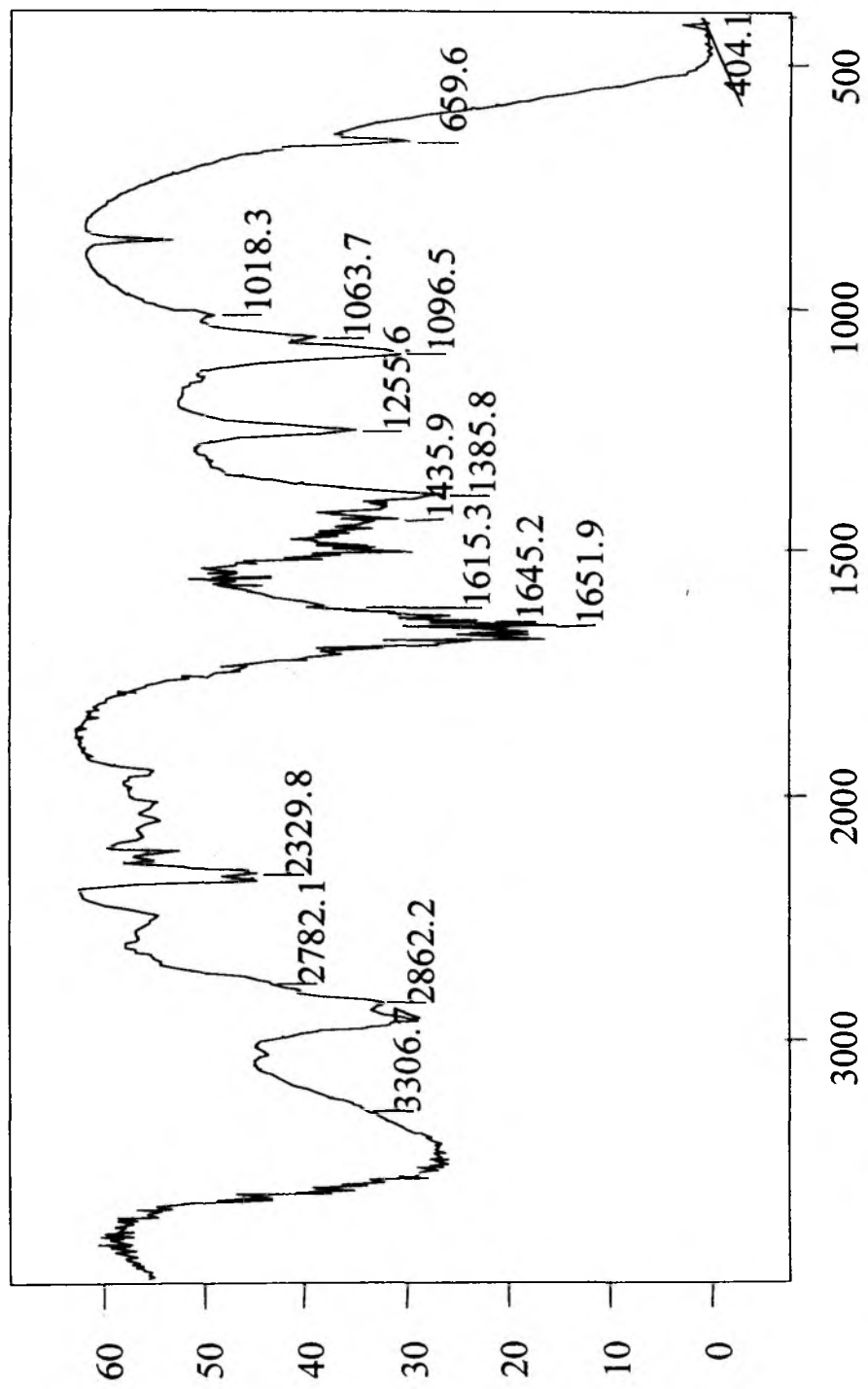


Figure 3.4c: FTIR spectra of a 7 % w/w PAN-C solution in pure DMF.





### 3.2.3 FT-IR studies of Salt + DMF + PAN

As shown in section 3.2.1, salt-DMF complexation results in breaking the dipolar alignment of DMF molecules. As a result of this solvent+salt complexation, we can expect a reduced solvation power of DMF for PAN.

The FT-IR spectra used to analyze the various interactions in DMF -PAN are shown in Figures 3.6a-c. The FT-IR spectra for various interactions in the DMF-salt-PAN ternary system are shown in Figures 3.7, 3.8 and 3.9 for DMF-L, DMF-Z and DMF-A, respectively. The effect of the salt and PAN together in DMF on  $>C=O$  stretching, OC-N stretching and O-C-N bending frequencies of DMF and the  $-C\equiv N$  stretching of PAN with the different polymers PAN-A, B and C are summarized in Table 3.4 to 3.6.

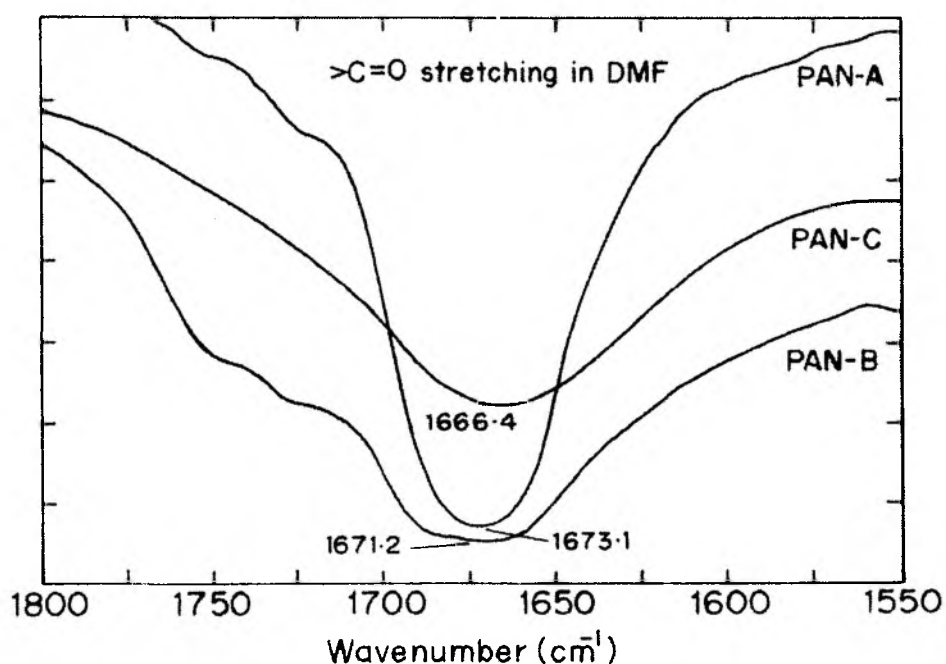


**Figure 3.6a:** Effect of PAN addition on  $>C=O$  stretching in neat DMF.

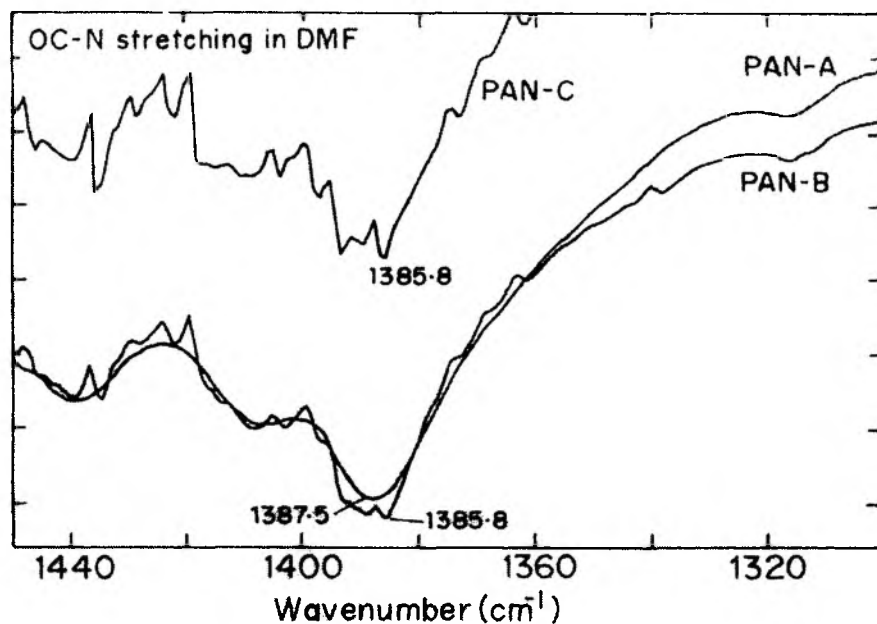


**Figure 3.6b:** Effect of PAN addition on OC-N stretching in neat DMF.

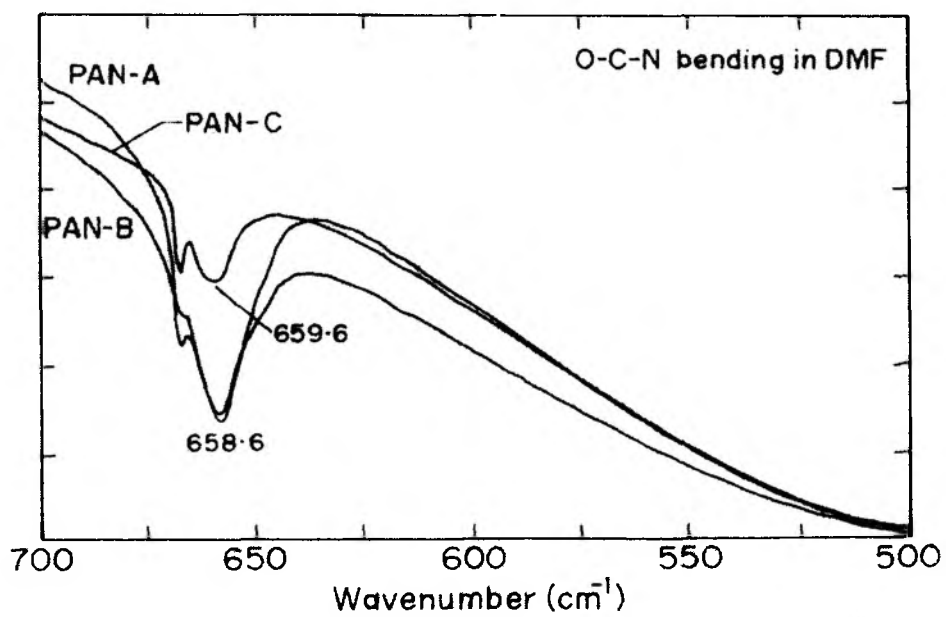


**Figure 3.6c:** Effect of PAN addition on O-C-N bending in neat DMF.

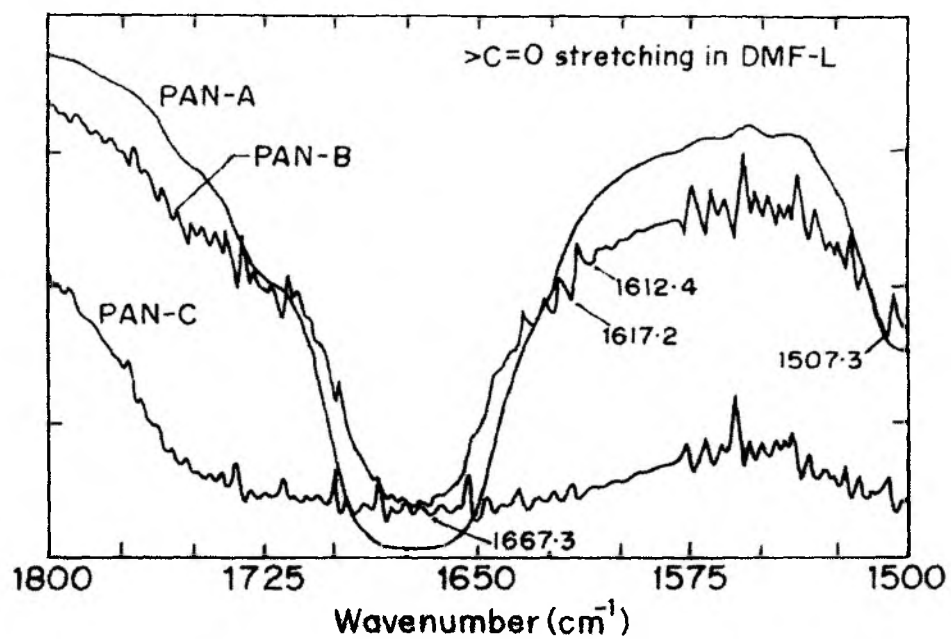


**Figure 3.7a :** Effect of LiCl and PAN addition on >C=O stretching in DMF.

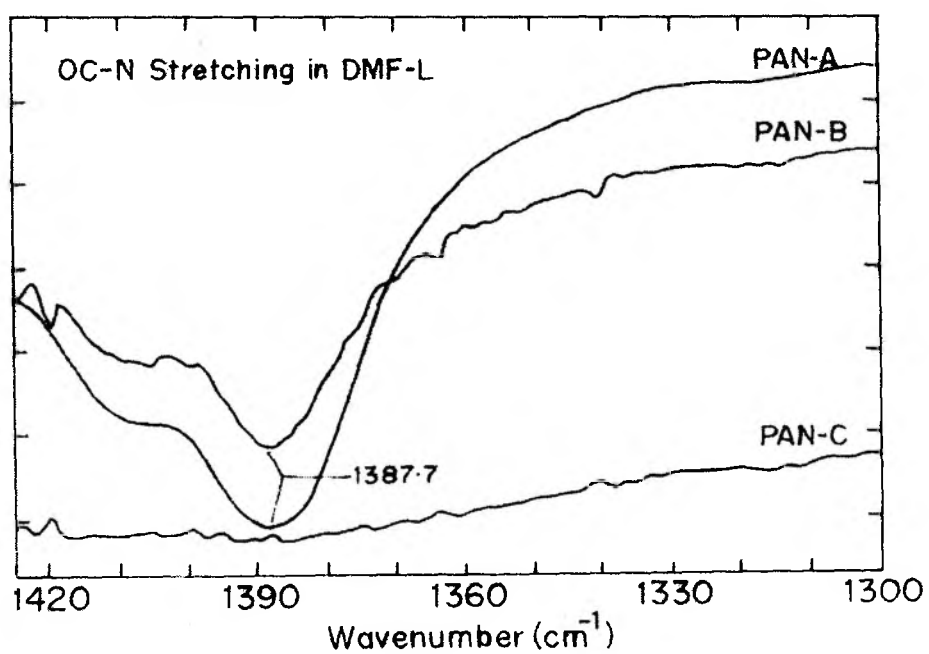


**Figure 3.7b:** Effect of LiCl and PAN addition on OC-N stretching in DMF.

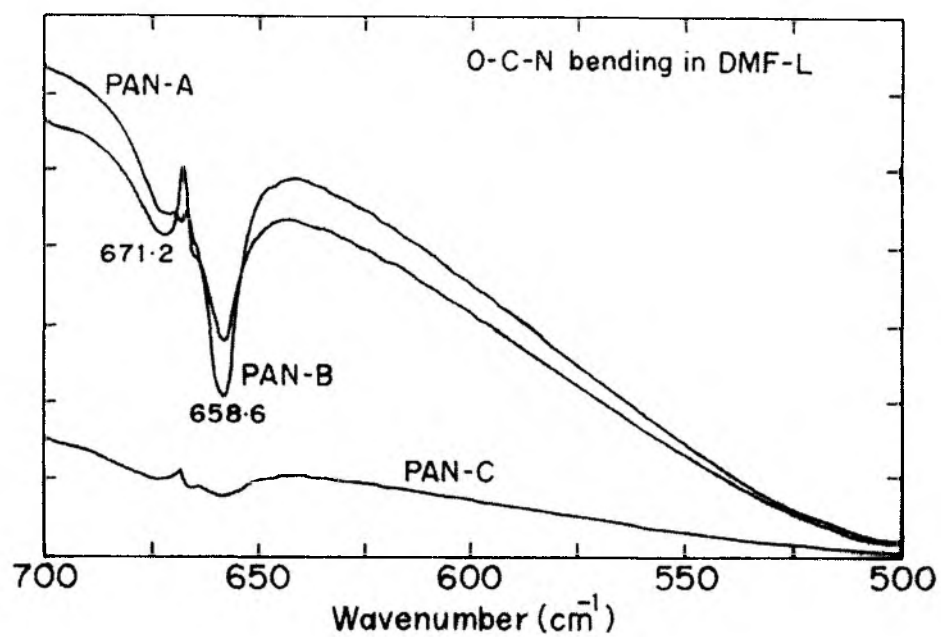


**Figure 3.7c:** Effect of LiCl and PAN addition on O-C-N bending in DMF.

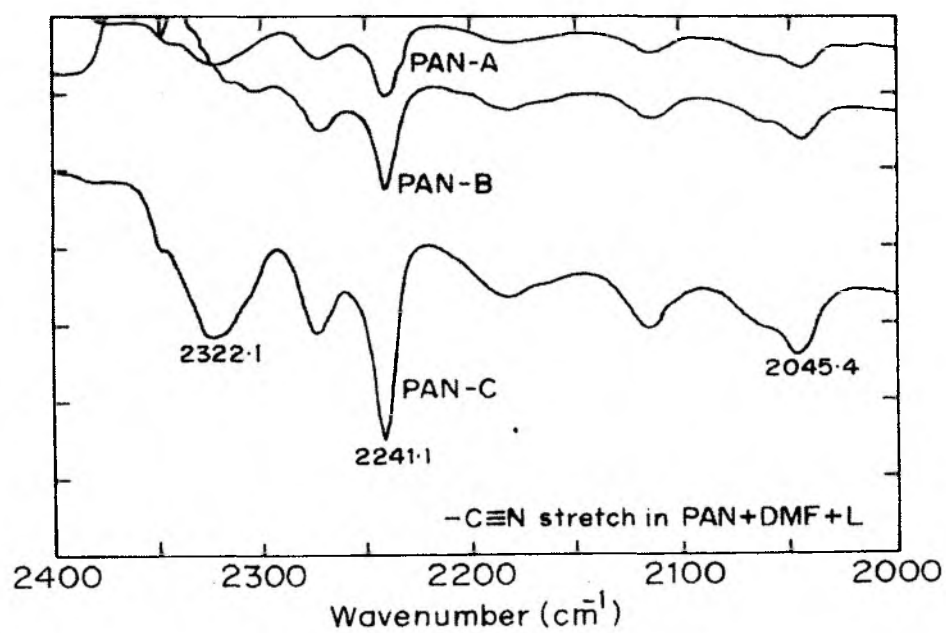


**Figure 3.7d:** Effect of LiCl on nitrile stretching in PAN + DMF.

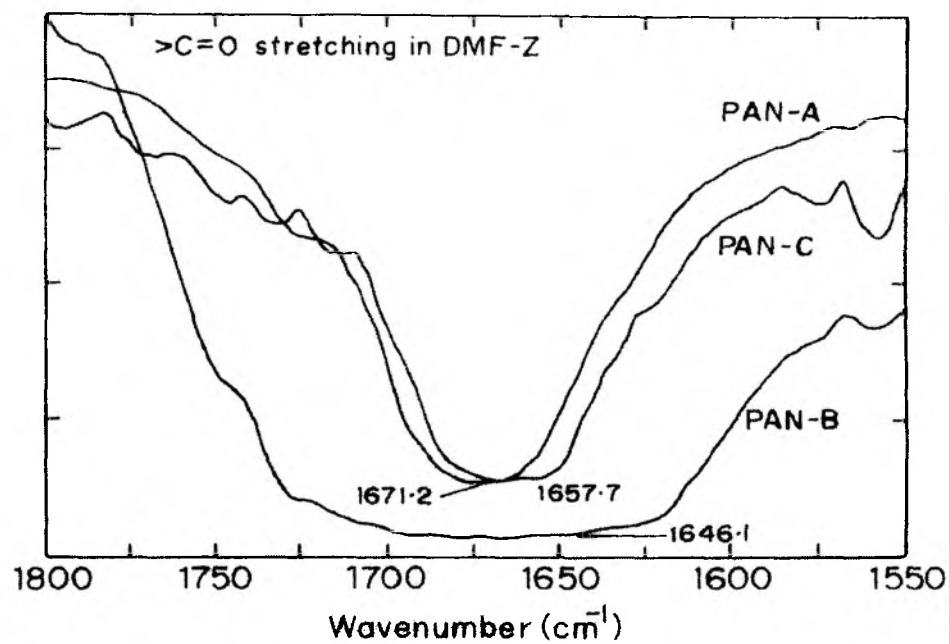


Figure 3.8a : Effect of  $\text{ZnCl}_2$  and PAN addition on  $>\text{C}=\text{O}$  stretching in DMF.

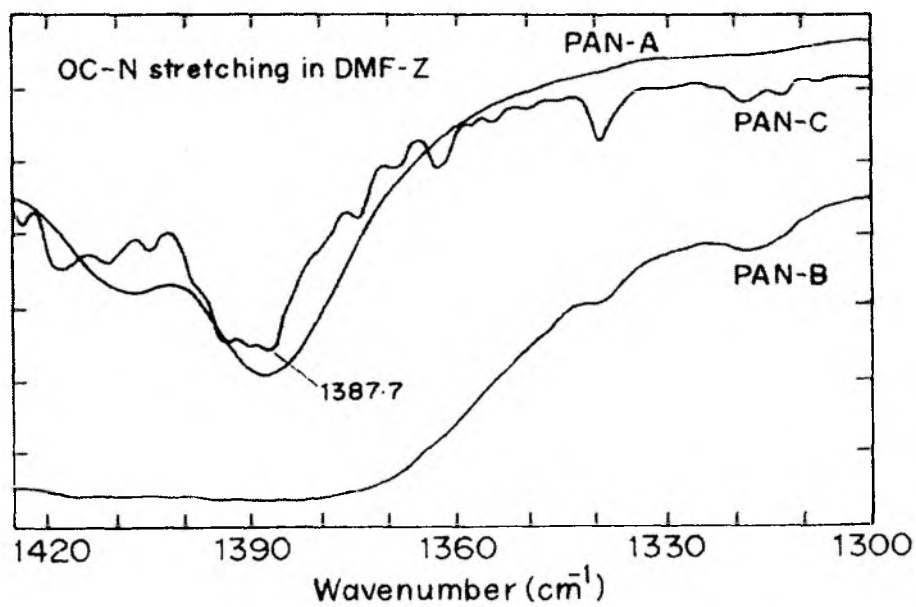


Figure 3.8b : Effect of  $\text{ZnCl}_2$  and PAN addition on OC-N stretching in DMF.

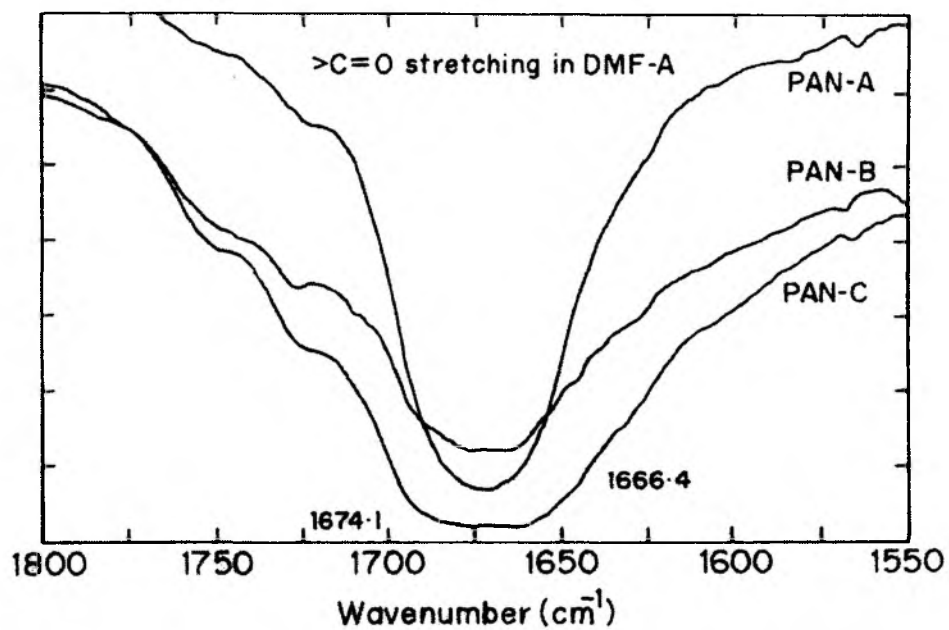


Figure 3.9a : Effect of  $\text{AlCl}_3$  and PAN addition on  $>\text{C}=\text{O}$  stretching in DMF.

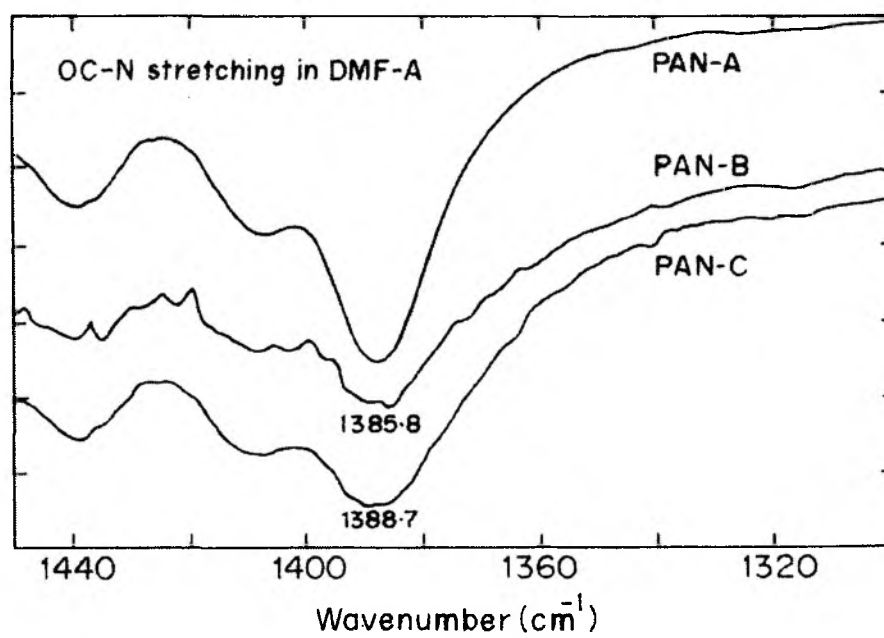


Figure 3.9b: Effect of  $\text{AlCl}_3$  and PAN addition on OC-N stretching in DMF.

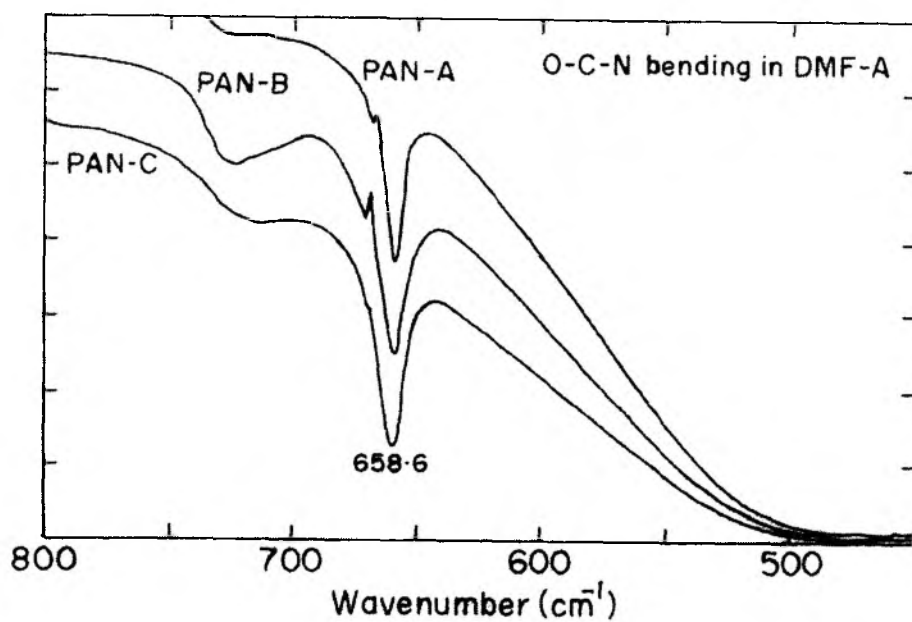


Figure 3.9c: Effect of  $\text{AlCl}_3$  and PAN addition on O-C-N bending in DMF.

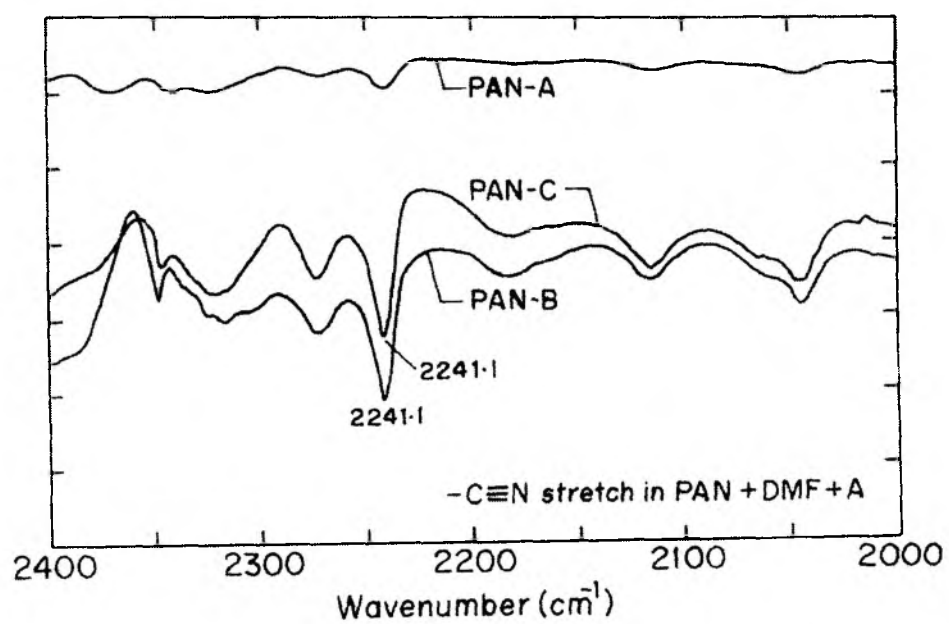


Figure 3.9d: Effect of  $\text{AlCl}_3$  on nitrile stretching in PAN + DMF.

**Table 3.4:** IR frequencies ( $\text{cm}^{-1}$ ) for  $>\text{C}=\text{O}$  stretching, OC-N stretching and O-C-N bending of DMF and  $-\text{C}\equiv\text{N}$  stretching of the polymer in the PAN-A+salt+DMF system.

Solution	IR frequencies of DMF			PAN freq.
	$>\text{C}=\text{O}$ stretching	OC-N Stretching	O-C-N Bending	$-\text{C}\equiv\text{N}$ stretching
DMF	1667.3	1390	661.5	-
DMF+PAN-A	1673.1	1387.5	658.6, 667	2241.1
DMF-L	1667.3	1388.7	658.6, 668.3	-
DMF-L+PAN-A	1671.2 blue shift vs DMF-L	1387.7	658.6, 668.8	2241.1
DMF-Z	1661.6	1386.7	658.6, 668.3, 682.5	-
DMF-Z+PAN-A	1671.2 blue shift vs DMF-Z	1388.5	658.6, missing, 679	2241.1
DMF-A	1667.3	1385.8	657.7, 668, 726.1	-
DMF-A+PAN-A	1674.1	1387	658.6, 668, 723.5	2241.1

The data for the ternary salt-DMF-PAN systems shown in Tables 3.4-3.6 are discussed below in the light of the previously presented binary system (DMF-salt, DMF-PAN) data in sections 3.2.1 and 3.2.2. The focus of the discussion is on the effect of the three salt additives: LiCl,  $\text{ZnCl}_2$ , and  $\text{AlCl}_3$ . Conventionally, a red shift (decrease) in frequency indicates a more thermodynamically favorable interaction while an increased frequency may indicate weakening of an existing complex formation.

The O-C-N bending vibration of neat DMF shows a red-shift in the original frequency as well as emergence of several new blue-shifted frequencies when DMF is in either binary system (DMF+salt or DMF+PAN) or in the ternary system (salt-DMF-PAN). In other words, these new higher frequencies are seen in the presence of any solute whether it is any of the 3 salts or PAN grades.



**Table 3.5:** IR frequencies ( $\text{cm}^{-1}$ ) for  $>\text{C}=\text{O}$  stretching, OC-N stretching and O-C-N bending of DMF and  $-\text{C}\equiv\text{N}$  stretching of the polymer in the PAN-B + salt + DMF system.

Solution	IR frequencies of DMF			PAN freq.
	$>\text{C}=\text{O}$ stretching	OC-N Stretching	O-C-N Bending	$-\text{C}\equiv\text{N}$ stretching
DMF	1667.3	1390	661.5	-
DMF+PAN-B	1671.2	1385.8	658.6, 667	2242.1
DMF-L	1667.3	1388.7	658.6, 668.3	-
DMF-L+PAN-B	1667.3	1385.8	658.6, 671.2	2241.1
DMF-Z	1661.6	1386.7	658.6, 668.3, 682.5	-
DMF-Z+PAN-B	1660.0	1387.3	658.6, 668, 688	2241.1
DMF-A	1667.3	1385.8	657.7, 668, 726.1	-
DMF-A+PAN-B	1672.0	1387.3	658.6, 670, 726(b)	2241.1

**Table 3.6.** IR frequencies ( $\text{cm}^{-1}$ ) for  $>\text{C}=\text{O}$  stretching, OC-N stretching and O-C-N bending of DMF and  $-\text{C}\equiv\text{N}$  stretching of the polymer in the PAN-C + salt + DMF system.

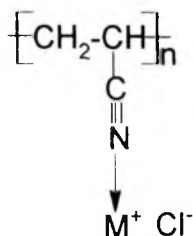
Solution	IR frequencies of DMF			PAN frequency
	$>\text{C}=\text{O}$ stretching	OC-N Stretching	O-C-N bending	$-\text{C}\equiv\text{N}$ stretching
DMF	1667.3	1390	661.5	-
DMF+PAN-C	1666.4	1385.8	659.6 (h), 667	2242.1
DMF-L	1667.3	1388.7	658.6, 668.3	-
DMF-L+PAN-C	~1640- 1680	1388.7	658.6, 671.2 (b)	2241.1
DMF-Z	1661.6	1386.7	658.6, 668.3, 682.5	-
DMF-Z+PAN-C	1661.6	1385.0	661.6(h), 665(h), 685	2241.1
DMF-A	1667.3	1385.8	657.7, 668, 726.1	-
DMF-A+PAN-C	1675 (vb)	1390	658.6, 715(b)	2241.1

As explained in sections 3.2.1.1 and 3.2.1.2, these new blue-shifted frequencies are mainly attributed to the complexation of salt or PAN with DMF. Since this effect appears to take place with every solute, it does not distinguish between the various salt types.

Likewise the  $\text{-C}\equiv\text{N}$  stretching of PAN at  $2241\text{ cm}^{-1}$  is the same for all PAN grades dissolved in any of the DMF+salt combinations. Observing this frequency also does not distinguish the effect of the various salt types.

In the competition between the DMF and the  $\text{-C}\equiv\text{N}$  group of PAN for forming a complex with the cations, DMF is clearly the preferred interaction partner. This may be due to the higher basicity of DMF (DN = 26.6) compared to the PAN nitrile group (DN for acetonitrile, a model compound for PAN = 14.1). DN is the donor number obtained from and defined by Gutmann [1982]. As shown in Table 3.4, the simultaneous presence of both salt and PAN gives rise to various new frequencies for both the  $\text{>C=O}$  and OC-N stretching frequencies of DMF while the nitrile stretching frequency of PAN-A remains constant even after addition of mono, di or trivalent salts in pure DMF. For the purer and higher molecular weight grades, PAN-B (Table 3.5) and PAN-C (Table 3.6), a small red shift in the  $\text{-C}\equiv\text{N}$  stretching frequency may be seen for all the salt additives. Though this difference was within experimental error, it suggests the possibility that the nitrile group of PAN may also form a weak complex with the cation as shown below.

Th 8572



We do see some more significant differences between the various salt-DMF-PAN ternary systems in terms of the OC-N and particularly the  $\text{>C=O}$  stretching in DMF. These differences are presented graphically in Figures 3.10 (a-c) for the  $\text{>C=O}$  stretching and OC-N stretching frequency, for each salt additive ( $\text{LiCl}$ ,  $\text{ZnCl}_2$  and  $\text{AlCl}_3$ )

respectively. The Y axis represent the frequency deviation ( $\Delta$ ) of the peak maximum in each solution from the peak frequency observed in neat DMF:

$$\Delta = \text{Frequency in binary or ternary solution} - \text{Frequency in neat DMF}$$

The neat DMF frequencies are  $1667.3 \text{ cm}^{-1}$  for the  $>\text{C}=\text{O}$  stretching and  $1390 \text{ cm}^{-1}$  for the OC-N stretching.

In the ternary systems, both the  $>\text{C}=\text{O}$  stretching and OC-N stretching (Figure 3.10 a-c) frequencies show the same trend vs PAN molecular weight. Comparing the  $\Delta$  values for DMF+PAN binaries shows that both frequencies show an increasing red shift i.e. the  $\Delta$  values trend more negative as the PAN MW increases.

In the case of DMF + salt binary solutions,  $\Delta$  becomes more negative for the OC-N stretching (Figure 3.10 a-c) as the cation valency increases from  $\text{Li} < \text{Zn} < \text{Al}$ . For the  $>\text{C}=\text{O}$  stretch,  $\Delta$  is 0 (no change) for Li and Al chlorides, while there is a strong red shift for DMF-Z.

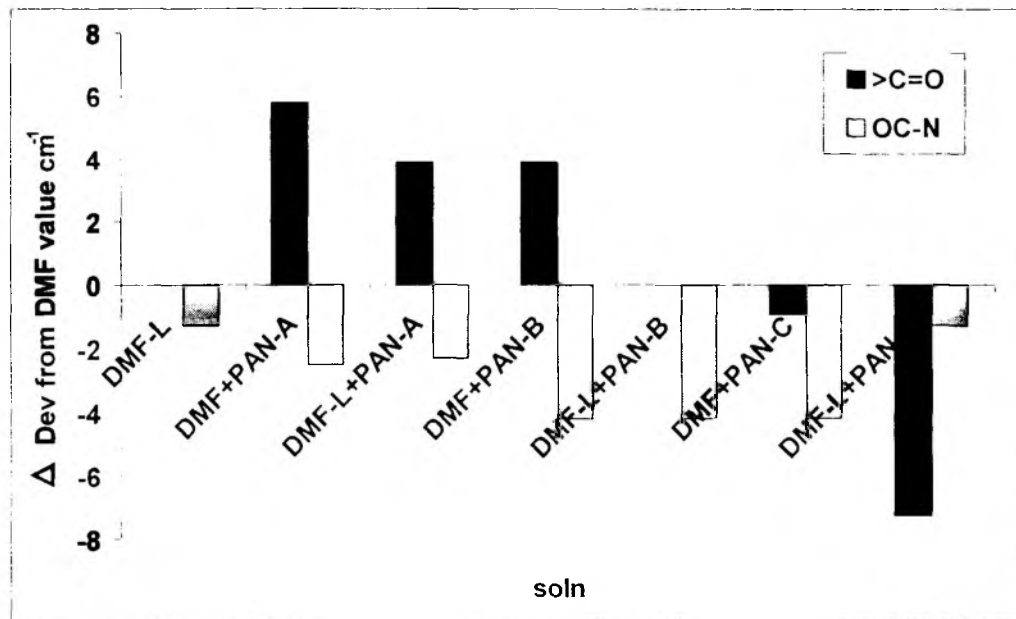


**Figure 3.10a:** Frequency shifts in PAN-DMF-LiCl binary and ternary system for  $>\text{C}=\text{O}$  and OC-N stretching.

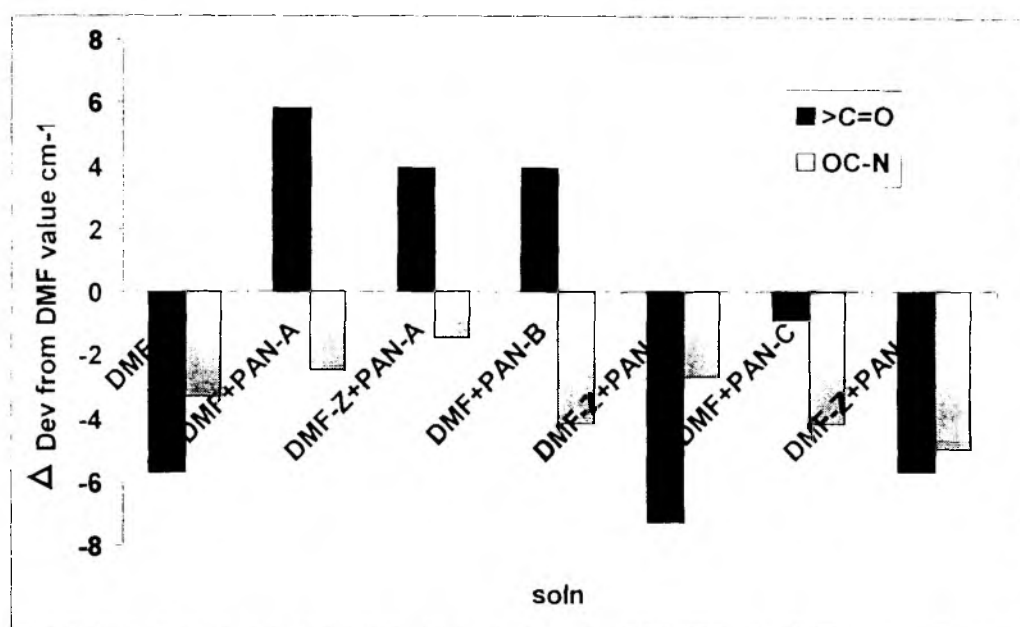


Figure 3.10b: Frequency shifts in PAN-DMF-ZnCl<sub>2</sub> binary and ternary system for >C=O and OC-N stretching.

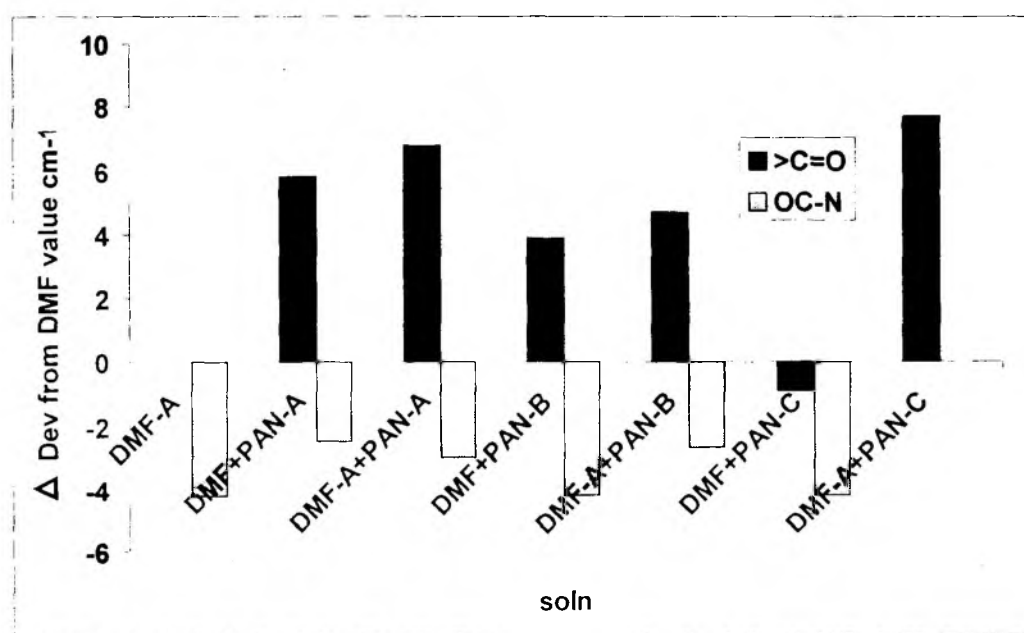


Figure 3.10c: Frequency shifts in PAN-DMF-AlCl<sub>3</sub> binary and ternary system for >C=O and OC-N stretching.

With the above binary information as a baseline, we can next compare the  $\Delta$  values between the ternary DMF+salt+PAN and the binary DMF+PAN systems for the various PAN grades and the three salts. No consistent effect is noticed in terms of any of the salts for the OC-N stretching frequency. However, we do see consistent trends for the important  $>C=O$  stretching frequency which is indicative of the strength of interactions between DMF and the solutes. For the LiCl additive (Figure 3.10 a) and each PAN grade, this frequency shows a consistent red shift. That is the  $\Delta$  values for each ternary DMF+LiCl+PAN system is less positive or more negative than the  $\Delta$  value for the corresponding DMF+PAN system for each of the three PAN grades.

Figure 3.10 b shows a similar effect with  $ZnCl_2$  as for LiCl when comparing the ternary and binary PAN solutions. The  $\Delta$  values for each ternary DMF+ $ZnCl_2$  +PAN system are less positive or more negative than the  $\Delta$  value for the corresponding DMF+PAN for each of the three PAN grades.

By contrast, this effect is reversed in the  $AlCl_3$  case. Here, the  $\Delta$  values for each ternary DMF+ $AlCl_3$ +PAN system (Figure 3.10 c) are more positive than the  $\Delta$  value for the corresponding DMF+PAN for each of the three PAN grades. This would indicate more complexed DMF molecules (with both salt and PAN) and less free DMF molecules.

Based on the spectroscopic data: we can postulate that four types of DMF molecules would be present in a salt-DMF-PAN solution: (i) free DMF molecules, (ii) molecules complexed with the salt (iii) molecules complexed with PAN and (iv) self – associated (dimer) DMF molecules. We can also postulate two effects of the salt on the solution properties: (i) Solvent effects- strong complexes formed with the DMF affect its solubilizing power and viscosity (ii) Polymer effects: weaker complexes formed with PAN affect its self-association and may lead to salt-mediated polymer chain bridging (in case of di- and trivalent metal ions). These various interactions would be expected to strongly affect solution properties viz. viscosity and phase boundary characteristics.

### 3.3 PAN-DMF-salt interactions: Dilute solution rheology studies

The interaction of PAN with DMF and the salt additives can also be probed by dilute solution rheology, which is highly sensitive to polymer chain configuration in solution. Similar inferences may also be drawn from other solution properties such as concentrated solution rheology and miscibility curves; however, in comparison to concentrated solutions, dilute solution behavior is easier to interpret theoretically. Concentrated solution properties with all 3 grades are discussed later in Chapter V. The dilute solution behavior of salt-PAN-DMF solutions and their consistency with the FT-IR analyses are discussed in this section.

#### 3.3.1 Solvent viscosity

The complexation of DMF to various salts is expected to result in changes in association behavior of DMF molecules and consequently in viscosity of the combined solvent. Figure 3.11 shows the ratios of flow times of salt solution ( $t_{\text{solution}}$ ) and DMF ( $t_{\text{DMF}}$ ) measured in the Ubbelohde viscometer at 25°C. It is clearly seen that addition of any of the salts results in an increased solvent viscosity. The ratio is highest for DMF-L (1.57), followed by DMF-A (1.37) and lowest for DMF-Z (1.2). These observations can be interpreted in light of the FT-IR results in section 3.2.1. It can be seen by referring to Table 3.1 that these changes in DMF-salt viscosity correlate with the strength of DMF complexation with each salt.

As depicted in Figure 3.2, neat DMF molecules are probably associated through anti-parallel dipolar alignment. As discussed in section 3.2.1, addition of the salt results in breaking of some of these dipoles, resulting in three types of DMF molecules, viz.-i) molecules still associated among themselves, (mole ratio salt:DMF = 0.094:1.52) ii) DMF molecules complexed with the cation and iii) free DMF molecules. All three salts complex with DMF molecules as evidenced by various IR spectra changes (eg. new IR peak at 667  $\text{cm}^{-1}$  in Table 3.1); this effect would result in increased viscosity. However in the case of the multivalent cations  $\text{AlCl}_3$  and  $\text{ZnCl}_2$ , the salts may even bridge between DMF molecules. In case of DMF-Z, as discussed in section 3.2.1, the

complexation of DMF carbonyl oxygen with the cation is the most favorable. In the case of  $\text{AlCl}_3$ , the electronic cloud around the  $\text{Al}^{3+}$  ion inhibits the approach of carbonyl oxygen of DMF towards  $\text{Al}^{3+}$  ion; however, the FT-IR red shift indicating favorable interactions with the OC-N moiety is the most pronounced. Comparatively, DMF-L has the least tendency for complexing with DMF.

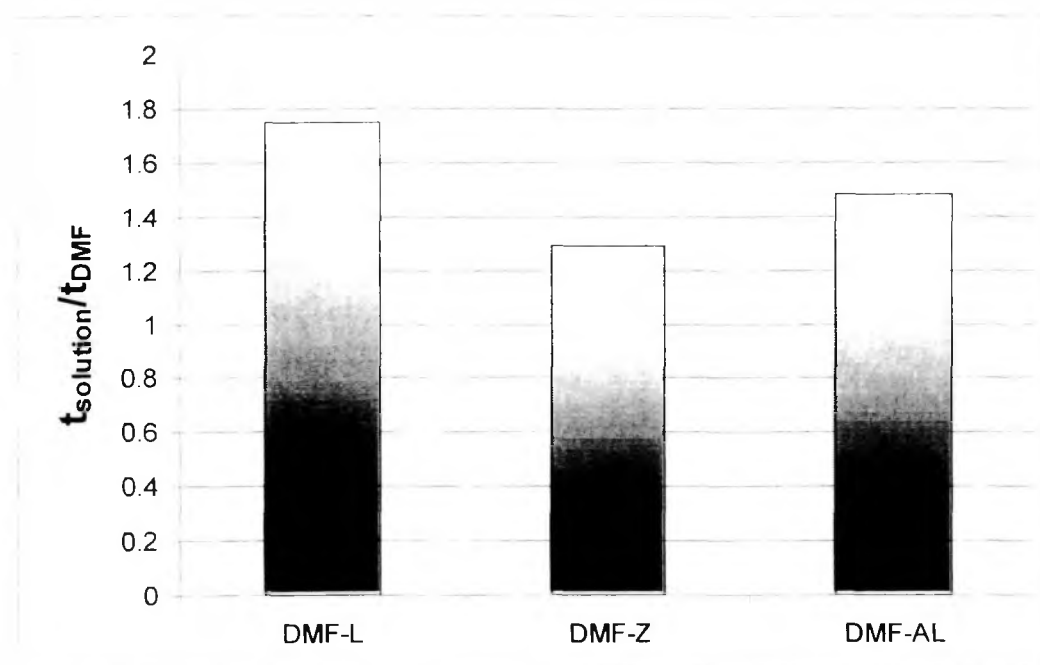


**Figure 3.11** : Effect of salt addition on viscosity ratio of DMF+salt vs neat DMF at 25°C.

### 3.3.2 Dilute Solution viscosity

Solution viscosities measured at 25-45°C at PAN concentrations of 0.1-0.3% are presented in Figures 3.12 a-c as Arrhenius plots. As discussed above, the neat solvent DMF has lower viscosity than the DMF+salt solvents. However in the case of the dilute PAN solutions, the solutions formed from DMF alone have higher viscosity than solutions from DMF+salt. This trend holds for all three PAN grades.

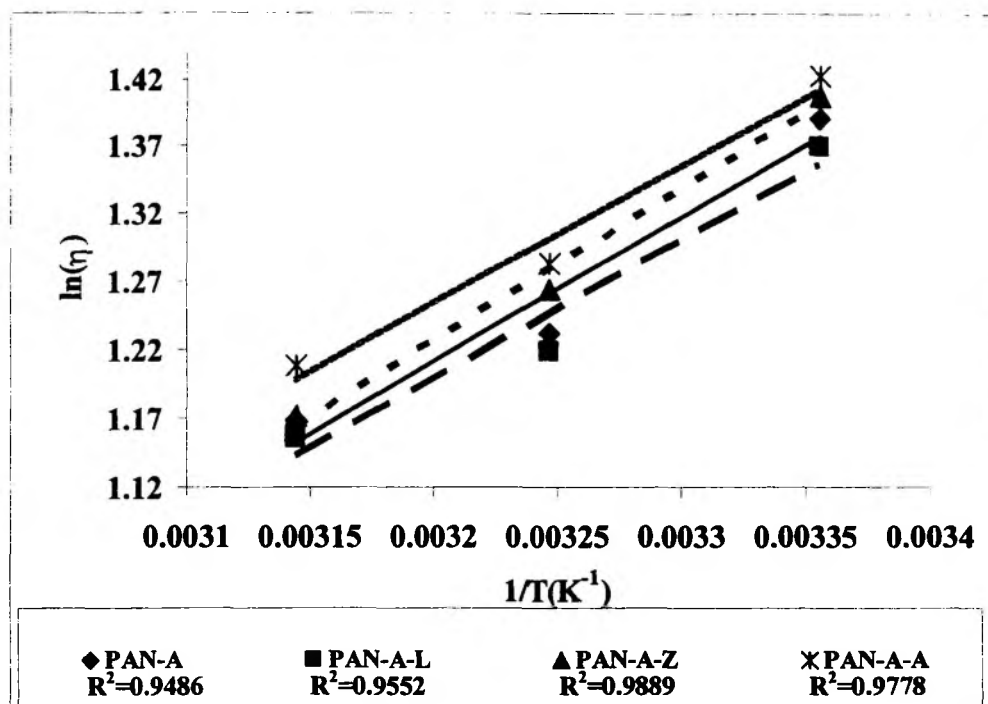


Figure 3.12a: Arrhenius plots of  $\eta$  vs  $1/T$  for PAN-A (0.1%) polymer solution with and without additives as function of temperature (298-318 K).

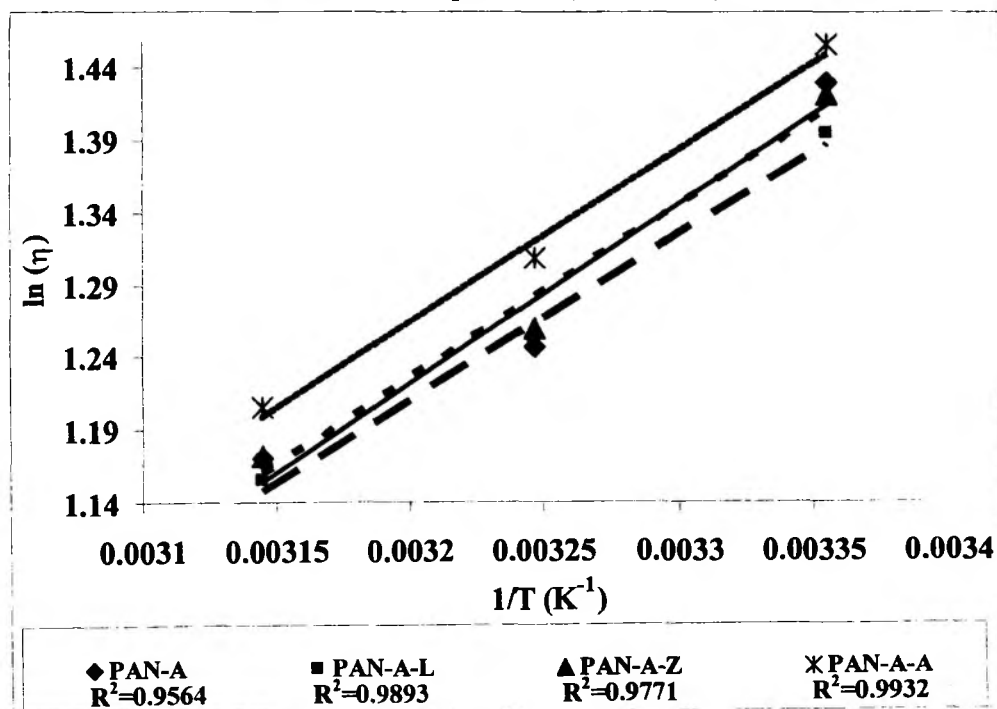


Figure 3.12b: Arrhenius plots of  $\eta$  vs  $1/T$  for PAN-A (0.2%) polymer solution with and without additives as function of temperature (298-318 K).



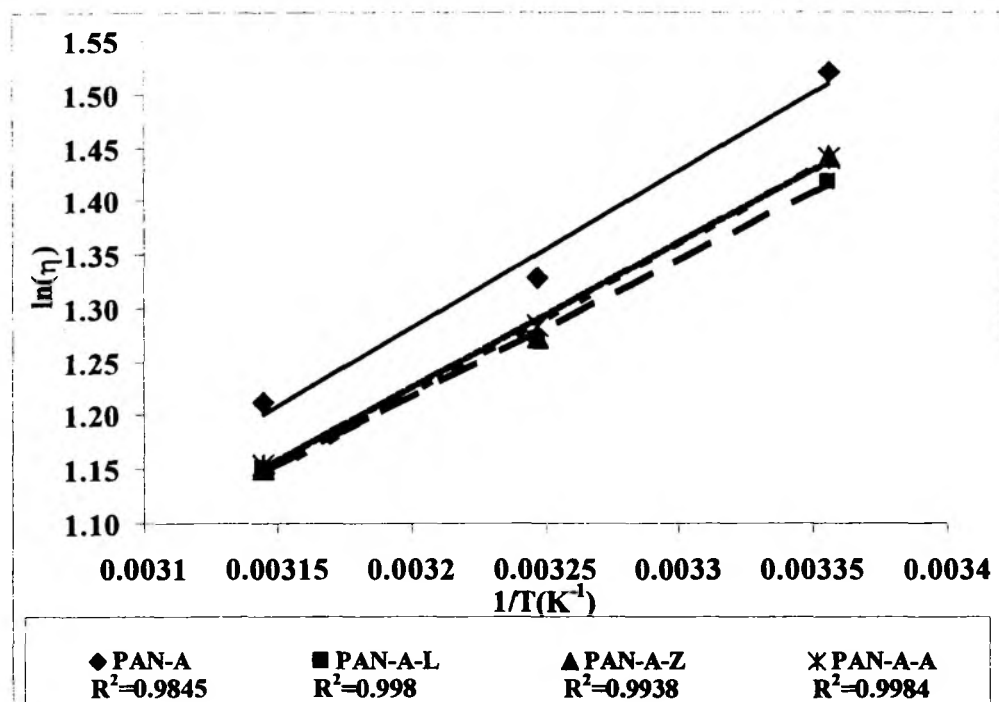


Figure 3.12c: Arrhenius plots of  $\eta$  vs  $1/T$  for PAN-A (0.3%) polymer solution with and without additives as function of temperature (298-318 K).

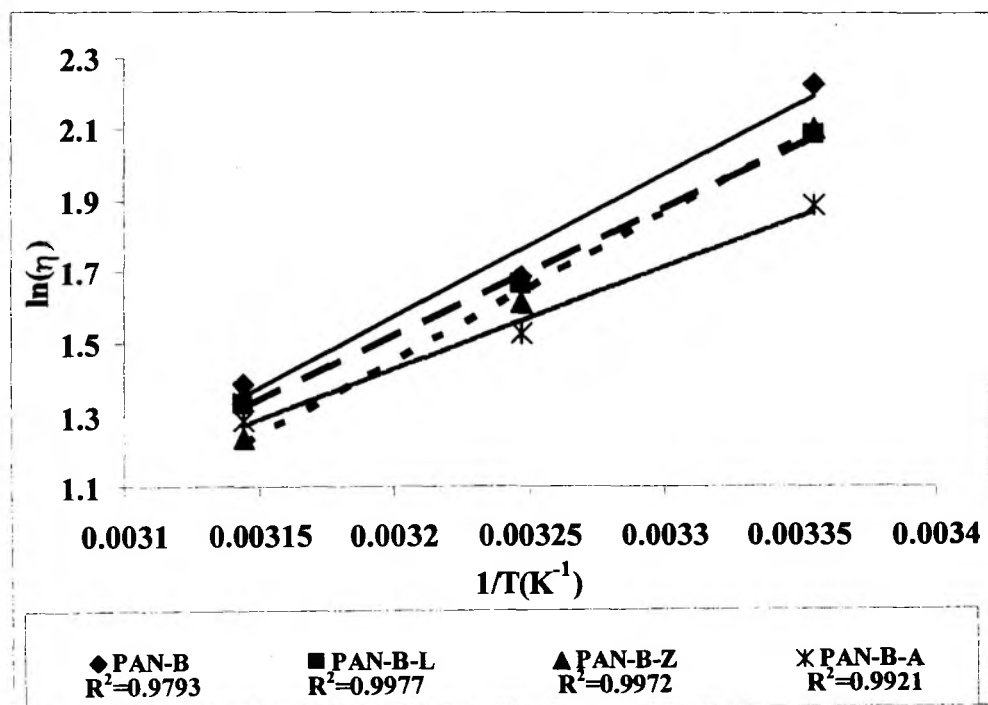


Figure 3.12d: Arrhenius plots of  $\eta$  vs  $1/T$  for PAN-B (0.1%) polymer solution with and without additives as function of temperature (298-318 K).

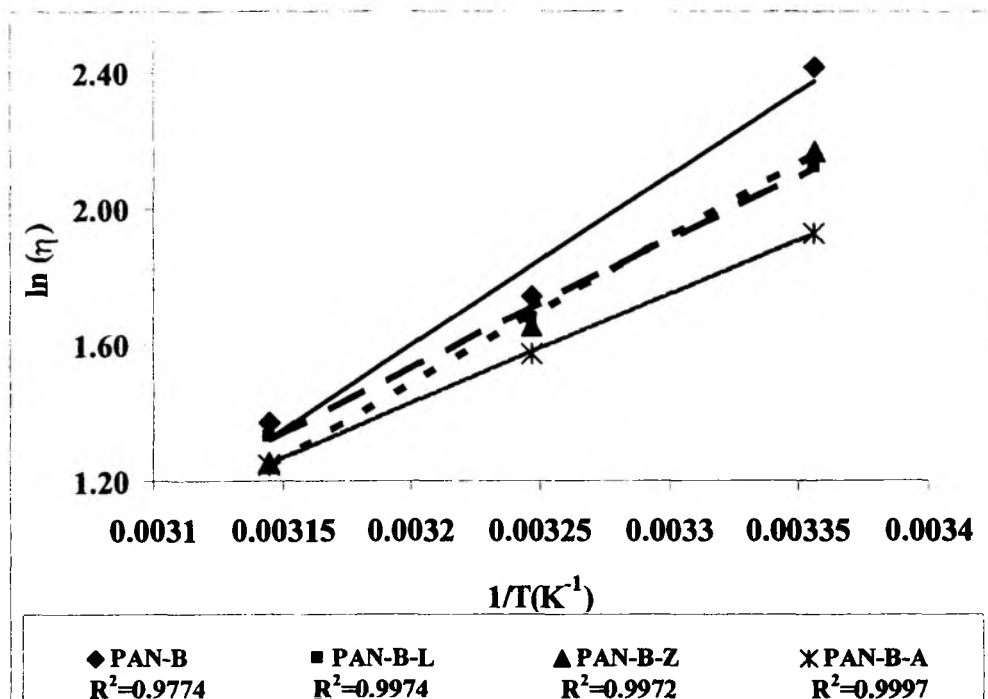


Figure 3.12e: Arrhenius plots of  $\eta$  vs  $1/T$  for PAN-B (0.2%) polymer solution with and without additives as function of temperature (298-318 K).

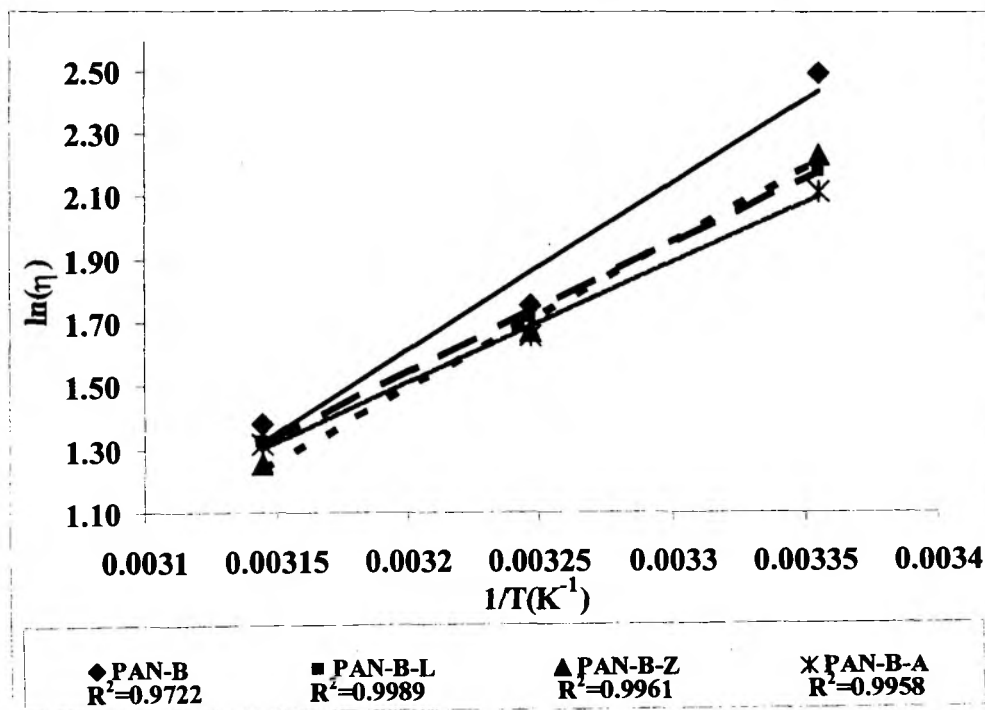
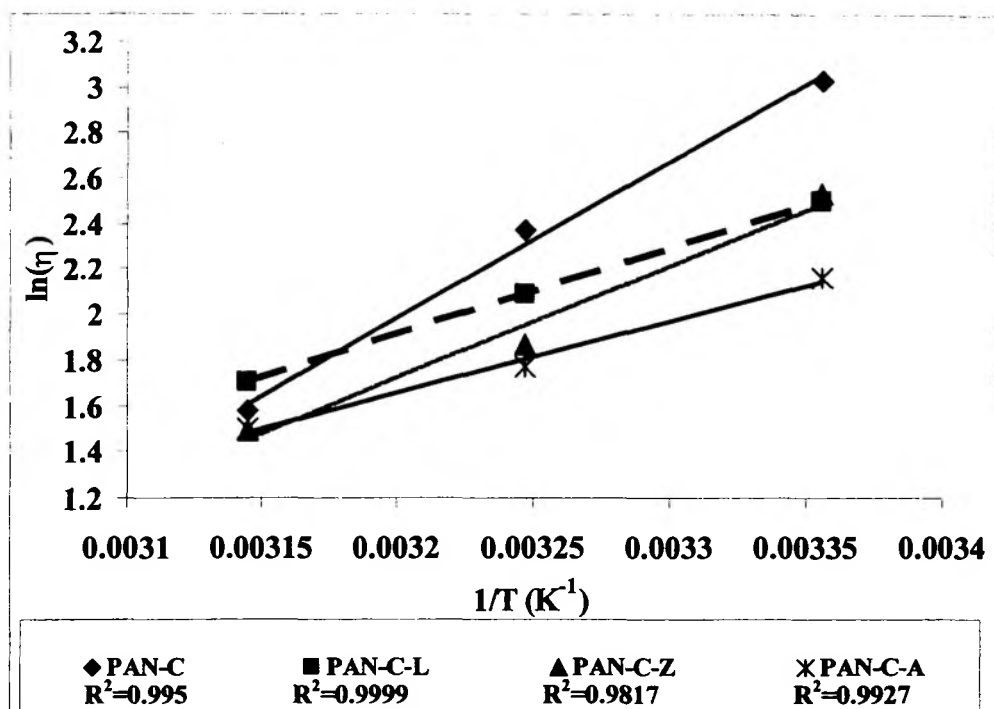
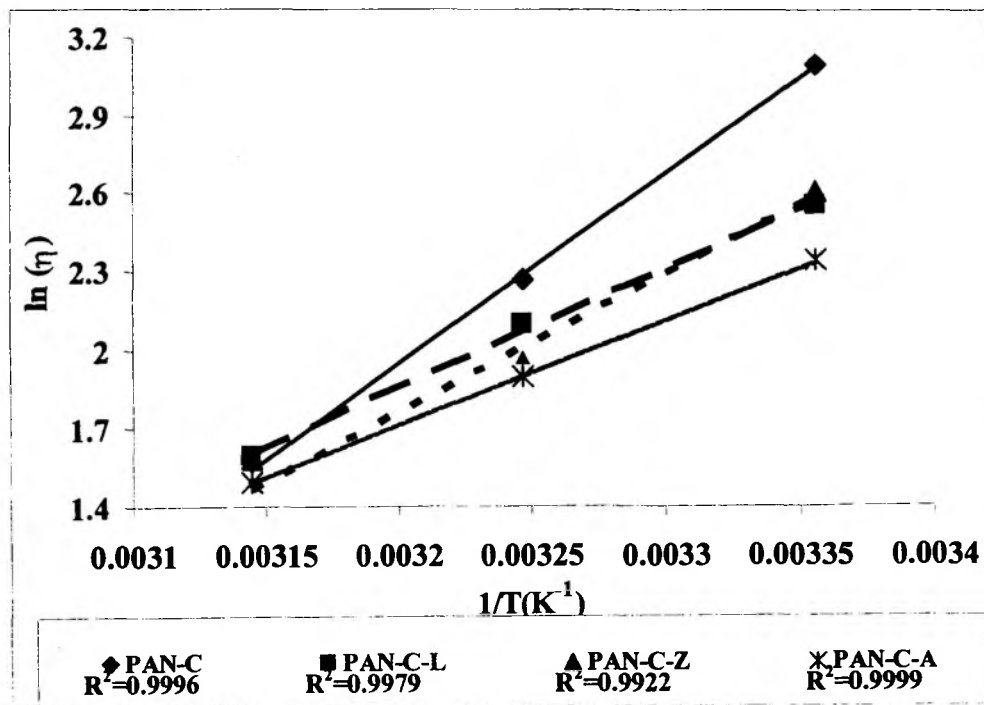


Figure 3.12f: Arrhenius plots of  $\eta$  vs  $1/T$  for PAN-B (0.3%) polymer solution with and without additives as function of temperature (298-318 K).



**Figure 3.12g:** Arrhenius plots of  $\eta$  vs  $1/T$  for PAN-C (0.1%) polymer solution with and without additives as function of Temperature (298-318 K).



**Figure 3.12h:** Arrhenius plots of  $\eta$  vs  $1/T$  for PAN-C (0.2%) polymer solution with and without additives as function of Temperature (298-318 K).

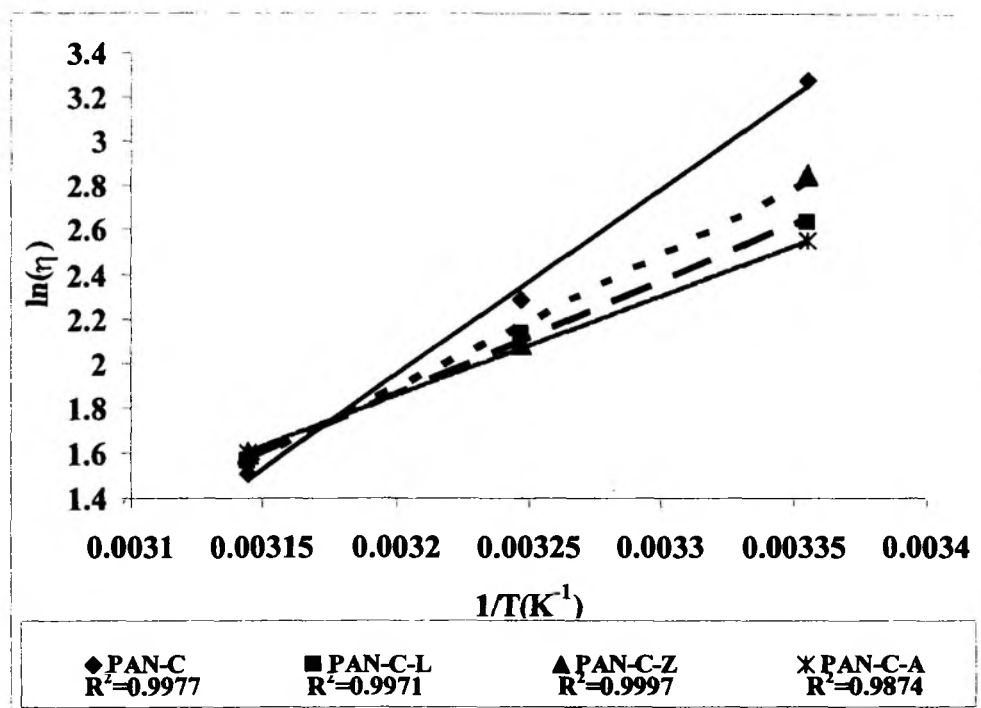


**Figure 3.12i:** Arrhenius plots of  $\eta$  vs  $1/T$  for PAN-C (0.3%) polymer solution with and without additives as function of Temperature (298-318 K).

The data are interpreted in the following sections where various rheology parameters: intrinsic viscosity, Mark-Houwink constants and viscosity activation energy are calculated.

### 3.3.3 Intrinsic Viscosity calculations and interpretation

The effect of additive type on intrinsic viscosity  $[\eta]$  is described in this section. For a given polymer of molecular weight  $M$ , intrinsic viscosity  $[\eta]$  is related to the chain expansion in that solvent as given in equation (3.1).

$$[\eta] = \phi \alpha^3 (r^2)^{3/2} / MW \quad (3.1)$$

where,  $\phi$  is a universal constant, and  $MW$  is the polymer molecular weight. Length  $(r^2)^{3/2}$  is the mean square end-to-end distance of the unperturbed coil i.e. in a theta solvent. The coil expansion coefficient,  $\alpha$ , is the ratio of the end-to-end distance of a

random coil in a particular solvent over the unperturbed end-to-end distance of the same polymer molecule.

Typically, a high  $[\eta]$  indicates a solvent which has a high solvation affinity for the polymer. For a given polymer-solvent combination  $[\eta]$  is higher for higher molecular weight grades.

Intrinsic viscosity was calculated by several methods. At first,  $[\eta]$  was calculated from the Huggins's method [Huggins, 1942] defined by extrapolation to zero concentration,  $c$ , using equation 3.2.

$$\eta_{red} = \frac{\eta_{sp}}{c} = [\eta] + k'[\eta]^2 c \quad (3.2)$$

The Huggins's parameter  $k'$  is also an indicator of the polymer solvating power of that solvent; for good solvents,  $k'$  is  $< 0.5$  [Billmeyer, 1984].

Table IIIA-3.7a in Appendix III-1 shows values for the intrinsic viscosity,  $[\eta]$  of PAN calculated from equation 3.2 measured both in neat DMF and in DMF containing various salts for all the three polymers PAN-A, B and C and at three temperatures 25, 35 and 45°C. Table IIIA-3.7b shows the corresponding values for  $k'$ . These analyses show a large amount of scatter. An explanation for this problem is given by a recent paper by Bercea [1999] who found that plots of  $\eta_{sp}/c$  vs  $c$  for PAN solutions in DMF show large deviations from linearity in the dilute region below 1.0 % polymer concentration. Our experience corroborates this observation (see Figure IIIA-2.1-2 in Appendix III-2).

Since the Huggins's equation cannot be used to estimate  $[\eta]$  in this concentration range, intrinsic viscosities were calculated by "one-concentration-point" techniques (see equation 1.8). The choice of the concentration at which  $[\eta]$  is calculated changes the estimate because of the nonlinearity of  $\eta_{sp}/c$  vs  $c$ . In order to gage the robustness of the one-point methods, estimates were made by several techniques. Table 3.7 shows  $[\eta]$  estimates at a polymer concentration of 0.2 g/dl by three different one-point calculation procedures: Under-root method [Raju and Yaseen, 1992] the Solomon-Ciuta method [Nero, 1982] and the Billmeyer equation [Billmeyer, 1984] (see Appendix III-1 for

details). These  $[\eta]$  estimates are based on the 25°C data set; within experimental error, there is no consistent trend for  $[\eta]$  with temperature.

**Table 3.7:** One point intrinsic viscosity estimates by three different methods at a polymer concentration of 0.2 g/dl

	<b>Under-root method</b>	<b>Solomon-Ciuta method</b>	<b>Billmeyer equation</b>
PAN-A	1.06	2.56	3.50
PAN-A-L	1.22	2.80	4.07
PAN-A-Z	1.23	2.75	3.94
PAN-A-A	1.17	2.80	4.07
PAN-B	2.70	4.87	9.39
PAN-B-L	2.56	4.73	9.02
PAN-B-Z	2.66	4.68	8.88
PAN-B-A	2.30	4.46	8.29
PAN-C	3.47	6.67	14.16
PAN-C-L	3.42	6.13	12.75
PAN-C-Z	3.33	5.94	12.26
PAN-C-A	3.28	5.65	11.44

All the three methods give different absolute intrinsic viscosity estimates; however, the relative trend shown by the different calculation methods for all solutions is the same.

The  $[\eta]$  estimates for PAN-A and the higher MW grades PAN-B and C show different trends. In the case of PAN-A, we see higher  $[\eta]$  values in solutions containing the salts compared to neat DMF. By contrast, in the case of PAN-B and PAN-C, salt addition has only a marginal effect or actually decreases the  $[\eta]$  value indicating that the polymer chain is less expanded. This seemingly contradictory behavior may be attributed to two opposing tendencies of the salt. We know that salt can promote association between the polymer chains thus the effectively higher MW chain would have a higher  $[\eta]$  value. This effect would be most pronounced for the lower MW grade

PAN-A. On the other hand, we also know (section 3.2.1) that the salt complexes with DMF, the complexed solvent would be expected to be a worse solvent in which the polymer chain would experience less affinity and coil expansion (low  $[\eta]$ ). The change in solvation capability would be more pronounced for the higher MW grades, PAN-B and C.

### 3.3.3.1 Mark-Houwink (M-H) constant estimation

The molecular weight of PAN was estimated by the Mark-Houwink equation:

$$[\eta] = K' M^a \quad (3.3)$$

where M is viscosity average molecular weight and K' and  $a$  are the Mark-Houwink constants. There is a specific set of Mark-Houwink constants for every polymer-solvent combination. The constant  $a$  is a scalar which relates to the "stiffness" of the polymer chains. If the polymer molecules in solution were rigid rods,  $a=2$ ; while if the polymers were hard spheres,  $a=0$ . If  $a=1$ , the polymers are semicoils. In a Flory theta solvent,  $a=0.5$ , and in a thermodynamically good solvent,  $a=0.8$ .

The Mark-Houwink constants for PAN at 25°C are reported to be  $K' = 3.17 \times 10^{-4}$  dl /g and  $a = 0.75$  [Beever, 1968]. These parameter estimates are also corroborated by several other researchers [Bisschops, 1955; Cleland and Stockmayer, 1965; Onyon, 1956]. As described above, the dilute solution viscosity measured at 0.2% polymer concentration and 25°C were used to estimate  $[\eta]$  values for the three PAN grades in neat DMF. The  $[\eta]$  values in neat DMF at 25°C and the corresponding molecular weights calculated from these data and the known M-H constants [Beever 1968] are shown in Table 3.8. The viscosity-average molecular weight increases in the order PAN -A < B < C. The copolymer has a comparatively smaller degree of polymerization.

**Table 3.8:** The intrinsic viscosities measured at 25°C and the molecular weight values calculated using reported Mark Houwink constants ( $K' = 3.17 \times 10^{-4}$  dl/g;  $a = 0.75$ ).

Polymer	Intrinsic Viscosity, $[\eta]$ at 25°C	Molecular weight (kDa)
PAN-A	1.06	50
PAN-B	2.63	168
PAN-C	3.55	250
PAN-1	0.81	35

With these molecular weights now known, we can estimate Mark-Houwink constants in different solvents (DMF+salts) from the equation:

$$\ln[\eta] = \ln K' + a \ln M \quad (3.4)$$

Plots of  $\ln[\eta]$  vs  $\ln M$  for each solvent type (DMF, DMF-L, DMF-Z and DMF-A) are shown in Figures 3.13(a-d) at 25, 35 and 45°C, respectively. The data show the same consistent trend which is typified by the Mark-Houwink plot from the data at 25°C (Figure 3.14) for the four solvents i.e. neat DMF, DMF+LiCl, DMF+ZnCl<sub>2</sub>, DMF+AlCl<sub>3</sub>. The corresponding M-H constants for each solvent type are summarized in Table 3.9.



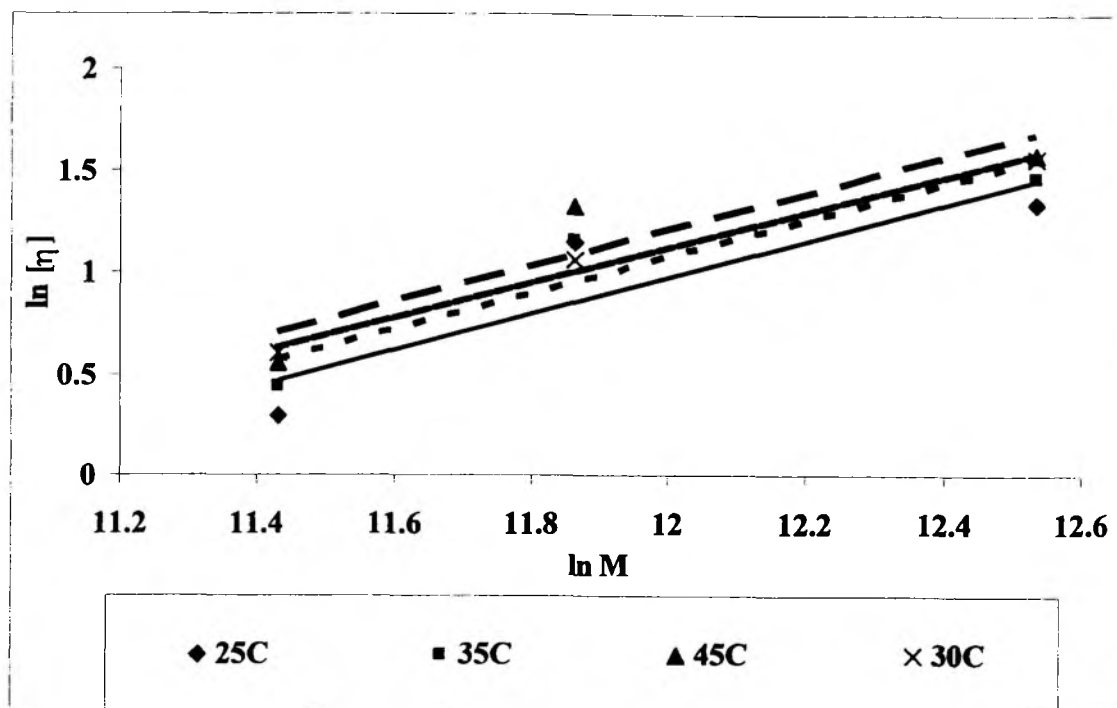


**Figure 3.13(a)** : Plot of  $\ln[\eta]$  vs  $\ln M$  for solvent type DMF at various temperatures; regression using equation 3.4; regression details as under:

Temperature (°C)	$R^2$	$A$	$\ln K'$
25	0.7911	0.8881	-9.6884
30	0.9911	0.8574	-9.1696
35	0.8832	0.8819	-9.5135
45	0.8414	0.8785	-9.3423

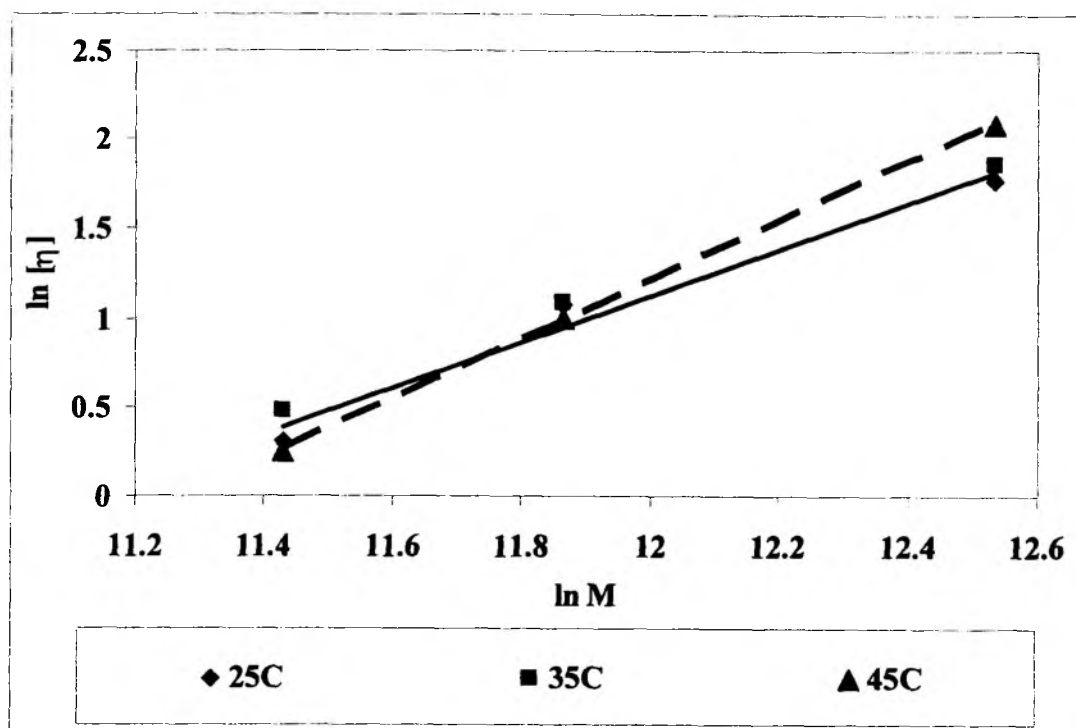


**Figure 3.13(b):** Plot of  $\ln[\eta]$  vs  $\ln M$  for solvent type DMF-L at various temperatures; regression using equation 3.4; regression details as under:

Temperature (°C)	$R^2$	$A$	$\ln k'$
25	0.9756	1.2939	-14.405
35	0.9975	1.2396	-13.664
45	0.9997	1.6548	-18.654

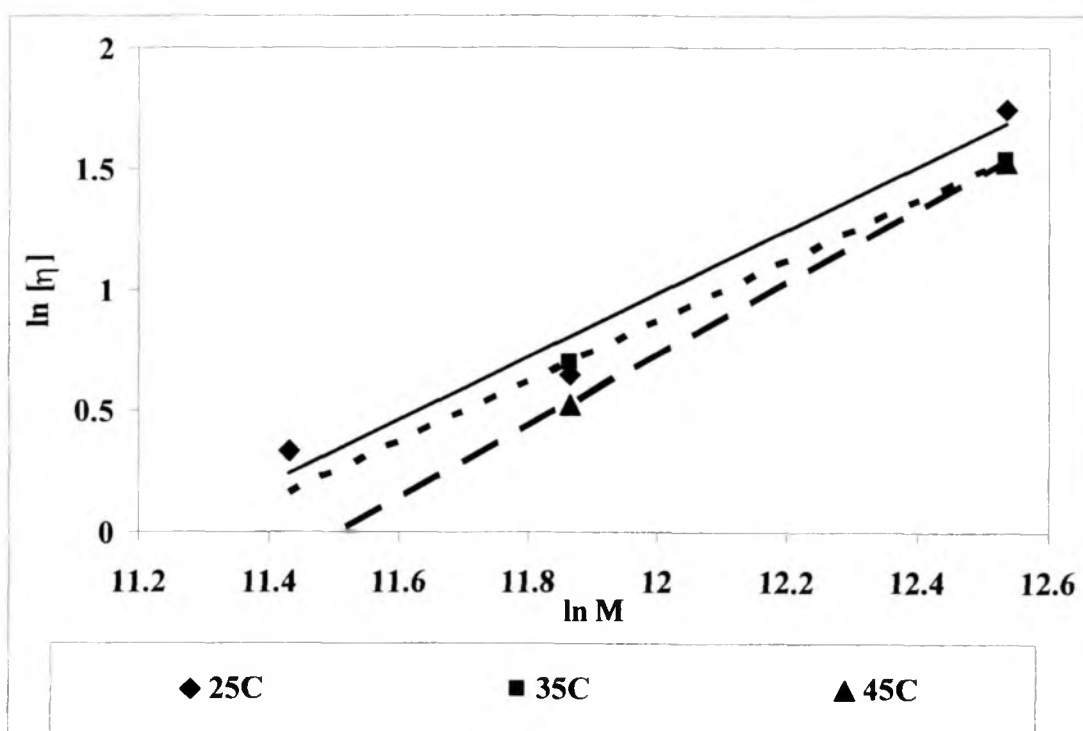


**Figure 3. 13(c) :** Plot of  $\ln[\eta]$  vs  $\ln M$  for solvent type DMF-Z at various temperatures; regression using equation 3.4; regression details as under:

Temperature (°C)	$R^2$	$A$	$\ln K'$
25	0.9672	1.3036	-14.66
35	1.0	1.2381	-13.99
45	1.0	1.4847	-17.089



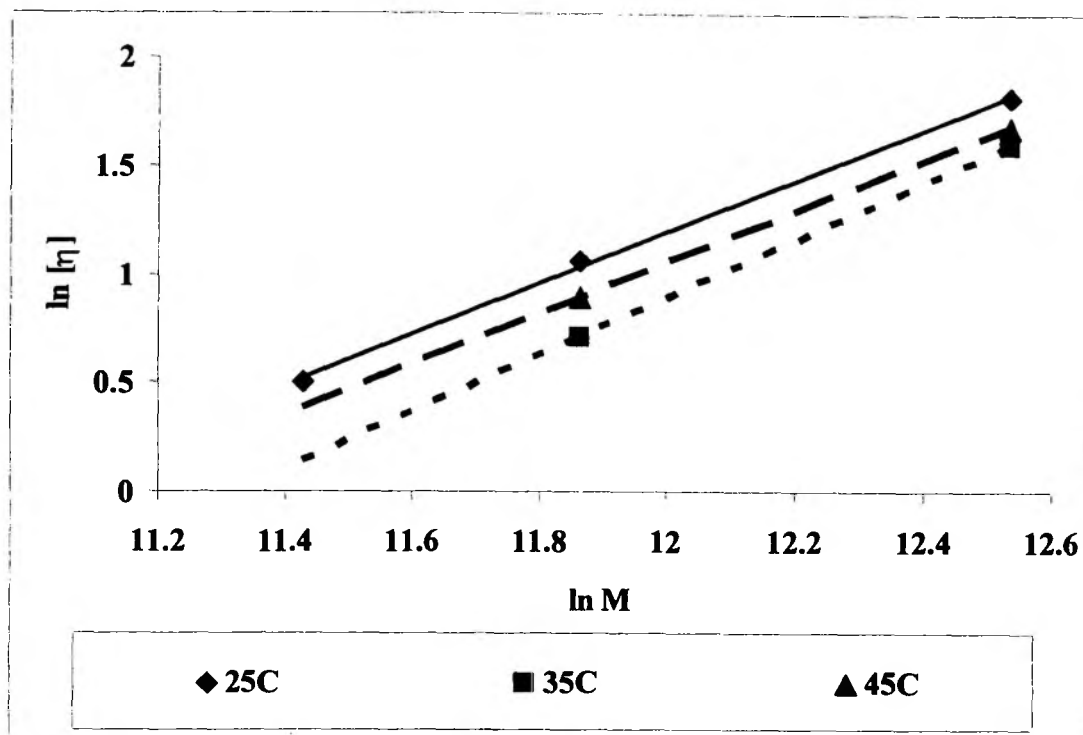


**Figure 3.13(d) :** Plot of  $\ln[\eta]$  vs  $\ln M$  for solvent type DMF-A at various temperatures; regression using equation 3.4; regression details as under:

Temperature (°C)	$R^2$	$A$	$\ln K$
25	0.999	1.1813	-12.98
35	1.0	1.3198	-14.949
45	1.0	1.1699	-12.99

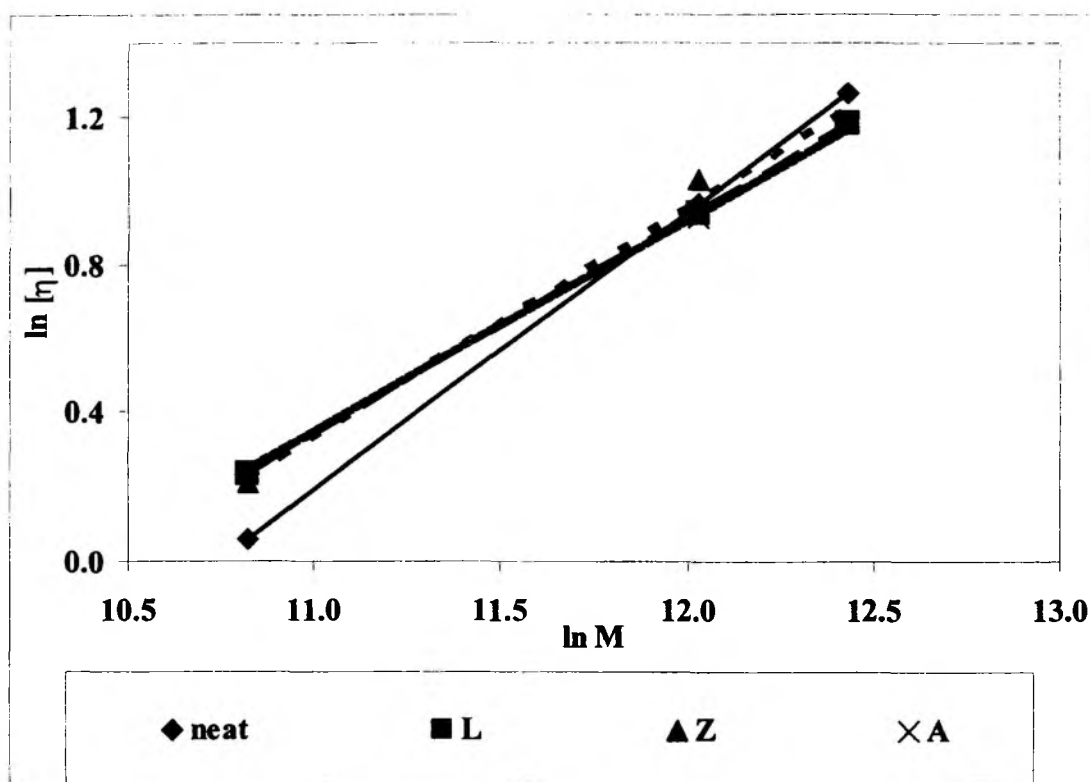


**Figure 3.14** : Mark-Houwink plot from the viscosity data at 25°C for all the four solvents i.e. neat DMF, DMF+LiCl, DMF+ZnCl<sub>2</sub>, DMF+AlCl<sub>3</sub>; regression details as under:

Salt	R <sup>2</sup>	<i>a</i>	lnK'
neat	1.0	0.7491	-8.0458
L	0.9998	0.5883	-6.1339
Z	0.9907	0.6193	-6.4761
A	0.9995	0.5797	-6.0334

**Table 3.9:** The Mark-Houwink constants at 25°C for the four solvents i.e. neat DMF, DMF+LiCl, DMF+ZnCl<sub>2</sub>, DMF+AlCl<sub>3</sub>.

Solvent	Mark-Houwink constants	
	K'	<i>a</i>
DMF	3.2E-04	0.75
DMF-L	2.2E-03	0.59
DMF-Z	1.5E-03	0.62
DMF-A	2.4E-03	0.58

The calculations of the Mark-Houwink constant in solutions made with the salt additives indicate that the general effect of the salt is to decrease the PAN chain expansion. As seen from the above table the exponent  $a$  decreases from 0.75 in DMF to  $\sim 0.6$  for DMF+salt solutions. Salt addition thus makes DMF approach the theta-solvent condition for PAN.

### 3.3.4. Activation energy correlations

Activation energies,  $E_a$ , were calculated from the dilute solution viscosity data presented in Figures 3.15(a-c) and the Arrhenius relation as:

$$\eta = \eta_{r_0} \exp\left(-\frac{E_a}{RT}\right) \quad (3.5)$$

where,  $R$  is the gas constant and  $T$  the absolute temperature. The calculated  $E_a$  are tabulated in Table IIIA-3.1 in Appendix III-3 and shown in Figures 3.15 (a-c).

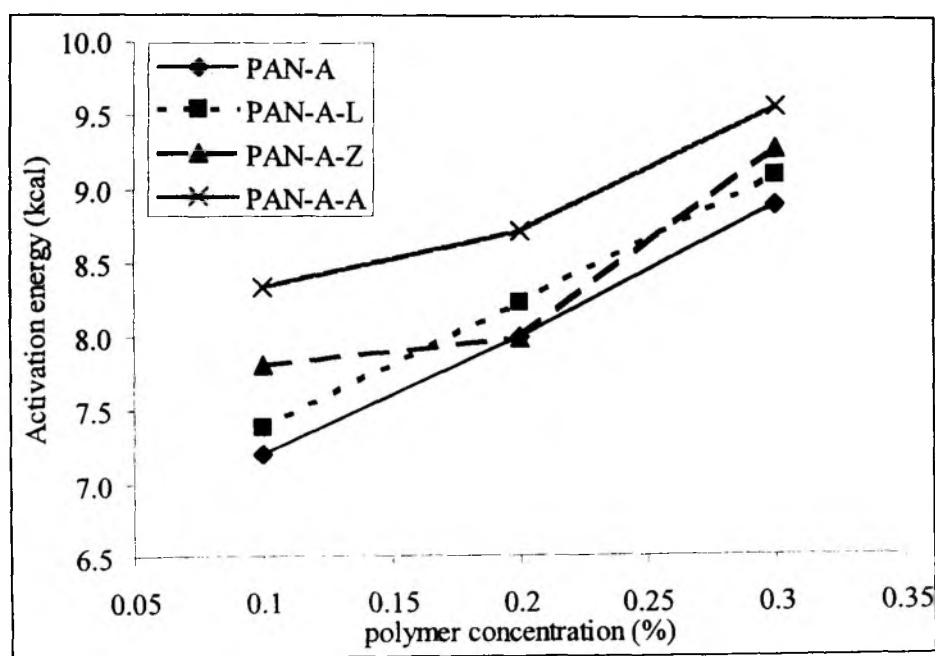


**Figure 3.15 (a):** Activation energy ( $E_a$ ) values for PAN-A as a function of polymer concentration for solvent types DMF, DMF-L, DMF-Z and DMF-A.

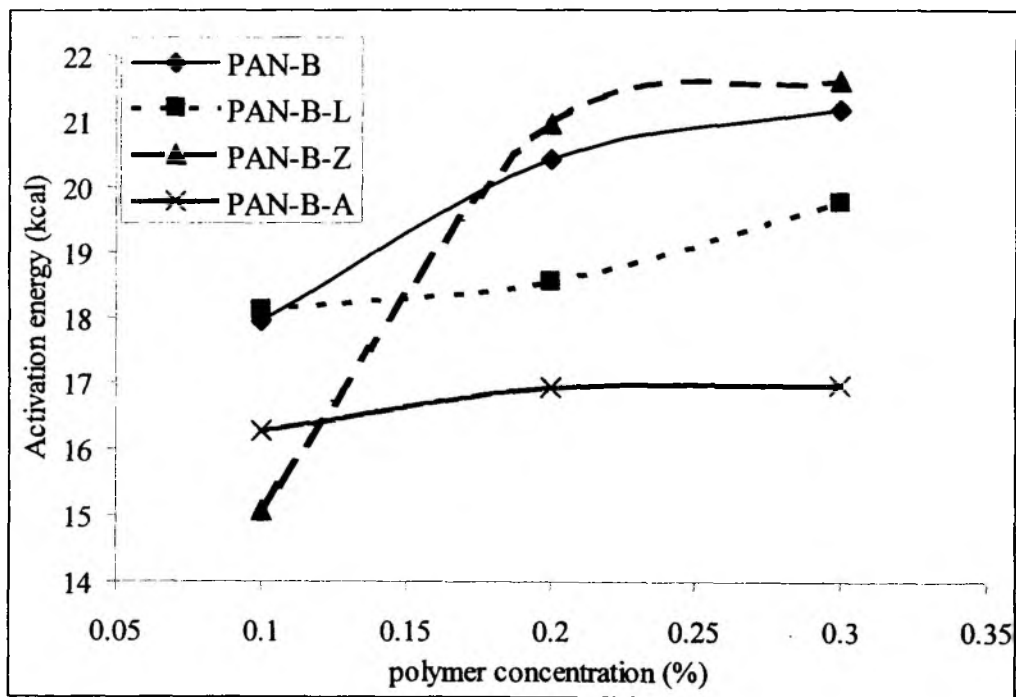


**Figure 3.15 (b):** Activation energy ( $E_a$ ) values for PAN-B as a function of polymer concentration for solvent types DMF, DMF-L, DMF-Z and DMF-A.

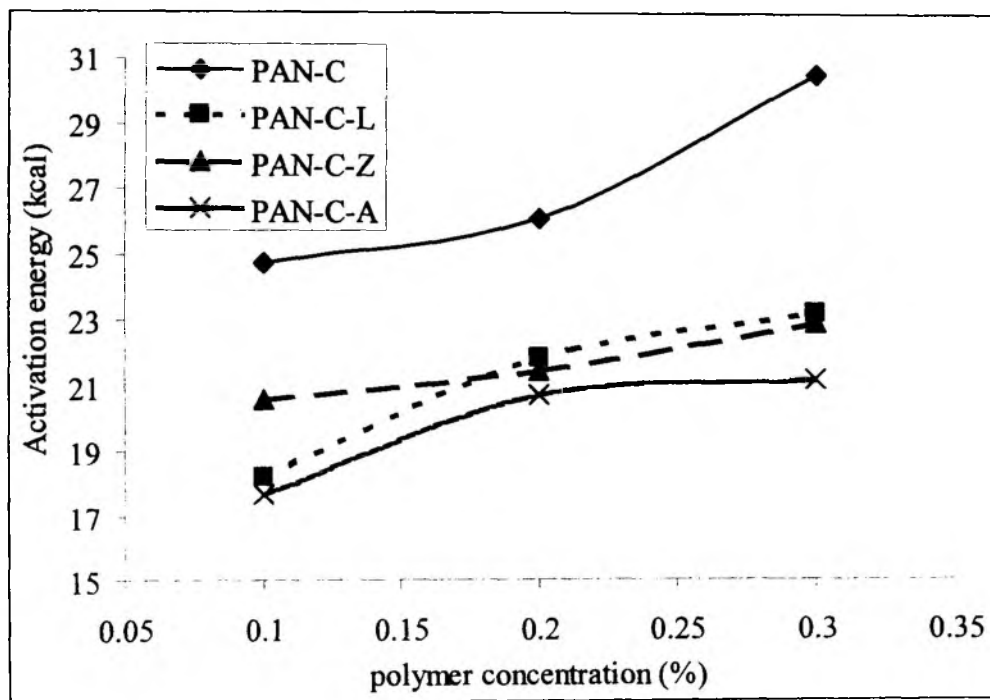


**Figure 3.15 (c):** Activation energy ( $E_a$ ) values for PAN-C as a function of polymer concentration for solvent types DMF, DMF-L, DMF-Z and DMF-A.

The theoretical justification for this relationship within a limited temperature region is given by the Eyring equation shown below:

$$\eta = \frac{2kT\beta}{\delta A} \frac{\sinh^{-1}(\beta \dot{\gamma})}{\beta \dot{\gamma}} \quad (3.6)$$

where,  $k$  is Boltzmann's constant and  $\beta$  ( $\equiv \lambda / 2\delta k_R$ ) is a cluster of constants;  $\lambda$  is the distance over which the displacement occurs,  $\delta$  is the forward distance a molecule moves in a single flow step,  $k_R$  the frequency of the steps,  $\dot{\gamma}$  is the shear rate and  $A$  is the frequency at which molecules cross the energy barrier. Eyring's theory postulates an energy barrier, to that must be overcome for a polymer motion to occur, thus  $k_R$  is expressed as:

$$k_R = A \exp\left(-\frac{\Delta\varepsilon^*}{kT}\right) \quad (3.7)$$

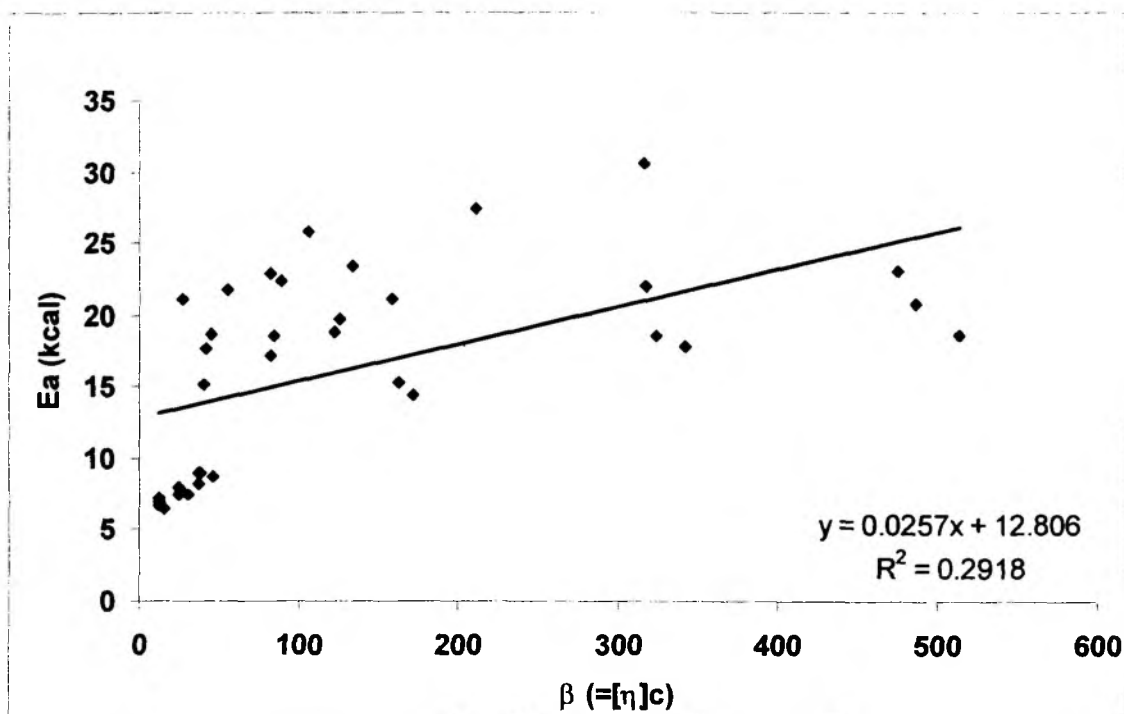
Based on the Eyring treatment, the activation energy is interpreted as the energy barrier that must be overcome for a polymer "jump" to occur.

The data in Figures 3.15 (a-c) shows the  $E_a$  values for each PAN grade as a function of polymer concentration for each solvent type. The solutions in DMF typically show the highest  $E_a$  values followed closely by the  $E_a$  estimates in DMF-Z. The  $E_a$  estimates in DMF-L and DMF-A are generally lower.

As shown in eqns ( 3.6-3.7)  $E_a$  is expected to correlate well with the chain size and the number density of chains in solution ie. it is a measure of the polymer chain interaction in a particular solution. A commonly accepted measures of chain interaction in solution is the coil overlap parameter or Berry number,  $\beta \equiv [\eta]c$ . This relation can be

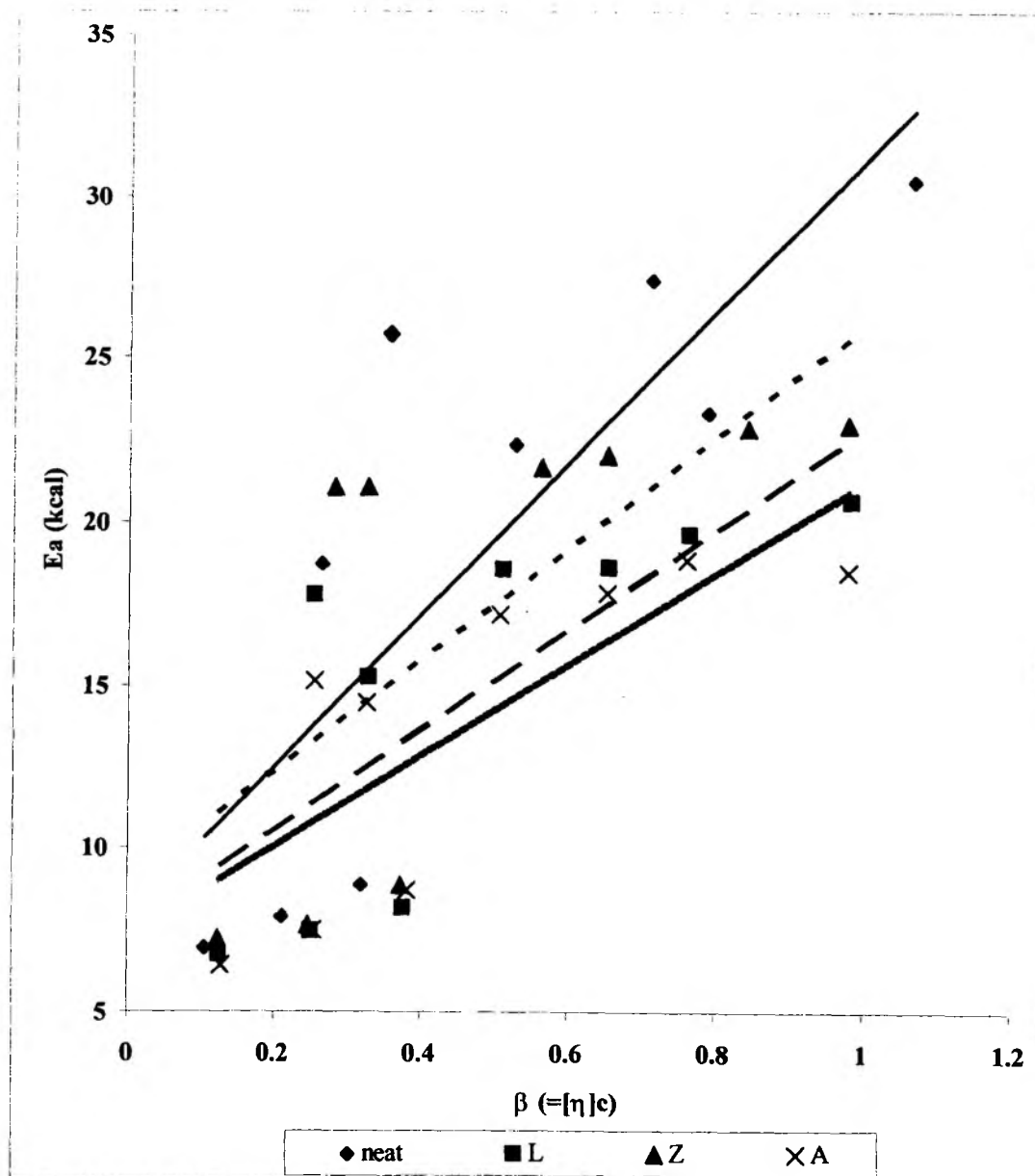


used to construct a “master” plot as shown in Figure 3.16 which shows a correlation between  $E_a$  and the coil overlap parameter,  $[\eta]c$ .



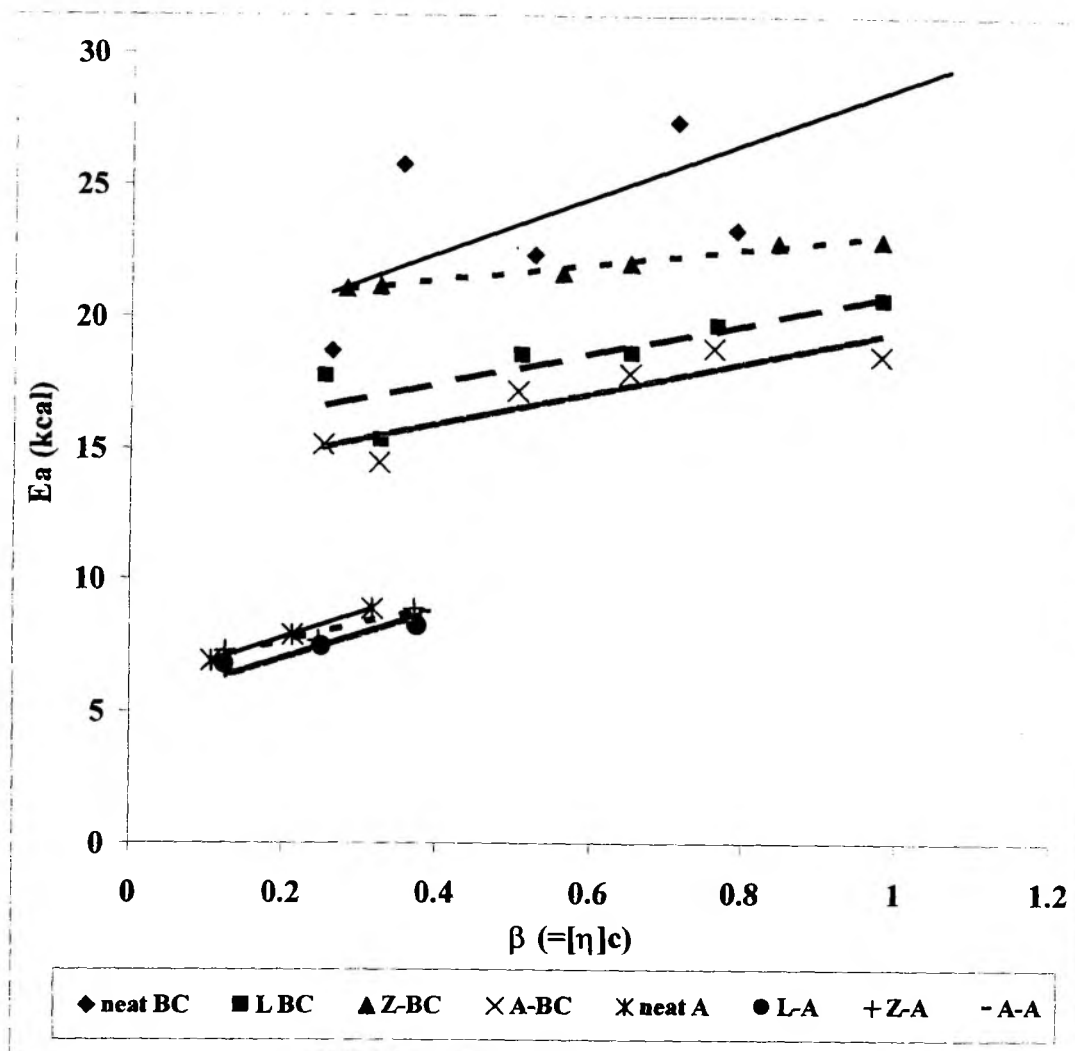
**Figure 3.16:** Correlation between the activation energy ( $E_a$ ) and the coil overlap parameter,  $[\eta]c$ .

Figure 3.17 shows the same data as in Figure 3.16 categorized according to solvent type. The  $E_a$  values show the clear trend: DMF > DMF-Z > DMF-L > DMF-A. Also the  $E_a$  values increase with increasing coil overlap in the same trend.



**Figure 3.17:** Correlation between the activation energy ( $E_a$ ) and the coil overlap parameter  $\beta$  categorized by solvent type i.e. neat DMF, DMF-L, DMF-Z and DMF-A; regression parameters as under:

Solvent	$R^2$	Slope	Intercept
neat	0.6656	23.359	7.8231
Z	0.4878	17	8.9989
L	0.5686	15.324	7.532
A	0.6177	14.071	7.2254



**Figure 3.18:** Correlation between the activation energy ( $E_a$ ) and the coil overlap parameter  $[\eta]c$  for the solvent type i.e. neat DMF , DMF-L, DMF-Z and DMF-A for the three polymer PAN-A, PAN-B and PAN-C; regression parameters as under:

Solvent	$R^2$	Slope	Intercept
Neat BC	0.5884	10.667	18.096
Z-BC	0.9738	2.9901	20.139
L-BC	0.7265	5.7666	15.058
A-BC	0.8205	6.0095	13.517
neat A	1.0	9.3652	5.9345
Z-A	0.9214	6.6784	6.2868
L-A	1.0	5.7514	6.017
A-A	0.9981	8.9879	5.2681

The correlation in Figure 3.17 is poor; it is obvious that the PAN-A data (lower  $E_a$  values) fit a different correlation than those for the higher MW grades. Figure 3.18 replots the same data with two different trend lines for PAN-A and the higher MW grades. However even with this distinction between PAN-A and the higher MW grades, the trend of  $E_a$  for the various solvent types remains the same ie: DMF > DMF-Z > DMF-L > DMF-A.

The lower  $E_a$  values for dilute PAN solutions with all three salt additives compared to neat DMF correspond with the chain expansion trends discussed in section 3.2.2. The relatively high  $E_a$  values for  $ZnCl_2$  compared to the other two salts may indicate a higher tendency to promote association between PAN chains.

### 3.4 Discussion summarizing Chapter III

The goal of this chapter was to define three issues: (i) the interaction of salts with solvent DMF, (ii) the interaction of salts with PAN and (iii) differences between the three salt additives ( $LiCl$ ,  $ZnCl_2$ ,  $AlCl_3$ )

(i) *Effect of salts on DMF*: FT-IR shows that all three salts complex with DMF. The strength of the cation interaction with the  $-OCN$  group of DMF is much stronger than the interaction with the  $-CN$  group of PAN. This is consistent with the known higher basicity of DMF compared to the PAN nitrile group.

The strong complex formed between the salt and DMF will reduce DMF's ability to solvate the polymer. Calculations of the Mark-Houwink constant in solutions made with the salt additives indicate that the general effect of the salt is to decrease the PAN chain expansion; the exponent  $a$  decreases from 0.75 in DMF to  $\sim 0.6$  for DMF in salt solutions. Similarly, the viscosity activation energy  $E_a$  increases more sharply with increasing coil overlap parameter  $\beta$  for neat DMF solutions compared to those with the salt additives. All these data show that these salt additives cause DMF to change from a good solvent towards a theta-solvent for PAN.

(ii) *Effect of salts on PAN*: IR was not able to detect any direct interaction between the salts and PAN. However, comparing the -OCN frequency shifts in the salt-PAN-DMF ternary systems with the binary PAN-DMF systems indicates that PAN is weakly affected by the presence of the salt.

The rheology studies show clear differences between the effect of the salt on the lower MW grade PAN-A compared to the higher MW materials. The viscosity and activation energies are markedly higher for PAN-B and PAN-C solutions. The effect of the salt on PAN appears to be via two mechanisms: (i) the decrease in the DMF solvation power which shrinks the polymer coils and (ii) increased inter-polymer chain entanglements via salt-promoted chain association. The  $[\eta]$  estimates for PAN-A are higher in DMF+salt solutions compared to those in neat DMF. The values for PAN-B are essentially unchanged with the salt while those for the highest MW grade, PAN-C decrease with salt addition. The decreased  $[\eta]$  seen for the highest PAN MW material correlates with the decreased DMF solvation power. The increase in  $[\eta]$  for the lower MW PAN-A (50k) may be attributed to interchain association promoted by the salts.

(iii) *Comparison between salt additives*: Though all three salts reduce the DMF solvation power, there are differences in their strength of complexation with the solvent. In particular, the Zn cation forms complexes with DMF more facily than the other two cations. The  $>C=O$  stretching frequency observed in pure DMF remained essentially unchanged in both DMF-L and DMF-A, whereas a red shift indicating more favorable complexation was observed in case of DMF-Z. This observation is correlated with the electronic cloud density around these cations. The energy involved in complexation of the electronegative carbonyl O of DMF with a cation is the highest for  $Al^{3+} > Li^+ > Zn^{2+}$ . Both anion ( $Cl^-$ ) and cation affect salt interaction with the OCN group of DMF. Red shifts (following the trend of  $Al^{3+} > Zn^{2+} > Li^+$ ) observed in the OC-N stretching frequency can be attributed to the increasing electron cloud density of  $Cl^-$  near slightly electropositive nitrogen (compared to oxygen).

The trend of the viscosity activation energies,  $E_a$  for the various solvent types is: DMF > DMF-Z > DMF-L > DMF-A. The relatively high  $E_a$  values for  $ZnCl_2$  compared to the other two salts may indicate a higher tendency to promote the association of PAN chains.

## Chapter IV

This chapter describes the rheological, phase-boundary and membrane properties of various DMF + salt solutions based on the commercial product PAN-A. The solution viscosity and the polymer-solvent-nonsolvent (water) phase boundary are considered critical variables affecting membrane pore formation.

The details of the solution preparations and experimental techniques are given in Chapter II. These conditions hold for all the data discussed in this chapter unless specifically mentioned otherwise. The various salt+DMF+PAN solutions are identified by the same nomenclature defined in Chapter III. The polymer solutions in DMF alone are denoted by the polymer notation alone (viz. PAN-A). Polymer solutions in DMF+salts is denoted by both the polymer and salt used e.g. PAN-A-Z represents the solution of PAN-A in DMF + ZnCl<sub>2</sub>.

The salt solutions discussed in Chapter III and later in Chapter V were made at constant ionic strength (0.83 M) of the various salts in DMF. The salt solutions discussed in this chapter were made at a constant 4% (wt) concentration of the various salts in DMF. The ionic strength (product of the salt molarity x cation valency) may be used as an upper limit estimate for solvent complexed with each cation. This product is 0.8357 M for LiCl, 0.2785 M for ZnCl<sub>2</sub> and 0.1393 M for AlCl<sub>3</sub>.

Dilute solution viscosity studies were described in Chapter III. These studies along with infra-red spectroscopy (IR) studies were used to draw inferences regarding various interactions in the DMF-PAN-salt system. The present chapter describes the concentrated solution rheology, solution phase-boundary characteristics and resulting properties of membranes cast from various salt (LiCl, ZnCl<sub>2</sub> and AlCl<sub>3</sub>) containing solutions based on the commercially available low MW grade PAN-A.

### 4.1 Rheological properties

The effect of solution temperature and additive type on dilute solution viscosity is described in section 3.3.2. The addition of both mono- and multivalent salts to PAN-A / DMF solution increased the measured PAN-A intrinsic viscosity  $[\eta]$ . However,

analysis of the Mark-Houwink exponent indicates that this effect is not related to chain expansion in salt-solutions but to salt-promoted polymer association for PAN-A. Literature [Cho et al, 1994; Edwards et al, 1992] supports our IR findings that cations can form complexes with DMF and to a weaker extent with PAN. All these effects point to reduced PAN – DMF affinity in presence of salts.

Salts can complex with DMF at either its electronegative carbonyl O or the more electropositive N. The strong complex formed between the salts and DMF will reduce DMF's ability to solvate the polymer. The dilute solution rheology data discussed in Chapter III show that all three salt additives cause DMF to change from a good solvent towards a theta-solvent for PAN.

Though all three salts reduce the DMF solvation power, there are differences in their strength of complexation with the solvent. In particular,  $ZnCl_2$  forms complexes with DMF more facilely than the other two salts. In addition, it may be possible for multivalent cations to bridge between chains

#### ***4.1.1 Concentrated solution viscosity***

Concentrated polymer solutions in the range of 1-17 % w/v were made with and without the additive for PAN-A, at room temperature on a mechanical stirrer. The viscosity of the polymer solutions was measured at 30°C using a Brookfield Cone and Plate viscometer (DV-I) as a function of shear rate.

Two different spindles were used to measure the polymer solution viscosity: cp-40 for solutions with low viscosities while cp-52 was used for concentrated/viscous solutions. The shear rate range for spindle cp-40 is between 3.75-750  $sec^{-1}$  while that for cp-52 is 1-200  $sec^{-1}$ . For comparison of data, a specific shear rate was chosen at which most of the solutions could be characterized from which the following significant features are observed:

1. The concentrated solution viscosity at 3.75  $sec^{-1}$  is shown as a function of polymer concentration in Figure 4.1a in the form of a semi-logarithmic plot. The viscosity increases with increasing concentration; the slope of these trend lines follow the ordering: PAN-A-Z > PAN-A > PAN-A-L. This trend indicates that

the polymer entanglement at high concentrations is more effective in the presence of ZnCl<sub>2</sub>. Gandhi et al [1971] have found that the increase in viscosity is greater in thermodynamically poorer solvents because of greater polymer-polymer interaction. By contrast at low concentration, viscosity is frequently higher in better solvents because of the chain expansion and excluded volume effect. There is insufficient data with PAN-A-A to define the slope on this graph; however, more extensive rheology measurements in Chapter V will show that the DMF-A solvent is positioned between DMF-Z and neat DMF on similar rheology correlations.

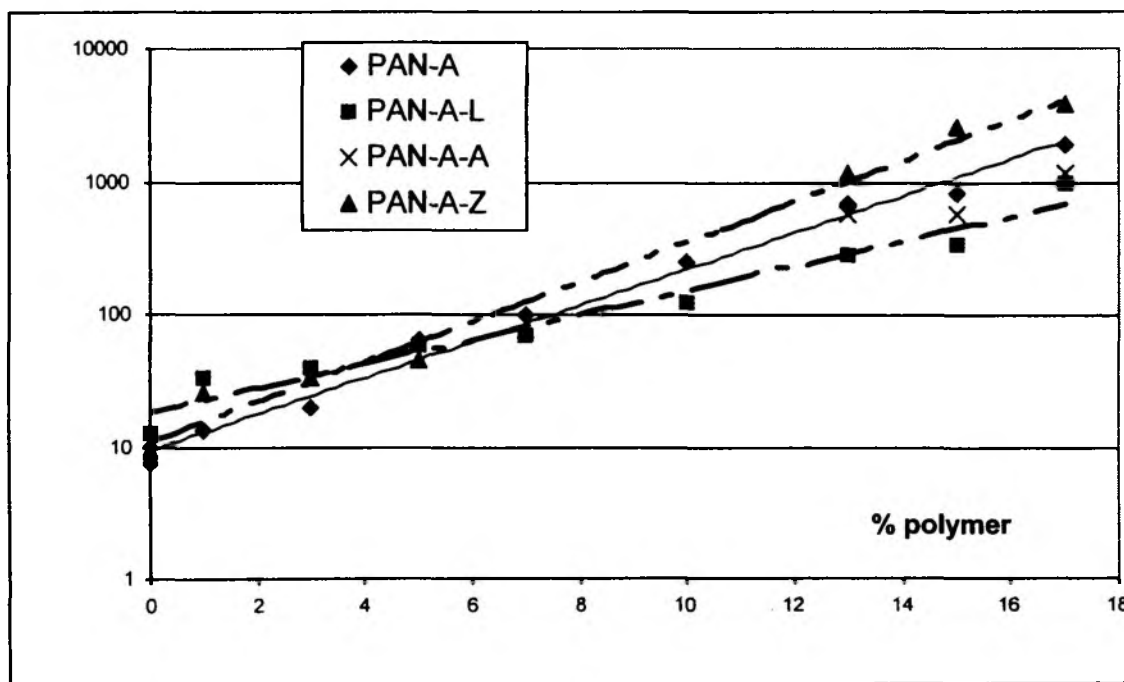


**Figure 4.1a.** Log viscosity (at 3.75 sec<sup>-1</sup> shear rate) as a function of PAN-A concentration in solutions with various solvents: DMF, DMF-L, DMF-Z and DMF-A. The trend lines are fitted to the empirical relation:  $\eta = I + S \cdot c$  where intercept  $I$  and slope  $S$  are given below:

Solvent	$I$	$S$	$R^2$
DMF	9.36	0.31	0.99
DMF-L	18.1	0.21	0.96
DMF-Z	10.8	0.35	0.98



- The data for each type of solution can be represented as two lines; the intersection of these lines represents the critical polymer concentration above which polymer entanglement in the solution leads to a more rapid increase in solution viscosity [Elias, 1977]. Cornet has defined the critical concentration  $c^*$  (concentration at which a plot of  $\ln \eta_0$  vs  $\ln c$  becomes linear) as the concentration at which a uniform segment density is achieved in the solution.

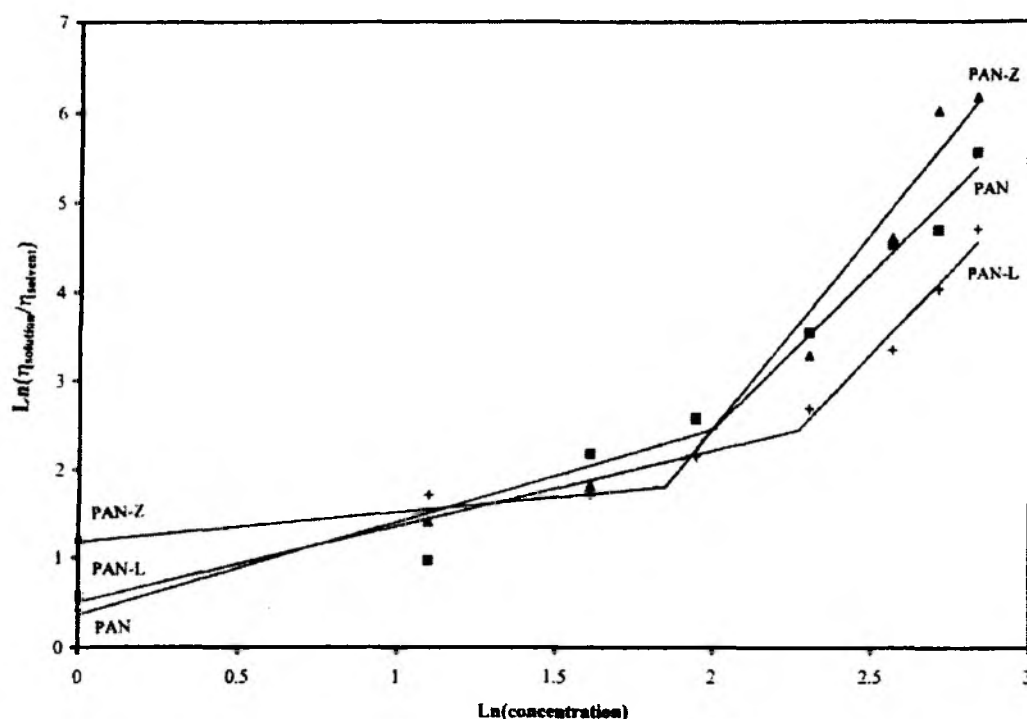


**Figure 4.1b:** Concentrated solution viscosity as a function of polymer concentration at a fixed shear rate of  $3.75 \text{ sec}^{-1}$ .

The two lines in Figure 4.1 were fitted by assuming the critical concentration point to lie between any two experimental points, fitting two least-squares lines to the up and downfield data and calculating the overall sum of squared errors (SSE). The critical point was varied to give an overall lowest SSE, which represents the best fit for the entire data. The range of critical concentrations in Figure 4.1b are also consistent with the  $[\eta]$  values reported in Chapter III and the Einstein equation [Meira et al, 1991]. PAN-A-Z has a smaller  $c^*$  value than PAN-A or A-L; this implies that it is easier for the PAN chains to associate in DMF-Z.

3. The  $ZnCl_2$  solution shows the highest viscosity over the whole range of polymer concentrations. This may be attributed to its divalent nature, which allows bridging [Tager, 1978]. At the polymer concentrations typical of casting solutions (10-17%), the solution viscosity is in the following order: PAN-L < PAN < PAN-Z. The low viscosity of the solution with LiCl agrees with the data of Lobanova et al [1969].

#### 4.2 Phase boundary studies

The presence of additives in the dope solution alters the ternary phase boundary. The experimentally observed cloud points for each type of solution are plotted in Figure 4.2 according to the empirical linearized cloud point (lcp) equation as:

$$\ln\left(\frac{\phi_{NS}}{\phi_P}\right) = b \ln\left(\frac{\phi_S}{\phi_P}\right) + a \quad (4.1)$$

where,  $\phi$  is the volume fraction and the subscripts  $NS$ ,  $S$  and  $P$  refer to the non-solvent, solvent and polymer respectively [Boom et al, 1993]. The values of the intercept  $a$  and slope  $b$  are shown in Table 4.1. Parameter  $a$  is expected to depend on enthalpy and molar volume factors while  $b$  [=  $(v_{NS}-v_P) / (v_S-v_P)$ ] depends on the respective molar volumes.

**Table 4.1:** Parameter  $a$  and  $b$  calculated by fitting eqn (4.1) to experimental lcp data.

	$a$	$b$
PAN-A	-5.4	1.8
PAN-A-L	-4.0	1.5
PAN-A-Z	-6.9	2.1
PAN-A-A	-4.2	1.5

The experimental data fitted to equation (4.1) were used to extrapolate the cloud point curves for still higher concentrations as shown in Figure 4.2.

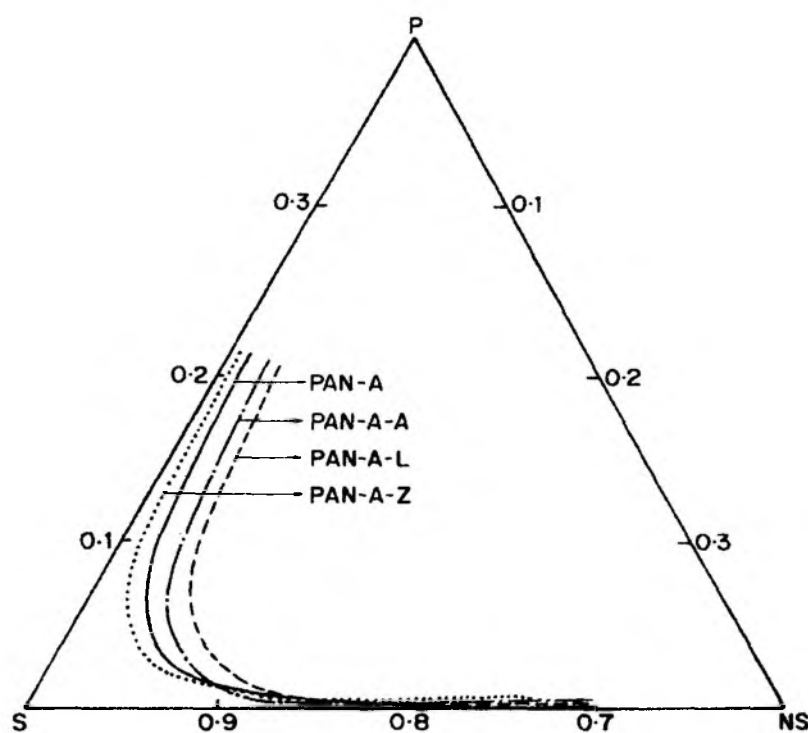


**Figure 4.2:** Ternary phase diagram plotted (theoretical points) for PAN-A, PAN-A-L, PAN-A-Z and PAN-A-A solutions using the lcp equation (4.1)

The ternary phase boundary obtained using the above data is re-plotted in Figure 4.3 for each solution to more clearly illustrate the difference in the precipitation behavior with the additives. The Y-axis of this plot is the water volume fraction at the cloud-point predicted from equation (4.1) and the phase diagram parameters in Table 4.1; this value of  $\phi_{NS}$  represents the water sensitivity of PAN solutions at varying polymer concentrations. The calculation procedure uses the  $a$  and  $b$  parameters for each type of

solution obtained by fitting the experimental data to the linearized cloud point equation. The water content (Figure 4.3) at the cloud point is calculated for a given polymer content: using eqn 4.1 and replacing  $\phi_S$  with  $(1 - \phi_{NS} - \phi_P)$ .

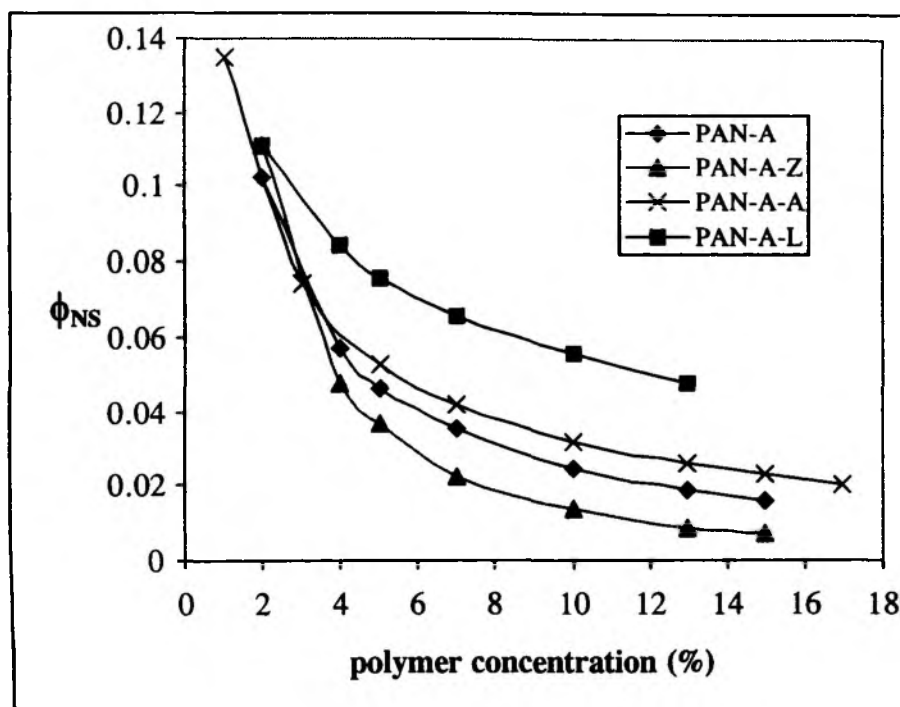


**Figure 4.3:** Water sensitivity plot for PAN-A, PAN-A-L, PAN-A-Z and PAN-A-A showing water volume fraction at the cloud point as a function of PAN concentration.

It is seen that PAN-A-Z solutions tolerate very little water prior to phase separation over the polymer concentration range of 3-17 % w/v. PAN-A-L or A-A solutions tolerate more water in comparison to A-Z or neat DMF. This type of difference between the solution properties with the various salts was also seen in section 4.1; specifically, concentrated A-Z solutions have higher viscosity compared to those with LiCl or AlCl<sub>3</sub>. The differences in the IR spectra and corresponding complex strength with DMF due to Zn and the other salts was shown in Table 3.1 (section 3.2.1.1). Clearly ZnCl<sub>2</sub> reduces the solvent power of DMF resulting in concentrated solutions with high viscosity that phase-separate with the introduction of a relatively small amount of nonsolvent.

### 4.3 Membrane morphology

SEM (surface and cross-section) has been used to define the changes in membrane structure as a result of the various solution compositions. The primary variables studied were the choice of additive (neat DMF, LiCl, ZnCl<sub>2</sub>, and AlCl<sub>3</sub>) and the PAN-A concentration. Samples for SEM were primarily examined in cross-section after cryo-fracturing as this gives a detailed picture of the membrane morphology. The details of the experimental procedure are given in section 2.3.4.

#### 4.3.1 Surface SEM

Surface SEM views of various PAN-A membranes cast from 13% solutions in various solvents are shown in Figures 4.4b-e and the resulting image analysis is summarized in Figure 4.4a below.

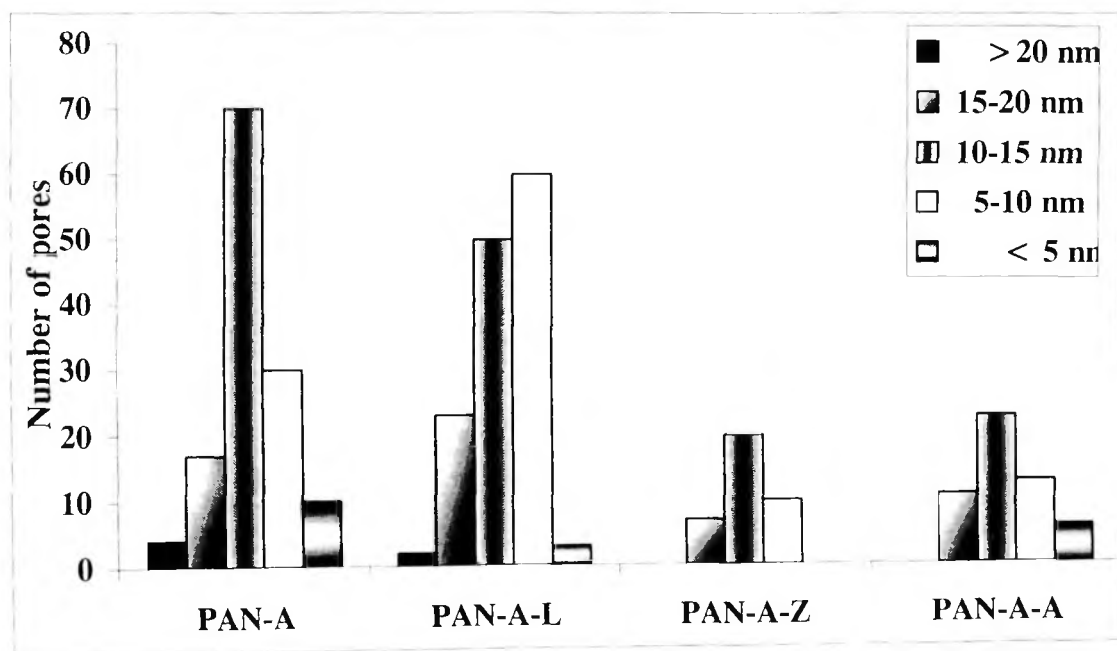


**Figure 4.4a:** Frequency distribution of the surface pore size for PAN-A, -A-L, -A-Z and A-A membranes cast (supported) from 13% polymer solutions. The legend shows the pore size in nm.

Examination of the membrane surface by SEM (13% polymer concentration) showed an overall reduction in pore number density, particularly of the larger pore sizes (>20nm), in the case of the PAN-A-Z and PAN-A-A membranes compared to PAN-A and PAN-A-L. The surface analysis is summarized in the bar chart (Figure 4.4a). In all

cases, the mode pore size (defined as the pore size corresponding to maximum number of pores [Zydney et al, 1994]) remained constant at 10-15 nm. The SEM resolution is not sufficient to detect pores below 5 nm. The surface of the 13% membranes cast on the polyester support were also examined directly for the surface views at a magnification of 50k [Figures 4.4 (b-e)]

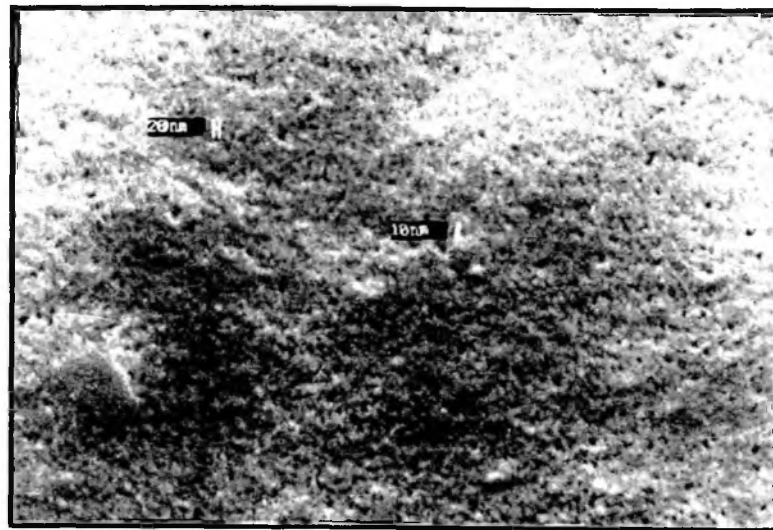


**Figure 4.4(b):** Surface view of 13% polyester supported PAN-A membrane at a magnification of 50k

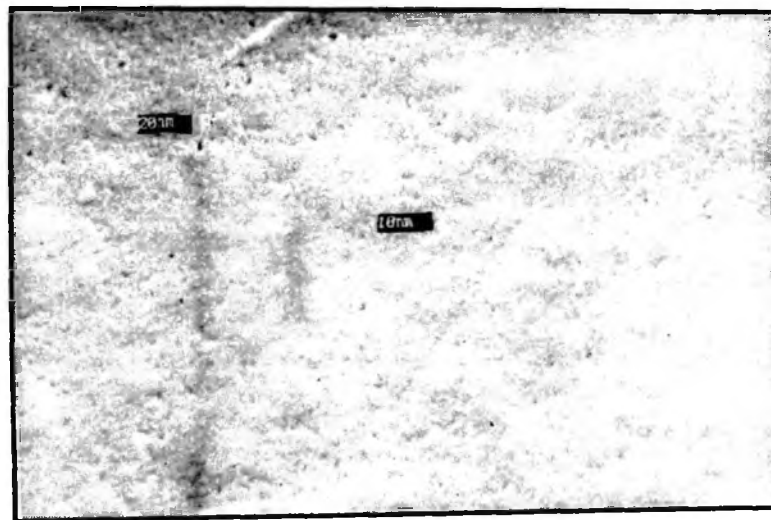


**Figure 4.4(c):** Surface view of 13% polyester supported PAN-A-L membrane at a magnification of 50k

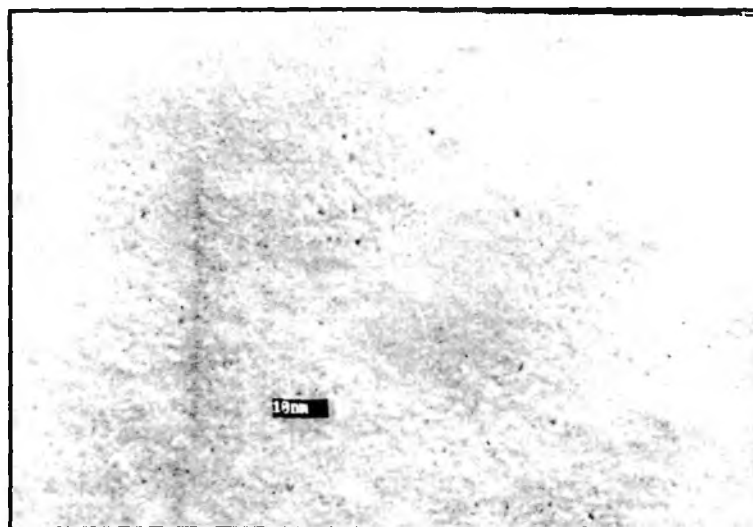


**Figure 4.4(d):** Surface view of 13% polyester supported PAN-A-Z membrane at a magnification of 50k

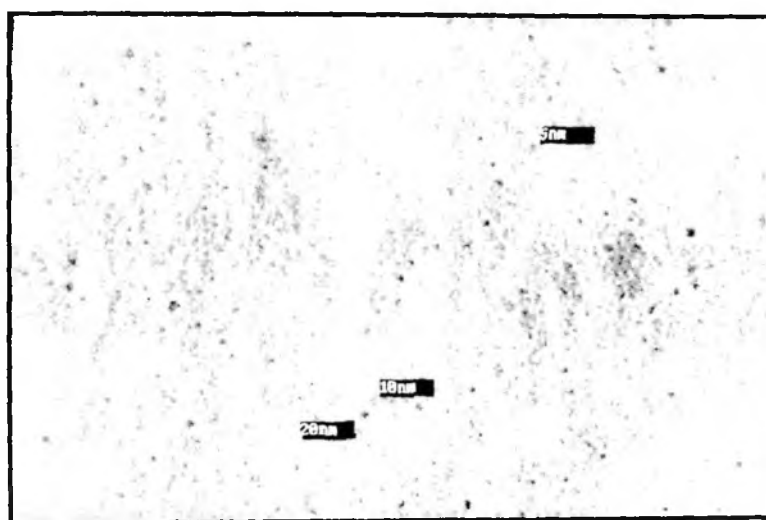


**Figure 4.4(e):** Surface view of 13% polyester supported PAN-A-A membrane at a magnification of 50k

The surface views Figure 4.4 (b-e) show that the pore number density of PAN-A-Z is less than that of PAN-A, PAN-A-L and PAN-A-A. The membranes PAN-A and

PAN-A-L (Figure 4.4 a & c) shows an increase in the overall porosity which correlates well with the pore size distribution analysis (Figure 4.10)

#### **4.3.2 Cross-section SEM**

As mentioned above the membrane morphology was studied in terms of two parameters: polymer concentration and additive choice. All the PAN membranes are highly asymmetric in density. In order to make systematic comparisons between the various morphologies; we define a common framework by identifying three distinct morphological features.

The total membrane thickness  $\sim 70-90 \mu\text{m}$  can be divided in 3 distinct zones.

Zone I which comprises of the dense skin with thickness  $< 1 \mu\text{m}$

Zone II is the supporting microporous layer with thickness  $\sim 5-20 \mu\text{m}$

Zone III is the bottom macroporous region with macrovoids

Figure 4.5 (a-h) identifies the various zones in the SEM cross-section. The various membrane morphologies are discussed below in terms of these three morphological zones.

##### **4.3.2.1 Effect of polymer concentration: Comparison of 7-17% polymer concentration variation for PAN-A and PAN-A-Z membranes**

A detailed comparison of the polymer concentration effect was made for solutions prepared with two solvent systems: neat DMF and DMF-Z.

##### ***PAN-A: Effect of polymer concentration***

Figures 4.5(a-h) show the cross-sectional views of PAN-A cast from solution of different polymer concentration (7-17%) in DMF at low (350-500x or *L*) and high (7500-10000x or *H*) magnification. Absolute size bars are included on each photograph.

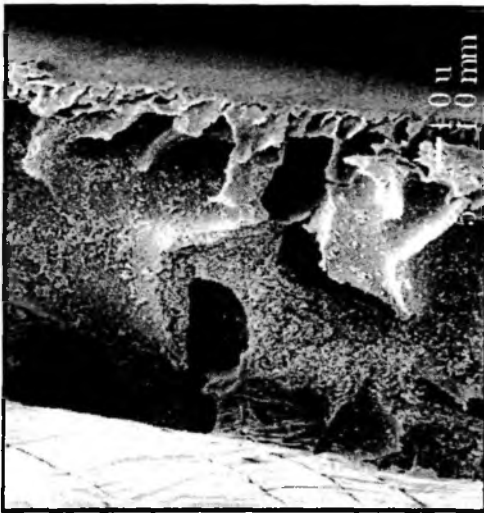




(a) PAN-A-7-L



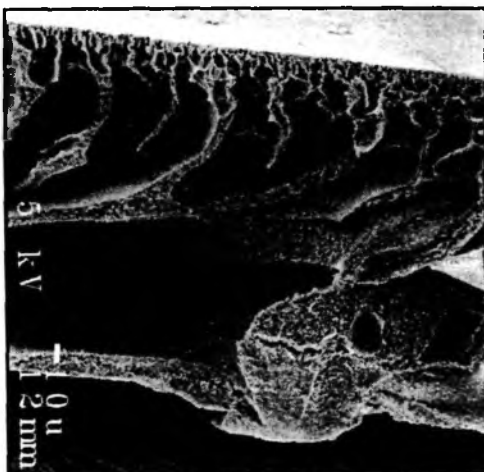
(b) PAN-A-7-H



(c) PAN-A-11-L



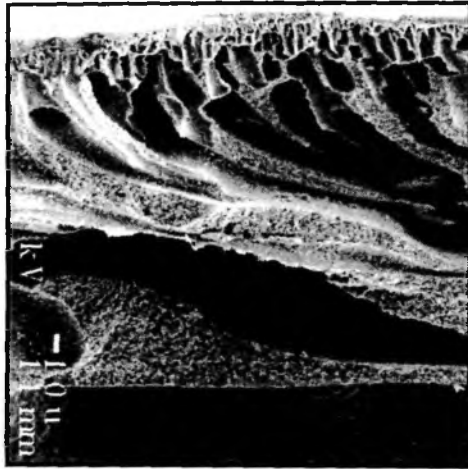
(d) PAN-A-11-H



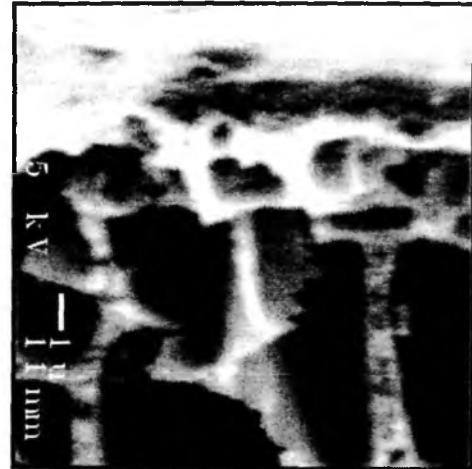
(e) PAN-A-13-L



(f) PAN-A-13-H



(g)PAN-A-17-L



(h)PAN-A-17-H

**Figure 4.5a-h:** Cross-sectional views of PAN-A membranes as a function of polymer concentration at (a,b) 7%, (c,d) 11%, (e,f) 13% and (g,h) 17%. Each set of two photographs shows both a low resolution (350-500x) and high resolution (7500-10000x) view. See 10 $\mu$ m and 1 $\mu$ m bar markers for actual dimensions.

The thickness of the skin (zone I) increases with increasing polymer concentration. At low polymer concentrations (7% PAN), the skin is difficult to detect at 10,000x magnification or “non-existent”. With an increase in PAN-A concentration from 7 to 13 %, the skin layer thickness increases from being non-existent at 7% to ~1-2- $\mu$ m at 13% PAN-A. For 17% PAN-A membranes the skin layer thickness increases to 4-5- $\mu$ m thick. The skin appears to be composed of a few fused nodular structures indicating that the skin formation is primarily through a nucleation and growth mechanism.

Polymer concentration has a similar effect on the thickness of the supporting microporous layer (zone II). At 7 % concentration, the supporting layer is only ~ 2-3  $\mu$ m thick and large macrovoids from the bottom layer penetrate into this layer. The reduced membrane strength due to this macrovoid structure is responsible for the collapsed lower sublayer structure in Zone III. At 11% concentration the supporting layer is ~4-5  $\mu$ m with 2-5  $\mu$ m pores which taper to smaller dimensions approaching the denser skin. In membranes cast from 13% polymer solutions, the supporting layer is ~8-

10  $\mu\text{m}$  thick with cylindrical pores of 2-5  $\mu\text{m}$  diameter which taper down as the skin layer approaches. For membranes cast from 17% polymer concentration solutions the supporting layer is very thick  $\sim 10 \mu\text{m}$ , with cylindrical pores which taper as they approach the skin.

All 4 PAN-A membrane structures (7-17% polymer concentration) show large macrovoids in the bottom macroporous region (zone III). Membranes cast from both the 7% and 11% polymer solutions show a Zone III structure dominated by large macrovoids. On increasing the concentration further to 13% a more finely porous structure is seen with the size of the large macrovoids reducing slightly and tapering towards the skin. This effect is related to the increased viscosity. As expected, with an increase in the polymer concentration beyond 13% we see a further trend away from macrovoids to a finely porous Zone III structure. Table 4.2 summarizes these observations.

**Table 4.2:** Summary of observations for cross-sectional SEM views (Figures 4.5a-h) of PAN-A cast from 7-17% polymer solutions in neat DMF.

PAN-A	Dense skin	Microporous	Macroporous
7%	non-existent	Very thin $\sim 2-3 \mu\text{m}$ thick Macrovoids from bottom section penetrate this layer	large macrovoids, structure weak
11%	Very thin non-existent, Some evidence of a nodular structure	Relatively thin $\sim 5-10 \mu\text{m}$ Pores are 2-5 $\mu\text{m}$ and taper to smaller dimensions approaching dense skin	Very large and numerous macrovoid fingers running
13%	$\sim 0.1 - 0.2 \mu\text{m}$ Few nodules seen	$\sim 10 \mu\text{m}$ thick Cylindrical pores 2-5 $\mu\text{m}$ in diameter taper as skin layer is approached	size of the macrovoid fingers reduces slightly and smaller number of pores are seen

17%	~ 0.4-0.5 $\mu\text{m}$ thick Nodular structure observed	~ 10 $\mu\text{m}$ thick Straight cylindrical pores 2-5 $\mu\text{m}$ in diameter, many small size pores also seen	Size of macrovoids reduces and more number of smaller pores visible
-----	--	---	--

We know that as polymer concentration increases the solution viscosity also increases, which will slow down the solvent exchange during precipitation. However, it is also known from the cloud point / water sensitivity studies that solutions with low polymer content precipitate slowly when exposed to water i.e. they tolerate a higher amount of non-solvent diffusing into the solution phase before phase separation. The second of these effects probably corresponds to the large macrovoids and weak substructure in zones II and III for membranes cast from the lowest polymer concentration solutions.

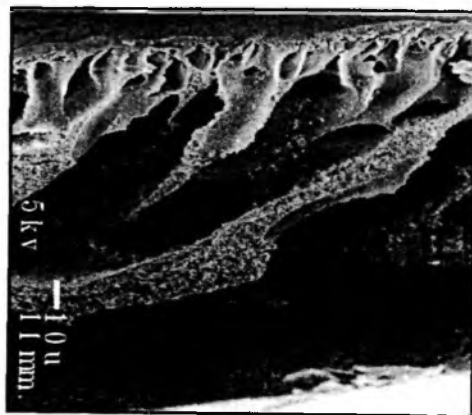
The morphology in zones II and III also has an effect on the integrity of the skin layer. The lack of support to the skin layer would most likely lead to defects in the skin layer. The low solution viscosity would also make the skin layer more sensitive to mechanical damage from fluid perturbations caused by random or natural vibrations during membrane casting. SEM can only give an indication of this effect; however, it is clearly seen in the bubble point measurements discussed later in section 4.4.1.

#### ***PAN-A-Z: Effect of polymer concentration***

A similar analysis for the effect of polymer concentration is discussed here for PAN-A-Z membranes. Figures 4.6(a-g) show the cross-sectional views of PAN-A cast from solution of different polymer concentration (7-17 %) in DMF + ZnCl<sub>2</sub>.



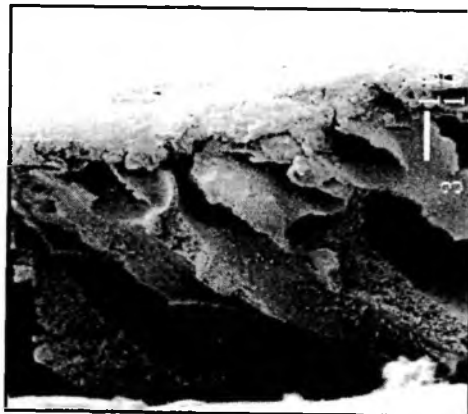
(a) PAN-A-Z-7-H



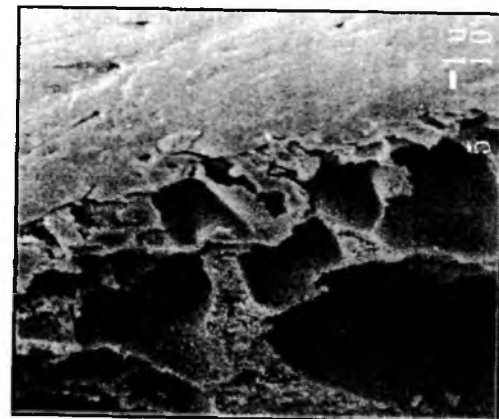
(b) PAN-A-Z-11-L



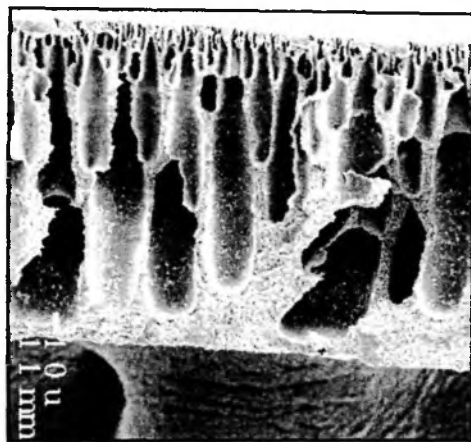
(c) PAN-A-Z-11-H



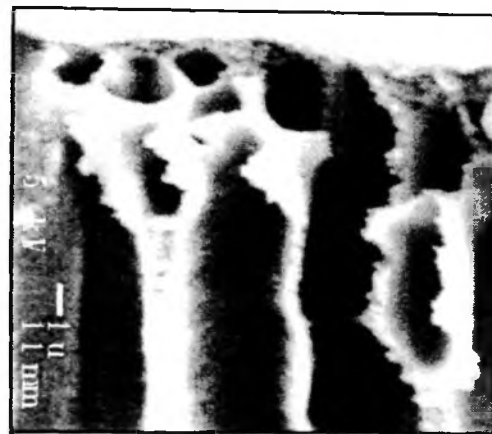
(d) PAN-A-Z-13-L



(e) PAN-A-Z-13-H



(f) PAN-A-Z-17-L



(g) PAN-A-Z-17-H

Figure 4.6a-g: Cross-sectional views of PAN-A-Z membranes as a function of polymer concentration at (a.) 7%, (b,c) 11%, (d,e) 13% and (f,g) 17%. Each set of two photographs shows both a low resolution (350-500x) and high resolution (7500-10000x) view. Only the high resolution view is shown for 7% PAN-A-Z. See 10 $\mu$ m and 1 $\mu$ m bar markers for actual dimensions.

The SEM micrographs in Figure 4.6 for PAN-A-Z can be analyzed similar to those in Figure 4.5 for PAN-A. The summary of these observations on the PAN-A-Z membrane structure is presented in table 4.3.

**Table 4.3:** Summary of observations for cross-sectional SEM views (Figures 4.6a-g) of PAN-A-Z cast from 7-17% polymer solutions in DMF+ZnCl<sub>2</sub>.

PAN-A-Z	Dense skin	Microporous	Macroporous
7%	Very thin – non-existent	Very thin ~ 2-4 μm thick Macrovoids from bottom section penetrate this layer	Almost completely filled with macrovoids
11%	Very thin ~ 0.1-0.2 μm Some evidence of nodules fusing into skin	Relatively thin ~ 5-10 μm Pores are 2-5 μm and taper to smaller dimensions approaching dense skin	Very large and numerous macrovoid fingers running ~ 50 μm long
13%	~0.2 –0.3 μm Nodules fusing into skin	~ 10 μm thick Cylindrical pores 2-5 μm in diameter taper as skin layer is approached	Very large and numerous macrovoid fingers running ~ 50 μm long
17%	~ 0.3 μ > Nodules fusing into skin	~ 10 μm thick Straight cylindrical pores 2-5 μm in diameter, many small size pores also seen	Very large and numerous macrovoid fingers running ~ 50 μm long opening at the skin layer only

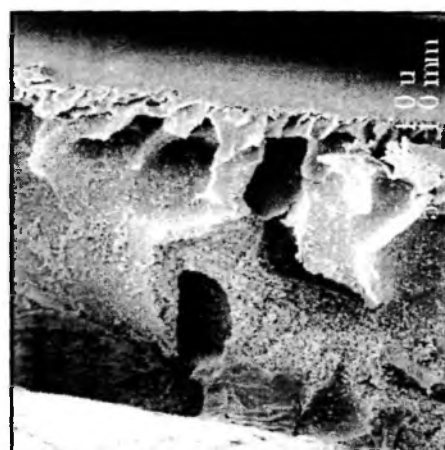
The cloud point studies in section 4.2 show that solutions with DMF-Z tolerate the least amount of non-solvent before phase separation. This effect may correspond to the tighter substructure in zones II and III for PAN-A-Z compared to PAN-A.

4.3.2.2 Effect of Salt additive: Comparison of Additive type for PAN-A membranes cast from 11 and 13% polymer concentration

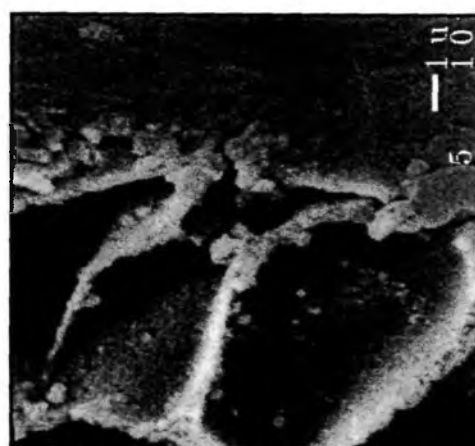
Two polymer concentrations (11% and 13%) were chosen for detailed SEM studies as it was felt the effect of the additives would be most evident at these intermediate PAN-A concentrations. At lower polymer concentration, the membrane morphology is dominated by macropores while at higher polymer concentration, the morphology is more uniformly tight and the effect of the additive is difficult to resolve clearly by SEM.

*11% PAN-A concentration: Effect of Additive*

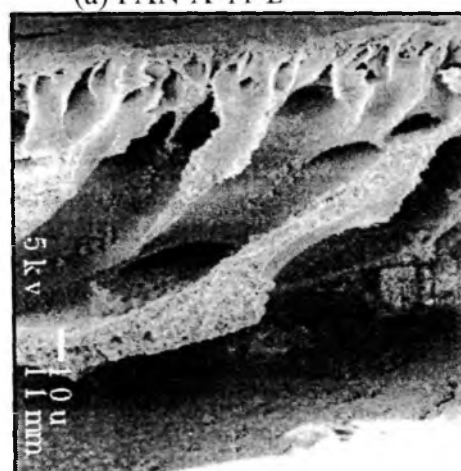
SEM cross-sections of PAN-A, PAN-A-Z, PAN-A-L and PAN-A-A cast from 11% polymer solutions are shown in Figures 4.7 (a-h).



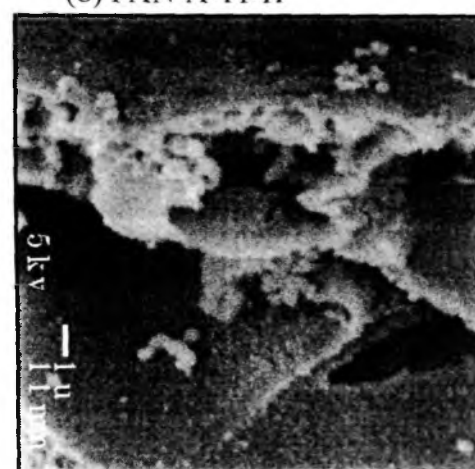
(a) PAN-A-11-L



(b) PAN-A-11-H



(c) PAN-A-Z-11-L



(d) PAN-A-Z-11-H



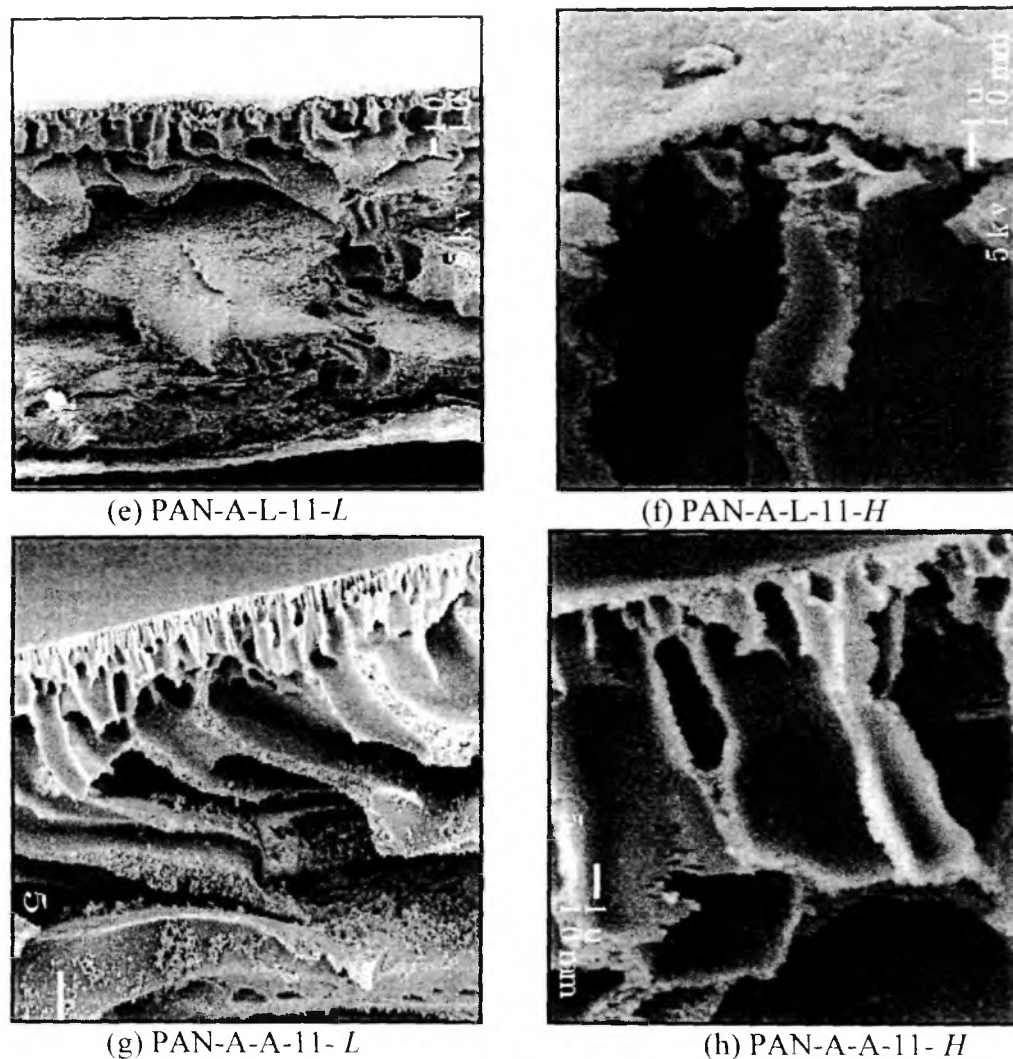


**Figure 4.7(a-h):** Cross-sectional views of PAN-A membranes cast from 11% polymer concentration as a function of combined DMF+ salt additive type: (a,b) neat DMF, (c,d) DMF-Z (e,f) DMF-L and (g,h) DMF-A. Each set of two photographs shows both a low resolution (350-500x, *L*) and high resolution (7500-10000x, *H*) view. See 10 $\mu$ m and 1 $\mu$ m bar markers for actual dimensions

A summary of the morphological changes in zones I-III of membranes made with various salt additives to 11% PAN-A / DMF solution is given in Table 4.4.

**Table 4.4:** Summary of observations for cross-sectional SEM views (Figures 4.6a-g) of PAN-A cast from 11% polymer solutions in various DMF+salt combined solvents.

11% PAN	Dense skin	Microporous	Macroporous
DMF	~ 0.3 $\mu\text{m}$ Rough appearance	~ 10 $\mu\text{m}$ thick Pores are large ~ 5-10 $\mu\text{m}$ and approach the dense skin without transition	Fine structure superimposed with ~ 30 wide $\mu\text{m}$ fingers
DMF-Z	Very thin ~ 0.1-0.2 $\mu\text{m}$ Some evidence of nodules fusing into skin	Relatively thin ~ 5-10 $\mu\text{m}$ Pores are 2-5 $\mu\text{m}$ and taper to smaller dimensions approaching dense skin	Very large and numerous macrovoid fingers running ~ 50 $\mu\text{m}$ long
DMF-L	Thin ~ 0.2 $\mu\text{m}$ Some evidence of nodules fusing into skin	~ 10 $\mu\text{m}$ thick Cylindrical pores 2-5 $\mu\text{m}$ in diameter	Nodular structure with few macrovoids
DMF-A	Thin ~ 0.2 $\mu\text{m}$	~ 10 $\mu\text{m}$ thick Cylindrical pores 1-3 $\mu\text{m}$ in diameter	Very large and numerous macrovoid fingers running ~ 50 $\mu\text{m}$ long

It is seen from the above SEM micrographs that PAN-A has a thicker and coarser skin in comparison to the others with additives. PAN-A-L and PAN-A-A have a similar Zone II morphology. It is seen that for both PAN-A-Z and PAN-A-A the Zone III shows the presence of large macrovoids while for PAN-A-L shows a tighter structure here which correlates well with the water permeability of the so formed membranes.

***13% PAN-A concentration: Effect of Additive***

Figures 4.8(a-c) show cross-sections of PAN-A, PAN-A-L and PAN-A-A membranes cast from a polymer concentration of 13% w/v at a magnification of 300x. Figure 4.8d shows a cross-section of PAN-A-Z (13% polymer concentration) at a

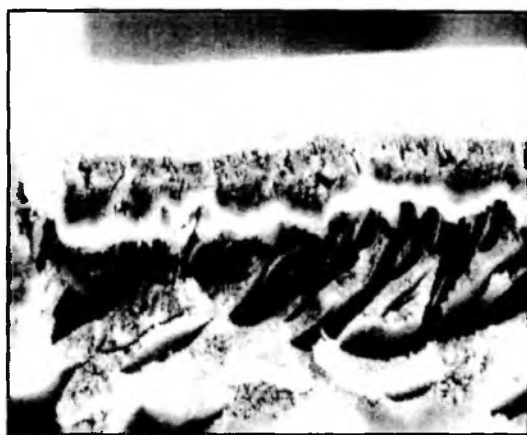
magnification of 50,000x. The low magnification view of PAN-A-Z is similar to that of PAN-A and A-A.



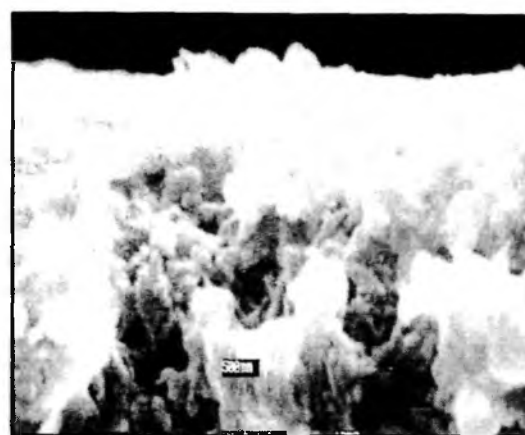
(a) PAN-A-13



(b) PAN-A-L-13



(c) PAN-A-A-13



(d) PAN-A-Z -13(skin layer)

**Figure 4.8(a-d):** Scanning electron micrographs for the cross-sectional view of membranes of 13% polymer concentration (a) PAN-A (b) PAN-A-L (c) PAN-A-A at 300x magnification and (d) skin layer of PAN-A-Z at 50k magnification

For the most part, the morphology trends at 13% polymer concentration mirror those at 11%. Figure 4.8d shows a representative view of the skin layer in PAN-A-Z showing the typical nodular surface. The other SEM photographs 4.8(a-c) show the

entire membrane morphology. Both PAN-A and PAN-A-A (as well as PAN-A-Z which is not shown) have large macrovoids in the underlying asymmetric structure; while the incidence and size of these macrovoids is considerably reduced in the case of monovalent salt (PAN-A-L Fig. 4.8b). This is consistent with the ternary cloud point data (Figure 4.2) which imply that the skin layer in PAN-A-Z and PAN-A would form rapidly with the exchange of only a small amount of water. In the PAN-A-A case, though the solution has intermediate water sensitivity, this salt also promotes chain association. The PAN-A-L solution had both lower viscosity as well as the least water sensitivity. In the case of PAN-A-L, precipitation would occur only after a considerable amount of DMF / water exchange had already taken place. The expected shallower concentration gradient in the PAN-A-L case would be consistent with the more homogenous support structure seen in the SEM cross-section.

#### **4.4 Permeation results**

The membrane structure was also characterized by various bubble point, water permeability and ultrafiltration tests.

##### **4.4.1 Bubble pt / Pore size distribution**

The effect of the polymer concentration and additive type on the effective membrane pore size is discussed in this section. While SEM cross-sections show the entire membrane morphology, the bubble point technique is sensitive to the critical separating skin layer porosity.

The determination of the largest pores present on the membrane surface (13.4 cm<sup>2</sup> samples) was made by the standard bubble point technique with both water and isopropanol wetted membranes. The pore and pore size distribution were determined by the extended bubble point method (Kesting 1971). The experimental and calculation procedures are described in Chapter II.

The pressure range of the bubble point measurements with water-wet membranes was 20- 400 kPa (0.2 - 4.0 bar) corresponding to a pore size range of 0.3 - 7.4 μm. Since the water-air interfacial tension is high (73 dynes/cm<sup>-1</sup>), the detection of smaller pores with this method requires correspondingly high pressures, which can cause pore

structure damage. Therefore, a second set of bubble point measurements were carried out where isopropanol (IPA) was used as the imbibed phase (interfacial tension 27 dynes/cm<sup>-1</sup>); this enables the measurement of smaller pores. In the case of isopropanol wetted samples, the air flux measurements were continued till 400 kPa in order to get the leading edge of the pore size distribution corresponding to pore sizes of ~0.1 μm.

Similar to the SEM work, a detailed study of the effect of polymer concentration (7-17%) on the pore size distribution for PAN-A and PAN-A-Z membranes was undertaken. The effect of the additive was examined for all four solvent systems (DMF, DMF-Z, -L and -A) at a fixed polymer concentration of 13%.

#### 4.4.1.1 Effect of additive on bubble point / pore size

The averaged bubble point data with isopropanol and water wetted membranes are shown in Figures 4.9a and 4.9b respectively. Appendix IV-1 contains the data used to construct these plots. The bubble point, which corresponds inversely to the diameter of the largest pore detected in the sample, is shown in each case for the various types of membranes. The standard deviation of these bubble point results is 45 kPa in case of the isopropanol displacement and 62 kPa in case of water displacement.

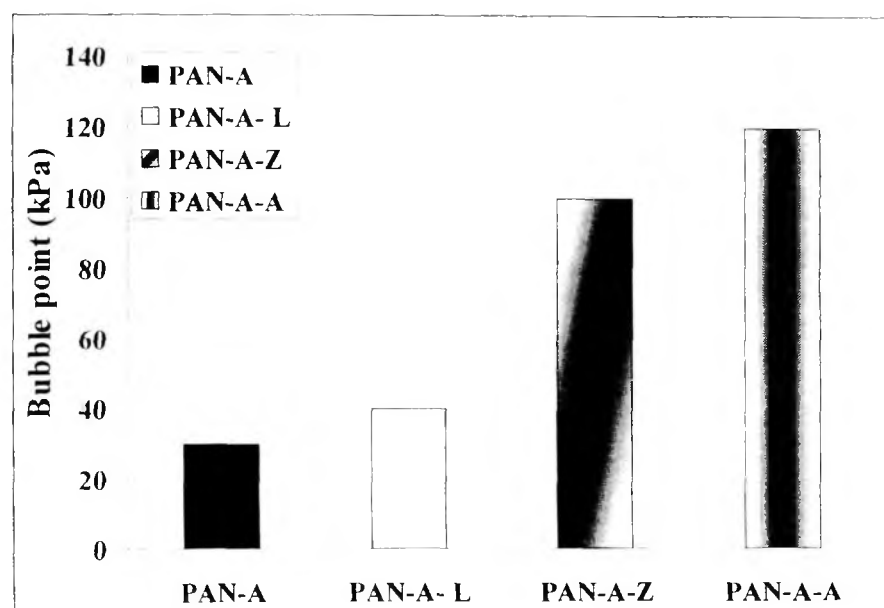


**Figure 4.9a:** Average membrane bubble points of isopropanol-wetted PAN-A, PAN-A-L, PAN-A-Z and PAN-A-A (polyester-supported) membranes cast from 13% polymer concentration solutions.

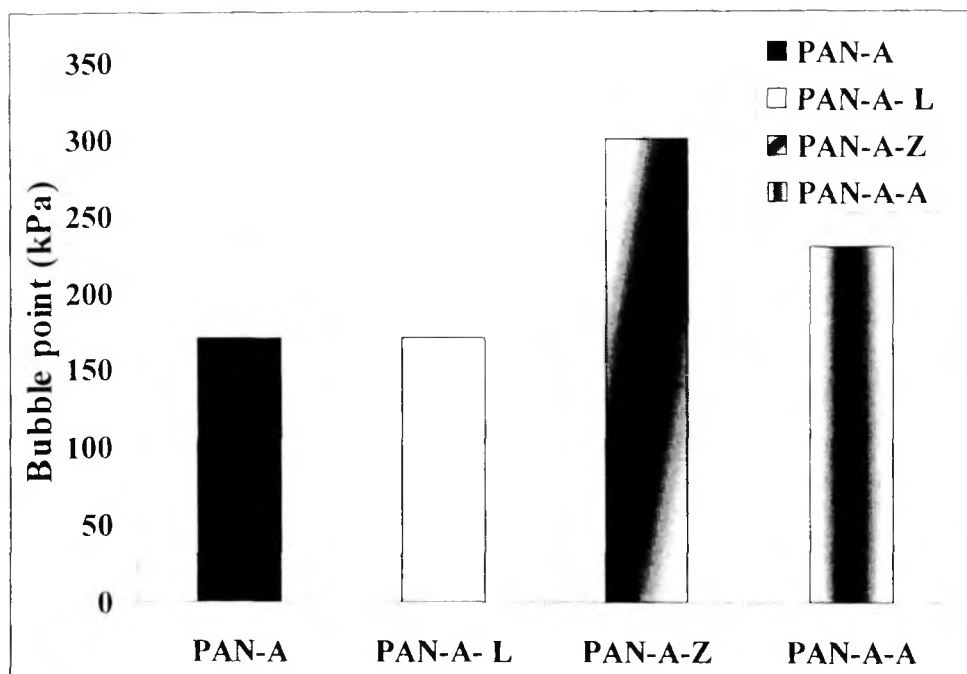


**Figure 4.9b:** Average membrane bubble points of water-wetted PAN-A, PAN-A-L, PAN-A-Z and PAN-A-A (polyester-supported) membranes cast from 13% polymer concentration solutions.

As shown in Figures 4.9 a-b, both PAN-A and PAN-A-L have low bubble points, indicative of defects large enough for bacterial passage. There is a good correlation between the low bubble point of these membranes with the low viscosity of the solutions (Figure 4.1 a-b) they are cast from. The slightly higher bubble point of PAN-A-L compared to PAN-A may be attributed to the more uniform support layer seen in the SEM study.

The addition of the multivalent salts that suppress these defects, also result in high concentrated solution viscosity (Figure 4.1a, section 5.1). This higher viscosity was attributed to increased polymer-polymer interactions in these solvent systems. Both membranes cast with the multivalent salts show increased bubble points. The increased viscosity rather than the water sensitivity appears to be the critical parameter defining the skin porosity. The water sensitivity on the other hand appears to be more important for defining the underlying support layer morphology.

A more detailed analysis of the pore size distribution using equations (2.2-2.3, section 2.3.3) is shown for all four additives in Figure 4.10. This is actually the leading edge of the entire pore size distribution based on higher pressure displacement of isopropanol. This analysis indicates that in addition to a higher bubble point, the multivalent salt additives lead to a narrower pore size distribution and particularly eliminate the pores large enough for bacterial passage. The elimination of these defects may be attributed to the higher viscosity / salt-promoted polymer chain association in the PAN-A-Z and PAN-A-A casting solutions. While both mono- and divalent salts decreased the DMF solvation capability, the higher viscosity in the case of multivalent salts may be attributed to increased interaction between polymer chains.

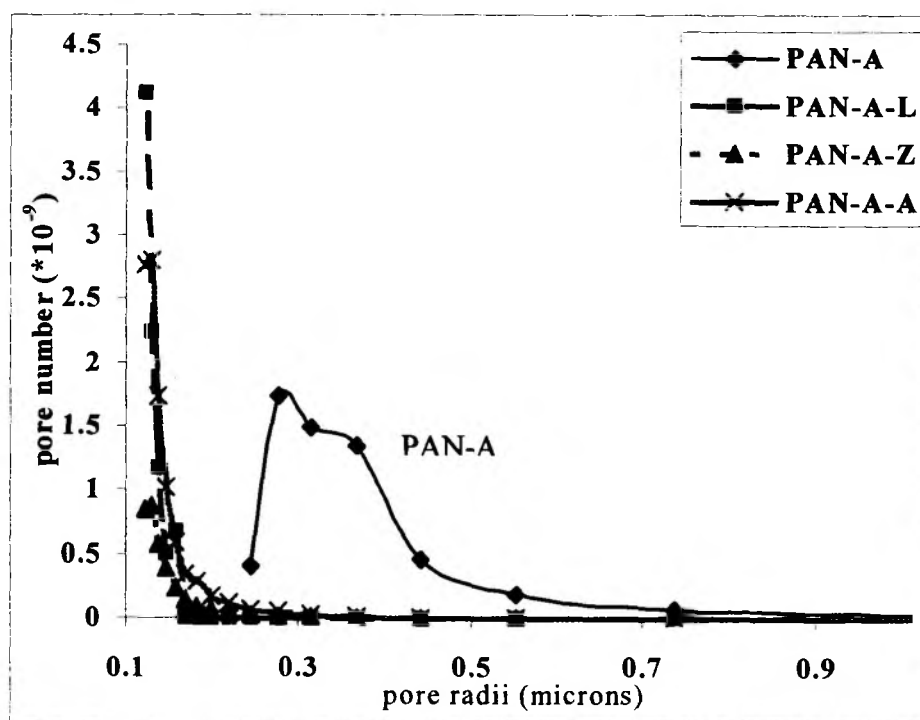


**Figure 4.10:** Pore size distribution curve for the 13% polymer concentration membrane (supported) of PAN-A, PAN-A-L, PAN-A-Z and PAN-A-A. Calculations based on air-isopropanol displacement data.

4.4.1.2 Effect of polymer concentration on bubble point / pore size of PAN-A and PAN-A-Z

The pore size distribution curves for water wetted membranes PAN-A and PAN-A-Z are shown in the Figure 4.11a and 4.11b, respectively. It would be expected that membrane pore size decreases with increasing polymer concentration; however, this correlation in Figures 4.11(a-b) is not consistent.

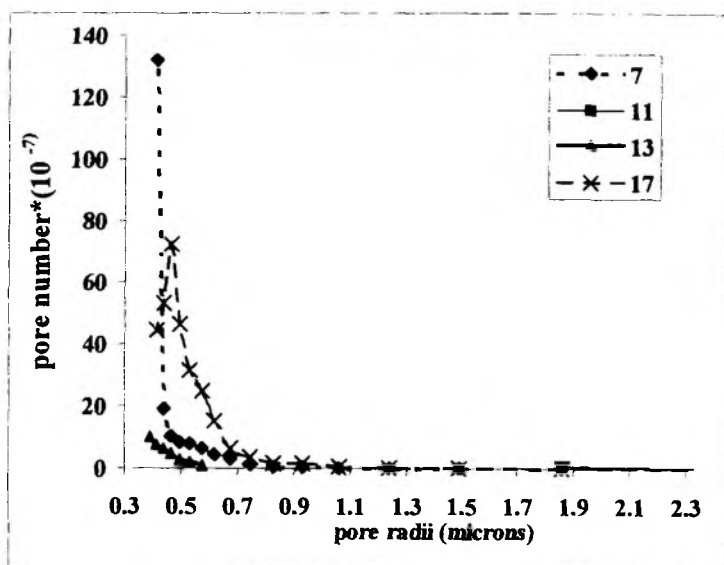


**Figure 4.11a:** Pore size distribution curve for PAN-A membranes (cast on glass plate) cast from 7, 11, 13 and 17% polymer concentration solutions. Calculations based on air-water displacement data.

PAN-A

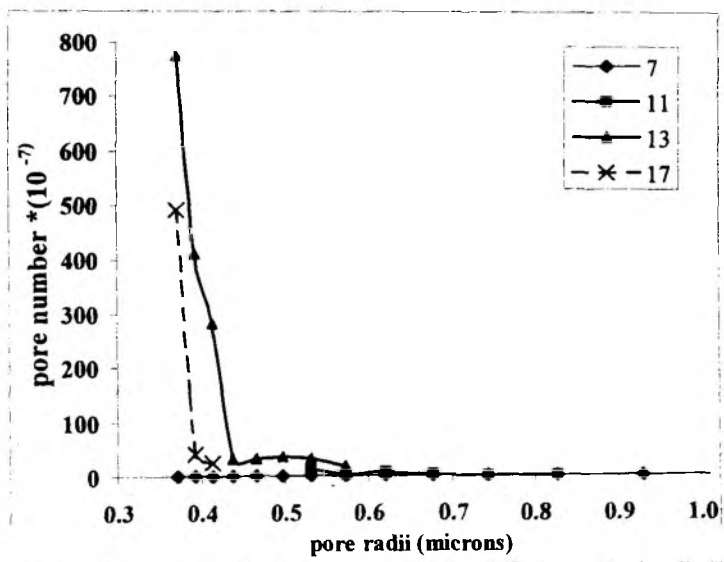


**Figure 4.11b:** Pore size distribution curve for the water wetted supportless PAN-A-Z membranes cast from different polymer concentrations.

PAN-A-Z



#### 4.4.2 Water permeability measurements

Distilled and filtered water fluxes were measured at 200 kPa (2.0 bar) in a 13.4 cm<sup>2</sup> stirred cell assembly at 25°C. The membranes were cast from 13% w/v PAN-A solutions in DMF with and without the salt additives. Figure 4.12 shows the average water permeability values for the various membranes; see Appendix IV-2 for the raw data. The standard deviations of the water fluxes are ~20% of the average value.

PAN-A-L has considerably lower flux than PAN-A; this is consistent with the more homogenous and tighter support structure observed in the SEM (Figures 4.7 and 4.8). PAN-A-Z and PAN-A-A have 75-80% of the PAN-A flux; this is consistent with the reduced number of larger pores in the skin layer (Figure 4.10) while retaining the open support structure.

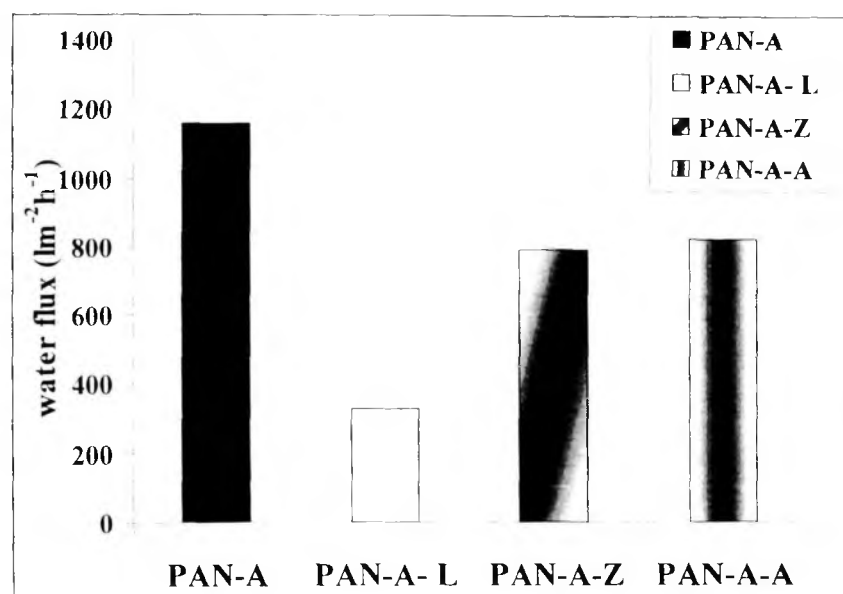


**Figure 4.12:** Average water permeation rates of PAN-A, PAN-A-L, PAN-A-Z and PAN-A-A (polyester-supported) membranes cast from 13% polymer concentration solutions. Based on data for operating pressure 200kPa, temperature 25°C in stirred cell.

Figure 4.13 shows the water permeability of PAN-A and PAN-A-Z membranes (machine cast on polyester support) as a function of polymer concentration. As expected, water flux decreases with increase polymer concentration, this is consistent with both the ternary phase diagram as well as the viscosity effect.

Interestingly, the graph shows that over the range of concentrations studied, the water permeability for neat PAN-A decreases more sharply than for PAN-A-Z. While PAN-A is more permeable at lower polymer concentrations, both membranes tend towards the same permeability as polymer concentration increases.

This trend is continued in Figure 4.14, which shows a semilog plot of the water permeability for supportless (cast directly on glass plate) membranes of PAN-A, PAN-A-L, PAN-A-Z and PAN-A-A as a function of polymer concentration. As expected, there is a decreasing trend of the water permeability with concentration; again, the slope is sharper for PAN-A than for PAN-A-Z. PAN-A-L and A-A membranes were studied at only two concentrations (11 and 13%); The permeability of these membranes are similar to the other two sets.

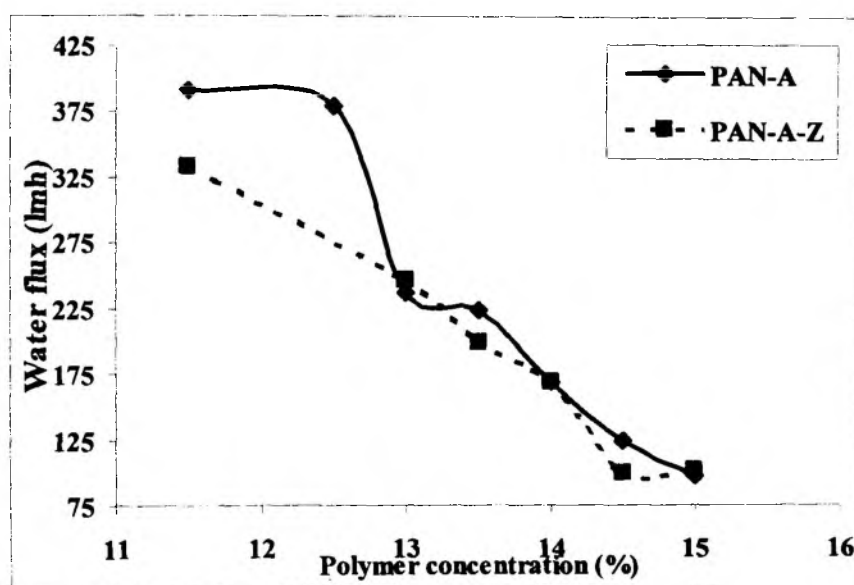


**Figure 4.13:** Water permeation rates as a function of polymer concentration (7-15%) for PAN-A and PAN-A-Z membranes cast on polyester support. The water permeability was measured at 70kPa, temperature 29°C

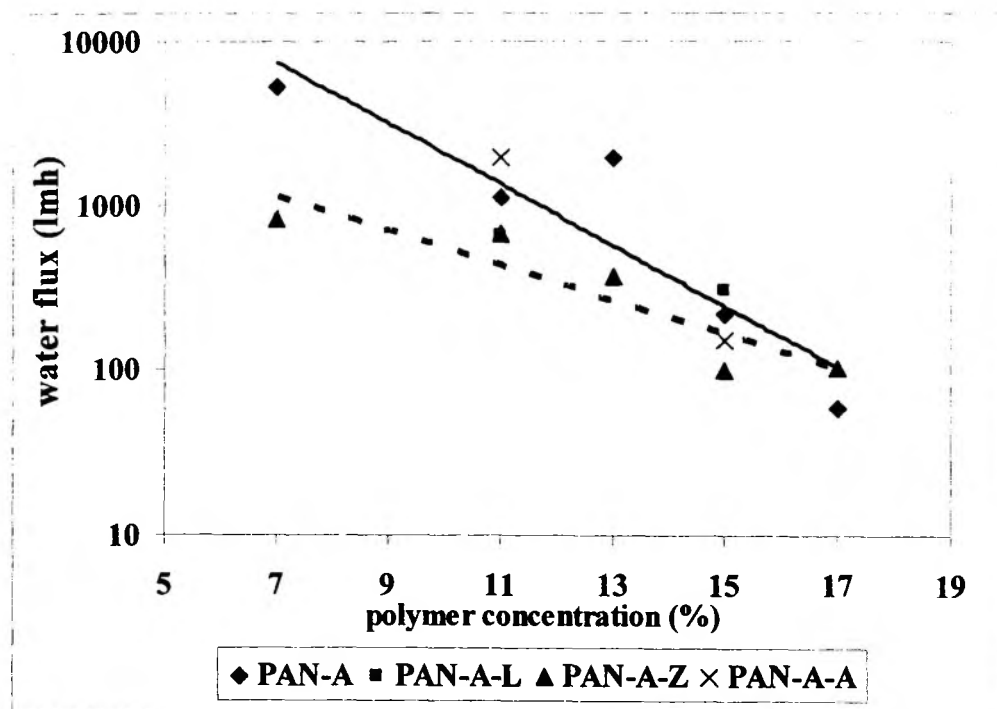


**Figure 4.14:** Water permeability for PAN-A ,PAN-A-L,PAN-A-Z, PAN-A-A supportless membranes as a function of polymer concentration range of 7-17%. The water permeability was measured at 70kPa, temperature 29°C. The trend lines for PAN-A and PAN-A-Z are fitted to the empirical relation:  $J(lmh) = I \exp(-S \cdot c)$  where pre-exponent  $I$  and slope  $S$  are given below:

Solvent	$I$	$S$	$R^2$
PAN-A	1.4E5	0.43	0.84
PAN-A-Z	6E3	0.24	0.83

#### 4.4.3 Ultrafiltration studies

The 13% polymer concentration membranes, cast on a polyester support with and without additives described in section 4.4.2, were also used for ultrafiltration (UF) experiments. The Amicon stirred cell assembly was used at 100 kPa (1.0 bar) and 25°C. The UF experiments were done with the following solutions: (i) BSA (M.W. 68,000 daltons) (0.1 g/dl) (ii) lysozyme (M.W. 14,000 daltons) (0.05 g/dl) solutions and (iii) PEG (M.W. 9,000 daltons) solution (0.5 g/dl).

The two protein solutions were prepared in phosphate buffer (pH 7.5) while the PEG was dissolved in distilled water. The phosphate buffer used was a mixture of a

0.2M solution of disodium hydrogen orthophosphate [A] and a 0.2M solution of Sodium dihydrogen phosphate [B]. The two were mixed well in a ratio of 87 ml of A + 17 ml of B to make up 100 ml of solution to which 100 ml of distilled water was added. The solution pH was approximately 7.5. If required, fine adjustments in the pH were made with 0.1N HCl and 0.1N NaOH solutions. All the feed solutions were filtered through Whatman paper (No. 1) prior to the UF run. The protein concentrations in the feed and permeate samples were determined using a spectrophotometer (Shimadzu, UV-240) at 280 and 260 nm [Jayaraman et al 1981]. The protein concentration was calculated from absorbances measured at two frequencies as follows:

$$\text{Protein conc (mg/ml)} = (1.55 * \text{Abs}_{280\text{nm}}) - (0.74 * \text{Abs}_{260\text{nm}}) \quad (4.2)$$

All the measurements were done in triplicates. The reproducibility of the rejection ( $R=1-C_p/C_f$ ) estimates was  $\sim \pm 4\%$ .

The analysis of the PEG concentrations in the feed and permeate samples was determined by the method of Sims and Snape [1980]. Typically, 4ml of PEG containing sample was mixed thoroughly with 1ml of each reagent C (5%BaCl<sub>2</sub> in 1N HCl) and reagent D (0.127g I<sub>2</sub> + KI 0.4g + 100ml H<sub>2</sub>O). The sample was allowed to stand for 20 mins followed by the measurement of the sample absorbance at 535nm. This absorbance was compared with the callibration plot of absorbance versus concentration of standard solution.

The permeate flux and solute rejection data at a volume concentration factor of 1.9 were obtained in triplicate for each solute and averaged. The raw data are tabulated in Appendix IV-3. The averaged solute rejections are plotted in Figure 4.15.

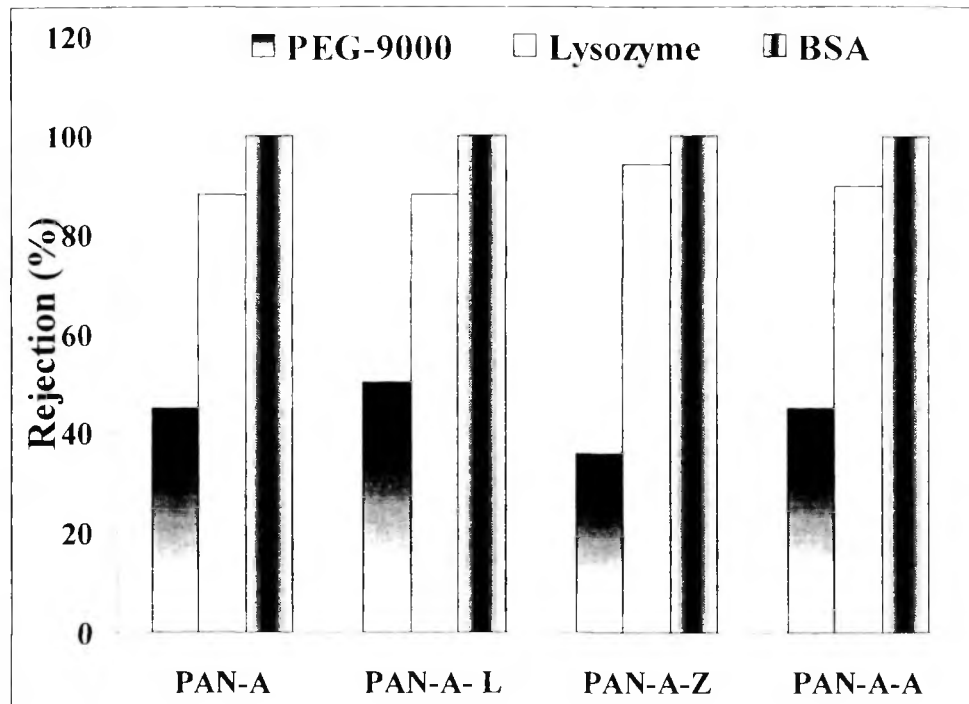


**Figure 4.15:** Average PEG, lysozyme and BSA rejections for PAN-A, PAN-A-L, PAN-A-Z and PAN-A-A supported membranes cast at 13% polymer concentration. Operating pressure 100kPa, temperature 25°C, stirred cell.

The average solute rejections shown in Figure 4.15 for the various membranes are similar for all 4 membrane types, indicating that the reduction of the few large pores as observed in the bubble point studies does not significantly change the average pore size. This is also consistent with the SEM surface analysis which showed that the modal pore size was relatively unaffected by the additives. (section 4.3.1).

BSA rejection for PAN-A and PAN-A-Z membranes is shown in Figure 4.16 as a function of polymer concentration. BSA rejection increases with polymer concentration for both membrane types. Within experimental error (4%), the BSA rejection for both membranes is essentially the same.

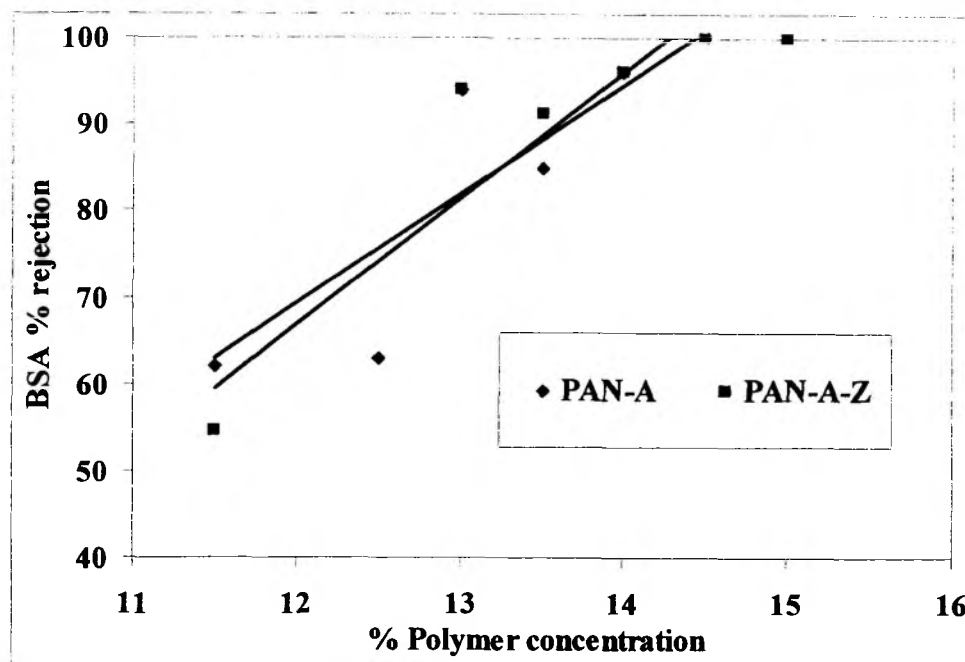


**Figure 4.16:** BSA rejection data for machine cast PAN-A and PAN-A-Z membranes cast on polyester support as a function of polymer concentration (11-15%). Operating conditions : pressure 70kPa, buffer 7.5 pH, and 0.1g/dl BSA in stirred cell. The trend lines for PAN-A and PAN-A-Z are fitted to the empirical relation:  $R(BSA)\% = S \cdot c - I$  where intercept  $I$  and slope  $S$  are given below:

Solvent	$I$	$S$	$R^2$
PAN-A	-108	14.6	0.72
PAN-A-Z	-82.3	12.6	0.81

In order to study the membrane performance for bacteria removal, PAN-A and PAN-A-Z membranes cast from 15% polymer solutions were wound in the form of small spiral-wound modules (0.3 m<sup>2</sup>) and tested for filtration of *E. coli* containing broth (10<sup>9</sup> bacterial counts/ml). Testing was done by circulating the broth through these modules at a pressure of 70 kPa and at a cross-flow rate of 1 liter / minute. The permeate samples were assayed for bacterial count using the serial dilution method [Collins et al, 1976] along with the diluted feed sample. This test was replicated after a sodium dodecyl sulfonate based cleaning of the membrane module between runs. The membrane rejection of the bacterial species can be measured in terms of the log

reduction (LR, defined in eqn 1.3). The bacterial challenge test results with these spiral wound modules based on PAN-A-Z and PAN-A are shown in Table 4.5

The PAN based module has an LR of 4.0-4.3 for *E.coli* compared to LR values of > 7 for the PAN-Z membrane tested at the same time. Thus, these membranes which have relatively similar separation characteristics for UF concentration have markedly different abilities to purify water in microbiological term

**Table 4.5:** Spiral wound module performance for bacteria removal. Operating conditions: ambient temperature,  $10^9$  Ecoli counts/ml in feed, 70kPa.

Spiral wound module	Water flux* (ml/min)	<i>E. coli</i> counts in permeate (per ml)	<i>E. coli</i> LR
PAN-A	420-470	5000,10000	4.0-4.3
PAN-A-Z	360-400	2,7	7.1-7.7

#### 4.5 Correlation of membrane structure / performance with solution properties

The solution viscosity and the polymer-solvent-nonsolvent (water) phase boundary are considered critical variables affecting membrane pore formation. Both solution properties are strong functions of the polymer concentration and the salt additives in the solution.

The addition of both mono and multivalent salts to PAN-A / DMF solution causes a increase in the polymer intrinsic viscosity  $[\eta]$  and a decrease in the solvation power of DMF. In the concentrated solution regime typical of casting solutions, the solution viscosity follows the trend: PAN-A-Z > PAN-A > PAN-A-L. The concentrated solution viscosity data (section 4.1.1) also shows that after the critical concentration entanglement point, the viscosity of the multivalent salt containing solutions increases more rapidly than that of neat PAN-A /DMF or PAN-A-L solution. Polymer entanglement at high concentrations is clearly more effective in the presence of  $ZnCl_2$ .

The presence of additives in the dope solution clearly alters the ternary phase boundary (section 4.2). Measurements of the cloud-point with PAN-A over a polymer concentration range of (1-13 % w/v) showed that solutions containing  $ZnCl_2$  can tolerate only a small amount of water before precipitation while those with LiCl can tolerate

more water than solutions of PAN-A in DMF only. The water sensitivity (inversely proportional to the water fraction at the cloud point) of these solutions follows the trend:

Water sensitivity of PAN-A-Z > PAN-A > PAN-A-A > PAN-A-L

The membrane structure was characterized by SEM studies and by the bubble point technique. The skin layer in PAN-A membranes shows a fused nodular surface with a well-defined transition layer between it and the macroporous substructure. Typically asymmetric membrane performance is governed by the skin layer; however the underlying support also affects the membrane flux and contributes to the skin integrity. The bubble point analysis is sensitive to the skin porosity while SEM characterizes the total membrane morphology.

SEM shows that PAN-A, PAN-A-A and PAN-A-Z have large macrovoids in the underlying asymmetric structure; while the incidence and size of these macrovoids is considerably reduced in the case of the monovalent salt (PAN-A-L). This is consistent with the ternary cloud point data, which imply that the skin layer in PAN-A-L would form slowly after a considerable amount of DMF / water exchange had already taken place.

Bubble point analyses show that PAN-A and -A-L have much lower bubble points / larger skin pores than PAN-A-A or -A-Z. The absence of these skin defects correlates well with the higher solution viscosity / salt promoted chain association due to the multivalent salts. Higher viscosity would presumably dampen perturbations which result in loss of skin integrity.

While there are clear differences in the propensity for micron size defects in membranes cast from the various additive solutions, the modal pore size appears to change only marginally with the additive used. Ultrafiltration studies show similar rejections for various solutes (BSA, lysozyme, PEG-9000) for membranes cast from solutions with and without the additives.

These observations help to explain why PAN-A-Z formulations work well for water purification. Both PAN-A-Z and PAN-A-A have fewer large pores / defects and consequently higher rejection for bacteria. The relatively high flux is due to retaining the macrovoid-containing substructure; this can be attributed to the low water tolerance of PAN-A-Z solutions. These findings explain why the addition of ZnCl<sub>2</sub> to the casting



solution increases the bacterial reduction capability of the membrane by 1000x (3-log) while retaining 80% of the water permeability of the corresponding membrane cast from DMF alone.

## Chapter V

This chapter describes the rheological, phase-boundary and membrane properties of various salt (LiCl, ZnCl<sub>2</sub> and AlCl<sub>3</sub>) containing solutions based on the higher MW grades PAN-B and PAN-C, These properties are then compared with those for PAN-A discussed in Chapter IV. As described in Chapter III (section 3.3.3), the MW of the three PAN grades increases in the order PAN –A < B < C. The main aim of this chapter is to examine the effect of the increased molecular weight vis-a-vis the interactions with the three salt additives. The approach of this chapter is the same as that for the PAN-A study in Chapter IV: we first define the concentrated solution behaviour (rheology and phase boundary) of the three PAN-DMF-salt solutions and then compare the resulting morphology of membranes cast from these solutions. In addition, the morphology of membranes made from the acrylonitrile-acrylamide copolymer PAN-1 (see section 2.1.3 for synthesis conditions) are also discussed.

### 5.1 Rheological properties:

The dilute solution rheological properties with all 3 PAN grades were discussed in Chapter III. The intrinsic viscosity values for PAN-A are higher in all three DMF + salt solutions compared to those in neat DMF. The  $[\eta]$  values for PAN-B are essentially unchanged with the salt while those for the highest MW grade, PAN-C decrease with the addition of salt. Calculations of the Mark-Houwink constant in solutions made with the salt additives indicate that the general effect of the salt is to decrease the PAN coil expansion; the exponent  $a$  decreases from 0.75 in DMF to  $\sim 0.6$  for DMF+salt solutions. This is consistent with the high affinity of the salts for DMF, measured by FT-IR. Viscosity activation energies,  $E_a$ , calculated in the dilute concentration regime (0.1-0.3 g/dl), correlate well with the coil overlap parameter,  $\beta$ . Plotting  $E_a$  vs  $\beta$  for various solution types show larger positive slopes for solutions made from neat DMF solutions compared to those with salt additives. Again this appears consistent with the solvent effects described above.

### 5.1.1 Concentrated solution viscosity

The experimental details for the concentrated solution rheology studies are described in section 2.2. The additives LiCl, ZnCl<sub>2</sub>, AlCl<sub>3</sub> were all added at 0.83 M concentration in solvent DMF. The higher molecular weight PAN polymers were difficult to dissolve at room temperature; hence the dissolution conditions were standardized at 75°C in a constant temperature bath with intermittent shaking for approximately 12-15 hrs. PAN-B and PAN-C solutions in DMF-Z were limited to polymer concentrations of 5 and 3% respectively. Their solutions in other solvents were limited to a maximum of 11-13% in DMF-L and DMF-A.

Wherever possible, the viscosity of the PAN- A, B and C solutions was measured for 3, 7, 9, and 11% w/v concentrations at 30°C ( $\pm 0.01^\circ\text{C}$ ) over a shear rate range of 1-750 sec<sup>-1</sup>. The entire data set describing the effect of polymer concentration and salt type on the solution viscosity, at 30°C as a function of shear rate is tabulated in Appendix V-1.

### 5.1.2. Low shear rate viscosity

In this section we compare the viscosity of concentrated solutions at low shear rates (1-3.75 sec<sup>-1</sup>). The viscosity of polymer solutions is commonly shear dependent. As described in section 1.6.3, the zero-shear rate viscosity  $\eta_0$  can be obtained from a plot of viscosity vs shear rate if the data obeys the power-law model well. In our case, it was found that the power law described the shear rate dependence well for PAN-C but not for PAN-A. Hence,  $\eta_0$  was approximated as the viscosity measured at the lowest shear rate at which consistent measurements could be made in the cone-and-plate apparatus. In the case of PAN-A, the lowest shear rate at which reliable measurements could be taken was 3.75 s<sup>-1</sup> while that for PAN-B and PAN-C was 1 s<sup>-1</sup>. (see for details in Appendix V-2). In this chapter, the symbol  $\eta_0$ , represents the low shear viscosity. This is not strictly correct since  $\eta_0$  usually represents *zero* shear viscosity.

Figure 5.1(a-c) shows semi-logarithmic plots of  $\eta_0$  as a function of polymer concentration and solvent-additive type for each PAN grade. Concentrated solution viscosity increases sharply with the increase in PAN MW. The discussion below

compares the effect of the salt additive on the solution viscosity of the various PAN materials.

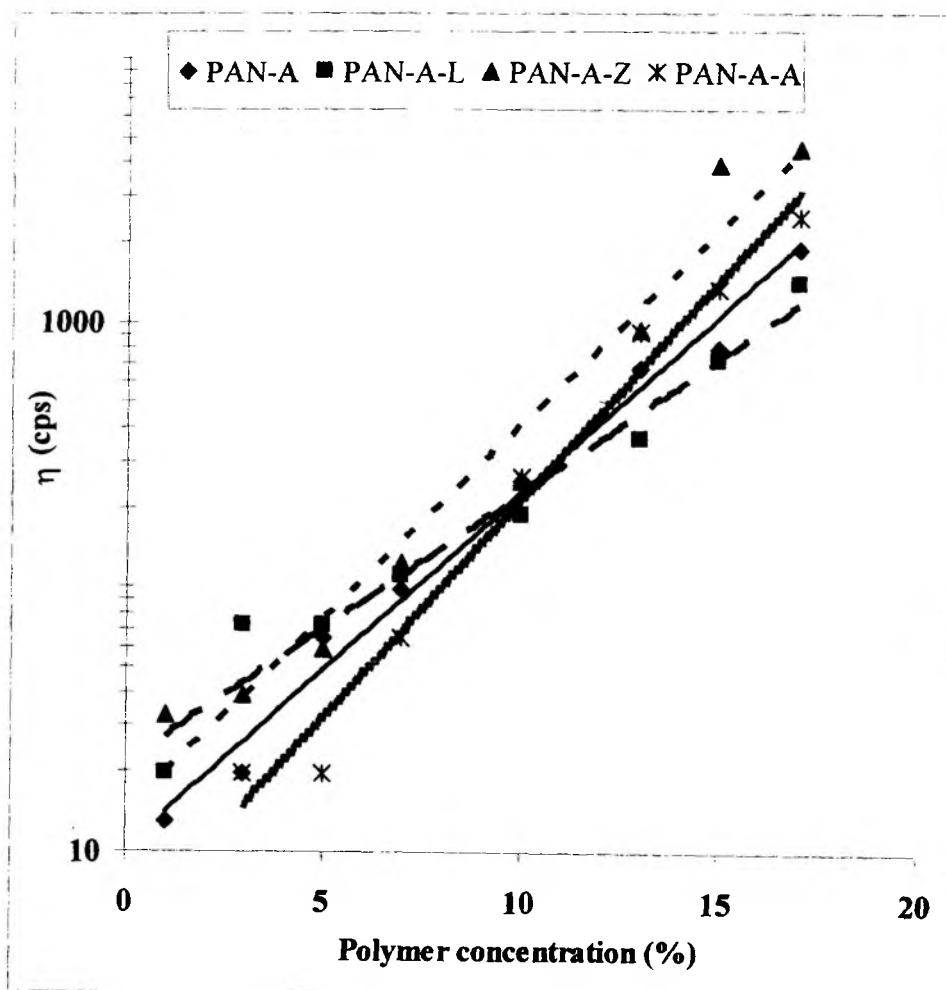


**Figure 5.1a:** Viscosity of PAN-A (DMF), PAN-A-L, PAN-A-Z and PAN-A-A solutions as a function of polymer concentration at a shear rate of  $3.75 \text{ sec}^{-1}$  and  $30^\circ\text{C}$ . The trend lines are fitted to the relation:  $\eta = I \exp(S \cdot c)$  where pre-exponent  $I$  and slope  $S$  are given below:

Solution	$I$	$S$	$R^2$
PAN-A	10.4	0.31	0.99
PAN-A-L	21.6	0.23	0.96
PAN-A-Z	14.2	0.34	0.96
PAN-A-A	4.8	0.38	0.98

William's and Gandhi [1971] examined the effect of solvent power and the polymer polarity on viscosity and found that  $\eta_0$  increases with concentration more rapidly in theta solvents than in good solvents. They attribute this result to increased polymer-polymer association in thermodynamically poor solvents. As discussed in Ch. IV, the viscosity of PAN-A-Z and PAN-A-A solutions increases faster with increasing polymer concentration than does the viscosity of neat PAN-DMF solutions. Above 10% PAN concentration, the viscosity's of solutions with the multivalent salts are clearly higher than that of PAN in DMF alone. The PAN-A-L solution generally shows lower viscosity value than the neat solution; this is consistent with the observations of Lobanov et al [1969]. We know from the studies discussed in Chapter III that all the salts decrease the solvation ability of DMF, hence, this increased viscosity in the case of the multivalent salts appears to be based on their promoting the association between PAN-A chains.

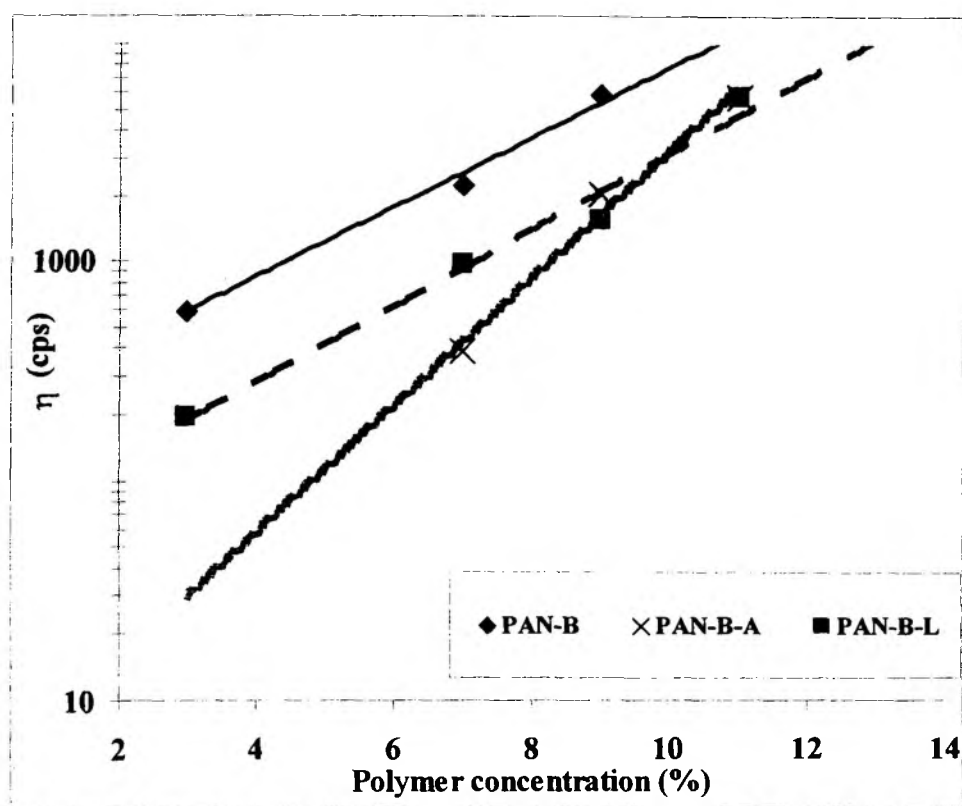


**Figure 5.1b** : Viscosity of PAN-B (DMF), PAN-B-L and PAN-B-A solutions as a function of polymer concentration at a shear rate of  $1 \text{ sec}^{-1}$  and  $30^\circ\text{C}$ . The trend lines

are fitted to the relation:  $\eta = I \exp(S \cdot c)$  where pre-exponent  $I$  and slope  $S$  are given below:

Solution	$I$	$S$	$R^2$
PAN-B	196	0.37	0.98
PAN-B-L	55.9	0.40	0.99
PAN-B-A	3.9	0.67	0.98

In the case of the two higher MW grades, PAN-B and PAN-C, (Figure 5.1 b-c) the  $\text{ZnCl}_2$  additive has a similar viscosity enhancing effect as seen for PAN-A. The reduction in the DMF solvent power is so large that that these grades are difficult to dissolve in DMF-Z. PAN-B-Z and PAN-C-Z solutions with > 5% polymer are gels. It will be shown in section 5.2 that the solutions of the all PAN grades in DMF+Z also tolerate very little water before phase separation. It should be mentioned that our results for the effect of  $\text{ZnCl}_2$  contradict those observed by Polatovskaya et al [1969]. We were unable to obtain the full Polatovskaya reference to resolve this discrepancy. Interestingly, our rheology, phase boundary and membrane permeability results with PAN+ DMF-Z based solutions parallel closely those observed for this additive in polysulfone solutions / membranes [Kim et al, 1996].

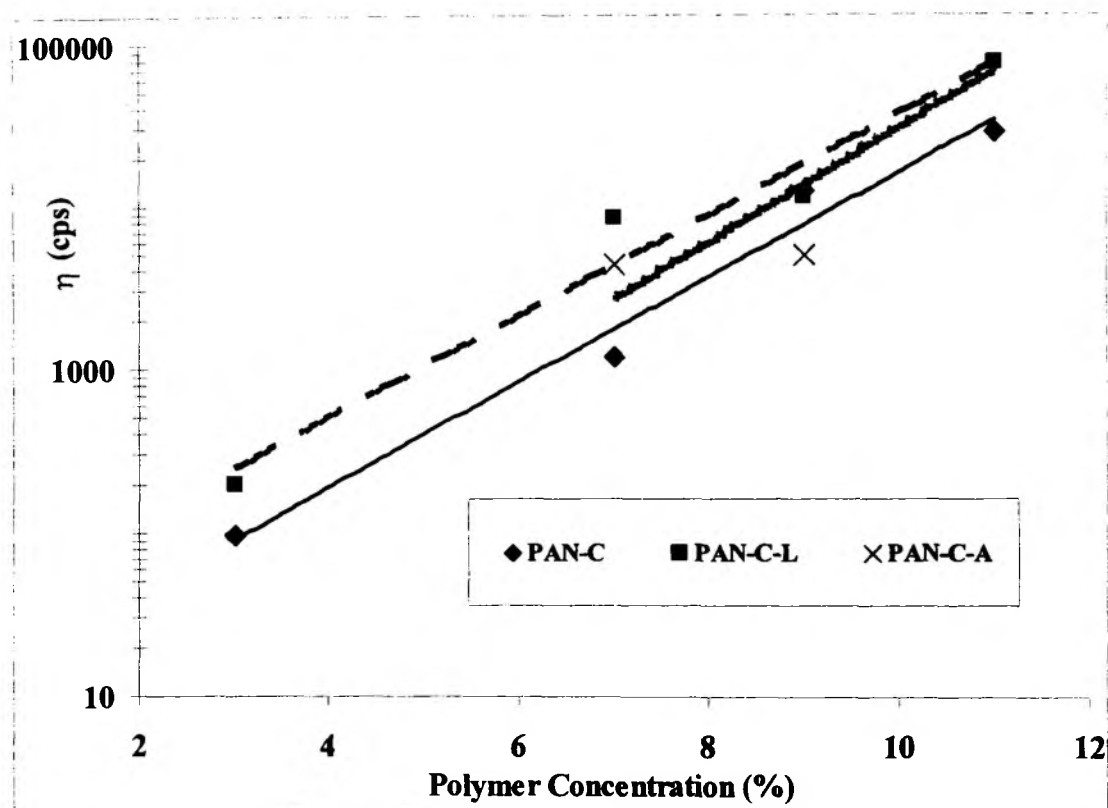


Figure 5.1c : Viscosity of PAN-C, PAN-C-L and PAN-C-A solutions as a function of polymer concentration at a shear rate of  $1 \text{ sec}^{-1}$  and  $30^\circ\text{C}$ . The trend lines are fitted to the relation:  $\eta = I \exp(S \cdot c)$  where pre-exponent  $I$  and slope  $S$  are given below:

Solution	$I$	$S$	$R^2$
PAN-C	9.8	0.74	0.98
PAN-C-L	28.6	0.71	0.96
PAN-C-A	9.4	0.81	0.78

In the case of the  $\text{LiCl}$  and  $\text{AlCl}_3$  additives, the trends with PAN-B and PAN-C are not clear. In the case of PAN-B, DMF-L and DMF-A based solutions have lower  $\eta_0$  over the entire concentration range than neat DMF solutions. This may be attributed to these salts (particularly  $\text{LiCl}$ ) breaking existing interchain interactions between the polymer chains. A similar viscosity reduction effect with  $\text{LiCl}$  has been observed before [Lobanov et al, 1969]. However, in the case of PAN-C, the salts appear to have only marginal effect on the solution viscosity.

### 5.1.3 : Solvent effect on viscosity in concentrated PAN solutions

In order to see the effect of the salt additive more clearly for concentrated solutions with the higher MW PAN grades, we examined “master” plots of the solution viscosity vs the coil overlap parameter  $\beta$  ( $\equiv [\eta] c$ ). Figure 5.2 shows a semi-logarithmic plot of  $\eta_0$  as a function of  $\beta$  using the data for all three PAN materials. The intrinsic viscosity values used for calculating  $\beta$  were given in Chapter. III Table 3.8.

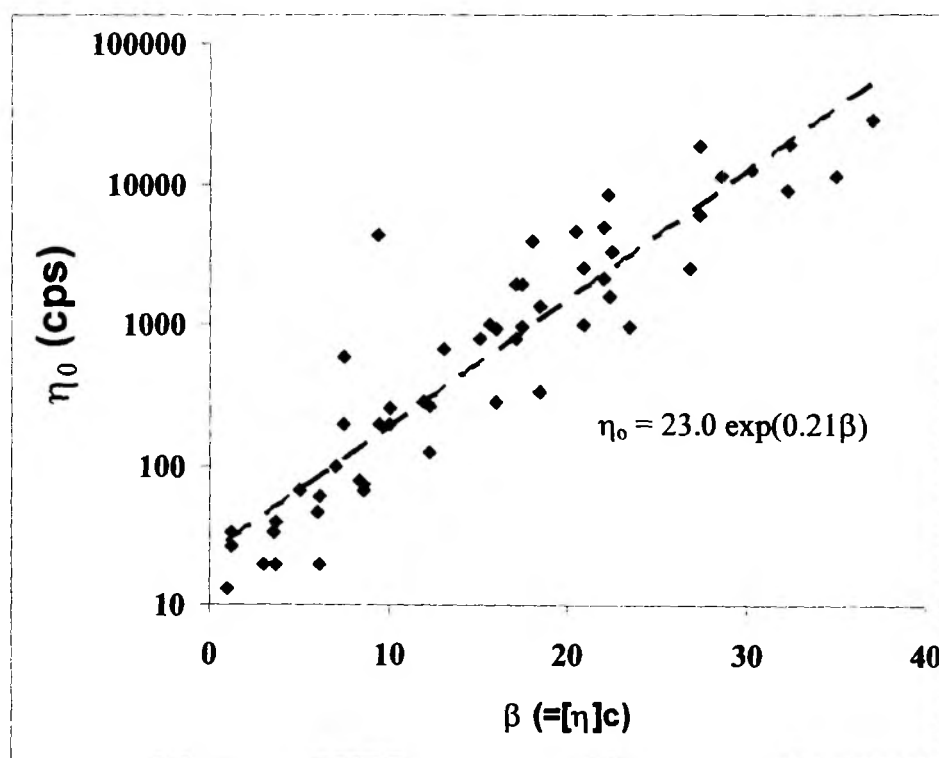


**Figure 5.2:** Correlation of  $\eta_0$  at 30°C with the coil overlap parameter  $\beta$  for all three PAN grades.

Fig 5.2 shows that the low-shear rate solution viscosity correlates well with the coil overlap parameter for all three PAN grades. This implies that the viscosity in the concentration and MW ranges studied here is determined by the degree of overlap of the individual polymer molecular domain [Graessley, 1974]. Frisch and Simha [1956] have shown that  $\beta$  is proportional to the average number of other polymer molecules with centers lying within the pervaded volume of any one given molecule.



We now re-classify the entire data set by the various solvent types to see the effect of the various salt additives. Figure 5.3a replots the data of Figure 5.2 and shows the varying dependence of  $\eta_0$  with  $\beta$  for the various DMF + salt solvent combinations. A larger slope on this graph (as for the multivalent salts) indicates an increased tendency for the polymer chains to associate in that solvent type.

A commonly used equation used to correlate solution viscosity  $\eta_0$  with  $\beta$  is Martin's equation (discussed in section 1.6.3):

$$\eta_0 - \eta_s = c[\eta] e^{k_M c[\eta]} \quad (5.1)$$

If we define a parameter Y as:

$$Y = \frac{(\eta_0 - \eta_s)}{c[\eta]} \quad (5.2)$$

Martin's equation would predict a linear semi-log relation between Y and  $\beta$  as shown in Figure 5.3b. This figure shows the trend lines for the various solvent types. The Martin's constant,  $k_M$ , has the same physical significance as the slope of Fig 5.3a and shows a similar trend :  $k_M$  for the  $ZnCl_2$  and  $AlCl_3$  containing solutions is greater than that for neat DMF or LiCl containing solutions . According to Kasaai [2000], higher value of  $k_M$  for the multivalent salts indicates a poorer solvent with low level of solvent-polymer interactions while the low value of  $k_M$  seen in DMF or DMF-L indicates a strong attraction between the solvent and PAN.

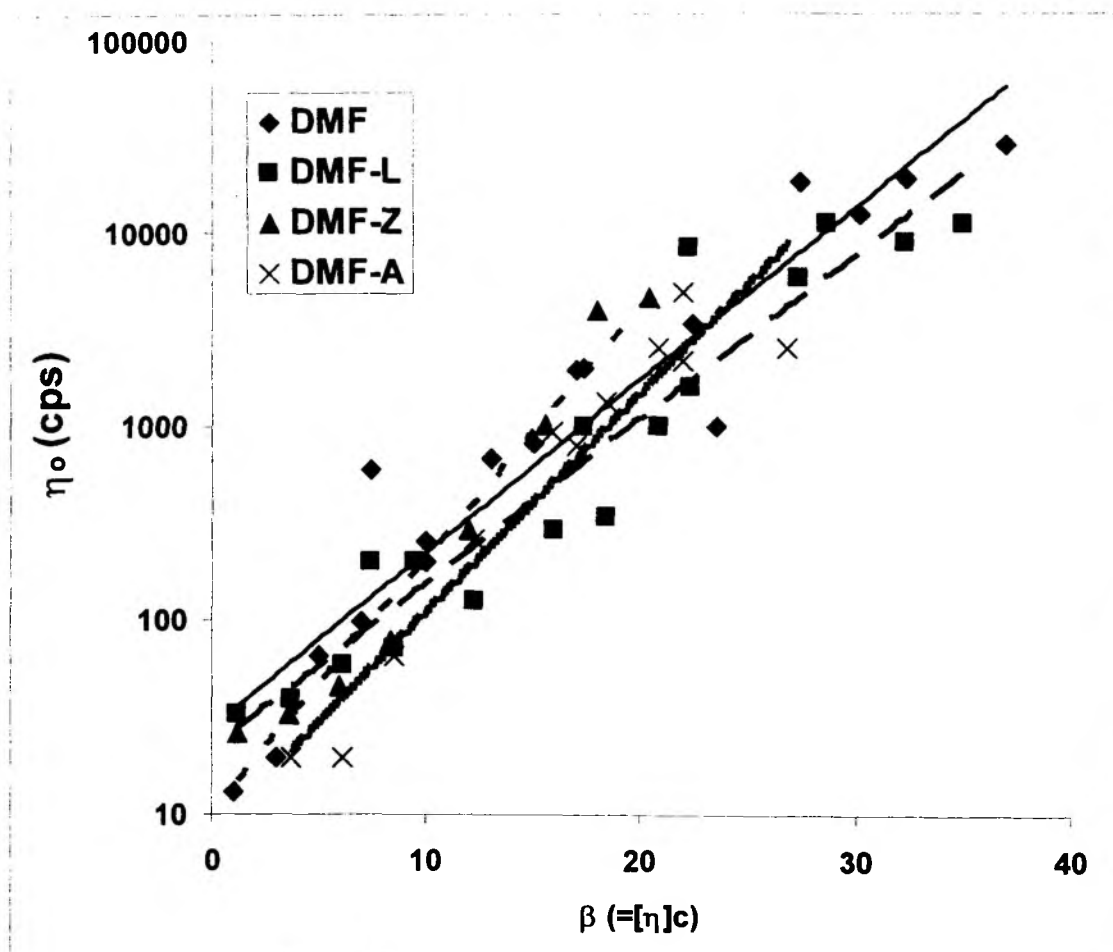


**Figure 5.3a:** Correlation of  $\eta_0$  with  $\beta$  ( $\equiv c[\eta]$ ) for the various DMF, DMF-L, DMF-Z and DMF-A based solutions for all three PAN grades. The trend lines are fitted to the relation:  $\eta_0 = I \exp(S \cdot \beta)$  where pre-exponent  $I$  and slope  $S$  are given below:

Solvent	$I$	$S$	$R^2$
DMF	28.0	0.21	0.91
DMF-L	21.7	0.20	0.91
DMF-Z	10.4	0.30	0.97
DMF-A	8.1	0.26	0.92

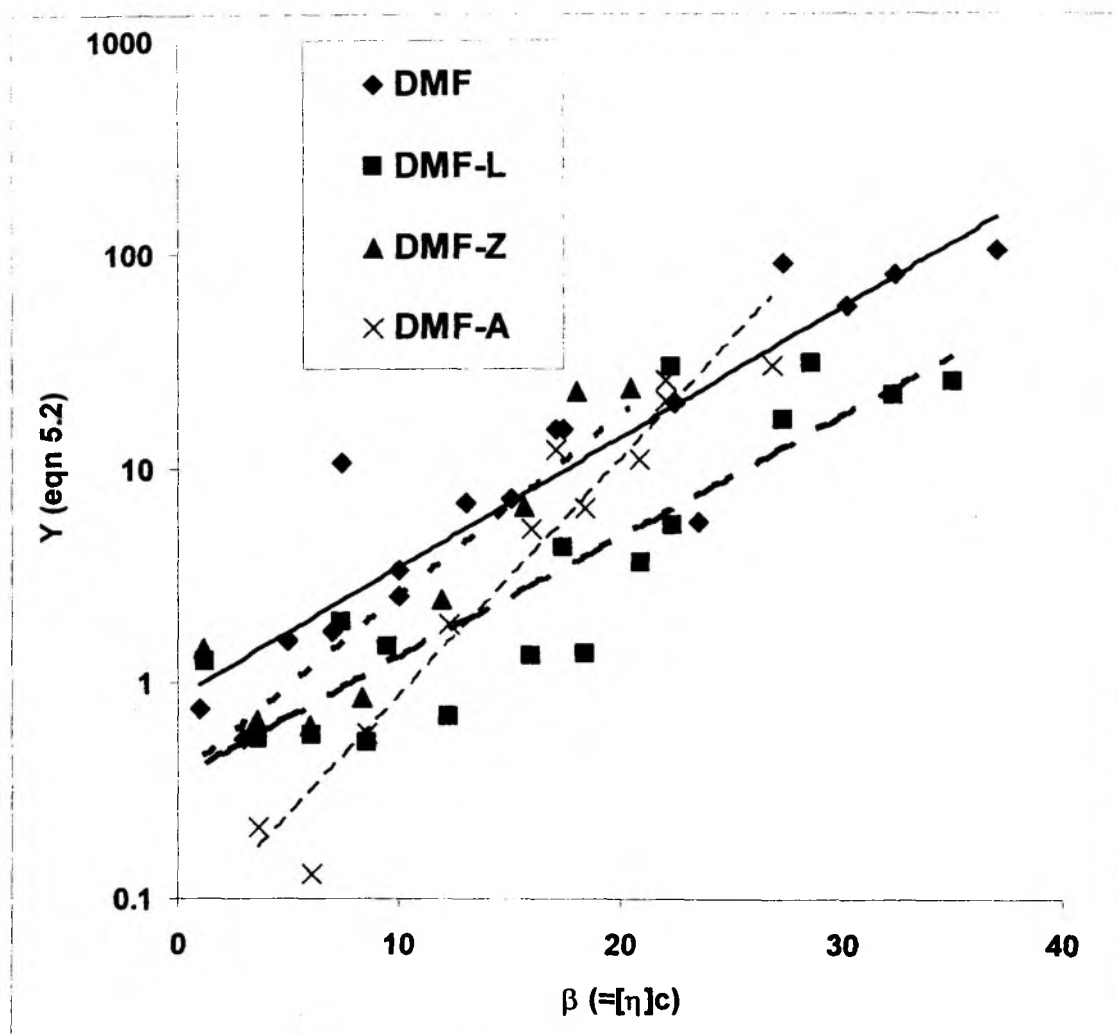


**Figure 5.3 b:** Correlation of  $Y$  (eqn 5.2) with  $\beta$  ( $\equiv c[\eta]$ ) for the various DMF, DMF-L, DMF-Z and DMF-A based solutions for all three PAN grades. This correlation is based on the Martin eqn (5.1). The trend lines are fitted to the relation:  $Y = I \exp(S \cdot \beta)$  where pre-exponent  $I$  and slope  $S$  are given below:

Solvent	$I$	$S$	$R^2$
DMF	0.85	0.14	0.85
DMF-L	0.36	0.13	0.77
DMF-Z	0.36	0.19	0.81
DMF-A	0.07	0.25	0.93

Another type of intermolecular interaction is based not on the coil overlap but segment-segment interactions. Bueche [1952] predicted that solution properties that were determined by inter-segment interactions would correlate with the product  $c \times MW$ . Figures 5.4a and 5.4b shows the analog of Figures 5.2 and 5.3a where  $\eta_0$  is correlated with the Bueche parameter ( $\lambda \equiv c MW$ ). Both the Bueche and Rouse [1970] model predict a linear variation of  $\eta_0$  with  $\lambda$ . The Rouse model is given by the equation below:

$$\eta_0 = \frac{\lambda N_A l^2 \zeta}{36 M_0^2} \quad (5.3)$$

where  $N_A$  is the Avogadro number,  $l$  is the (monomer) link distance,  $M_0$  is the monomer molecular weight and  $\zeta$  is the friction coefficient between polymer chains. The different slopes of the  $\eta_0$  vs  $\lambda$  (or  $\beta$ ) plots for PAN in the various solvent types can thus be attributed to changes in the interchain friction coefficient  $\zeta$ .

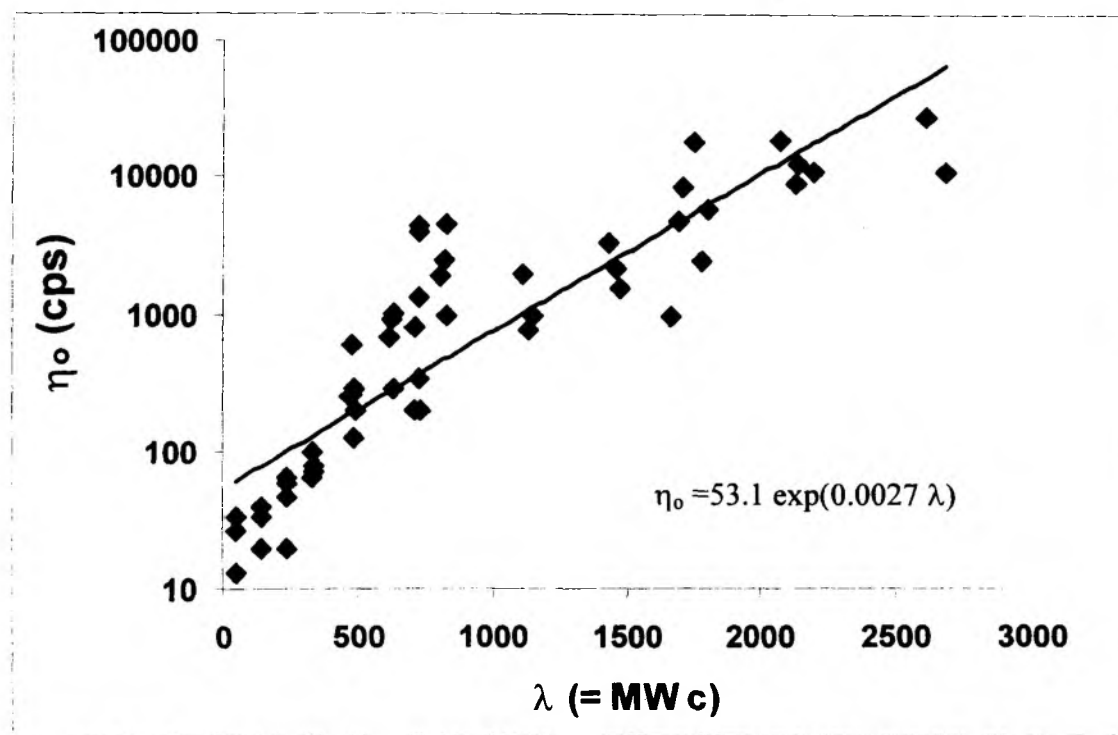


**Figure 5.4 a:** Correlation of  $\eta_0$  at 30°C with the Bueche parameter ( $\lambda \equiv MW c$ ) for all three PAN grades.

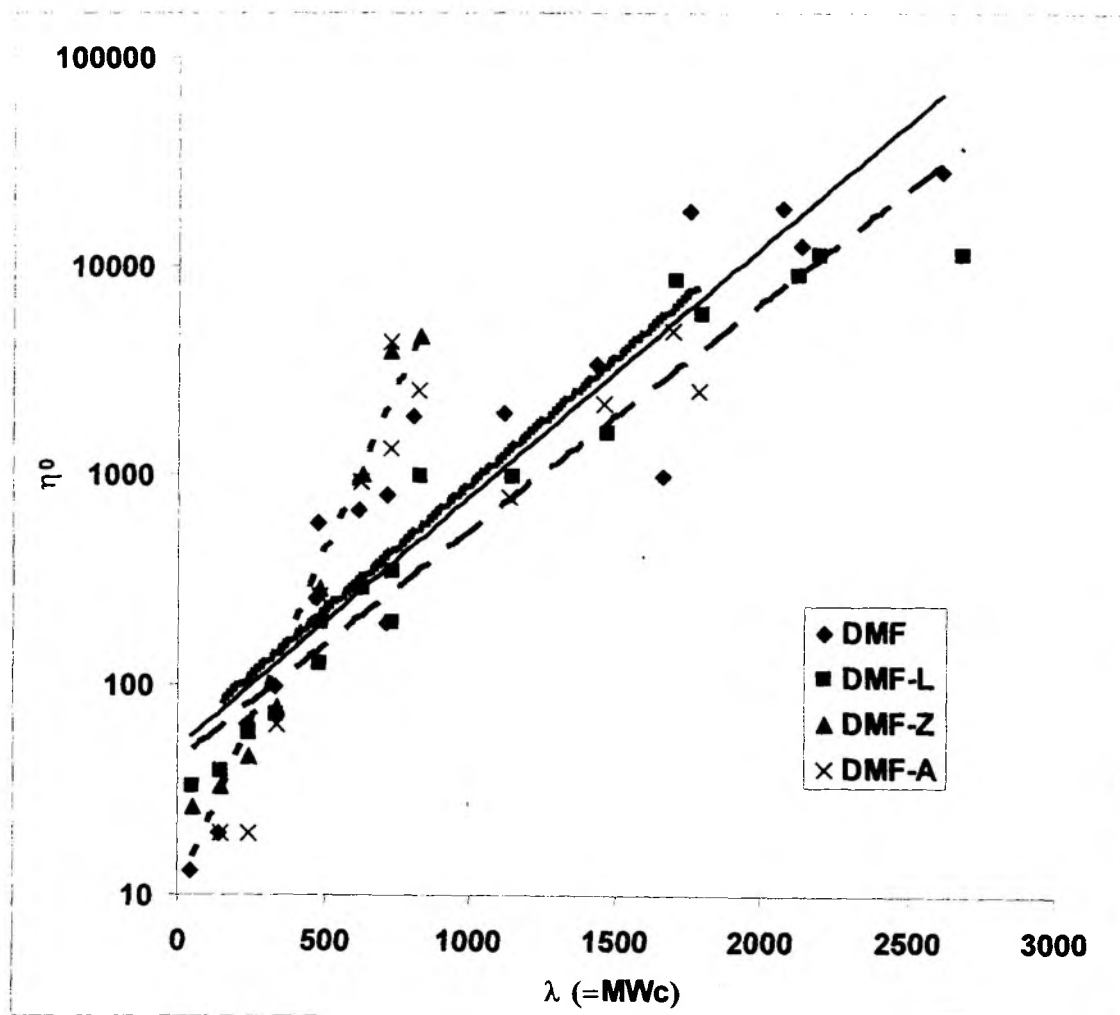


**Figure 5.4b** : Correlation of  $\eta_0$  at 30°C with the Bueche parameter ( $\lambda \equiv c \text{ MW}$ ) for the various DMF, DMF-L, DMF-Z and DMF-A based solutions for all three PAN grades. The trend lines are fitted to the relation:  $\eta_0 = I \exp(S \cdot \lambda)$  where pre-exponent  $I$  and slope  $S$  are given below:

Solvent	$I$	$S \cdot 10^4$	$R^2$
DMF	50.3	28	0.84
DMF-L	44.0	25	0.93
DMF-Z	10.5	74	0.97
DMF-A	55.8	28	0.60

The correlations in Figures 5.4(a-b) with the Bueche parameter are slightly weaker than those shown in Figures 5.2 and 5.3a for the coil-overlap parameter. Hence,

the coil overlap model terminology discussed in connection with Figures 5.2-5.3 will continue to guide our view of the solution properties.

#### 5.1.4 Shear dependent rheology

The behaviour of the various solutions was measured as a function of shear rate. All the solutions exhibit shear thinning behaviour. The data at 30°C for solutions with varying polymer concentration and different additives are tabulated in Appendix V-3. Representative data at 7% PAN concentration for each polymer grade and solvent type are shown in Figures 5.5 (a-c) as plots of reduced viscosity vs reduced shear rate:

$$(\eta / \eta_{ref}) = (\dot{\gamma} / \dot{\gamma}_{ref})^{n-1} \quad (5.4)$$

No consistent trend is seen in these plots. PAN-A and PAN-B show more shear thinning tendency than solutions with the salts; however, the opposite is true for PAN-C based solutions.

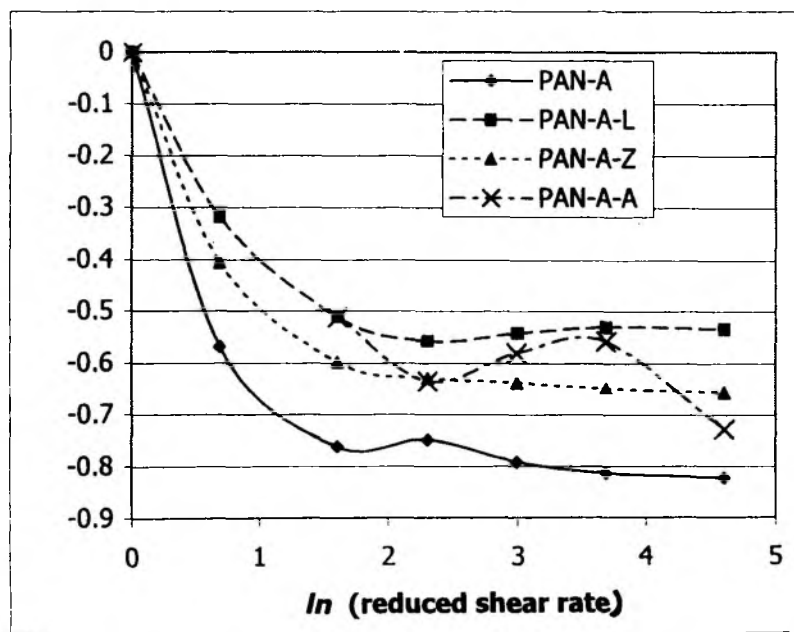


**Figure 5.5a:** Reduced shear viscosity vs reduced shear rate for PAN-A in DMF, DMF+L, DMF+Z and DMF+A. The reference condition was at 3.75 cm<sup>-1</sup> shear rate. The viscosity data does not fit the power law dependence (eqn 5.4) with shear rate ( $R^2 \sim 0.2$ ).

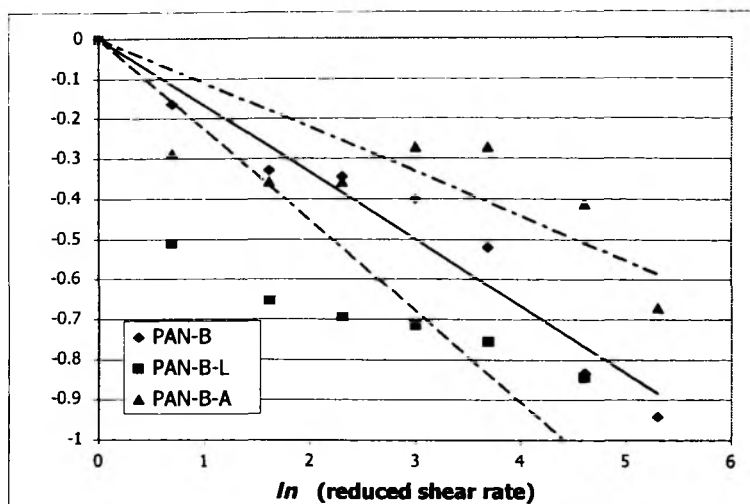


**Figure 5.5b:** Reduced shear viscosity vs reduced shear rate for PAN-B in DMF, DMF+L and DMF+A. . The trend lines are fitted to the power law relation (eqn (5.4)): where the reference condition was at  $1 \text{ cm}^{-1}$  shear rate and slope ( $n-1$ ) is given below:

Solution	$n-1$	$R^2$
PAN-B	0.17	0.95
PAN-B-L	0.23	0.40
PAN-B-A	0.11	0.48

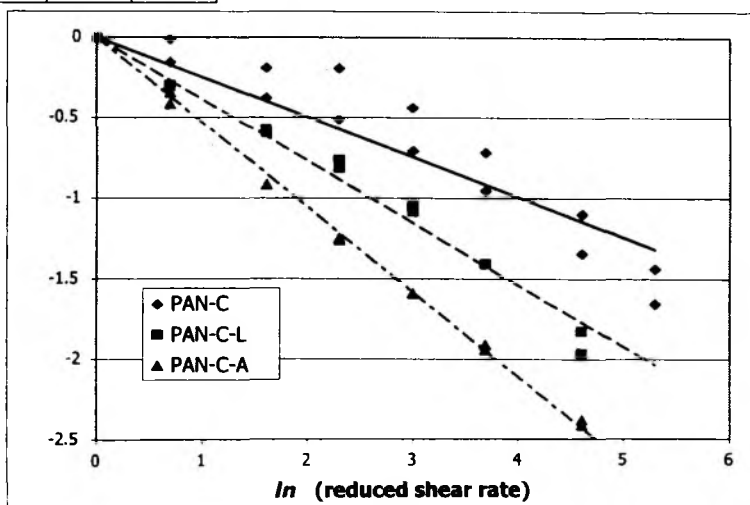


**Figure 5.5c:** Reduced shear viscosity vs reduced shear rate for PAN-C in DMF, DMF+L and DMF+A. . The trend lines are fitted to the power law relation (eqn (5.4)): where the reference condition was at  $1 \text{ cm}^{-1}$  shear rate and slope ( $n-1$ ) is given below:

Solution	$n-1$	$R^2$
PAN-C	0.17	0.95
PAN-C-L	0.23	0.40
PAN-C-A	0.11	0.48

## 5.2 Phase boundary studies

The cloud points for the PAN – solvent –water systems at 30°C were obtained by the procedure described in section 2.2.3. The experimentally observed cloud points for each type of solution were correlated by the empirical linearized cloud point equation 4.1 and extrapolated to a higher concentration range than can be accurately measured experimentally. The solvent was either DMF alone as a reference or DMF + 0.83M of one of the 3 salts (LiCl, ZnCl<sub>2</sub> and AlCl<sub>3</sub>). Figures 5.6-5.7 depict the ternary phase diagrams of the polymers PAN-B and PAN-C with and without additives. The ternary phase diagrams of PAN-A was shown in Figure 4.2. Chapter IV.

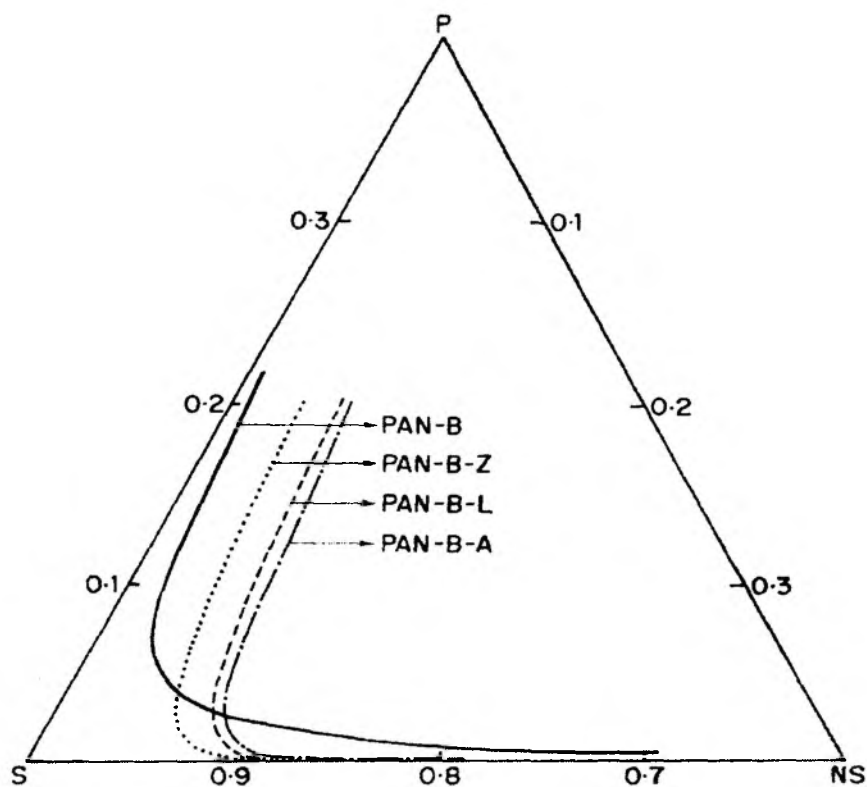


**Figure 5.6:** Ternary phase diagram for PAN-B (P) in solvents (S) DMF, DMF+L, DMF+Z and DMF+A in contact with non-solvent (NS) water.



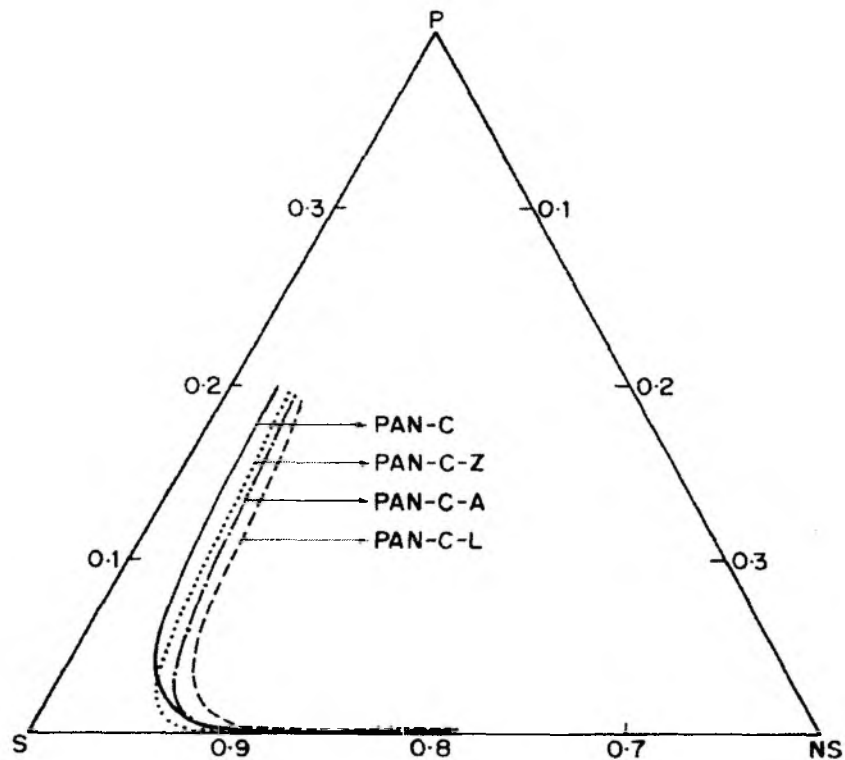


**Figure 5.7:** Ternary phase diagram for PAN-C (P) in solvents (S) DMF, DMF+L, DMF+Z and DMF+A in contact with non-solvent (NS) water.

Figures 5.6-5.7 show that the phase boundary curves for PAN-B and -C move away from the P-S axis i.e.. towards increasing water contents when salt is present.. The cloud point curve also depends on the PAN grade. For PAN- A-Z, the phase boundary is very close to the P-S axis while PAN-A-L AND PAN-A-A tolerate more water than solutions of neat polyacrylonitrile in DMF. In the case of PAN-B and PAN-C, all solutions with salts phase separate at higher water content than solutions in DMF only.

The values of the intercept  $a$  and slope  $b$  (parameters of the linearized cloud point eqn (2.4)) for the various solutions with all three PAN grades are shown in Table 5.1. Though both parameters  $a$  and  $b$  have theoretical significance [Boom et al 1993, see section 1.7.1), Appendix V-4 shows that these parameters do not follow the predicted trends. For example, for a given solvent-non-solvent pair, parameter  $b$  [=  $(v_P - v_{NS}) / (v_S - v_{NS})$ ] should increase with increasing PAN MW. However, the estimates do not show

even this basic trend. Though this equation correlates the data well, we cannot infer any fundamental information from the values of the parameters themselves.

**Table 5.1.** Summary of lcp equation (4.1) parameters obtained by regression analysis of experimental cloud point data.

System	$a$	$b$
PAN-A	-5.44	1.77
PAN-A-L	-3.97	1.46
PAN-A-Z	-6.89	2.15
PAN-A-A	-4.25	1.47
PAN-B	-6.40	2.12
PAN-B-L	-2.92	1.13
PAN-B-Z	-3.36	1.18
PAN-B-A	-2.76	1.11
PAN-C	-3.91	1.28
PAN-C-L	-3.24	1.18
PAN-C-Z	-3.37	1.13
PAN-C-A	-3.44	1.19

The water sensitivity of the polymer solutions is defined as the amount of solvent-water exchange that can take place before phase separation. This important characteristic is highlighted in Figures 5.8(a-c). These figures are based on the cloud point data; specifically on the correlative linearized equation (4.1) and the parameter estimates in Table that were fitted to these data. The plots for all three PAN grades are shown below

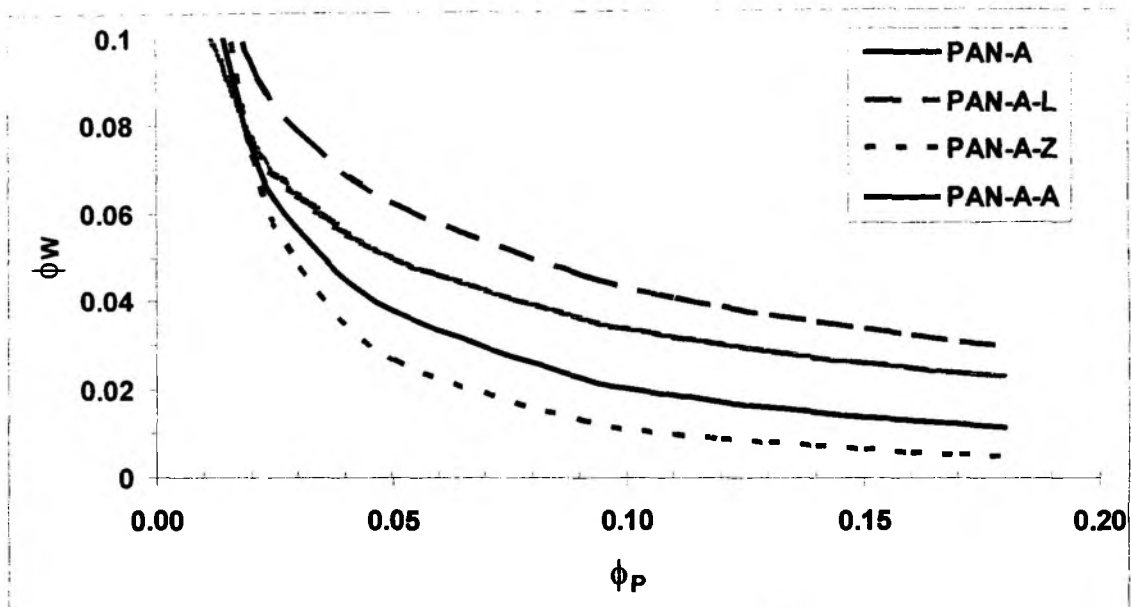


**Figure 5.8a:** Predicted curves for the water sensitivity of PAN-A solutions as a function of polymer volume fraction with and without salt additives.

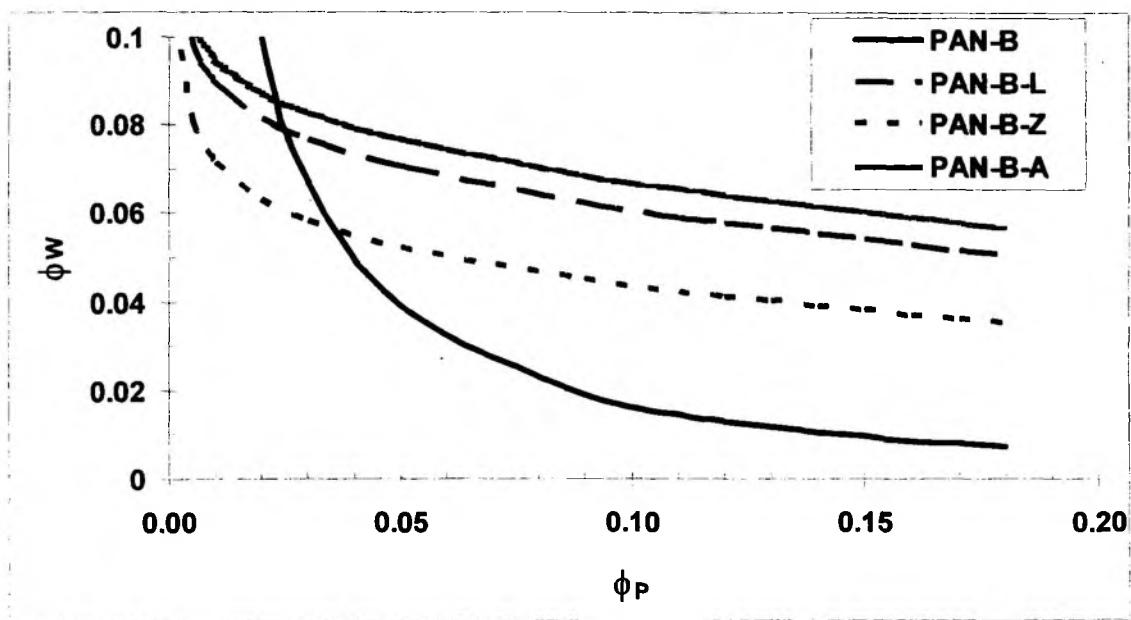


**Figure 5.8b:** Predicted curves for the water sensitivity of PAN-B solutions as a function of polymer volume fraction with and without salt additives.

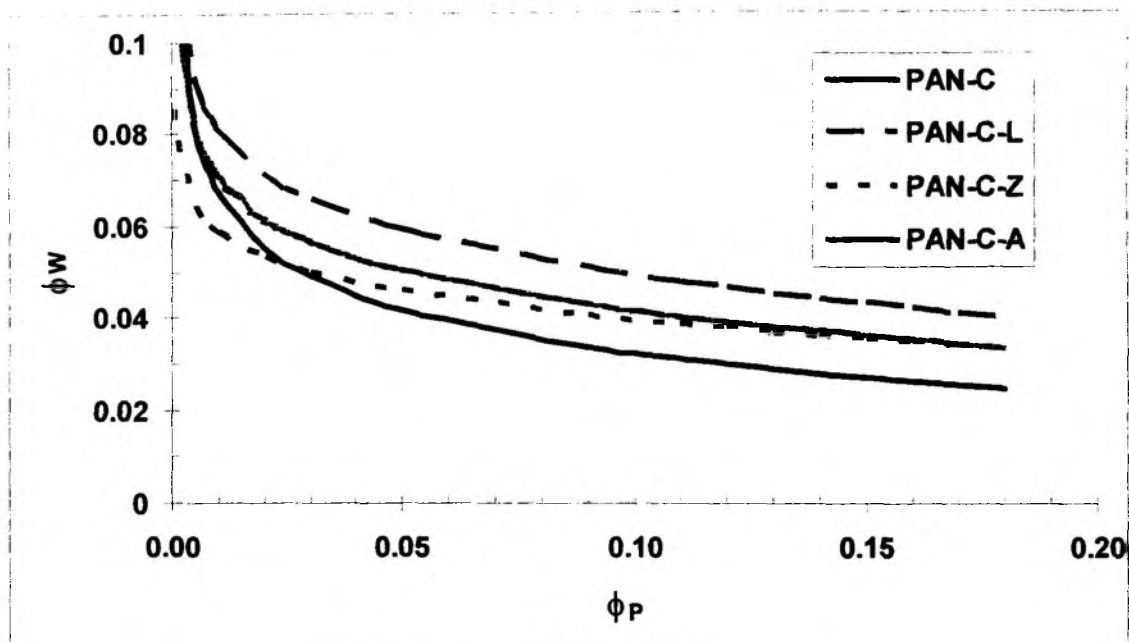


**Figure 5.8c:** Predicted curves for the water sensitivity of PAN-C solutions as a function of polymer volume fraction with and without salt additives.

As discussed in Chapter IV, in the case of the low MW grade, PAN-A-Z has the highest water sensitivity while PAN-A-L and A-A are less sensitive to water than the solution in neat DMF. The water sensitivity of these solutions can be ordered as:

$$\text{PAN-A-Z} > \text{PAN-A} > \text{PAN-A-A} > \text{PAN-A-L}$$

Two different trends are seen for the higher MW grades PAN-B and -C depending on the polymer concentration. At low polymer concentrations (0-3%) the water sensitivity for these higher MW PAN grades follows the same trend as for PAN-A. At higher polymer concentrations, the trends change and the solution in neat DMF is more water sensitive than those with salts. This water sensitivity trend at higher polymer concentrations can be expressed as:

$$\text{Neat DMF} > \text{DMF-Z} > \text{DMF-A and L} \quad \text{for } >3\% \text{ PAN-B and PAN-C}$$

The trend is more marked for PAN-B than for PAN-C; in the PAN-C case, the difference between the various curves is relatively small. The water sensitivity does not correlate well with the PAN MW.

### 5.3 Membrane properties

The morphology of PAN-B and -C membranes were studied mainly by SEM and bubble point measurements. These results are compared with the more extensive characterization for PAN-A discussed in Chapter IV.

#### 5.3.1 Pore size and pore size distribution:

The use of membranes in water purification may be hindered by the occurrence of pores large enough to affect the leak-through of bacteria or spores. The bubble point, which corresponds to the largest pore detection in the sample, is thus an important membrane property. As discussed in Chapter IV, section 4.4.1, the bubble point method can be extended to obtain the leading edge (large pore sizes) of the pore size frequency distribution. The bubble point data / pore size distribution with water and isopropanol wetted membranes for PAN-A are shown again in Figure 5.9a.

These results for PAN-A are compared here with those for membranes based on PAN-B and PAN-C. However, a full direct comparison is not possible. PAN-B and PAN-C can be dissolved only at low concentrations (< 11% polymer); whereas PAN-A membranes cast at such low polymer concentrations are mechanically too weak to be extensively tested. PAN-B-Z and C-Z solutions can be made only with < 5% polymer content; membranes made with these PAN grades and the ZnCl<sub>2</sub> additive were also not testable.

Table 5.2 compiles the average bubble point for various PAN membranes measured by the water-air displacement technique; Table 5.3 shows the corresponding data for isopropanol wetted membranes. As expected, the bubble points in Table 5.3 are lower than those in Table 5.2. The ratio of these bubble points is not always equal to the corresponding surface tension ratio, probably due to the higher experimental error in measuring the low bubble points with isopropanol wetted membranes. The isopropanol-air displacement technique is more useful for measuring the pore size distribution (Figures 5.9a-c).



**Table 5.2 :** Average bubble point ( $\text{kg/cm}^2$ ) in water –air displacement tests for membranes cast from various PAN materials and salt additive

Additive	7% PAN-A	13%PAN-A	7% PAN-B	7% PAN-C
Neat DMF	0.4	2.0	1.8	2.0
LiCl	*	-	2.0	0.8
ZnCl <sub>2</sub>	2.2	2.4	#	#
AlCl <sub>3</sub>	*	-	1.2	2.4

**Table 5.3 :** Average bubble point ( $\text{kg/cm}^2$ ) in isopropanol –air displacement tests for membranes cast from various PAN materials and salt additives

Additive	7% PAN-A	13%PAN-A	7% PAN-B	7% PAN-C
Neat DMF	0.2	0.6	1.2	0.2
LiCl	*	-	0.4	0.2
ZnCl <sub>2</sub>	0.8	1.2	#	#
AlCl <sub>3</sub>	*	-	0.2	0.8

Common notes to Tables 5.2 and 5.5:

\* The asterix denotes membranes that were too weak to be tested. PAN-A-L and PAN-A-A membranes could not be formed at 7% polymer content. The viscosity of these casting solutions was low

# PAN-B and PAN-C could not be dissolved in DMF-Z above 5% polymer concentration.

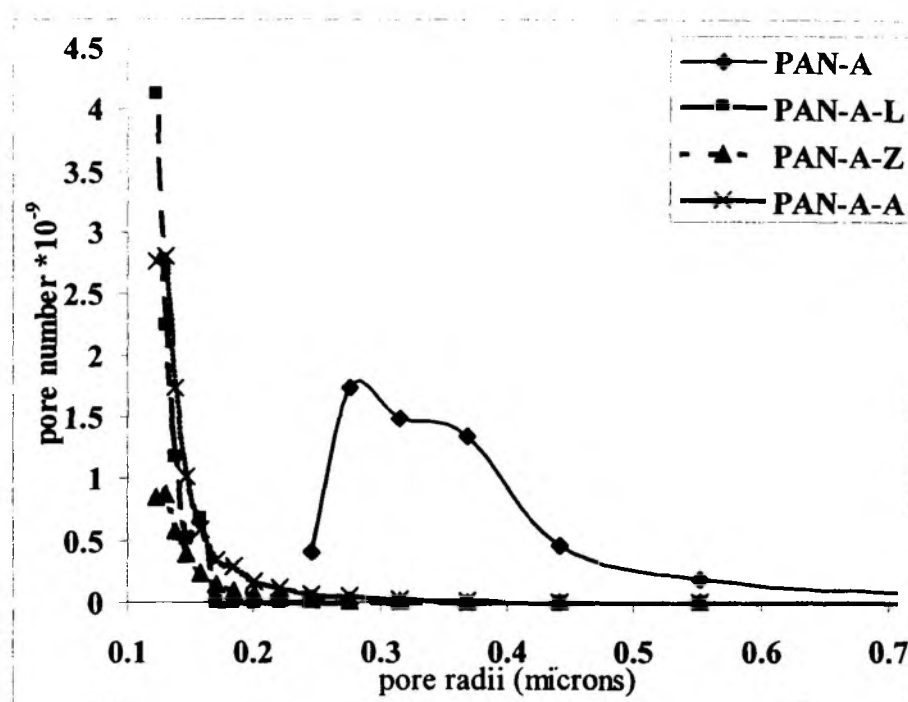


Figure 5.9a : Pore size distribution in isopropanol of PAN-A, PAN-A-L, PAN-A-Z and PAN-A-A 13% solutions cast on polyester support

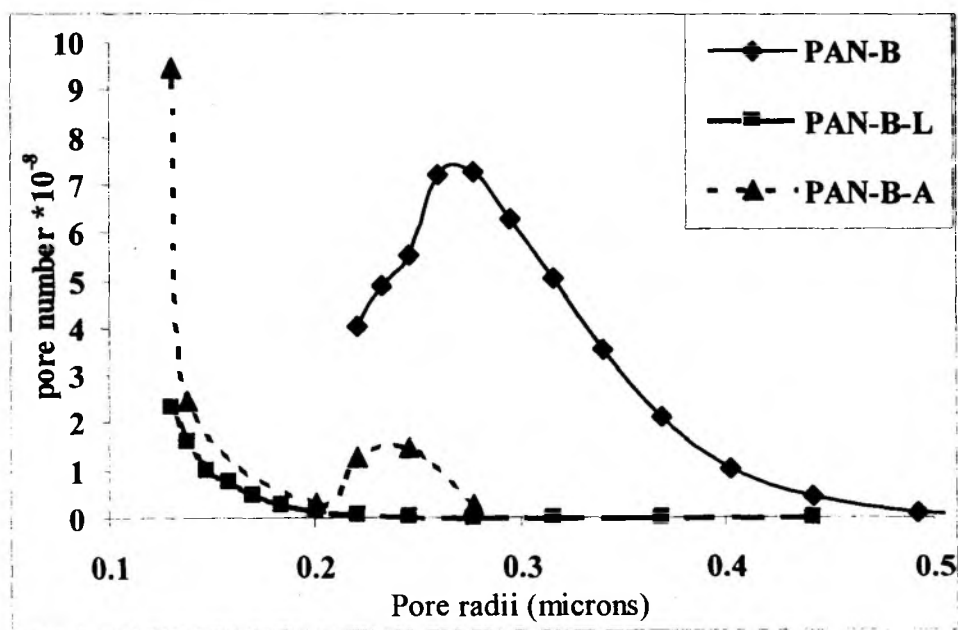
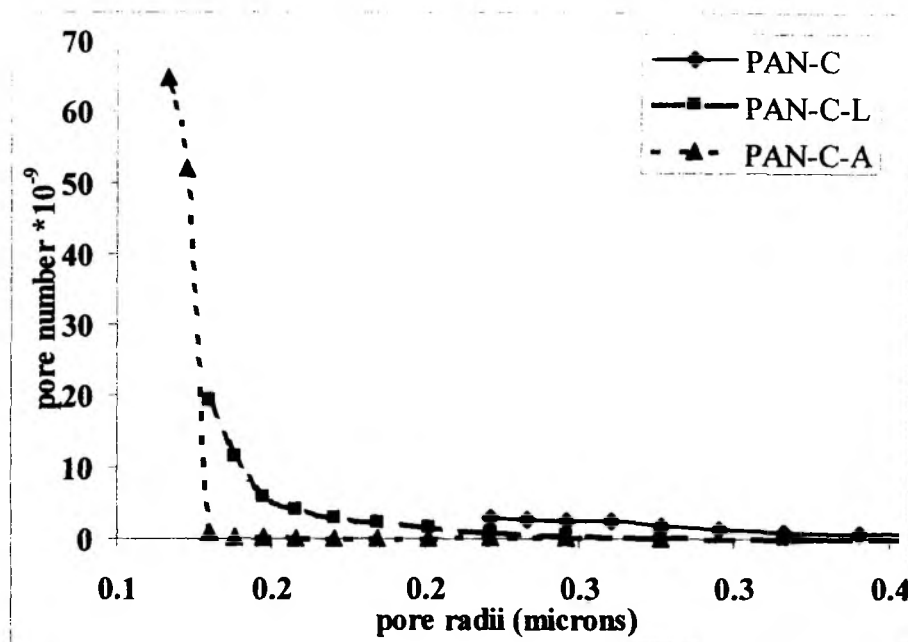


Figure 5.9b : Pore size distribution measured by isopropanol –air displacement tests of PAN-B, PAN-B-L and PAN-B-A membranes (supportless) cast from 7% polymer solutions



**Figure 5.9c :** Pore size distribution measured by isopropanol –air displacement tests of PAN-C, PAN-C-L and PAN-C-A membranes (supportless) cast from 7% polymer solutions

Figures 5.9(b-c) show the pore size distribution for PAN-B and PAN-C membranes cast from various 7% polymer content solutions; these can be compared with the analogous figure for PAN-A membranes cast from solutions with 13% polymer content in Figure 5.9a. Though the bubble point could be measured for PAN-A membranes cast from 7% solution (as shown Tables 5.2-5.3), the membranes were too weak to be tested at the higher pressures necessary to obtain the extended pore size distribution curve. However, the results seem quite clear in terms of the effect of the salt additives.

For all three PAN grades, all the salt additives cause an increase in bubble point and reduce or eliminate the larger size ( $> 0.2 \mu\text{m}$ ) pores. This benefit is more marked for the multivalent salts. For PAN-A, the proportion of larger pores (Figure 5.9a) follows the trend:

$$\text{PAN-A-Z} < \text{PAN-A-A} < \text{PAN-A-L} < \text{PAN-A}$$

For PAN-B and PAN-C, data with the  $\text{ZnCl}_2$  additive is not available, however, the other additives show the same trend (Figures 5.9b-c) as seen as for PAN-A:



PAN-B- or PAN-C- with  $\text{AlCl}_3 < \text{LiCl} < \text{neat DMF}$

Though Figures 5.9a-c do not show the entire pore size distribution, the pore sizes in the detectable range ( $\geq 0.1\mu\text{m}$ ) does not change significantly with the higher MW grades PAN-B and PAN-C. However, protein rejection testing of PAN-B (section 5.3.3) show that there may be some coarsening for even smaller pore sizes ( $< 0.01\mu\text{m}$ ) affecting ultrafiltration performance

### 5.3.2 Pure water permeation

The pure water fluxes at 70 kPa for each membrane type were averaged over 3 - 4 measurements. The standard deviation of the pure water flux measurements corresponds to  $\pm 5\%$ . The average water flux data for membranes cast from all three PAN grades and various polymer concentrations is shown in Appendix V-5. Figure 5.10 depicts the averaged water flux for membranes made at 7% polymer content for all the three polymers with various salt additives.

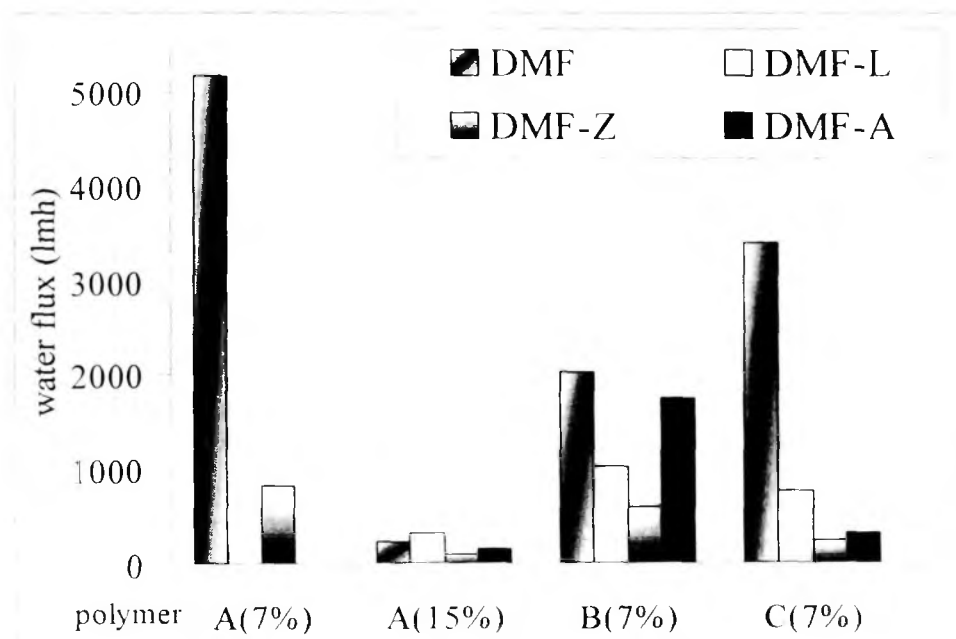


**Figure 5.10** : Water flux (lmh) data at 70kPa and 30°C for membranes cast from 7 % PAN- A, 15% PAN-A 7% PAN- B and 7% PAN-C solutions with DMF, DMF-Z, DMF-L and DMF-A solvents

As mentioned before, membranes from PAN-A-L and PAN-A-A solutions with 7% polymer could not be tested. For completeness, Figure 5.10 also shows the water flux for 15% PAN-A membranes cast with all three salts additives in DMF. Clearly all three salt additives decrease the water permeability. It is observed that DMF-Z results in the least water permeable membrane for all three PAN grades. The trends with the other two salts are less clear. Since the pore size distribution and separation data (section 5.3.1) indicate marginal change in the mode pore size, the reduced water permeability may be caused by a decrease in the total number of pores in addition to the elimination of the larger pores.

### 5.3.3 Protein rejection

Protein (BSA) rejections were not measured with PAN-C at all and only limited measurements were made with PAN-B due to the limited amount of these polymers that was synthesized. Data for PAN-B cast from different polymer concentrations in neat DMF are tabulated in Table 5.3. This can be compared with the equivalent data for PAN-A in Table 5.4, which shows the data for PAN-A with 11 and 13% polymer concentration. The experimental conditions were the same as defined in section 4.4.

**Table 5.3.** Water permeability, air-water bubble point and BSA rejection at 70kPa - 30°C / 0.1 % BSA concentration in stirred cell for PAN-B membranes.

% Polymer	Water Flux (lmh)	Bubble pt. (kg/cm <sup>2</sup> )	% BSA rejection
7	2027	2.9	53.5
9	321	1.5	64.0
11	148	2.7	66.5
13	117	2.9	78.5

**Table 5.4.** Water permeability, air-water bubble point and BSA rejection at 70kPa – 30°C / 0.1 % BSA concentration in stirred cell for PAN-A membranes. More extensive data for PAN-A membranes can be found in sections 4.4.2 and 4.4.3.

% Polymer	Water Flux (lmh)	Bubble pt. (kg/cm <sup>2</sup> )	% BSA rejection
11	1117	0.4	63
13*	428	1.8	85

- Data for membrane cast from 13% polymer concentration was obtained at 200kPa

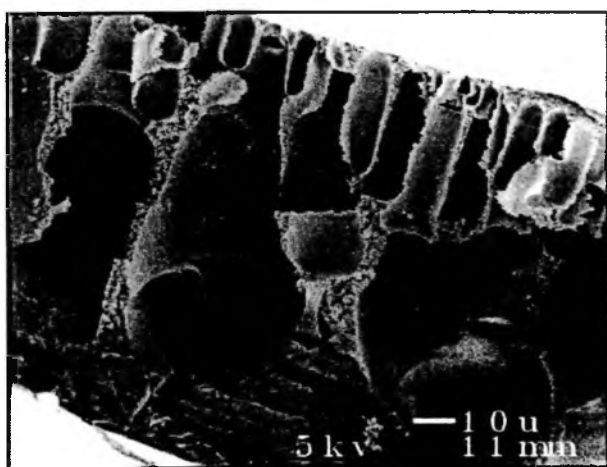
The water flux for the lower molecular weight PAN-A is higher and the bubble points are lower than the corresponding membranes made from PAN-B. In spite of this, PAN-B has similar BSA rejection as PAN-A. The majority of PAN-A pores are small enough to reject BSA but this membrane has a greater propensity for a minute number of surface defects. These surface defects have little effect on the UF separation but show up clearly in bubble point and bacterial challenge tests.

It is seen from the PAN-B data that the water flux decreases markedly and the BSA rejection increases slightly as the polymer content increases. The bubble point for PAN-B membranes is not very sensitive to the polymer concentration.

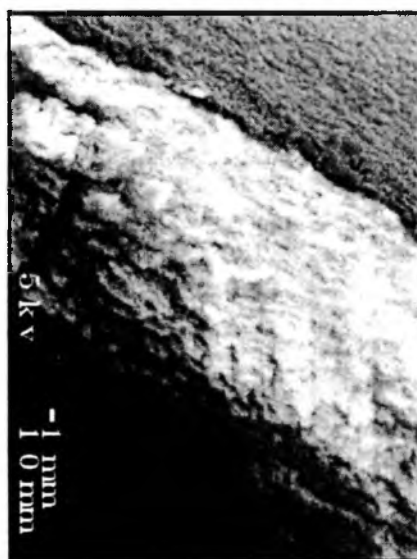
#### 5.4 Membrane morphology studies

The cross sectional SEM views of membranes cast from the higher molecular weight polymers PAN- B and C are shown in Figures 5.11(a-g). These cross-section views of membranes cast with the neat polymers B and C at 7 % polymer concentration be compared to PAN-A cast from 11% polymer in Figure 4.7. As mentioned before, the PAN- B and -C concentration was limited to 7% due to solubility constraints; hence a concentration study analogous to that done for PAN-A (section 4.3.2.1) was not possible. However, we can compare the morphology of membranes cast from these higher MW grade materials with those cast at several PAN-A concentrations.

Figure 5.11 (a-g): Cross-sectional views of PAN-B and PAN-C membranes with and without additives (a,b) 7% PAN-B and PAN-C from neat DMF (c,d,e) 7% PAN-B and PAN-C from DMF-L (f,g) 5% PAN-B from DMF-Z. The last letter *L* =low resolution (35-500x) and *H*= high resolution (7500-10000x) magnification. See size bars for actual dimensions.



(a)PAN-B-7-L



(b)PAN-C-7-L

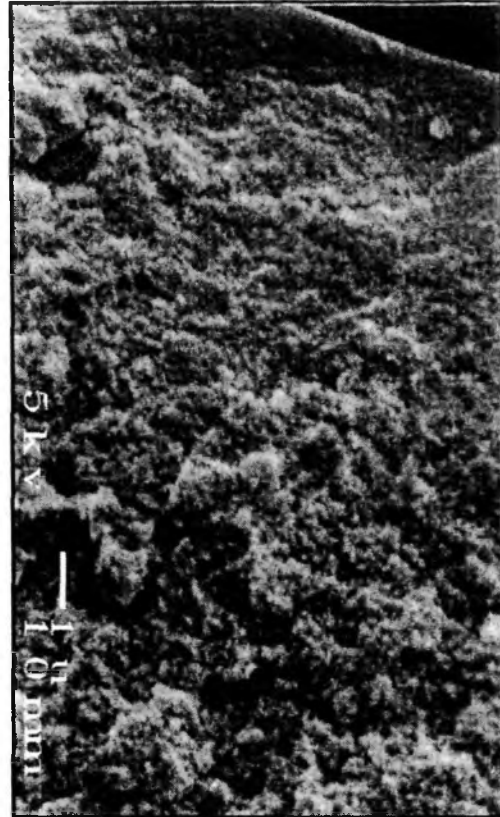


(c)PAN-B-L-7-L

Figure 5.11 (Continued)



(d) PAN-C-L-7-L



(e) PAN-C-L-7-H



(f) PAN-B-Z-5-L



(g) PAN-B-Z-5-H

We can also compare the effect of the various salt additives on membranes made from PAN-B and PAN-C vis-à-vis the effects on PAN-A discussed in section 4.3.2.2. PAN-B-L and -C-L were also cast at 7% polymer concentration, which can be compared to PAN-A-L cast at 11% in Figure 4.7. Figure 5.11(f-g) also shows the cross-section of PAN-B-Z cast from 5% polymer concentration, which is the highest possible at with this solvent + salt combination.

The comparison between these various morphologies follows the same format as used in Chapter IV (section 4.3.2), in terms of the three morphological zones in which the membrane cross-section is divided. Table 5.5 summarizes the various morphological features in zones I-III for these membranes and compares them with the most relevant PAN-A based membranes discussed in section 4.3.2.

**Table 5.5** Summary of observations for the cross-sectional views of PAN-B and PAN-C membrane cross-sectional views in Figure 5.11. The observations are compared with those for PAN-A membranes summarized in Table 4.3. Table continues overleaf.

Polymer PAN - %	Dense skin	Microporous zone	Macroporous zone
<b>Neat DMF membrane</b>			
A 7%	non-existent	Very thin~ 2-3 $\mu\text{m}$ thick Macrovoids from bottom section penetrate this layer	large macrovoids, structure weak
A 11%	Very thin to non-existent, Some evidence of a nodular structure	Relatively thin ~ 5-10 $\mu\text{m}$ Pores are 2-5 $\mu\text{m}$ and taper to smaller dimensions approaching dense skin	Very large and numerous macrovoid fingers
B 7%	Very thin – to non-existent	Non-existent Macrovoids from bottom section penetrate this layer	Almost completely filled with macrovoids
C 7%	Nodular skin Rough surface texture Low degree of asymmetry	Completely collapsed structure Structure appears to be fine nodules	

PAN- %	Dense skin	Microporous zone	Macroporous zone
<b>DMF+ LiCl</b>			
A-L 11%	Thin -0.2 $\mu\text{m}$ Nodules fusing into skin	$\sim 10 \mu\text{m}$ thick Cylindrical pores 2-5 $\mu\text{m}$ in diameter	Nodular structure with few macrovoids
B-L 7%	Relatively smooth skin	Completely collapsed structure Structure appears to be fine nodules	
C-L 7%	Skin layer difficult to distinguish. Thick combination skin+transition layer $\sim 30 \mu\text{m}$	Merges with skin Fused nodules clearly visible	Few macrovoids towards center of film
<b>DMF+ZnCl<sub>2</sub></b>			
A-Z 7%	Very thin – non-existent	Very thin $\sim 2-4 \mu\text{m}$ thick Macrovoids from bottom section penetrate this layer	Almost completely filled with macrovoids
A-Z 11%	Very thin $\sim 0.1-0.2 \mu\text{m}$ Some evidence of nodules fusing into skin	Relatively thin $\sim 5-10 \mu\text{m}$ Pores are 2-5 $\mu\text{m}$ and taper to smaller dimensions approaching dense skin	Very large and numerous macrovoid fingers running $\sim 50 \mu\text{m}$ long
B-Z 5%	Skin layer difficult to distinguish Low degree of asymmetry	Merges with skin Fused nodules clearly visible	Collapsed structure



#### ***5.4.1 Effect of PAN grade***

The most noticeable general feature seen for the PAN-B and PAN-C membranes are their reduced asymmetry in morphology / density compared to PAN-A. In several of the cases shown in Table 5.5, and specific Figs 5.11 (a-g) , the skin layer is relatively thick or merges imperceptibly into Zone II. The Zone III macroporosity also appears low in several instances (Figures 5.11 b-g) reflecting either an intrinsically uniform morphology or a weak porous structure that collapsed to a denser form.

We know from the rheology study (section 5.1) that the higher MW grade PAN solutions are more viscous than solutions with PAN-A. We also know from the cloud point data that 7% solutions with these polymers have very similar water sensitivity. These facts point to a kinetic difference in the phase separation behaviour of the higher MW grade PAN materials. Diffusivity in solution is known to correlate strongly with viscosity. The higher MW PAN solutions will phase separate at a similar non-solvent content; however, that solvent exchange will take place much more slowly. This explanation appears consistent with the tendencies towards more homogenous (less asymmetry) morphologies of the higher MW grades.

#### ***5.4.2 Effect of salts***

The LiCl effect on the membrane morphology appears to be similar for PAN-B and PAN-C as for PAN-A. PAN-A-L showed a more homogenous and uniform morphology than PAN-A; we attributed this to the decreased water sensitivity of the LiCl containing solution. This effect would be slow down the phase separation and give a more uniform morphology. As discussed above, in the PAN-B and PAN-C case, there is already a tendency towards a more homogenous morphology due to slow solvent interchange. This effect would only be strengthened by the reduced water sensitivity of the LiCl containing solutions.

PAN-B-Z shows an interesting effect of water sensitivity in addition to the viscosity /diffusivity effect. Both PAN-B-Z and PAN-C-Z have less water sensitivity than PAN-A-Z. This effect coupled with the kinetic effect would explain why PAN-A-Z has a highly asymmetric morphology while PAN-B-Z shows a more homogenous structure.

### 5.5 Membrane morphology: Comparison of PAN-A with copolymer PAN-1

We understand (without formal documentation) that the commercial product PAN-A contains a small amount of a polar co-monomer (perhaps methacrylate), which is added to increase dyeability. The co-monomer amount is so small that it was not detected by our spectroscopic analyses; hence, we believe that the comparisons between PAN-A and the laboratory synthesized grades PAN-B and PAN-C are not affected by this. However, to increase our faith in this assumption, we synthesized an (88:12) acrylonitrile-acrylamide copolymer, designated PAN-1, as described in section . The MW of PAN-1 is also relatively low, comparable to PAN-A (Table 3.8).

Films were cast from 13% and 17% polymer content of PAN-1 in neat DMF and DMF-Z. The SEM cross-sections, at low and higher magnification, of these membranes are shown in Figures 5.12(a- h). There is a great deal of similarity in the morphological features of the membranes cast from these two polymers. This similarity can be seen by comparing Figures 5.12(a-d) for PAN-1 cast from DMF with the analogous SEM Figures 4.5(e-h) for PAN-A also cast from neat DMF. Similarly, Figures 5.12(e-h) for PAN-1 cast from DMF-Z can be compared with the analogous Figures 4.6(d-g) for PAN-A-Z at the same 13% and 17% casting solution concentrations. The surprisingly similar morphologies supports our assumption that the membrane morphology comparisons between PAN-A and the laboratory synthesized pure grades are not grossly affected by the small amount of unknown co-monomer in PAN-A.

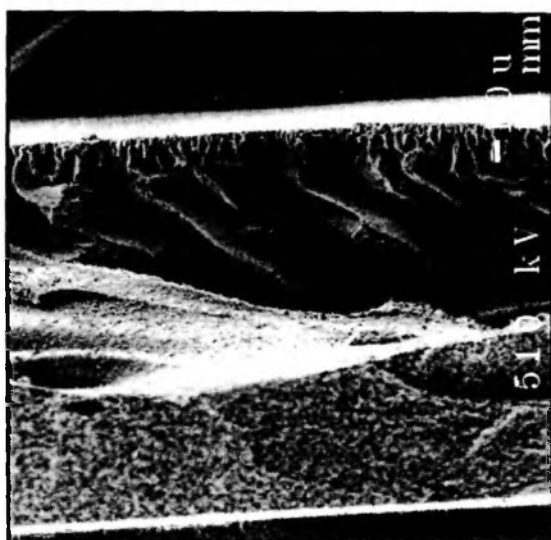
**Figure 5.12 (a-h):** Cross-sectional views of PAN-1 membranes cast from neat DMF at (a,b) 13% and (c,d) 17% solutions. Views (e,f) 13% and (g,h) 17% show the analogous views for PAN-1 cast from DMF-Z. The last letter *L* =low resolutions and *H*= high resolution views. See size marker for absolute dimensions.



(a)PAN-1-13-*L*



(b)PAN-1-13-*H*

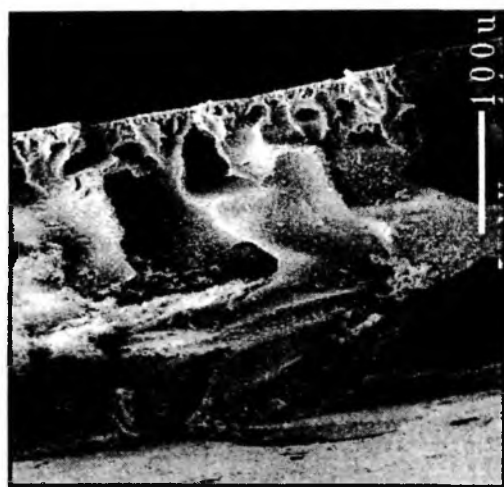


(c)PAN-1-17-*L*

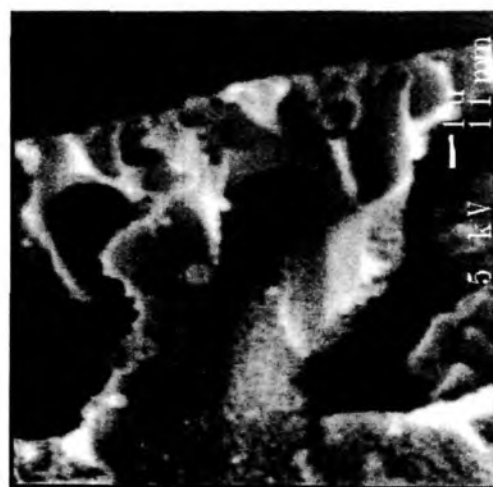


(d)PAN-1-17-*H*

Figure 5.12 (continued)



(e) PAN-1-Z-13-L



(f) PAN-1-Z-13-H



(g) PAN-1-Z-17-L



(h) PAN-1-Z-17-H

## 5.6 Correlation of PAN membrane structure / performance with solution properties

This chapter built on the results presented in Chapter IV by examining the effect of the three salt additives on the solution and resulting membrane morphology of the higher MW grades PAN-B and -C. We can now attempt to correlate the effect of various spectrometric, rheology and phase boundary properties on the characteristics of

membranes made from PAN-B and -C. These results are compared with those for PAN-A.

The FTIR analysis presented in Chapter III showed that all three salt additives complex strongly with DMF and reduce the solvent-polymer interactions. This phenomena will promote association between the PAN chains. These effects result in a complex dependence of the salt additives on  $[\eta]$  for the various PAN grades. For the lowest MW sample PAN-A,  $[\eta]$  increases after salt addition; this is attributed to the increased association between PAN chains. For the higher MW grades, interchain or intersegmental association would be intrinsically easier and  $[\eta]$  is more affected by the reduced coil expansion in DMF+salt solvents. Thus for the intermediate MW material PAN-B,  $[\eta]$  does not change significantly with salt addition while for the highest MW grade, PAN-C,  $[\eta]$  decreases with salt addition.

The FTIR results also indicated that  $ZnCl_2$  complexes with DMF more facilely than the other two salts. The resulting lower solvation ability of the combined solvent is magnified for the higher MW PAN grades. PAN-B and -C cannot be dissolved in DMF-Z above 5% polymer concentration.

As expected, solutions with the higher MW PAN grades have higher viscosity than similar solutions with PAN-A. However, the concentrated solution viscosity data for all three PAN grades can be correlated well by the coil overlap parameter  $\beta$ . The slope of these plots is larger for the two multivalent additives,  $ZnCl_2$  and  $AlCl_3$  than for neat DMF or with the LiCl additive. Depending on the model chosen to fit these data, the results can be interpreted as either increased interchain association or a larger interchain friction factor in solutions with DMF-Z or DMF-A. These results are consistent with the trends seen for PAN-A alone.

Also, as may be expected from the complex affects of the salts and PAN MW on  $[\eta]$ , we also see a complex dependence of these variables on the ternary phase boundary (ref 73-75 from Witte). In the case of the low MW grade, PAN-A-Z has the highest water sensitivity while PAN-A-L and A-A are less sensitive to water than the solution in neat DMF. The higher MW grades PAN-B and -C show two different trends depending on the polymer concentration. At low polymer concentrations (0-3%) the water sensitivity for these higher MW PAN grades follows the same trend as for PAN-A. At

the higher polymer concentrations typical of casting solutions, the trends change and the solution in neat DMF is predicted to be more water sensitive than those with salts. This water sensitivity trend at higher polymer concentrations for PAN-B and PAN-C can be expressed as:

$$\text{Neat DMF} > \text{DMF-Z} > \text{DMF-A and L}$$

The trend is more marked for PAN-B than for PAN-C. The water sensitivity does not correlate well with the PAN MW.

The membrane structure was characterized mainly by SEM studies and by the bubble point technique. The most striking change between PAN-B and -C membranes compared to PAN-A is the more homogenous morphology (decreased asymmetry of structure) for the higher MW based membranes. This effect can be attributed to the higher solution viscosity of the PAN-B and -C solutions. Higher viscosity generally correlates with reduced diffusivity, which would result in slower solvent-non-solvent exchange during the phase inversion process.

The effect of the salts on membrane morphology is consistent with the water sensitivity data. In the case of PAN-B, solutions in DMF have higher water sensitivity than the salt containing solutions. The lower water sensitivity of the salt containing casting solutions prevents rapid skin formation, resulting in homogenous morphology at a polymer concentration (7%) where the neat DMF solution leads to an asymmetric morphology.

PAN-B and -C membranes cast from neat DMF have higher bubble points than PAN-A based membranes cast at the same polymer concentration. PAN-B and -C membranes cast from DMF-Z were too weak to be tested reliably by bubble point or permeability tests because of the low polymer concentration (<5%) that can be achieved in this solvent combination. However, we continue to see the same trend for the LiCl and AlCl<sub>3</sub> additives as seen earlier with PAN-A: membranes with either additive have lower bubble points than those cast from neat DMF. In the case of PAN-A, we had correlated the presence of these skin defects with the solution viscosity trend. The PAN-B and PAN-C cases indicate that while the solution viscosity may indeed be important to dampen surface perturbations during phase inversion, the homogenous morphology for membranes cast with salt additives is also responsible for their higher

bubble point. The similar BSA rejection data with PAN-B membranes compared to PAN-A indicates that the modal pore size responsible for UF performance remains the same even as the maximum pore size decreases for PAN-B.

Though spectroscopic studies had failed to show any significant chemical differences between the three PAN grades, there is a possibility that the commercial grade PAN-A may have a small content of a polar co-monomer. However, when the membrane morphology of PAN-A membranes was compared with membranes cast with PAN-1 (similar MW as PAN-A with 12% acrylamide co-monomer), a close resemblance was seen. This resemblance, coupled with the consistency in rheology data with the laboratory synthesized grades, leads us to believe that the small content of co-monomer in PAN-A is not sufficient to bias the results presented in the thesis.

## Chapter VI

### CONCLUSIONS

This chapter summarizes the conclusions drawn from the present study and the scope to further continue this work. This thesis studied the effect of PAN molecular weight and that of various metal chloride additives (LiCl, ZnCl<sub>2</sub> and AlCl<sub>3</sub>) on the solution and separation properties of the resulting membranes. The approach used was a step-wise investigation involving:

1. Spectroscopic and dilute solution rheology studies to describe the interaction between salt, solvent and polymer.
2. Measurement of rheology and phase boundary characteristics in concentrated solutions and correlation with spectroscopic and dilute solution rheology.
3. Detailed description of membrane morphology and correlation with the casting solution properties

This approach was intended to clarify the following major issues: (i) the interaction of salts with solvent DMF, (ii) the interaction of salts with PAN (iii) differences between the three salt additives (LiCl, ZnCl<sub>2</sub>, AlCl<sub>3</sub>), and (iv) effect of PAN molecular weight.

#### 6.1 Spectroscopic and dilute solution rheology studies

These studies were undertaken to understand the interaction between salt, solvent and polymer on a molecular scale.

##### 6.1.1 *Effect of salts on solvent DMF:*

FT-IR studies show that all three salts complex with DMF. The cation interaction with the -OCN group of DMF is much stronger than the interaction with the -CN group of PAN (Table 3.1). This is consistent with the known higher basicity of DMF compared to the PAN nitrile group.

Salts can complex with DMF at either its electronegative carbonyl O or the more electropositive N. The strong complex formed between the salts and DMF will reduce DMF's ability to solvate the polymer. Calculations of the Mark-Houwink constant in



solutions made with the salt additives indicate that the general effect of all salts is to decrease the PAN chain expansion; the Mark-Houwink exponent  $a$  decreases from 0.75 in DMF to  $\sim 0.6$  for DMF in salt solutions (Table 3.10). Similarly, the viscosity activation energy  $E_a$  increases more sharply with increasing coil overlap parameter  $\beta$  for neat DMF solutions compared to those with the salt additives (Figure 3.17). All these data show that these salt additives cause DMF to change from a good solvent towards a theta-solvent for PAN.

Though all three salts reduce the DMF solvation power, there are differences in their strength of complexation with the solvent. In particular,  $\text{ZnCl}_2$  forms complexes with DMF more readily than the other two salts. This can be seen by the effect of these salts on two characteristic DMF IR frequencies:

(i) The  $>\text{C}=\text{O}$  stretching frequency observed in pure DMF remained essentially unchanged in both DMF-L and DMF-A, whereas a strong red shift indicating more favorable complexation was observed in case of DMF-Z. This observation is correlated with the electronic cloud density around these cations. Thus, the likelihood of complexation of the electronegative carbonyl O of DMF with a cation is the highest for  $\text{Zn}^{2+} > \text{Li}^+ > \text{Al}^{3+}$ .

(ii) Both anion ( $\text{Cl}^-$ ) and cation affect salt interaction with the OCN group of DMF. Red shifts observed in the OC-N stretching frequency can be attributed to the increasing electron cloud density of  $\text{Cl}^-$  near slightly electropositive nitrogen (compared to oxygen). Thus, the likelihood of complexation of the amide N of DMF with the salt is the highest for  $\text{AlCl}_3 > \text{ZnCl}_2 > \text{LiCl}$ .

Based on the spectroscopic data: we can postulate (Figures 3.2 and 3.5) that four types of DMF molecules would be present in a salt-additive-PAN solution: (i) free DMF molecules, (ii) molecules complexed with the salt (iii) molecules complexed with PAN and (iv) self-associated DMF molecules.

### ***6.1.2 Effect of salts on dissolved PAN:***

Comparing the -OCN frequency shifts in the salt-PAN-DMF ternary systems with the binary PAN-DMF systems indicates that the PAN-DMF interaction is affected by the presence of the salt. Considering the strong complexation of all three salts with

DMF, this result is as expected. However, IR was not able to detect any direct interaction between the salts and PAN. Surprisingly, for unknown reasons, we were not even able to detect a clear interaction between the nitrile group of PAN and DMF, as previously reported by Padhye and Karandikar [1985].

The rheology studies show clear differences between the effect of the salt on the lower MW grade PAN-A compared to the higher MW materials. The dilute solution viscosity and activation energies are markedly higher for PAN-B and PAN-C solutions. The effect of the salt on PAN chains in DMF solution appears to be via two mechanisms:

- (i) The FTIR analysis showed that all three salt additives complex strongly with DMF, thus preventing these solvent species from solvating the polymer. The resulting decrease in the DMF solvation power reduces expansion of the polymer coils in the combined DMF+salt solvent.
- (ii) The reduced solvation power of the combined DMF+salt solvent will promote association between the PAN segments or chain.

These two effects result in a complex dependence of the salt additives on intrinsic viscosity  $[\eta]$  for the various PAN grades. For the lowest MW sample PAN-A,  $[\eta]$  increases after salt addition; this is attributed to the increased association between PAN chains. For the higher MW grades, interchain or intersegmental association would be intrinsically easier and  $[\eta]$  is more affected by the reduced coil expansion in DMF+salt solvents. Thus for the intermediate MW material PAN-B,  $[\eta]$  does not change significantly with salt addition while for the highest MW grade, PAN-C,  $[\eta]$  decreases with salt addition.

The trend of the viscosity activation energies,  $E_a$  for the various solvent types is: DMF > DMF-Z > DMF-L > DMF-A. For these systems  $E_a$  correlates well with the coil overlap parameter,  $\beta$ . The relatively high  $E_a$  values for  $ZnCl_2$  compared to the other two salts may indicate a higher tendency to bridge the PAN chains.

## 6.2 Concentrated solution properties

The study focused on the concentrated solution rheology and ternary (polymer-solvent-non-solvent) characteristics of the PAN+DMF+salt systems. These properties

are generally considered to be important parameters affecting final membrane morphology and performance.

### **6.2.1 Concentrated solution rheology**

At dilute concentrations, viscosity is higher in the better solvent (DMF) because of the greater chain expansion and excluded volume effect.; however we see the well-known cross-over as concentration increases in poorer solvents (DMF+mivalent salts). Also as expected, solutions with the higher MW PAN grades have higher viscosity than similar solutions with PAN-A.

The concentrated solution viscosity data for all three PAN grades both with and without the salt additives can be correlated (section 5.1.3) by the coil overlap parameter  $\beta$  and to a lesser degree by the Bueche parameter. The slope of these plots is larger for the two multivalent additives,  $ZnCl_2$  and  $AlCl_3$  than for neat DMF or with the LiCl additive. Depending on the model chosen to fit these data, these results can be interpreted as either increased interchain association (Coil overlap model,) or a larger interchain friction factor (Rouse model) in solutions with DMF-Z or DMF-A. These results are consistent for all three PAN grades.

Several similar scenarios on a molecular scale would be consistent with the salt effect on the rheology data:

(i) As discussed above, the reduction in DMF solvation power caused by the salts would promote the self-association of PAN chains. Polymer interchain entanglement at high concentrations would thus be more effective in the presence of the salts.

(ii) The self-association promoted by the salts may cause the polymer chain to form a “pearl necklace” type configuration where a series of associated segment clusters are connected by flexible polymer chain “strings”. Such a chain configuration would also lead to higher viscosity.

(iii) The rheology data would be consistent with the multivalent salts bridging polymer chains to give an effectively higher MW. However, we did not find any proof of such an interaction in the FTIR studies.

### 6.2.2 Ternary phase boundary

As may be expected from the complex effects of the salts and PAN MW on  $[\eta]$ , we also see a complex dependence of these variables on the ternary phase boundary (PAN+DMF+water). The water sensitivity or miscibility gap i.e. the composition difference between the polymer-solvent axis and the phase boundary would determine the amount of solvent-nonsolvent exchange before phase inversion. In the case of the low MW grade, the water sensitivity follows the trend (section 5.2):

Water sensitivity : PAN-A-Z > PAN-A > PAN-A-A > PAN-A-L

The higher MW grades PAN-B and -C show two different trends depending on the polymer concentration. At low polymer concentrations (0-3%) the water sensitivity for these higher MW PAN grades follows the same trend as for PAN-A. At the higher polymer concentrations typical of casting solutions where polymer chain entanglement would be dominant, the trends change and the solution in neat DMF is predicted to be more water sensitive than those with salts. This water sensitivity trend at higher polymer concentrations for PAN-B and PAN-C can be expressed as:

Water sensitivity : PAN-B and -C in Neat DMF > DMF-Z > DMF-A and L

This trend is more marked for PAN-B than for PAN-C.

## 6.3 Correlation of PAN membrane morphology / performance with solution properties

Very different morphologies are seen with membranes cast from PAN-A compared to the higher MW grades. PAN-A membrane morphologies can be described in terms of a skin layer with a well-defined transition layer between it and the macroporous substructure. PAN-B and PAN-C membranes are less asymmetric in structure.

### 6.3.1 PAN-A membrane morphology and structure

SEM shows that PAN-A, PAN-A-A and PAN-A-Z have large macrovoids in the underlying asymmetric structure; while the incidence and size of these macrovoids is considerably reduced in the case of the monovalent salt (PAN-A-L) (section 4.3.2). This is consistent with the ternary cloud point data, which imply that the skin layer in

PAN-A-L would form slowly after a considerable amount of DMF / water exchange had already taken place.

Bubble point analyses (section 4.4.1) show that PAN-A and -A-L have lower bubble points / larger skin pores than PAN-A-A or -A-Z. The absence of these skin defects in PAN-A-A and A-Z correlates well with the idea that the multivalent salts promote polymer chain association. The resulting higher solution viscosity would presumably dampen perturbations that result in loss of skin integrity. While there are clear differences in the propensity for micron size defects in membranes cast from the various additive solutions, the modal pore size appears to change only marginally with the additive used. Ultrafiltration studies (section 4.4.3) show similar rejections for various solutes (BSA, lysozyme, PEG-9000) for PAN-A membranes cast from solutions with and without the additives. PAN-A-Z membrane has 1000x (3-log) higher bacterial rejection while retaining 80% of the water permeability of the corresponding membrane cast from DMF alone. The relatively high flux is due to retaining the macrovoid-containing substructure; this can be attributed to the low water tolerance of the PAN-A-Z casting solution.

### ***6.3.2 Morphology of membranes from higher MW grades in comparison to PAN-A***

The most striking change between PAN-B and -C membranes compared to PAN-A is the more homogenous morphology for the higher MW based membranes. The higher viscosity of the PAN-B and -C solutions indicates reduced diffusivity. This would result in slower solvent-non-solvent exchange during the phase inversion process and thereby produce less asymmetric structures. Correspondingly, PAN-B and -C membranes cast from neat DMF have higher bubble points than PAN-A based membranes cast at the same polymer concentration (section 5.4).

The effect of the salts on membrane morphology is consistent with the water sensitivity data. In the case of PAN-B, solutions in DMF have higher water sensitivity than the salt containing solutions. The lower water sensitivity of the salt containing casting solutions prevents rapid skin formation, resulting in homogenous morphology at a polymer concentration (7%) where the neat DMF solution leads to an asymmetric morphology.

PAN-B and -C membranes cast from DMF-Z were too weak to be tested reliably because of the low polymer concentration (<5%) that can be achieved in this solvent combination. PAN-B and -C membranes cast using either LiCl or AlCl<sub>3</sub> additives have higher bubble points than those cast from neat DMF. In the case of PAN-A, we had correlated the presence of these skin defects with the solution viscosity trend. The PAN-B and PAN-C cases indicate that while the solution viscosity is indeed important to dampen surface perturbations during phase inversion, the more homogenous morphology for membranes cast with salt additives is also responsible for their higher bubble point. The similar BSA rejection data with PAN-B membranes compared to PAN-A indicates that the modal pore size remains the same even as the maximum pore size decreases for PAN-B.

Comparison of the morphology of PAN-A membranes with membranes cast with PAN-1 (similar MW as PAN-A with 12% acrylamide co-monomer) showed a close resemblance (section 5.5). This resemblance, coupled with the consistency in rheology data with the laboratory synthesized grades, leads us to believe that a small polar co-monomer content (if present) in the commercial grade PAN-A is not sufficient to bias the comparisons with the laboratory synthesized PAN-B and -C.

#### **6.4 Scope for future work:**

This thesis establishes a linkage from the basic physical chemistry to solution properties to the membrane morphology obtained with various PAN grades and three different salts. However, the conclusions are essentially qualitative and in some cases require assumptions as to the effect of kinetic variables. Further understanding of this system could be gained by:

(i) Quantitative description incorporating kinetic and thermodynamic variables. Though we can make some “educated guesses” based on the solution property characterization in this thesis, it has still not been possible to clearly delineate basic thermodynamic effects relating to the phase inversion from kinetic effects. A light transmission setup has been designed using a diode array detector for determining the precipitation kinetics. Combining this kinetic information with the binodal curve equation would give a quantitative description of the phase inversion process.

(ii) Varying additive concentration. The thesis studies were done at a fixed ionic strength of additives. Potentially, further information may be obtained by varying the additive concentrations.

## References

- Alexander. P.I, Zinc -67 NMR study of Zn ion in water and in some non-aqueous and mixed solvents, *J. Soln. Chem.*, 11 (1982) 17
- Alia. J.M., Edwards. H.G.M., Ion solvation and ion association in lithium trifluoromethanesulfonate solutions in three aprotic solvents : An FT-Raman spectroscopic study, *Vib. Spectrosc.*, 24(2) (2000) 185
- Alia. J.M., Edwards. H.G.M., Moore. J., Fourier Transform, Raman spectroscopic study of the association between Co(II) ions and acrylonitrile in aqueous solution, *J. Mikrochim. Acta. Suppl.*, 14 (1997) 733
- Alia. J.M., Edwards. H.G.M., Navarro. F.J.G., Lawson. E.E., FT-Raman spectroscopic study of preferential solvation and ionic association in lithium and silver triflate solutions in acrylonitrile / N,N-dimethylformamide mixed solvent, *J. Mol. Struct.* 43(51) (2001) 565
- Beevers R.B., The physical properties of poly(acrylonitrile) and its polymers, *Macromol. Rev.*, 3 (1968) 113
- Bercea M., Morariu S., Ioan C., Ioan S., Simionescu B.C., Viscometric study of extremely dilute polyacrylonitrile solutions, *European Polym J.*, 35 (1999) 2019
- Bhadani S. N. and Kundu S., Acid initiated copolymerization of acrylonitrile with acrylamide, *Makromol. Chem, Rapid Commun.*, 1 (1980) 281
- Billmeyer F.W. Jr., Textbook of polymer science, 3<sup>rd</sup> ed., John-Wiley and Sons, NY, 1984
- Bisschops J., Viscosity, Diffusion and Sedimentation of Polyacrylonitrile solutions, *J. Poly. Sci.*, 17 (1955) 81
- Biyang. H, Sumin. W, Xuejie. H, Ronjian. X, Liquan. C, Vibrational spectroscopic investigations of Polyacrylonitrile based electrolytes with dimethylformamide plasticizer, *J. Electrochem. Soc.*, 144(1) (1997) 44



- Boom. R.M., Boomgaard. Th.van den, Van den Berg. J.W.A. and Smolders. C.A., Linearized cloud point curve correlation for ternary systems consisting of one polymer, one solvent and one non-solvent, *Polymer*, 34 (1993) 2248
- Bottino. A., Capanelli. G., Munari. S. and Turturro. A., High performance ultrafiltration membranes cast from LiCl doped solutions, *Desalination*, 68 (1988) 167
- Bueche. F, Viscosity, self diffusion and allied effects in solid polymers, *J. Chem. Phys.*, 20 (1952) 1959
- Chai. P.V and Samalenko. V.M, Formation of solvate complexes of  $AlCl_3$  with some organic solvents, *Uzb. Khim. Zh.*, 37 (1971) 642 (Russian)
- Chiang W.Y and Hu C.M., Studies of reactions with polymer II. The reaction of maleic anhydride with acrylonitrile onto PVA and properties of the resultant, *J. Appl. Polym. Sci.*, 30 (1985) 4045
- Cho. S.H., Park J.S., Jo S.M. and Chung I.J., Influence of  $ZnCl_2$  on the structure and mechanical properties of poly(acrylonitrile) fibres, *Poly. Int.*, 34 (1994) 333
- Cleland R.L., Stockmayer W.H., An Intrinsic Viscosity-Molecular weight relationship for Polyacrylonitrile, *J. Poly. Sci.*, 17 (1965) 473
- Collin. C.H., *Microbiological Methods, Estimating Bacterial Numbers*, Butterworths publication, UK, 1976. p194
- Cornet. C.F, The determination of unperturbed dimensions of polymer molecules by viscometry of moderately concentrated solutions, *Polymer (London)*, 6 (1965) 373
- Dubroniva. L.V, Bronshtein. L.M, Bragina. T.P, Valetskii. P.M, Association of polyacrylonitrile macromolecules, *Vysokomol. Soedin. Ser A, Ser B*, 40 (1998) 472
- Dunn. P, Samson. G.F, The stress cracking of polyamides by metal salts (i) Metal halides, *J. Appl. Polym. Sci.*, 13 (1969) 1641
- Edwards. H.G.M., Hoskins. A.R., Johnson A.F. and Lewis I.R., Raman spectroscopic studies of poly(acrylonitrile)-zinc complexes in aqueous solutions of zinc chloride and bromide, *Poly. Int.*, 30 (1992) 25
- Elias. H.G., *Macromolecules, Part 1, Structure and properties*, John Wiley and Sons Inc. NY, 1977, p274
- Farona. M.F., Bremer. N.J., Succinonitrile derivatives of halogenpentacarbonyl manganese (I), *J. Amer. Chem. Soc.*, 88 (1966) 3735

- Ferry. J.D, Viscoelastic properties of Polymers 2<sup>nd</sup> Edn. New York, Wiley Interscience, 1970
- Frisch. H.L and Simha. R, The viscosity of colloidal suspensions and macromolecular solutions, Vol. 1, Chapter 14, In. Erich, F.R (Ed) Rheology New York: Academic Press, 1956
- Fritzsche. A.K., Cruse. C.A., Kesting. R.E., Murphy. M.K., Hollow fiber membranes spun from Lewis acid: base complexes. I. Structure determination by oxygen plasma Ablatio, J. Appl. Polym. Sci. 40 (1990) 19
- Frommer. M. A, Matz. R and Rosenthal. U, Ind. Eng. Chem. Prod. Res. Develop. 10 (1971) 193
- Gallarado. A.M, Livel. J, Lilly. T.H, Enthalpies of interaction of alkali metal halides with N-Methylacetamide and DMF in water at 25°C, J. Chem. Soc, Faraday. Trans. 1, 85 (1989) 2909
- Gandhi. K.S and Williams. M.C, Solvent effects on the viscosity of moderately concentrated polymer solutions, J. Polym. Sci. Pt.C., 35 (1971) 211
- Gerrard. W, Lappert. M.F, Pyzora. H, Wallis. J.W, Spectra and structure of amide complexes, J. Chem. Soc., (1960) 2144
- Glasstone S., Elements of Physical Chemistry, Van Nostrand Co., NY, 1946
- Goldammer. V, Schollmeyer. E, Peter. H, Wilfried. A, Heinz. H, Carbon-13 NMR investigations on the influence of inorganic salts on the solvation of N'N' dibenzoyl-m-phenylenediamine in N'N'-dimethylacetamide, Makrom. Chem. , 180 (1979) 1013
- Gopal. R, Rastogi. P.P, Study of ion-solvent interaction of some tetraalkyl ammonium and common ions in polar, hydrogenbonded, non-hydrogenbonded solvents from the viscosity data, Z. Phys. Chem., 69 (1970) 1
- Graessley. W.W, The entanglement concept in Polymer Rheology, Adv. Polym. Sci., 16, (1974) 38
- Gupta A.K. and Chand N., Glass transition in polyacrylonitrile : Analysis of dielectric relaxation data, J. Poly. Sci.: Part B., 18 (1980) 1125

Gurunadham. G., Thyagarajan. G., Intensity studies of Raman bands of dimethyl formamide (DMF) and Dimethylsulfoxide (DMSO) in solutions of different concentrations, *Indian. J. Pure. Appl. Phys.*, 20 (1982) 886

Gutmann V., Resch G., Linert W., *Coord. Chem. Rev.*, Structural variability in solutions, 43 (1982) 133

Hoskins. A.R., Edwards. H.G.M., Johnson. A.F., Infrared spectroscopic study of acetonitrile in aqueous solutions and comparison with related polyacrylonitrile solutions, *J. Mol. Struct.* 263 (1991) 1

Huggins M.L., The viscosity of dilute solutions of long chain molecules. IV. Dependence on concentration, *J. Am. Chem. Soc.*, 64 (1942) 2716

Jacob M.M.E. and Arof A.K., FTIR studies of DMF plasticized polyvinylidene fluoride based polymer electrolyte studies, *Electrochim. Acta.*, 45 (2000) 1701

Jamroz. D., Wojcik. M., Lindgren. J., Stangret J., Solvation of  $Al^{3+}$ ,  $Fe^{3+}$  and  $Cr^{3+}$  cations in water-acetonitrile mixtures studied by IR spectroscopy, *J. Phys. Chem., B*, 101 (1997) 6758.

Jayaraman. J., *Laboratory Manual in biochemistry*, John Wiley and Sons Inc. NY, 1981, p80

Jungbaeur. J.A.M, Curran. C, N-C=O bending vibration in complexes of dimethylformamide with metal halides, *Nature*, 202 (1964) 290

Kabisch. G., Kalman. E., Palinkas. G and Radnai. T., Complex formation and solvation of zinc bromide in N,N-Dimethyl formamide solution: An electron diffraction and Raman Study, *Chem. Phys. Lett.*, 107(4-5) (1984) 463

Kasaai. M.R., Charlet. G. and Arul. J., Master curve for the concentration dependance of semi-dilute solution viscosity of chitosan homologes : the Martin's eqn., *Food Research Int.*, 33 (2000) 63

Kesting. R.E, *Synthetic Polymeric Membranes*, John Wiley and Sons Inc. NY, 1971, p80

- Khotsyanovskii. O.I, Telyakova. V.Sh, Bromide complexes of Zinc in DMF, Zh. Neorg. Khim., 16 (1971) 61 (Russian)
- Kim. J., Lee. H, Ho. K., Effect of PEG additive on membrane formation by phase inversion, J. Membr. Sci 138 (1998) 153.
- Kim. S.R., Lee. K.H. and Jhon. M.S., The effect of  $ZnCl_2$  on the formation of polysulfone membrane, J. Membr. Sci. 119 (1996) 59.
- Kim. T.P, Imanakunov. B.I, Kazybaer. S.A, Complexes of dimethyl formamide with a bivalent cobalt ion, Zh.Neor. Khim, 27(12), (1985) 3190
- Kim. T.P., Infrared spectroscopic study of several metal complexes of DMF, Zh. Neorg. Khim, 30, (1985) 2817 (Russian)
- Kiyoshi. J, Takeo. S, Fujio. T, Mechanism of dissolution of PAN in concentrated aqueous solutions of magnesium and calcium thiocyanate, Nippon. Kagaku. Kaishi, 10 (1979) 1384
- Kobayashi. T., Ono. M., Shibata. M. and Fuji. N., Cutoff performance of *Escherichia Coli* by charged and noncharged poly(acrylonitrile) ultrafiltration membranes, J. Memb. Sci. 140 (1998) 1
- Kraus. M.A., Nemas. M., Frommer. M.A., The effect of low molecular weight additives on the properties of aromatic polyamide membranes, J. Appl. Polym. Sci., 23 (1979) 445.
- Kuhn. S.J, Mc Intyre. J.S, Reactions of amides and related compounds, NMR (proton) investigations of N,N'dimethylformamide-lewis acid adducts and remarks on the relative strengths of Lewis acids, Indian. Journ. Chem., 43 (1965) 375
- Kulkarni. S.S, Funk. E.W and Li. N.N, in Ho. W.S.W and Sirkar. K.K (Eds), Membrane Handbook, Van Nostrand Reinhold, NY, 1992a ,Chapter 26
- Kulkarni. S.S, Funk. E.W and Li. N.N, in Ho. W.S.W and Sirkar. K.K (Eds), Membrane Handbook, Van Nostrand Reinhold, NY, 1992b ,Chapter 30
- Kulkarni. S.S, Shinde. M.H and Musale. D.A, An improved process for the manufacture of ultrafiltration membranes based on poly(acrylonitrile) and its copolymers, Indian Pat. Appl, 1811/DEL/96, 1996

- Kurdi. J., Trembley. A.Y., The influence of casting solution structure on the microporosity of polyetherimide gas separation membranes prepared by the coagulation post-leaching method, *J. Membr. Sci.*, 184 (2001) 175.
- Lassaigne. C, Baine. P, Solvation studies of lithium salts in DMF, *J. Phys. Chem.*, 75 (1971) 3188
- Lee. H.J, Won. J., Lee. H., Kang. Y.S., Solution properties of Poly (amic -acid)- NMP containing LiCl and their effects on membrane morphology, *J. Membr. Sci.* 196 (2002) 267.
- Liang C.Y. and Krimm S., Infrared spectra of High Polymers. VII. Polyacrylonitrile, *J. Poly. Sci.*, 31 (1958) 513
- Lirova. B.I, Tager. A.A, Lyutikova. E.A, Behaviour of solutions of Polyacrylonitrile and cellulose acetate in dimethylformamide in the presence of inorganic salts, *Vysokomol. Soedin, Ser.B*, 22 (1980) 99
- Lobanova. G.A., Polatoskaya. R.A., Pakshever. A.B. and Pakshver. E.A., Effect of LiCl additive on properties of solutions of Poly(acrylonitrile) in DMF, *Sin. Volokna.*, (1969) 81; CA 73: 99322y
- Matsuzaki. K, Uryu. T, Ishigure. K, NMR spectra of Polyacrylonitriles, *J. Poly. Sci. Polymer Letters*, 4 (1960) 93
- Meira. G.R., Data reduction in size exclusion chromatography of polymers, in H.G. Barth and J.W. Mays (Ed.s) *Modern methods of polymer characterization*, John Wiley and Sons, NY, 1991, Chap.2
- Minagawa. M, Shirai. H, Monita. T, Fujikura. Y, Kameda. Y, Dynamic nuclear magnetic resonance and Raman spectroscopic measurements of five different kinds of N'N' dimethylformamide derivatives in relation to the dissolution mechanism of polyacrylonitrile, *Polymer*, 37 (1996) 2353
- Morariu S. Bercea. M Ioan .C, Ion. S Simonescu. B.C, Conformational characteristics of oligo and polyacrylonitrile in dilute solutions, *Eur. Polym. J.*, 35 (1999) 377
- Nero J.R. and Sikdar S.K., One point determination of intrinsic viscosity for Polycarbonate, poly(phenylene) oxide and poly(etherimide), *J.Appl.Polym.Sci.* 27 (1982) 4687

- Nishio. Y.Sh., Roy. S.K., Manley. J., Blends of Cellulose with PAN prepared from DMAc / Lithium solutions, *Polymer.*, 28 (1987) 1385.
- Nunes. S.P, Recent advances in the Controlled formation of pores in membranes, *Trip*, 5(6) (1997) 187
- Onyon R.F., The Molecular Weight-Viscosity relation for Polyacrylonitrile, *J. Poly. Sci.*, 22 (1956) 13
- Padhye M.R. and Karandikar A.V., The effect of alkali salts on solvent-Poly(acrylonitrile) interactions, *J. Appl. Poly. Sci.*, 30 (1985) 667
- Padhye M.R. and Karandikar A.V., The effect of alkali salts on solvent-Poly(acrylonitrile) interactions, *J. Appl. Poly. Sci.*, 30 (1985) 667
- Panar, Beste. L.F., Structure of poly (1,4- benzamide) solutions, *Macromolecules.*, 10 (1977) 1401.
- Paul R.C, Guraya P.S., Sreenathan B.R., Dimethyl formamide as a Polar solvent: Part I ; Autoprotolysis of DMF and electrochemical studies of the solutions of protonic acids and bases, *Indian. J. Chem.*, 1 (1963) 335
- Pereira. C.C., Nobrega. R., Borges. C.P., Membrane formation with presence of Lewis Acid - Base complex in polymer solution, *J. Appl. Polym. Sci.*, 83 (2002) 2022.
- Pereira. C.C., Souza. J.N. M., Nobrega. R., Borges. C.P., Hollow fiber formation using Lewis Acid : Base complex in the polymer solution, *J. Appl. Polym. Sci.*, 81 (2001) 908
- Petrov. S., Dimov. A., Petrova. S., Preparation of poly(acrylonitrile) ultrafiltration membranes from polymer solutions containing glycerol, *J. Membr. Sci.*, 64 (1991) 183.
- Polatovskaya. R.A, Pakshevar. A.B, Pakshever. E.A, Formation of Pan fiber from a solution containing Lifol salts, *Sin. Volokna.*, (1969) 86 (Russian)
- Porter. M.C in Schweitzer. P (Eds) Handbook of Seperation techniques for chemical engineers, 2<sup>nd</sup> Ed., Mc. Graw-Hill, NY, 1988, 2.3
- Powell. D.B., Woolins. A., Vibrational Spectra of metal formamide complexes, *Spectrochim Acta, Part A, Molecular Spectroscopy* , 41(1985),1023.
- Prince M., Hornyak J., High Pressure reactions III. Hydrolysis of PAN, *J. Poly. Sci. A-1*, 5 (1967) 161.

- Rae. P.C, Jeon. K.Y, The hyperstructure of polyacrylonitrile FeCl<sub>3</sub> hybrid composite, *Polym. Prepr.*, 41 (1) (2000) 452
- Raju K.V.S.N. and Yaseen M., A New equation for estimating  $[\eta]$  from single-viscosity measurement in solution, *J. Appl. Poly. Sci.* 45 (1992) 677
- Rode. B.M, Fussenger. R, Influence of small cations on the rotational barrier to amides, *J. Chem. Soc, Faraday. Trans. 2*, 71 (1975) 1959
- Salmova. U. U, Masimov. A.A, Effect of inorganic salts on the main parameters of the dilute aqueous PVP solutions, *Polymer*, 37 (12)(1996) 2415
- Saum. A.M, Intermolecular association inorganic nitriles; the CN dipole-pair bond, *J. Polym. Sci.*, XLII (1960) 57
- Schneider. W, DMF solvates of metal perchlorates, *Helv. Chim. Acta.*, 46 (1963) 1842 (German)
- Seong. J.S., Park. T.K., Lee. J.O., The effect of inorganic additives contained in precipitant (water) on the formation mechanism of asymmetric polysulfone membranes, *Polymer.*, 14 (1990) 50.
- Sims. G.E.C and Snape. T.J., A method for estimation of PEG in plasma protein fractions, *Anal. Biochem.*, 107 (1980) 60
- Sims. G.E.C and Snape. T.J., A method for estimation of PEG in plasma protein fractions, *Anal. Biochem.* 107 (1980) 60
- Spange S., A. Reuter, E. Vilsmeier, T. Heinze, D. Keutel, W Linert, Determination of empirical polarity parameters of cellulose solvent N,N'-dimethyl acetamide/LiCl by means of the Solvatochromic technique, *J. Appl. Polym. Sci.: Polym.Chem*, 36 (1998) 1945
- Staudinger. H and Heuer. W, Highly polymerized compounds XXXIII A relation between the viscosity and the molecular weight of polystyrenes, *Bev.Dtsch. Chem. Ges B*, 63 (1930) 222
- Stoiko. P.P, Conditions for obtaining ultrafiltration membranes from a solution of Polyacrylonitrile in Dimethylformamide in the presence of Formamide, *J. Appl. Polym. Sci.*, 62 (1996) 267
- Strathmann. H, Scheible. P and Baker. R.W, A Rationale for the preparation of Loeb-Sourirajan-Type Cellulose Acetate membranes , *J. Appl. Polym. Sci.*, 15 (1971) 811

- Streigel. A.M, Piotrowiak, Bove. M.S, Cole. B.R, Polarizability and inductive effect contribution to solvent cation binding observed in electrospray ionization mass spectroscopy, *J. Am. Soc. Mass. Spectrom.*, 10(3) (1999) 254
- Stropanik. C, Musil. V, Brumen. M, The polymeric membrane formation by wet phase separation; turbidity and shrinkage phenomena as evidence for the elementary process, *Polymer*, 41(26) (2000) 9227
- Tager. A., *Physical Chemistry of Polymers*, Mir Publishers, Moscow, 1978 p362
- Tao. H., Cheng. J. Zhang, Effect of non-solvent additives on the performance of Polyethersulfone microporous membranes, *Mo. Kexue. Yu. Jishu.*, 18, (1998) 43
- Tarasov. V.P., Kirakosyan. G.A., Randaverich. S.B., Buslaev. Y.A., Formation of solvate separated ion pairs in dimethylformamide solutions of aluminium trihalides, *Koord. Khim.*, 8 (1982) 1087.
- Turner. A, Goldberg. J.A.I, Price. J.A, Dilute solution viscosity of polymethyl methacrylate and the methyl methacrylate styrene copolymer, *J. Colloid. Sci.*, 5 (1950)a 251
- Turner. A, Goldberg. J.A.I, Price. J.A, The influence of the solvent composition on the specific viscosities of polymer solutions , *J. Colloid. Sci.*, 2 (1947)b 99
- Waghorne W.E. and Rubalcava H., Infrared spectroscopic studies of the effect of different cations on N,N-dimethylacetamide and fully deuterated N,N-dimethylformamide, *J. Chem. Soc. Faraday. Trans.*, 1 78 (1982) 1199
- Witte. P. Van. de, Dijkstra. P. J. , Berg. J. W. A. Van.den., Feijen. J., Phase separation processes in polymer solutions in relation to membrane formation, *J. Membr. Sci.* 117 (1996) 1
- Wu C.R., Leidberg, The influence of copper-nitrile complexing on the electronic structure of PAN, *Synthetic Metals* 26 (1988) 21.
- Yang. C R, Perng. J T, Wang. Y Y. and Wan. C.C., Conductive behaviour of lithium ions in polyacrylonitrile, *Journal of Power Sources*, 62 (1996) 89
- Yih. L.J., Jane. H.S., Hsiung. C.S., Polymethyl (methacrylate) / DMF / metal complex membrane for gas separation, *J. Membr. Sci.*, 74 (1992) 71.



- Yilmaz. V. T, Topcu. Y, Preparation, characterization and thermal reactivity of N'N' Dimethylformamide complexes of some transition metal chlorides, *Thermochim. Acta*, 307(2) (1997) 143
- Ying. K., Yonglie. W., Jinnong. Y., Jiping. X., Preparation of asymmetric microporous hydrophobic PVDF membranes for distillation and morphology study, *Mo. Kexue. Yu. Jishu.*, 10 (1990) 119. (Chinese)
- Zagar. E., Zigon. M., Solution properties of carboxylated polyurethanes and related inomers in polar solvents, *Polymer*, 41 (2000) 3513.
- Zazuhiko. O, Makoto. K, Honoh. S, Shinichi. I, Solvation structure of divalent transition metal ions in DMF and DMAc, *J. Phys. Chem.*, 97 (1993) 500
- Zhu. D, Pappa. H, Jiongxin. Z, Chengxun. W, Baojun. Q, Effect of entanglement measurement of intrinsic viscosity of ultrahighmolecular weight polyacrylonitrile, *Zhonggua. Fangzhi. Daxue. Xuebao.*, 22 (1996) 1
- Zydney. A.L., Aimar. P., Meireles. M., Pimbley.J.N. and Belfort. G., Use of the log-normal probability density function to analyze membrane pore size distributions: functional forms and discrepancies, *J. Memb. Sci.*, 91 (1994) 293

## Appendix I-1

### Reported properties of commercially available PAN membranes

The commercially available membranes made of polyacrylonitrile are tabulated as follows:

KROSEP provides a hollow fiber module configuration which is made from hydrophilic polyacrylonitrile material for water treatment application.

product	unit	specification
Product no		Krosep-N11030-4040
Membrane material		High molecular wt. PAN
Nominal molecular wt. cut off	Dalton	50,000
Initial pure water flow rate	L/hr	1,200
optimum operating pressure	Kg/cm	1-1.3
Optimum operating temperature	°C	5-45
pH		2-10

Applied Membrane Inc. (AMI) polyacrylonitrile membranes are as follows

Model No	Pure water flux (gfd)	Nominal active surface area ft <sup>2</sup>	MWCO
M-UB8040PAN50	230	350	20,000
M-UB8040PAN100	350	350	20,000
M-UB8040PAN400	900	350	20,000

### Rochem FM ultrafilters

Code	J <sub>w</sub> lmh	Avg. Pore dia. (nm)	MWCO(dalton)
HV1 / T	6150	37.7	15.7 x 10 <sup>4</sup>
HV2 / T	688	11.6	2.0 x 10 <sup>4</sup>
HV3 / T	330	6.7	9.5 x 10 <sup>4</sup>

J<sub>w</sub> is the water permeability measurements (lmh) at 3 bar and the cutoff is determined using Dextran T<sub>250</sub>

The maximum operating pressures is 600 psi, maximum feed flow rate is 75 gpm, operating temperature is 45 degree, and pH is 2-11. Chlorine tolerance for the membranes is 5000 ppm, PEG 30k used for the study.

PAN can be welded by heat or ultrasound. This makes the production of membrane envelopes possible, which are used in several filtration module types like Amafilter PM and Rochem FM.

The reported performances of these PAN membranes can be compared with the more common polysulfone UF membrane. For example, Pall Corporation provides 10k Nova<sup>TM</sup> membranes made of Polyether sulfone (PES) with a water flux of 700 lmh and 4% Albumin flux of 55 lmh. This membrane is stable to biological degradation and organic solvent and can be used safely within the pH range of 2-12. Many attempts are being made to improve its performance, like blending, surface modification, copolymerization etc. and recently a few studies are related to the properties of the membrane to the molecular weight of the material.

### Appendix III.1

The intrinsic viscosity calculations using the Huggins equation (eqn. 3.2) are as follows:

**Table IIIA-1:** Dilute solution intrinsic viscosities measured at a temperature range of 25-45°C for solutions with and without salts for PAN-A, B and C calculated using Huggins's equation

Solution	Temperature (°C)		
	25	35	45
PAN-A	1.34	1.55	1.73
PAN-A-L	1.36	1.62	1.28
PAN-A-Z	1.39	1.82	1.86
PAN-A-A	1.66	2.38	2.45
PAN-B	3.14	3.17	3.76
PAN-B-L	2.96	3.10	3.20
PAN-B-Z	1.92	2.01	1.69
PAN-B-A	2.88	2.03	2.79
PAN-C	3.80	4.31	4.83
PAN-C-L	5.84	6.42	8.03
PAN-C-Z	5.71	4.62	4.58
PAN-C-A	6.16	4.93	5.34

The intrinsic viscosity values do not show any specific trend with an increase in temperature

**Table IIIA-2:**  $k_H$  parameter calculated from the dilute solution viscosities using the Huggins's equation (eqn.3.2)

Solution	Temperature (°C)		
	25	35	45
PAN-A	0.30	-1.54	-2.12
PAN-A-L	-0.54	-1.14	-1.62
PAN-A-Z	0.29	-1.50	-1.67
PAN-A-A	-0.52	-3.01	-3.81
PAN-B	4.14	3.63	-0.73
PAN-B-L	4.21	2.77	2.04
PAN-B-Z	7.74	6.87	7.83
PAN-B-A	3.50	5.31	0.82
PAN-C	4.37	15.38	11.59
PAN-C-L	-0.25	-3.52	-10.31
PAN-C-Z	2.07	3.12	2.08
PAN-C-A	-2.66	-0.98	-4.99

The averaged values of  $k_H$  (Table IIIA-2) show a great deal of scatter making this an unreliable indicator of solvent efficacy. On the whole the  $k_H$  values are less than 0.5; this indicates that all 4 solvents (DMF, DMF+salts) are good solvents but we cannot draw useful comparisons between them because of the estimation inaccuracy.

### Appendix III.2

Deviations in the dilute solution regime (0.1-0.3%) was observed similar to Bercea [1999]. Solutions with additive-Z show the deviation as depicted below

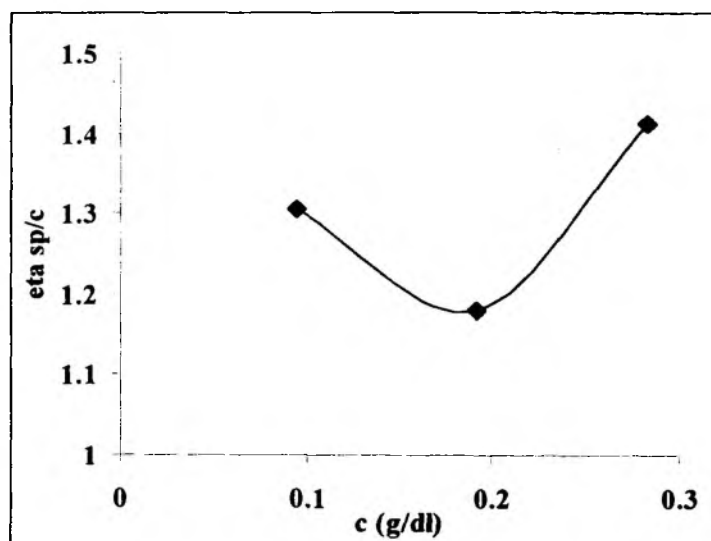


Figure III-A-2.1: Deviations observed from the Huggin's equation for PAN-A-L solution as a function of polymer concentration

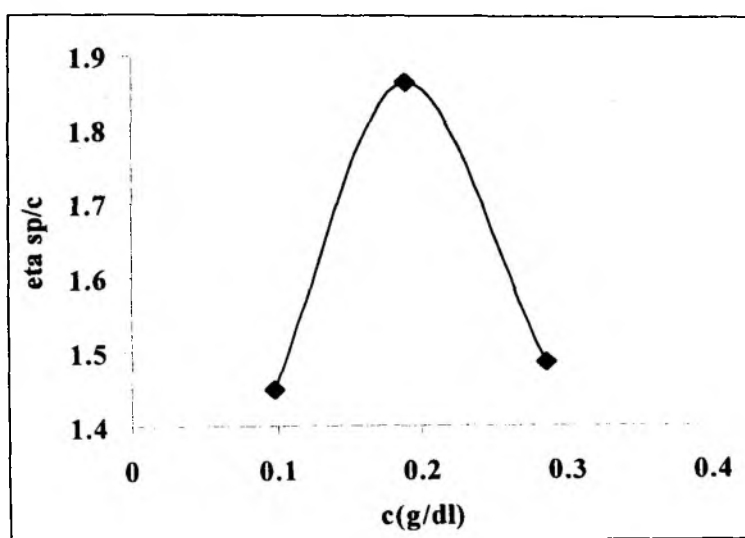


Figure III-A-2.2: Deviations observed from the Huggin's equation for PAN-A-Z solution as a function of polymer concentration

### Appendix III.3

The dilute solution viscosities were used to calculate the activation energies as per the Arrhenius equation. The values as a function of concentration are tabulated below:

**Table III-A-3.1:** Activation energy (kcal) values calculated from the dilute solution viscosities

Solution	PAN Concentration (%)		
	0.1	0.2	0.3
PAN-A	6.93	7.93	8.91
PAN-A-L	6.74	7.47	8.19
PAN-A-Z	7.24	7.66	8.91
PAN-A-A	6.44	7.49	8.72
PAN-B	18.72	22.36	23.34
PAN-B-L	17.73	18.56	19.66
PAN-B-Z	21.06	21.68	22.89
PAN-B-A	15.15	17.17	18.85
PAN-C	25.73	27.41	30.56
PAN-C-L	15.25	18.61	20.67
PAN-C-Z	21.10	22.03	22.97
PAN-C-A	14.45	17.84	18.52

As the polymer concentration increases the activation energy also shows an increase.

The trend of Solutions with Z as an additive show an increase in the energy required which correlates somewhere with the complex formation

### Appendix IV.1

The bubble point data for the supported 13% polymer membrane are discussed in section 4.4.1 is tabulated below followed by the data for the supportless membranes over the polymer concentration range of 7-17%.

**Table IV-A-1:** Bubble point data for the 13% PAN-A supported membrane with and without additives

Code	Bubble point (kg/cm <sup>2</sup> )	
	water	Isopropanol
PAN-A	1.7	0.3
PAN-A-L	1.7	0.4
PAN-A-Z	3.0	1.0
PAN-A-A	2.3	1.2

**Table IV-A-2:** Bubble point data for the PAN-A supportless membrane with and without additives at different polymer concentrations

polym.conc. (%)	Bubble point (kg/cm <sup>2</sup> )			
	PAN-A	PAN-A-L	PAN-A-Z	PAN-A-A
7	0.4	-	0.4	-
11	0.4	2.2	0.4	0.2
13	2.0	-	2.0	-
15	2.2	3.2	2.2	3.1
17	0.4	-	0.4	

Aluminum and Lithium solutions were studied only at two concentrations, the lower concentrations could not be studied due to the viscosity problems.



## Appendix IV-2

**Table IV-A-2.1 : Water fluxes for the 13% PAN-A supported membrane with and without additives**

code	water flux (lmh)
PAN-A	1162
PAN-A-L	329
PAN-A-Z	795
PAN-A-A	826

\* operating pressure 200 kPa

**Table IV-A-2.2: Water fluxes for PAN-A with and without additives supportless membranes over a polymer concentration range of 7-17%**

polym.conc. (%)	water flux (lmh)			
	PAN-A	PAN-A-L	PAN-A-Z	PAN-A-A
7	5170	-	815	-
11	1118	653	680	1944
13	1988	-	378	-
15	220	310	100	152
17	59	-	102	-

\* operating pressure 70 kPa

The decrease in flux with polymer concentration is not very sharp in case of solutions with additives in comparison to those without additives.

---

### Appendix IV.3

**Table IV-A-3.1 : Protein rejection data for 13% supported PAN-A membranes with and without additives**

Code	PEG-9000	Lysozyme	BSA
PAN-A	45	88	100
PAN-A-L	50	88	100
PAN-A-Z	36	94	100
PAN-A-A	45	90	100

\* operating pressure 100 kPa and filtrations done in a 13.4 cm<sup>2</sup> stirred cell assembly (Amicon) at 25°C

It is seen from the protein rejection data that the MWCO of the membrane is not affected by the presence of additives but improving the separation abilities by slight changes in the structure of the membrane formed.

### Appendix V-1

The effect of polymer concentration and salt type on the solution viscosity (cps), at 30°C as a function of shear rate

**Table V-A-1:** The viscosity for PAN-A (1-17% concentration) in DMF as a function of shear rate.

Ln(shear) conc (%)	Ln(viscosity)									
	17	15	13	10	7	5	3	1		
1.321756	7.554691	6.690122	6.522328	5.541499	4.585987	4.180522	2.976549	2.571084		
2.014903	7.614509	6.698219	6.50291	5.327925	4.018003	3.749739	2.283402	1.18479		
2.931194		6.487099	6.493058	5.265712	3.823847	3.487375	1.877937	0.268499		
3.624341				5.311924	3.838032	3.4255	2.140301	0.268499		
4.317488				5.31031	3.79486	3.370841	2.249501	0.673964		
5.010635					3.772554	3.342349	2.266595	0.754007		
5.926926					3.763491	3.310638	2.228594	0.856286		
6.620073						3.310638	2.225067	0.883685		

PAN-A spindle used :Cp-40 Shear rate 3.75-750 sec<sup>-1</sup>

**Table V-A-2:** The viscosity for PAN-A (1-17% concentration) in DMF+L as a function of shear rate.

Ln(shear) conc (%)	Ln(viscosity)									
	17	15	13	10	7	5	3	1		
1.321756	6.895217	5.829181	5.662127	4.822376	4.275832	4.075162	3.669697	3.487375		
2.014903	6.911638	5.738667	5.566817	4.480627	3.957379	3.669697	3.1307	2.283402		
2.931194	6.736198	5.702221	5.483435	4.200325	3.765007	3.446553	2.666395	1.367112		
3.624341		5.634475	5.480714	4.257483	3.718487	3.4255	2.571084	1.521262		
4.317488			5.515523	4.150063	3.734235	3.382015	2.595777	1.447154		
5.010635				4.170472	3.745886	3.370841	2.571084	1.407934		
5.926926				4.134478	3.743566	3.336552	2.571084	1.399901		

PAN-A-L spindle used :Cp-40 Shear rate 3.75-750 sec<sup>-1</sup>

**Table V-A-3:** The viscosity for PAN-A(1-17% concentration) in DMF +Z as a function of shear rate.

PAN-A-Z spindle used :Cp-40 Shear rate 3.75-750 sec<sup>-1</sup>

Ln(shear) conc (%)	Ln(viscosity)										
	17	15	13	10	7	5	3	1			
1.321756	8.429018	8.274867	6.908375	5.662127	4.362844	3.823847	3.487375	3.264232			
2.014903			6.888572	5.627441	3.957379	3.264232	2.794228	2.283402			
2.931194			6.698219	5.515523	3.765007	3.041088	2.571084	1.367112			
3.624341				5.533777	3.734235	3.009339	2.465724	1.18479			
4.317488				5.418896	3.726392	2.976549	2.465724	1.18479			
5.010635					3.714511	2.959742	2.479517	1.133497			
5.926926					3.707313	2.959742	2.476774	1.101408			
6.620073						2.95294	2.474023	1.056957			

**Table V-A-4:** The viscosity for PAN-A (1-17% concentration) in DMF+A as a function of shear rate.

PAN-A-A spindle used :Cp-40 Shear rate 3.75-750 sec<sup>-1</sup>

Ln(shear) conc (%)	Ln(viscosity)										
	17	15	13	10	7	5	3				
1.321756	7.836362	7.191143	6.833764	5.566817	4.180522	2.976549	2.976549				
2.014903	7.790088	7.362734	6.8919	5.579239	4.180522	2.976549	2.571084				
2.931194			6.765274	5.362249	3.669697	2.833449	2.347941				
3.624341				5.383495	3.545644	2.871189	2.347941				
4.317488				5.398398	3.600704	2.889538	2.408565				
5.010635					3.62278	2.889538	2.451738				
5.926926					3.452784	2.719504	2.235612				
6.620073						2.763769	2.259792				



**Table V-A-5: The viscosity for PAN-B (1-17% concentration) in DMF as a function of shear rate**  
**PAN-B** spindle used :Cp-52 Shear rate 1-200 sec<sup>-1</sup>

Ln(shear)	Ln(viscosity)				
conc (%)	3	7	9	11	13
0	6.379783	7.583756	8.114385	9.813771	9.855882
0.693147	5.281171	7.421237	8.05376	9.455558	9.700012
1.609438	4.36488	7.255252	7.861388	9.494779	9.365465
2.302585	4.075671	7.239739	7.756183	9.317418	9.157076
2.995732	4.077198	7.183279	7.627773		8.921385
3.688879	4.157241	7.064562	7.441617		
4.60517	4.109988	6.751347	7.121721		
5.298317	4.077198	6.642148			

**Table V-A-6: The viscosity for PAN-B (1-17% concentration) in DMF+L as a function of shear rate**  
**PAN-B-L** spindle used :Cp-52 Shear rate 1-200 sec<sup>-1</sup>

Ln(shear)	Ln(viscosity)				
conc (%)	3	7	9	11	13
0	5.281171	6.890609	7.360613	8.682369	9.109813
0.693147	4.588024	6.379783	7.072931	8.648467	8.994743
1.609438	3.671733	6.236683	6.890609	8.577008	8.853517
2.302585	3.670206	6.195935	6.889082	8.518323	8.735961
2.995732	3.671733	6.177259	6.86015	8.423166	8.586225
3.688879	3.671733	6.135587	6.796298	8.29056	8.387998
4.60517	3.566373	6.046639	6.644709		

**Table V-A-7: The viscosity for PAN-B (1-17% concentration) in DMF+ A as a function of shear rate**  
**PAN-B-A** spindle used :Cp-52 Shear rate 1-200 sec<sup>-1</sup>

Ln(shear)	Ln(viscosity)			
conc (%)	3	7	9	11
0	0.000000	6.667466	7.679066	8.648467
0.693147	0.000000	6.379783	7.478396	8.558316
1.609438	0.000000	6.310791	7.385305	8.325694
2.302585	2.977059	6.309264	7.346507	8.255174
2.995732	3.384051	6.396313	7.269046	8.140511
3.688879	4.077198	6.396313	7.149120	7.948399
4.605170	3.854055	6.255731	6.894601	
5.298317	3.566373	5.996569	6.658677	

**Table V-A-8: The viscosity for PAN-C (1-17% concentration) in DMF as a function of shear rate**

PAN-C spindle used :Cp-52 Shear rate 1-200 sec<sup>-1</sup>

Ln(shear) conc (%)	Ln(viscosity)			
	3	7	9	11
0		7.227081	9.455558	10.278383
0.693147	4.588024	7.072931	9.141901	9.995196
1.609438	4.364880	6.849787	8.695614	9.665695
2.302585	4.768818	6.714729	8.324167	9.215384
2.995732	5.118652	6.519545	7.740760	8.967548
3.688879	5.255853	6.274423	7.714785	
4.605170	4.895509	5.885487	7.169755	
5.298317	4.577974	5.573841		

**Table V-A-9: The viscosity for PAN-C (1-17% concentration) in DMF+ L as a function of shear rate**

PAN-C-L spindle used :Cp-52 Shear rate 1-200 sec<sup>-1</sup>

Ln(shear) conc (%)	Ln(viscosity)			
	3	7	9	11
0	5.281171	9.018841	9.358709	11.183805
0.693147	4.588024	8.715158	9.065361	11.090814
1.609438	4.364880	8.425323	8.662166	
2.302585	4.586497	8.208168	8.356956	
2.995732	4.588024	7.930886	7.872688	
3.688879	4.536731	7.613315	7.332085	
4.605170	4.413671	7.192194	7.168241	
5.298317	4.259520			

**Table V-A-10: The viscosity for PAN-C (1-17% concentration) in DMF+ A as a function of shear rate**

PAN-C-A spindle used :Cp-52 Shear rate 1-200 sec<sup>-1</sup>

Ln(shear) conc (%)	Ln(viscosity)	
	3	7
0	8.416665	8.539268
0.693147	8.171543	8.198942
1.609438	7.846121	7.622977
2.302585	7.602032	7.281124
2.995732	7.379189	6.948878
3.688879	7.039029	6.596238
4.60517	6.586798	6.160798
5.298317		6.037293

**Appendix V-2:**

The zero shear viscosities for the polymers PAN-A-B and C as a function of polymer concentration with and without additives is tabulated. ( Ref. Figure 5.1 (a-c))

**Table V-A-2-1: The Zero shear viscosities  $[\eta_0]$  for the polymers PAN-A-B and C as a function of polymer concentration**

Conc %	PAN-A	PAN-A-L	PAN-A-A	PAN-A-Z	PAN-B	PAN-B-L	PAN-B-A	PAN-C	PAN-C-L	PAN-C-A
1		2.99		2.96						
3		3.47		3.21						8.43
5	4.07	4.02		3.62						8.46
7	4.45	4.20		4.28	7.59	6.43	6.55	7.24	9.07	
10	5.53	4.78			8.19	7.23	7.68	9.46	9.40	
13	6.54	5.69	6.93	6.76	9.73	8.65	8.69	10.29		
15	6.90	5.92	6.64	7.69	9.88	9.27				
17	8.20	7.06		8.15						

**Table V-A-2-1: The Power law fit  $[\eta]$  for the polymers PAN-A-B and C as a function of polymer concentration**

Conc %	PAN-A	PAN-A-L	PAN-A-A	PAN-A-Z	PAN-B	PAN-B-L	PAN-B-A	PAN-C	PAN-C-L	PAN-C-A
1		0.70		0.65						
3		0.83		0.86						0.61
5	0.86	0.86		0.88						0.50
7	0.86	0.90		0.88	0.83	0.88	0.92	0.72	0.60	
10	0.94	0.87			0.79	0.87	0.83	0.49	0.50	
13	0.98	0.95	0.90	0.88	0.82	0.92	0.80	0.55		
15	0.87	0.92	0.96	0.92	0.68	0.81				
17	0.98	0.90		0.93						

**Appendix V-3: Shear dependence of concentrated solution shear viscosity**

**Table V-A-3-1 : reduced shear data vs reduced shear viscosity data for PAN-A with additives for 7% polymer concentration at a fixed shear rate of  $3.75\text{sec}^{-1}$**

red shear	PAN-A	PAN-A-L	PAN-A-Z	PAN-A-A
1	1.000000	1.000000	1.000000	1.000000
2	0.566667	0.727273	0.666667	1.000000
5	0.466667	0.600000	0.550000	0.600000
10	0.473333	0.572727	0.533333	0.530000
20	0.453333	0.581818	0.529167	0.560000
40	0.443333	0.588636	0.522917	0.572500
100	0.439333	0.587273	0.519167	0.483000

**Table V-A-3-2 : reduced shear data vs reduced shear viscosity data for PAN-B with additives for 7% polymer concentration at a fixed shear rate of  $1\text{sec}^{-1}$**

red shear	PAN-B	PAN-B-L	PAN-B-A
1	1.000000	1.000000	1.000000
2	0.850000	0.600000	0.750000
5	0.720000	0.520000	0.700000
10	0.708917	0.499237	0.698932
20	0.670000	0.490000	0.762500
40	0.595000	0.470000	0.762500
100	0.435000	0.430000	0.662500
200	0.390000		0.511250



**Table V-A-3-3** : reduced shear data vs reduced shear viscosity data for PAN-C with additives for 7% polymer concentration at a fixed shear rate of  $1\text{sec}^{-1}$

red shear	PAN-C	PAN-C	PAN-C-L	PAN-C-L	PAN-C-A	PAN-C-A
1	1.000	1.000	1.000	1.000	1.000	1.000
2	0.857	0.986	0.738	0.744	0.660	0.712
5	0.686	0.825	0.552	0.563	0.400	0.400
10	0.599	0.823	0.445	0.467	0.288	0.284
20	0.493	0.645	0.337	0.351	0.204	0.204
40	0.386	0.489	0.245	0.245	0.148	0.143
100	0.261	0.333	0.161	0.140	0.090	0.093
200	0.191	0.238				

The shear behaviour for the three different molecular weight polymers was studied using the reduced viscosity vs shear plots (Figure 5.5a-c). It is seen that the transition/plateau region is between 10-100 shear rate in case of PAN-A which remains mostly unaffected with the additives of course the viscosity is affected. This is related to the strength of the complex formed of the additive and solvent as well as polymer that on application of shear shows the trend which is related to the viscosity also. Hence the observed trend is PAN-A>PAN-A-Z>PAN-A-L>PAN-A-A

PAN-A-DMF solutions show more shear thinning than solutions containing salts. For PAN-C we see the opposite trend and PAN-B shows similar power-law indices for DMF, DMF-L and DMF-A solvent systems. We must note from Figure 5.5c for PAN-C the slope increase.

Appendix V-4: LCP equation parameters.



Figure V-A-4-1 : Plot of parameter a vs PAN MW for the various solvent types DMF, DMF-L, DMF-Z and DMF-A.

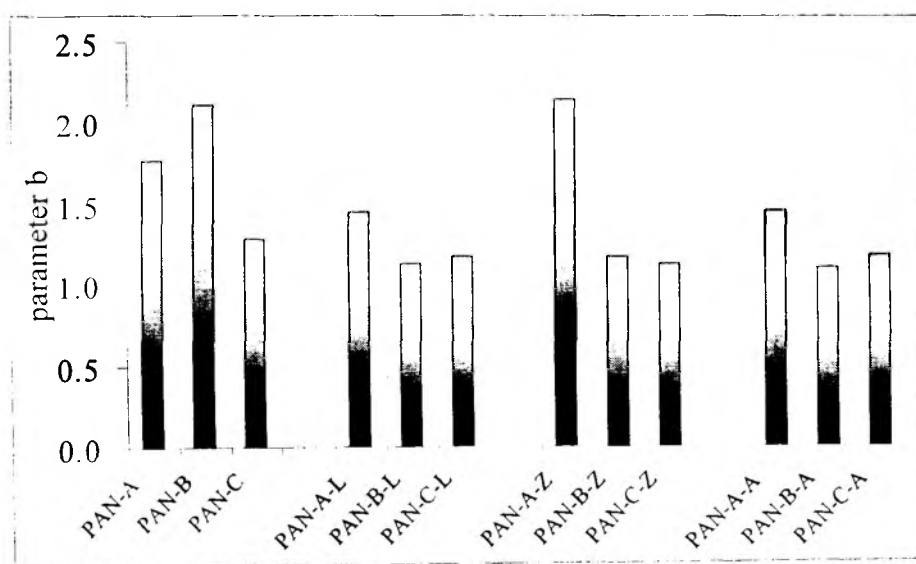


Figure V-A-4-2 : Plot of parameter b vs PAN MW for the various solvent types DMF, DMF-L, DMF-Z and DMF-A.

The parameter a and b do not obey the predicted trends. For example, for a given solvent-non-solvent pair, parameter  $b [= (v_P - v_{NS}) / (v_S - v_{NS})]$  should increase with increasing PAN MW. However, the estimates do not show even this basic trend

## Appendix V-5

The water permeability for the supportless membranes cast from two different concentrations for PAN-A (7 and 15%) and PAN-B and PAN-C 7% respectively with additives is tabulated below.

Table V-A-5-1: Water permeance (lmh) at 70 kPa for membranes of PAN-A, PAN-B and PAN-C cast from 7% solutions with and without salts

	A (7%)	A (15%)	B (7%)	C (7%)
DMF	5170	220	2027	3402
DMF-L	-	310	1024	754
DMF-Z	815	100	590	234
DMF-A	-	152	1738	317

The water permeabilities show a standard deviation of  $\pm 5\%$  approximately. The data shows a trend for the reduction of the water permeation in the case of DMF- and the polymers A, B and C. The obvious trend is that with PAN-C with all the additives there is a noticeable reduction in the permeability.